# UNIVERSIDAD COMPLUTENSE DE MADRID

FACULTAD DE CIENCIAS FÍSICAS

Departamento de Física de la Tierra, Astronomía y Astrofísica I



## TESIS DOCTORAL

# Upwelling in the tropical lower stratosphere
# Effects on tracer transport and drivers of variability
# Ascenso en la baja estratosfera tropical
# Efectos en el transporte de trazadores y fuentes de variabilidad

MEMORIA PARA OPTAR AL GRADO DE DOCTOR

PRESENTADA POR


**Marta Ábalos Álvarez**

Directores

Encarna Serrano Mendoza
William J. Randel


**Madrid, 2014**

Depto. de Física de la Tierra, Astronomía y Astrofísica I
Facultad de Ciencias Físicas
Universidad Complutense de Madrid

# Upwelling in the tropical lower stratosphere: effects on tracer transport and drivers of variability

Ascenso en la baja estratosfera tropical:
efectos en el transporte de trazadores y fuentes de variabilidad

Memoria de Tesis presentada para obtener el grado de Doctor por

Marta Ábalos Álvarez

Directores de Tesis:

Dra. Encarna Serrano Mendoza
Dr. William J. Randel

Madrid, 2013

Este trabajo ha sido financiado por la beca de Formación de Personal Investigador (FPI) BES-2009-013082 asociada al proyecto nacional CGL2008-06295, y en parte por el proyecto CGL2012-34997.

*Agradecimientos/Acknowledgements*

En primer lugar, quiero agradecer a mis directores de Tesis su esfuerzo y dedicación, sin los cuales no existiría esta Tesis. Encarna, gracias por confiar en mí, darme alas y apoyar mis decisiones, por las largas horas de trabajo y por cuidar todos los detalles. Bill, thank you for teaching me so much, for being always enthusiastic and motivating; I will try to follow your example as a scientist.

A mis súper-compañeros, por estar siempre dispuestos a ayudar, por compartir buenos y malos momentos, por el compañerismo y el buen rollo, y por las risas. Gracias por hacer del camino lo mejor de la tesis. Gracias Jorge (*etupendo*), Mariano (el auténtico), Iñigo (y sus ciclones explosivos), Cahlo (Nishi) ¡Gracias Altintop! Gracias Blanca por compartir charlas (sobre estratosfera y no) y por tu buen humor, Marta M. por cuidarnos, Jesús por las discusiones dinámicas. A los que estabais al principio, gracias Teresa, Irene, Bea, Javi, Javi BF, por el buen ambiente que encontré al empezar, y a los llegados más tarde, Julián, Roberto, Ibrahima. No puedo imaginar mejores compañeros. Y gracias a los compañeros de comidas y/o cafés, fundamentales para la productividad (para rebajarla, claro): Javi P., Ana, Juan, Maurizio, Sara, Luis D., Luis, Elsa. Y a los compañeros de la Semana de la Ciencia, que ha sido una experiencia única para mí. Belén, gracias por tu empuje y tu entusiasmo sin límites (¡anda que no hay gente aquí para el centro de investigación en la playa!). Gracias Carlos, porque siempre se pueda contar contigo. Pablo, Natalia, gracias por vuestro apoyo, cercanía y ayuda. Gracias al Depto. de Geofísica y Meteorología, a Salva y a Lucía por ayudar siempre con una sonrisa.

I would like to acknowledge Rolando Garcia (NCAR) and Thomas Birner (CSU) for insightful comments and suggestions on the Thesis.

I'd also like to thank ACD (NCAR) for hosting my visits, in particular the Satdat/UTLS group for the weekly meetings, where I have learned a lot thanks to a relaxed environment. Special thanks to Mijeong, Hella, Aurélien, Cameron and Tao. D. Kinnison, F. Wu, M. Park and C. Homeyer directly contributed to this thesis by providing data.

Gracias a mis amigos del cole (Viole, Laura, Ire, Eva) por esas tardes de juegos, y a los de la facultad (Ana, Vir, Julia, Bea, Leti, Cova, Rosi, Roi, Fierro, Crespo) por mantener la amistad como nueva. Gracias a TONTO, por haberme esperado tantas veces. Y gracias a mis nuevos amigos de París por hacer de esta ciudad un sitio acogedor.

Gracias a mi familia (Fernando, Elena, Lucía y Javi), por absorber todos los golpes para que me mantenga en pie.

Y por supuesto, gracias a Álvaro. Por su ayuda como científico y compañero, por su apoyo incondicional y por sacar lo mejor de mí.

# Contents

# 1. Motivation

The chemical composition of the stratosphere[1] largely controls the radiative balance of the atmosphere, directly affecting climate at the Earth surface. For instance, the importance of stratospheric ozone absorption of solar ultraviolet radiation for protecting life on the planet is well-recognized. By limiting the anthropogenic emissions of ozone-depleting substances around the world, the Montreal Protocol (1987) has reduced stratospheric ozone loss over the Antartic and presumably avoided its total collapse (Newman et al. 2009, Garcia et al. 2012). In addition to ozone, several other trace gases in the stratosphere play crucial roles in determining global radiative budgets. Solomon et al. (2010) pointed out the important role of stratospheric water vapor (through its greenhouse gas effect, GHG) on observed decadal changes in surface temperatures. The radiative forcing[2] of surface climate is particularly sensitive to the temperature structure and tracer distribution in the upper troposphere and lower stratosphere (UTLS) (Riese et al. 2012). The UTLS constitutes a transition region between the well-mixed troposphere and the strongly stratified stratosphere, and the interplay of dynamics, radiation and chemistry is particularly complex in this region. Quantifying the processes that control the chemical composition of the UTLS is thus an important and challenging task.

In addition to chemical sources and sinks, changes in the spatial distribution and temporal variability of ozone, water vapor and other radiatively active tracers in the stratosphere are determined by transport processes. The global mean meridional mass circulation in the stratosphere

[1] Region of the atmosphere between ~10 km and ~50 km characterized by stable stratification.

[2] Radiative forcing is the change in the net, downward minus upward, irradiance (expressed in $Wm^{-2}$) at the tropopause or top of atmosphere due to a change in an external driver of climate change, such as, for example, a change in the concentration of a greenhouse gas (IPCC 2013).

consists in upwelling in the tropics, poleward drift and downwelling over the high latitudes (e.g. Andrews et al. 1987). Air masses and chemical constituents are transported by this overturning circulation from the tropics towards the poles over timescales of ~5 years. State-of-the-art chemistry-climate models consistently show an intensification of the stratospheric circulation, associated with increased emissions of GHG (e.g. Butchart et al. 2006). A stronger overturning circulation can lead to changes in stratospheric and tropospheric ozone distribution, potentially impacting climate and air quality (Waugh 2009). Dynamical causes for such increase in the strength of the stratospheric circulation have been identified in models (e.g. Garcia and Randel 2008, Shepherd and McLandress 2011), and are ultimately associated with the overall warming of the troposphere and cooling of the stratosphere resulting from increased GHG concentrations in the atmosphere (IPCC 2007, 2013). However, no robust evidence of such change has been identified so far in the limited available observational record (Waugh 2009, Engel et al. 2009, Garcia et al. 2011). Moreover, global stratospheric temperature trends are still under debate due to inconsistencies among different datasets (Thompson et al. 2012).

Tropospheric air is carried upwards into the lower stratosphere across the tropical tropopause (~16-17 km altitude) by the ascending branch of the stratospheric circulation. This is the primary pathway for air masses to enter the stratosphere, such that the upwelling in this region determines the rate of troposphere-to-stratosphere transport. The tropical UTLS is often referred to as the tropical tropopause layer (TTL), and is characterized by sharp transitions in chemical composition and thermal stratification, which enhance the role of transport processes. In particular, changes in tropical upwelling have important effects on the distribution and variability of tracers with steep vertical gradients in this region and on lower stratospheric temperatures.

Despite its relevance, this very slow ascent (< 1 $mm \cdot s^{-1}$) remains poorly quantified, mainly due to the lack of direct observations (e.g. Randel and Jensen 2013). In order to evaluate its influence on tracer

concentrations and temperature in the tropical lower stratosphere, it is necessary to explicitly quantify upwelling variability and assess the uncertainties. Indirect methods to infer upwelling have been proposed in the literature. Sufficiently accurate upwelling estimates near the tropical tropopause are required for exploring these links and their implications for tracer and thermal budgets in the tropical lower stratosphere (in relation to other transport and chemical processes).

Furthermore, although it is well-known that the global mean stratospheric circulation is dynamically (and not thermally) driven[3], there are at the moment several open questions regarding the specific forcings of upwelling (e.g. Ueyama et al. 2013 and references therein). For instance, the spatial distribution of annual-mean upwelling in the tropical lower stratosphere is not fully understood from the current theoretical framework (Plumb and Eluskiewicz 1999). A deep understanding of the dynamical mechanisms that control upwelling across a wide range of timescales constitutes an essential step towards improving the representation of the stratospheric circulation in chemistry-climate models.

In conclusion, upwelling variability and tracer transport in the tropical lower stratosphere are topics of broad interest, with important questions that remain uncertain and require further research. Some of these open issues motivate the analyses carried out in this Thesis. First, updated dynamical estimates of upwelling magnitude based on improved datasets are required. Second, the impact of the fluctuations in upwelling intensity on the variability of lower stratospheric temperature and tracers has not been directly quantified and compared to other transport processes. Finally, although the forcing of tropical upwelling sub-seasonal timescales is understood from theoretical models, more observational studies are needed on the dynamical sources of upwelling transient variability.

[3] This is true outside the tropics. Near the equator it is possible to have angular momentum-conserving mean meridional circulations that are thermally driven.

# 2. Introduction and state-of-the-art

To first-order approximation, the stratospheric circulation can be analyzed from a zonal mean perspective (Andrews et al. 1987). The longitudinal deviations from the zonal mean can usually be considered smaller than the magnitude of the zonal mean field. Nevertheless, these zonal anomalies (denoted *eddies* in the literature and in this Thesis) have been proven to play a key role in stratospheric transport, as will be discussed in this Chapter. Therefore, it is important to bear in mind the background zonal mean structure of temperature and zonal wind in the stratosphere. Figure 2.1 shows the zonal mean climatology of temperature and zonal wind for thirty-three years of reanalyzed ERA-Interim data from the European Center for Medium-Range Weather Forecast (ECMWF), for boreal winter (December through March, DJFM) and summer (June through September, JJAS). The tropopause separates two clearly distinct regions in terms of stratification. One outstanding feature in Figure 2.1 is the band of extremely low temperatures around the tropical tropopause, which constitutes one of the coldest regions in the atmosphere. This exceptional region around the tropical tropopause is the focus of the present Thesis. The altitude corresponding to the lowest temperatures is known as the *cold point tropopause*, and has important implications for stratospheric transport, especially for water vapor, as will be discussed below in this Chapter.

There is a strong seasonality in the stratosphere evident in Fig. 2.1, with coldest polar temperatures on the winter hemisphere, associated with strong eastward winds. This westerly jet is known as the polar vortex, and represents a dominant feature of the stratospheric circulation and dynamics (e.g. Andrews et al. 1987). The summer hemisphere is characterized by weak easterly winds. Two westerly jets in the subtropics persist throughout the year. The climatological subtropical jet cores are approximately co-located with the latitudes at which the tropopause

changes abruptly its altitude from the tropical tropopause (around ~16-17 km) to the extra-tropical tropopause (near ~8-10 km altitude).

The general structure of the mean zonal wind in Figure 2.1 can be interpreted in terms of thermal wind balance. Under assumptions of geostrophic and hydrostatic balance, the thermal wind relation directly relates the vertical shear of the zonal wind to the meridional gradient in temperature (with opposite sign in the NH):

$$f \cdot \overline{u}_z = -\frac{R}{aH}\overline{T}_\phi \qquad (1)$$

Subscripts indicate partial derivatives throughout the Thesis. In Eq. (1) $\phi$ is the latitude, $f = 2\Omega sin\phi$ is the Coriolis parameter (with $\Omega$ the Earth's angular velocity), $H$ is a mean scale height in the stratosphere (usually 7 km), $a$ is the Earth radius, $z \equiv -H\ln(p/p_s)$ is the log-pressure height (with $p_s$ a reference pressure) and $R = 287 m^2 s^{-2} K^{-1}$ is the ideal gas constant for the dry air.

In Figure 2.1, the polar vortex core shows positive vertical wind shear, and is co-located with large negative meridional temperature gradients (note that the Coriolis parameter in Eq. (1) changes sign in the SH). The closed subtropical jets are consistent with the change in sign of the meridional gradient in temperature crossing the tropopause (i.e. negative below the jet core and positive above in the NH).

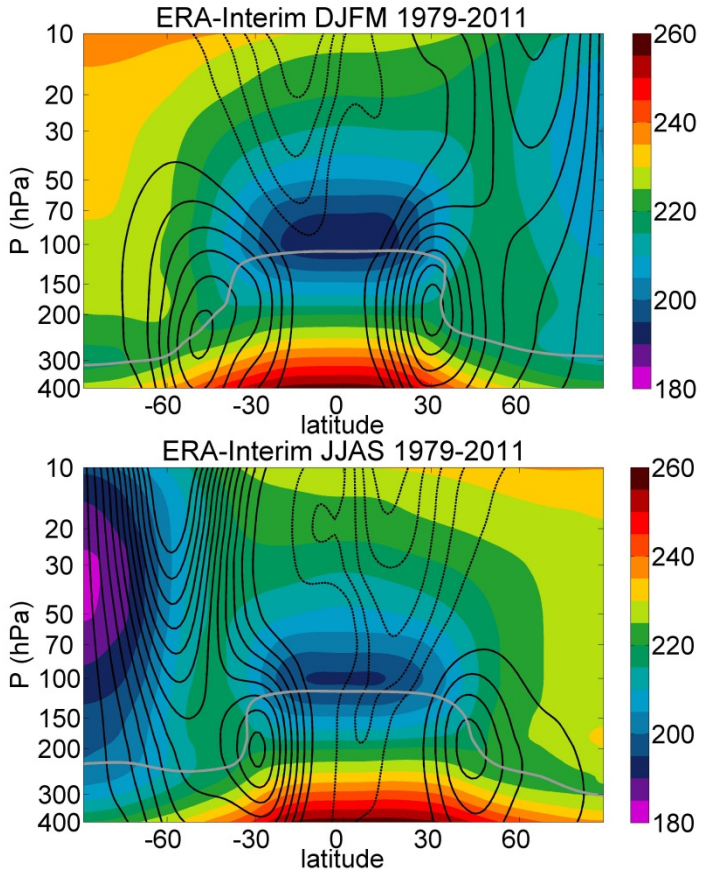


**Figure 2.1**. Zonal mean temperature (shading) and zonal wind (contours) climatology from the ERA-Interim reanalysis for the period 1979-2011 in DJFM (top panel) and JJAS (bottom panel). Temperature in K. Zonal wind contour spacing: $5m \cdot s^{-1}$. Solid: eastward flow, dotted: westward flow. The gray line is the thermal tropopause (WMO definition). Computed from ERA-Interim reanalysis daily mean data for 1979-2011.

The temperature structure in Figure 2.1 arises from the balance between the shortwave radiative heating on one hand, and thermal (infrared) relaxation and the effects of transport by the circulation, on the other. The net radiative equilibrium stratospheric temperatures are notably colder than the observed temperatures in the winter poles and warmer in the tropics. The fact that the observed stratospheric thermal structure is not as deduced from radiative equilibrium points toward the

existence of a global zonal mean meridional circulation, which must provide adiabatic heating/cooling such as to produce the observed balanced distribution.

This Chapter is divided in three Sections. The aim of Section 1 is to describe this global mean meridional mass circulation and the underlying dynamics. Section 2 focuses on tropical upwelling, presenting the known features and the open issues. Section 3 described the main characteristics of the tropical tropopause layer (TTL) and reviews the current understanding of tracer transport near the tropical tropopause and in the tropical lower stratosphere.

# 1 The zonal-mean stratospheric mass circulation

In contrast with the troposphere, dominated by turbulence and convection, the stratosphere is strongly stably stratified, such that vertical motions are inhibited to a large extent. The horizontal components of the wind are ~$10^4$-$10^5$ times stronger than the vertical velocity in the stratosphere (in the zonal mean). Nevertheless, the physical and chemical properties of the stratosphere would be completely different from what is observed if vertical motion was identically zero. The ultimate responsible for the large-scale ascents and descents in the stratosphere are the waves propagating from the troposphere, which drive the stratosphere away from radiative equilibrium, as will be discussed below.

The characteristics of stratospheric transport have been largely deduced from observations of tracers, which have become gradually available in the last decades (e.g. Andrews et al. 1987, Plumb 2002, Shepherd 2007). The following subsections present the main characteristics of the global stratospheric circulation. Section 1a reviews the general structure of the zonal mean meridional circulation, as anticipated by the seminal works of Brewer (1949) and Dobson (1929, 1956). Section 1b describes the current picture of tracer transport in the stratosphere. In Section 1c the *residual circulation* is defined, in the context of the *Transformed Eulerian Mean* framework, which constitutes the mathematical formulation to be used throughout this Thesis. Finally Section 1d presents the dynamical causes of the Brewer-Dobson circulation (BDC).

## a. *Historical perspective*

Water vapor concentrations in the stratosphere are extremely low as compared to those in the troposphere. Brewer (1949) first[1] had the

[1] This article cites Dobson (1929), where the possibility of an overturning circulation in the stratosphere is mentioned but discarded in the same manuscript,

intuition that such dryness of the stratosphere could only be explained if the stratospheric air masses had traveled across the tropical tropopause, and been dehydrated in this region, where the coldest climatological annual mean temperatures are observed (see Fig. 2.1). The proposed circulation, as depicted by Brewer (1949), is reproduced in Figure 2.2. It shows air rising from the troposphere into the stratosphere through the cold point tropopause in the tropics and sinking at higher latitudes. Overlaid on this circulation, the isothermes demonstrate the coldest temperatures at the tropical tropopause. Such meridional circulation could also explain the high concentrations of ozone in the extra-tropical lower stratosphere, and new measurements of vertical ozone profiles supported this view (Dobson 1956). This original idea of Brewer and Dobson was not supported by a dynamical explanation, and the development of a theory that could justify such circulation had to wait until the 1970's (e.g. Holton, 2000). This theoretical framework will be presented in Sections 1c and 1d.

Besides the theoretical development, the advance in the understanding of the global stratospheric circulation was largely boosted as more measurements of the stratosphere became available. The picture of stratospheric zonal mean circulation illustrated in Figure 2.2 was modified and upgraded as the number of satellite and ground-based observations increased.

as it could not be proven due to the lack of ozone vertical profiles measurements (Holton, 2000).

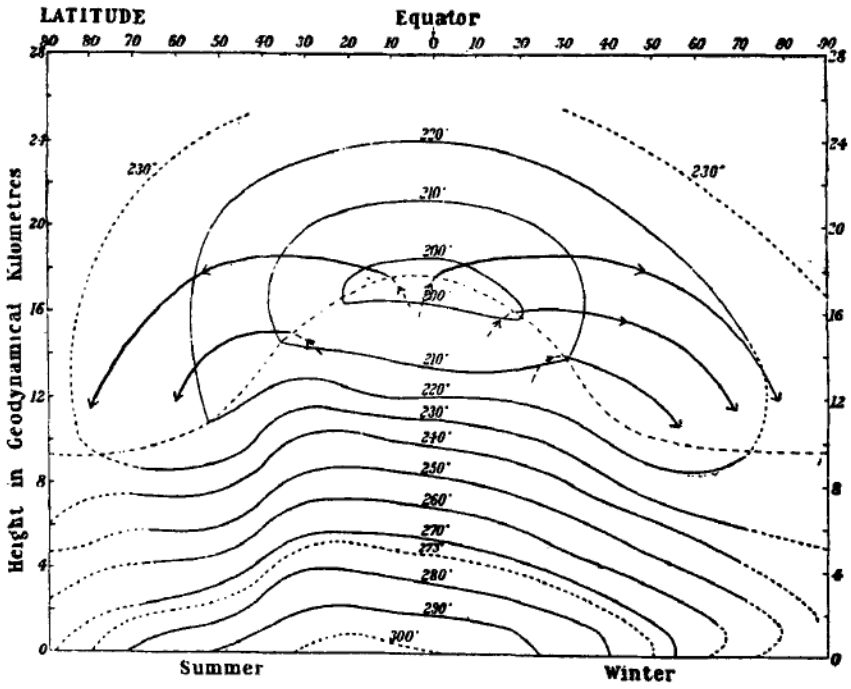


**Figure 2.2**. Schematic of transport envisioned by Brewer to explain low water vapor concentrations in the stratosphere. From Brewer (1949).

## b. *Tracer transport in the stratosphere*

- Observations of tracer distribution

Figure 2.3 shows the latitude versus height cross-section of zonal mean $N_2O$ concentrations, as derived from measurements taken aboard the UARS satellite in the early 1990's one day in austral summer. Several tracers with tropospheric sources and lifetimes of decades exhibit similar spatial distributions. This similarity indicates that the structure shown in Figure 2.3 is not determined only by chemical processes, but transport plays a central role (Plumb 2002, Shepherd 2007). The high concentration bulge in the tropics is indicative of upwelling over this region, carrying high tracer concentrations into the stratosphere. The opposite behavior is observed over the winter pole (i.e. in the SH), which shows lower concentrations consistent with sinking of upper stratospheric air. The black

arrows in Fig. 2.3 illustrate these vertical motions. Hence, the distribution of $N_2O$ (and other tracers) in the stratosphere is strongly suggestive of a hemispheric overturning circulation, with upwelling across the tropics lifting tropospheric air into the stratosphere, poleward drift across the middle latitudes and downwelling over the winter high latitudes. Note that the concentrations are higher in the summer pole (NH) than in the winter pole (SH), indicating weaker downwelling over the more quiescent summer hemisphere.

The departure from radiative equilibrium of the stratospheric climatological temperature structure shown in Figure 2.1 is consistent with the described circulation. Upwelling in the tropics leads to adiabatic cooling of the tropical lower stratosphere, which is balanced by net diabatic heating in this region. In contrast, the extra-tropical stratosphere is adiabatically heated by the BDC downwelling, and this heating is compensated by diabatic cooling. The question of why this circulation appears in the stratosphere is addressed in Section 1d.

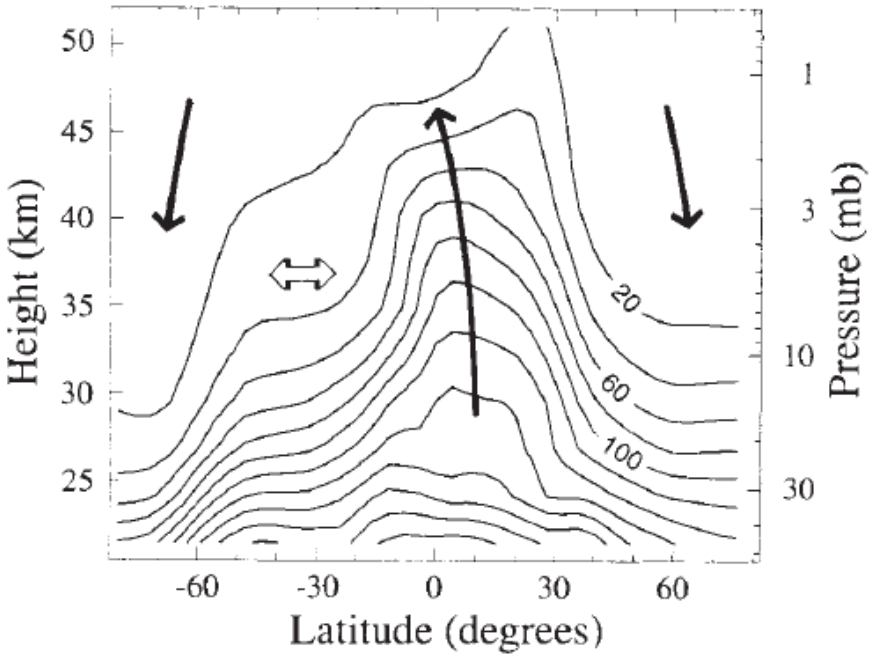


**Figure 2.3**. Zonal mean cross-section of $N_2O$ measurements from the Cryogenic Limb Array Etalon Sounder (CLAES) instrument onboard the Upper Atmosphere Research Satellite (UARS) satellite on September 20, 1992. Contour labels indicate $N_2O$ mixing ratios in ppbv. From Randel et al. 1993.

The $N_2O$ concentrations in Figure 2.3 show an almost flat shape in the middle latitudes of the winter hemisphere, confined by two narrow bands of strong meridional gradients. This behavior suggests strong quasi-horizontal mixing in this region (e.g. McIntyre and Palmer 1983, Garcia 1991, Holton 1995, Plumb 2002), and is indicated in Fig. 2.3 by the two-directional horizontal arrow. The small slope of the tracer isopleths results from the balance between the sharpening effect of downwelling by the mean meridional circulation and the flattening by horizontal mixing (Plumb 2002). In contrast, the steep meridional gradients are indicative of small mixing. Accordingly, the bands presenting steep slopes in tracer concentrations are usually referred to as transport barriers. This feature is observed in the subtropics in both hemispheres, implying an isolation of

the tropics from the extra-tropics. The other transport barrier in Figure 2.3 separates the polar region from the middle latitudes, coinciding with the polar vortex edge (see Fig. 2.1). Hence, from tracer observations the stratosphere can be divided in four main regions, separated by transport barriers with weak mixing across them (i.e. the summer stratosphere, the tropics, the winter middle latitudes and the inside of the polar vortex) (Plumb 2002, 2007). It is important to note that, as well as seasonally and spatially variable, these barriers are also permeable, such that transport across them, although limited, is not impossible (Plumb 1996, Haynes and Shuckburgh 2000a). In fact, these relatively infrequent events have a large impact on the background tracer concentrations, given the steep changes from one side of the barrier to the other (e.g. Randel et al. 1993, Holton 1995).

- ## Advective transport and two-way mixing

The transport features deduced from the tracer distribution in Figure 2.3 reveal two distinct (although closely related, as will be shown below) ways of transport in the stratosphere: advection by the hemispheric Brewer-Dobson circulation[2] (BDC) and quasi-horizontal two-way mixing. The current picture of mass transport in the stratosphere, including these two transport components, is illustrated in the schematic in Figure 2.4 (taken from Bönisch et al. 2011). The white arrows indicate advection by the BDC, and the wavy orange arrows indicate two-directional mixing. The green bands indicate transport barriers, with weak mixing across them (e.g. Plumb 2002).

[2] In this Thesis the term Brewer-Dobson circulation (BDC) will refer to the advective part of stratospheric transport. Note that occasionally the term BDC is used for the combined effect of advection and mixing. In this Thesis we denote the latter “stratospheric transport”.

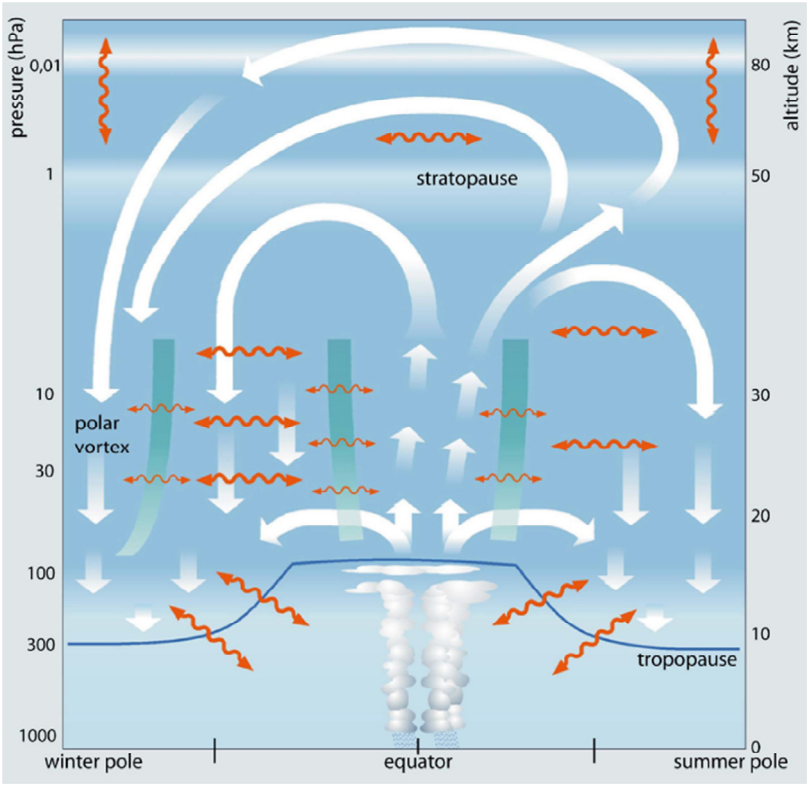


**Figure 2.4**. Schematic of the zonal mean mass circulation in the stratosphere. The white arrows indicate advective transport by the Brewer-Dobson circulation[2]. The wavy orange double-headed arrows represent two-way eddy transport and mixing. Green bands are transport barriers. From Bönish et al. 2011.

In the stratosphere (i.e. from the tropopause up to ~1 hPa, ~50 km) there are two hemispheric branches of the BDC, with the winter hemisphere having significantly stronger circulation than the summer hemisphere. This is true for the so-called deep branch of the circulation, which penetrates high into the stratosphere and overturns near the stratopause. The origin of this seasonality will be discussed in Section 1d. In contrast, the so-called shallow branch of the circulation is limited to altitudes in the lower stratosphere (below ~20 km), and does not show a pronounced seasonality. Upwelling near the tropical tropopause contributes to feed both branches, although in terms of mass flux, due to

the decrease in density with height, a large fraction of the air entering the lower stratosphere will be removed by the shallow branch and will not reach the upper stratosphere. Note that above the stratopause there is an inter-hemispheric circulation, with upwelling over the summer pole and downwelling over the winter pole (contributing to the stratospheric downwelling).

As described above in relation to Figure 2.3, the BDC accounts for part of the mean distribution of long-lived tracers. However, in order to explain the shallow slopes in tracer concentrations in middle latitudes, quasi-horizontal mixing is required. Strong perturbations of the zonal mean flow occur in this region (i.e., eddies or waves), and these wavy structures eventually become unstable and break, producing planetary-scale tongues of air which fold around stirring the air and ultimately leading to (molecular) mixing (e.g. Randel et al. 1993, Holton et al. 1995). The resulting irreversible mixing, as indicated by the wavy arrows in Fig. 2.4, is largest in the middle latitudes (consistently with the tracer distribution in Fig. 2.3) but is also present in other regions of the atmosphere. Notably, there is mixing across the tropopause causing stratosphere-troposphere exchange, with interesting implications as it strongly changes the chemical and physical characteristics of the mixed air (Holton et al. 1995).

## c. *The residual circulation*

- ### Transformed Eulerian Mean formulation

In the previous sections a global zonal mean mass stratospheric circulation has been presented as deduced from observations of tracers, consisting on global advection by the BDC plus quasi-horizontal mixing. In the beginning of this chapter it was stated that the stratospheric circulation can be considered approximately longitudinally symmetric. If the circulation of the stratosphere was exactly zonally symmetric, the mass circulation in the latitude-height plane should follow the zonally-averaged

circulation $(\overline{v},\overline{w})$[3]. In this case the zonally-averaged Eulerian equations would be able to represent mass transport, which is fundamentally a Lagrangian process. However, the Eulerian zonal mean circulation does not present hemispheric cells as deduced from the observations, but two cells in one hemisphere, with upwelling both over the tropics and over the poles (Vincent 1968). This discrepancy underscores the importance of the zonal anomalies or eddies for stratospheric transport. In order to approximate the observed zonal mean mass overturning circulation (BDC) from an Eulerian point of view, the main effects of the eddies need to be accounted for. This was the approach followed to derive the Transformed Eulerian Mean (TEM) formulation (Andrews and McIntyre 1976), which is described in this section.

Any zonal mean field is defined as the longitudinal average:

$$\overline{A}(\phi,z,t) \equiv \frac{1}{2\pi}\int_0^{2\pi} A(\lambda,\phi,z,t)d\lambda \tag{2}$$

and the zonal anomaly, or eddy, is then:

$$A'(\lambda,\phi,z,t) \equiv A-\overline{A} \tag{3}$$

where $\lambda$ is the longitude and $\phi$ is the latitude.

The primitive equations include momentum balance equations for the three components of the velocity field, the thermodynamic balance equation and an equation for mass continuity (Eqs. 3.1.3 in Andrews et al. 1987). It is useful to express these equations in terms of the fields decomposed into the zonal mean component plus the anomaly (Eq. 3). The interaction between the zonal mean flow and the eddies (perturbations of the mean state) is a central issue in stratospheric dynamics, as will be discussed below. If the decomposed equations are subsequently averaged zonally, the resulting expressions (Eqs. 3.3.2 in Andrews et al. 1987) contain two types of terms: zonal mean terms (e.g. $\overline{T},\overline{u},...$) and zonally

[3] More precisely, the divergence between the Eulerian zonal-mean and the zonal-mean mass transport is associated to Rossby wave breaking in the stratosphere (Matsuno 1980).

averaged products of anomalies (e.g. $\overline{v'T'}, \overline{u'v'}, \ldots$)[4]. The former terms represent the zonal mean background state of the stratosphere, and the latter are eddy fluxes that perturb this basic state.

In order to approximate the zonal-mean mass (Lagrangian) transport by the BDC using an Eulerian expression, the following definition of the *mean meridional residual circulation* on (isobaric) log-pressure coordinates is introduced (Eq. 3.5.1 of Andrews et al. 1987):

$$\overline{v}^* \equiv \overline{v} - e^{z/H}\left(e^{-z/H}\frac{\overline{v'T'}}{S}\right)_z \tag{4a}$$

$$\overline{w}^* \equiv \overline{w} + \frac{1}{a\cos\phi}\left(\cos\phi\frac{\overline{v'T'}}{S}\right)_\phi \tag{4b}$$

where $S$ is the static stability parameter, $S = H \cdot N^2/R$, a function of the squared Brunt-Väisälä frequency: $N^2 = \frac{R}{H}\left(T_z + \frac{\kappa T}{H}\right)$ and $\kappa \equiv R/c_p \approx 0.286$.

The zonal-mean residual circulation defined by these components $(0, \overline{v}^*, \overline{w}^*)$ is non-divergent, and thus it can be expressed in terms of a streamfunction. Substituting the Eulerian mean circulation $(\overline{v}, \overline{w})$ as a function of the residual circulation $(\overline{v}^*, \overline{w}^*)$ in the Eulerian-mean equations, the Transformed Eulerian Mean (TEM) set of equations is obtained (Eqs. 3.5.2 in Andrews et al. 1987, Andrews and McIntyre 1976, 1978).

In particular, the zonal momentum equation states that the perturbation of the zonal mean flow by the eddies (on the right-hand side of Eq. 5) is balanced by the meridional residual circulation $(\overline{v}^*, w^*)$ plus changes in the background flow ($\overline{u}_t$):

$$\overline{u}_t + \overline{v}^*\left[(a\cos\phi)^{-1}(\overline{u}\cos\phi)_\phi - f\right] + \overline{w}^*\overline{u}_z = (e^{-z/H}a\cos\phi)^{-1}\nabla\cdot\mathbf{F}, \tag{5}$$

[4] This is straightforward noting that $\overline{A'} = \overline{A'\overline{A}} = 0$.

where a dissipative term (e.g. friction or viscosity) has been neglected because its effects are small on large scales. In this equation, the eddy terms have been grouped into the divergence[5] of the so-called Eliassen-Palm flux (EP flux in the following), $\mathbf{F} \equiv \left(0, F^{(\phi)}, F^{(z)}\right)$, defined as (Eliassen and Palm 1961):

$$F^{(\phi)} \equiv e^{-z/H} a \cos\phi \left[ \left( \overline{u}_z \frac{\overline{v'T'}}{S} \right) - \overline{u'v'} \right], \tag{6a}$$

$$F^{(z)} \equiv e^{-z/H} a \cos\phi \left\{ \left[ f - (a\cos\phi)^{-1} (\overline{u}\cos\phi)_\phi \right] \frac{\overline{v'T'}}{S} - \overline{w'u'} \right\} \tag{6b}$$

Considering the typical magnitude of the different terms in Eq. (6) for the stratosphere, it can be shown that, in the extra-tropics, the horizontal component of the EP flux ($F^{(\phi)}$) mainly depends on the meridional eddy flux of zonal momentum ($\overline{u'v'}$), while the vertical component ($F^{(z)}$) is a function primarily of the meridional eddy heat flux ($\overline{v'T'}$) (Andrews et al. 1987). However, this approximation is not true in the tropics. Denoting the absolute vorticity as $\hat{f} \equiv f - \left(1/a\cos\phi\right)\left(\partial/\partial\phi\right)\left(\overline{u}\cos\phi\right)$ and the scaled EP flux divergence $DF \equiv (e^{-z/H} a\cos\phi)^{-1} \nabla \cdot \mathbf{F}$, and neglecting the term $\overline{w}^* \overline{u}_z$ by scaling considerations, Eq. (5) may be re-written more compactly:

$$\overline{u}_t - \hat{f}\overline{v}^* = DF \tag{7}$$

The TEM thermodynamic equation is:

$$\overline{T}_t = -\overline{v}^* \overline{T}_y - \overline{w}^* S + \overline{Q} - e^{z/H} \left[ e^{-z/H} \left( \overline{v'T'} \frac{\overline{T}_y}{S} + \overline{w'T'} \right) \right]_z \tag{8}$$

This equation gives the rate of change in temperature as a function of the mean meridional heat transport by the residual circulation, the diabatic

[5] Note that on spherical coordinates:
$\nabla \cdot \mathbf{F} \equiv (a\cos\phi)^{-1} (F^{(\phi)} \cos\phi)_\phi + (F^{(z)})_z$.

heating ($\bar{Q}$) and an eddy transport term (last term on the right-hand side). In the stratosphere $\bar{Q}$ is approximated by the radiative heating alone, since other sources of heat are negligible compared to the radiative effects (e.g. Andrews et al. 1987). Note that the quasi-geostrophic version of the thermodynamic equation is much simpler:

$$\bar{T}_t = -\bar{w}^* S + \bar{Q} \tag{9}$$

In this equation there are no explicitly included eddy terms, only those embedded in the residual circulation components. Hence, temperature transport is only due to the vertical component of the residual circulation, $\bar{w}^*$. The simplicity of Eq. (9) justifies the definition of the residual circulation given in Eqs. (4), and hence the TEM formulation in general.
Finally, the TEM mass continuity equation for the residual circulation is:

$$(a\cos\phi)^{-1}(\bar{v}^*\cos\phi)_\phi + e^{z/H}(e^{-z/H}\bar{w}^*)_z = 0 \tag{10}$$

## • Wave propagation and breaking

The eddies disturbing the mean stratospheric flow are waves generated by topography, baroclinic instabilities or heating, which propagate in the stratosphere (e.g. Holton 2005). Rossby waves are planetary to synoptic scale oscillations in the meridional plane that are mainly forced in the troposphere[6] and propagate vertically into the stratosphere (Andrews et al. 1987). Based on theoretical calculations, calculation Charney and Drazin (1961) predicted planetary Rossby waves to be dominant features of the stratospheric circulation in winter. The presence of these waves in the winter stratosphere has been confirmed later, as well as their absence during the summer season. In contrast with the inter-hemispheric asymmetry observed at high levels, in the lower stratosphere synoptic-scale Rossby waves, mainly associated with baroclinic instability, dissipate in the subtropics in both winter and summer

[6] Rossby waves exist due to the latitudinal variation on an isentrope of the potential vorticity, $PV = (\xi_\theta + f)/(-g\partial\theta/\partial dp)$, with $\xi_\theta$ the relative vorticity.

hemispheres (Held and Hoskins 1985, Shepherd 2007). In linear theory, a refractive index can be defined to determine the direction of propagation of waves in the stratosphere[7]. Waves are not able to penetrate or travel across regions where the squared refractive index is negative. Based on this index, the Charney-Drazin criterion states that waves are able to propagate vertically only if they satisfy the following condition:

$$0 < \overline{u} - c < U_c \tag{11}$$

where $U_c$ is the Rossby critical velocity, which depends on the inverse of the zonal wavenumber squared, and $c$ is the wave phase-speed. The expression (11) implies that Rossby waves can propagate upward only in westerly flows weaker than $U_c$. Given the climatology of the stratospheric background zonal wind shown in Fig. 2.1, one fundamental consequence of Eq. (11) is that propagation is only possible in the winter stratosphere (through westerlies), in agreement with the observed behavior. The criterion is more restrictive for higher wavenumbers, since they require even weaker (but still positive) winds, and this is why planetary waves (small wavenumbers) are predominant in the stratosphere, while synoptic-scale waves are observed only at the lower levels. Matsuno (1970) further explored the refractive index using a realistic background wind structure. Figure 2.5 shows the direction of wave energy propagation for a stationary wave number 1 propagating from the troposphere into the winter stratosphere derived by Matsuno (1970) for a wind structure similar to that in Fig. 2.1 (i.e., including the polar vortex and a subtropical jet). The waves propagate upward deep into the stratosphere, and they are refracted subsequently towards the equator. A shallower wave guide is

[7] The refractive index for Rossby waves can be expressed as:
$n^2 = \frac{N^2}{f^2}\left[\frac{\partial PV / \partial y}{\overline{u} - c} - \left(k^2 + l^2\right)\right] - \frac{1}{4H^2}$, with $k$ and $l$ the zonal and meridional wavenumbers, respectively; the rest of the notation is previously defined in the text.

observed as well, propagating mostly equatorward in the lower stratosphere and upper troposphere (below ~20 km). The components of the EP flux give the direction of propagation of the wave energy (Edmon et al. 1980), so the arrows in Fig. 2.5 are proportional to the EP flux vectors (Eq. 6).

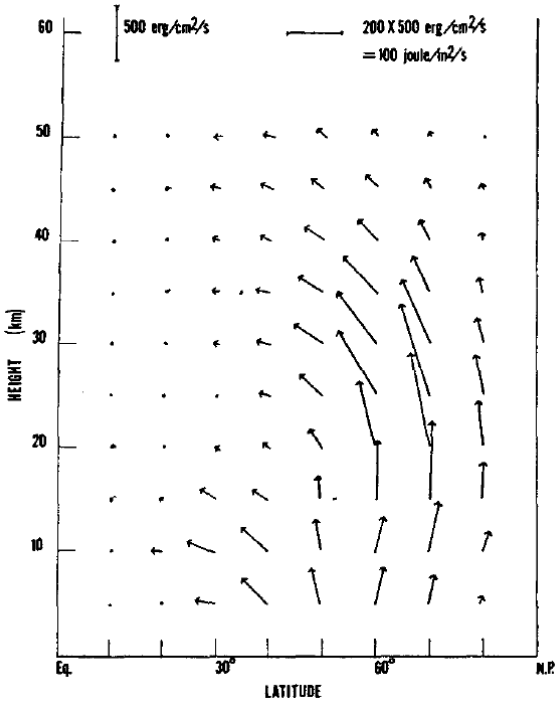


**Figure 2.5**. Energy flux for a stationary zonal wave number 1 with a realistic background zonal wind structure. From Matsuno (1970).

Dickinson (1968) pointed out the importance of the background zonal wind structure for wave propagation and breaking. Where the phase speed equals the background velocity ($c = \overline{u}$) the refractive index becomes infinite (see footnote 6 of this Chapter), and this region is denoted a *critical line* in the latitude-height plane. Note that for stationary waves the critical lines coincide with the zero wind lines. Hence, for the climatological background wind structure of the stratosphere shown in Figure 2.1, the critical lines for stationary waves are located in the subtropics. When a

wave reaches the critical line, it cannot propagate further, the amplitude becomes unstably large and it breaks, leading to wave-mean flow interactions (e.g. McIntyre and Palmer 1983). As the wave is absorbed, it transfers energy and momentum to the background flow. The momentum carried by the waves is transferred to the zonal mean flow and the subsequent dynamical changes have important implications. Since Rossby waves have westward phase speeds, they transfer westward momentum to the eastward background winds as they dissipate, hence decelerating the mean flow (Shepherd 2007). This forcing exerted by the waves (or eddies) on the mean flow is given by the divergence of the EP flux (usually in $m \cdot s^{-1} day^{-1}$).

The zonal-mean acceleration produced by wave dissipation is eventually balanced by the Coriolis force (in the stationary case, as will be discussed below), which is associated to a poleward velocity. An illustrative way to understand this dynamical mechanism is through the angular momentum conservation. The zonal mean angular momentum can be written as a contribution due to the zonal mean flow plus the rotation of the Earth (i.e., the Coriolis acceleration): $\overline{m} = a\cos\phi(\Omega a\cos\phi + \overline{u})$. The angular momentum budget is[8]:

$$\overline{m}_t + \overline{\mathbf{v}}^* \cdot \nabla \overline{m} = a\cos\phi \cdot DF \tag{12}$$

with $\overline{\mathbf{v}}^* \equiv (\overline{v}^*, \overline{w}^*)$ the meridional residual circulation vector. The angular momentum isolines are mainly vertical in the latitude-height plane outside the tropical region (see Figure 2.6). The angular momentum gradient is approximately horizontal, pointing towards the equator. In the steady case (i.e., $\overline{m}_t = 0$), Eq. (10) shows that: 1) if there is no wave drag ( $DF = 0$ ), there cannot be flow across angular momentum surfaces, and 2) if there is a wave drag ( $DF < 0$ ) outside the tropics, it must be balanced by a poleward flow ( $\overline{v}^* > 0$ ).

[8] Neglecting dissipative forces not included in the EP flux divergence.

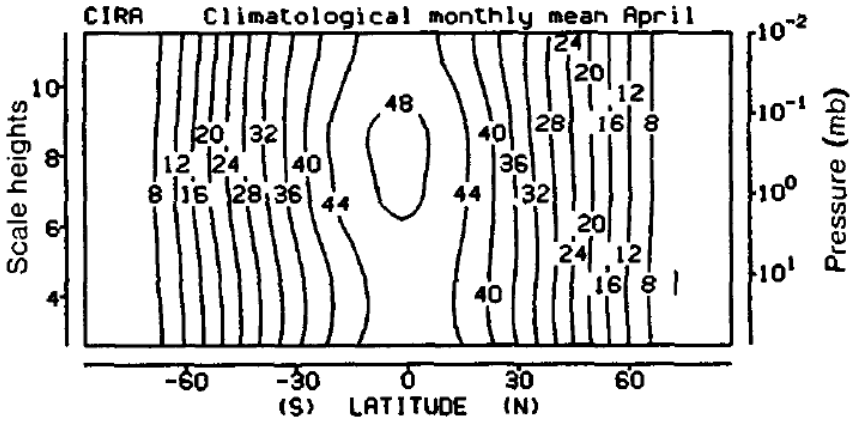


**Figure 2.6**. Zonal mean angular momentum distribution. April climatology from CIRA data (in units of $6.4\times10^{7}\,m^{2}s^{-1}$). The overall structure does not change significantly with the season. From Haynes et al. 1991.

In order to satisfy mass continuity (Eq. 10), the induced poleward flow requires upwelling on the equatorial side and downwelling on the poleward side of the wave breaking region. As illustrated in Figure 2.5, planetary Rossby waves mainly propagate vertically within a band in the middle latitudes (roughly ~45° to ~75°), such that the induced circulation leads to upwelling over the tropics and downwelling over the high latitudes. This hemispheric circulation cell constitutes the deep branch of the Brewer-Dobson circulation (Figure 2.4), mathematically approximated by the mean meridional residual circulation (Eqs. 4) in the TEM framework. Hence, the above demonstrates the dynamical origin of the BDC. Note that, as well as driving the mean meridional circulation (which in turn advects the tracers) the breaking of planetary Rossby waves in the winter middle latitudes has another important effect on tracer transport. The connection between wave breaking, meridional mixing and the mean-meridional circulation was shown by Garcia (1991) based on simple theoretical arguments. In particular, it leads to deformation of the zonal flow and development of large-scale tongues, which produce stirring and ultimately mixing of air masses, as seen in Figures 2.3 and 2.4.

The fact that Rossby waves can only propagate (and thus eventually break) in westerly winds has important implications for the BDC circulation. Figure 2.7 shows the climatology for boreal winter and summer of the EP flux (arrows) and its divergence (shading).

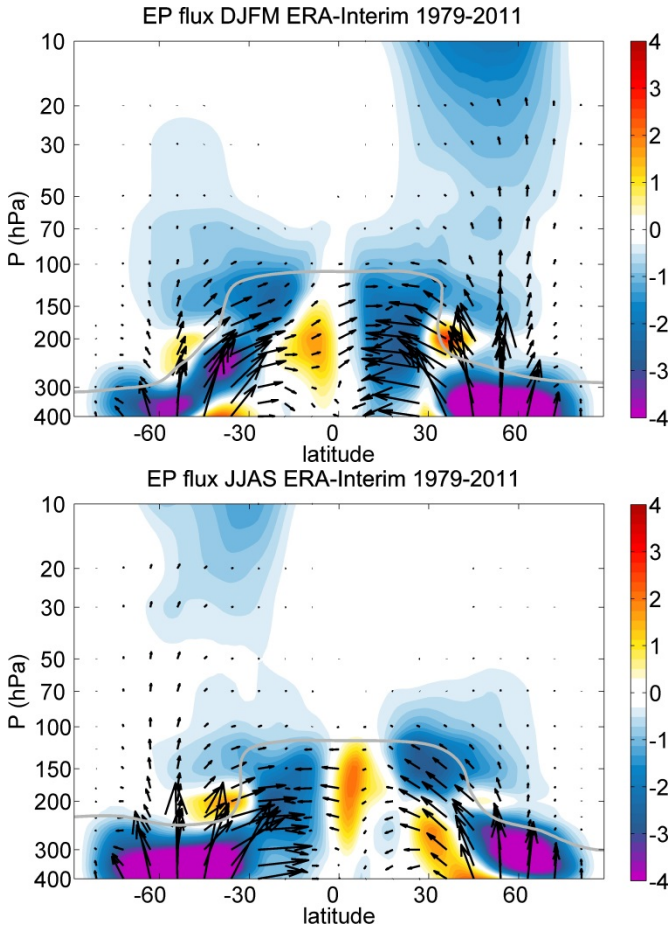


**Figure 2.7**. EP flux (arrows) and scaled divergence (shading, in $mm \cdot s^{-1} day^{-1}$) for DJFM (top) and JJAS (bottom) climatology. Computed from ERA-Interim reanalysis daily mean data for 1979-2011.

Deep propagation and wave drag is observed in the extratropical winter stratosphere, mainly associated with planetary Rossby waves, while the summer hemisphere remains quiescent. It also stands out from Figure 2.7 the stronger boreal winter (top panel) wave activity as compared to the

austral winter (bottom panel). This inter-hemispheric asymmetry is explained to first order by greater planetary wave emission from the troposphere due to larger ocean-land contrast and topography in the northern hemisphere (NH). In addition (and not unrelated), the NH polar vortex is weaker than the SH counterpart (see Fig. 2.1), such that the Charney-Drazin criterion (Eq. 11) is more easily satisfied in the NH. The stronger wave drag in boreal winter produces more intense BDC in the NH than in the SH winter season.

Further details can be appreciated in Fig. 2.7, such as the subtropical wave drag in both hemispheres, associated with equatorward planetary wave propagation on the winter side of the equator (as in Fig. 2.5), and synoptic-scale waves associated with baroclinic instabilities on both hemispheres[9]. Also, there are positive values of $DF$ in the upper troposphere deep tropics, corresponding to generation of equatorial waves forced by convection. In addition to the planetary Rossby waves, there are several types of waves in the stratosphere, which can be classified based on their restoring mechanisms. While Rossby waves are maintained by the latitudinal dependence of the potential vorticity gradient, gravity waves are mainly forced by buoyancy or stratification and inertia-gravity waves, due to the combined effect of stability and the Coriolis acceleration (Andrews et al. 1987). It is important to keep in mind that not all waves can be resolved in climate models due to the limited spatial extension of the model grid, and physical parameterizations are included to simulate their effects on the stratospheric circulation. Although the planetary Rossby waves dominate the overall variability of the stratosphere, other waves can have important roles in driving the stratospheric circulation, as has been shown in particular for tropical upwelling, as will be discussed in the next Section.

[9] This result is based on spectral wavenumber decomposition of the EP flux and its divergence, result not shown.

# 2 Tropical upwelling

Figures 2.1-2.3 highlight the relevance of the upwelling branch of the BDC as a vehicle for tropospheric air masses to enter the stratosphere. Upwelling across the TTL and in the lower stratosphere is particularly interesting because 1) it involves large mass fluxes (relative to the stratospheric mass) due to the decrease in density with height and 2) the TTL provides the chemical and physical boundary conditions for the entire stratosphere. This Section describes tropical upwelling to the present state of knowledge, including the main spatial and temporal characteristics (Section 2a) and the dynamical drivers (Section 2b)).

## a. *Mean structure and variability*

### • Upwelling estimates

There are no direct measures of tropical upwelling. In the literature, the intensity of this vertical velocity has been estimated indirectly using different methodologies, three of which are used in the present Thesis and will be described in detail in the Chapter *Methodology*. A different way to deduce upwelling is through the ascent rates of trace gases exhibiting "tape recorder" signals. Mote et al. (1996) first used this term[10] to refer to the observed behavior in water vapor concentrations in the tropical lower stratosphere (as derived from satellite measurements). Seasonal variations in tropical mean water vapor near the tropopause are transported upward by the slow but continuous ascent in the tropical lower stratosphere, producing a pattern reminding of a tape recorder in a time-altitude section (Figure 2.8). Such changes in stratospheric water vapor entry values are due to seasonality in temperature and dehydration processes near the cold point tropopause (e.g. Figs. 2.1 and 2.2). Similar behavior has been found in other species with seasonally-dependent entry concentrations at tropopause level (due to annual changes in tropospheric chemical sources),

[10] M. E. McIntyre invented this term, which was first used in the literature in this article.

such as $CO_2$ (Andrews et al. 1999), CO (Schoeberl et al. 2006) and HCN (Pumphrey et al. 2008).

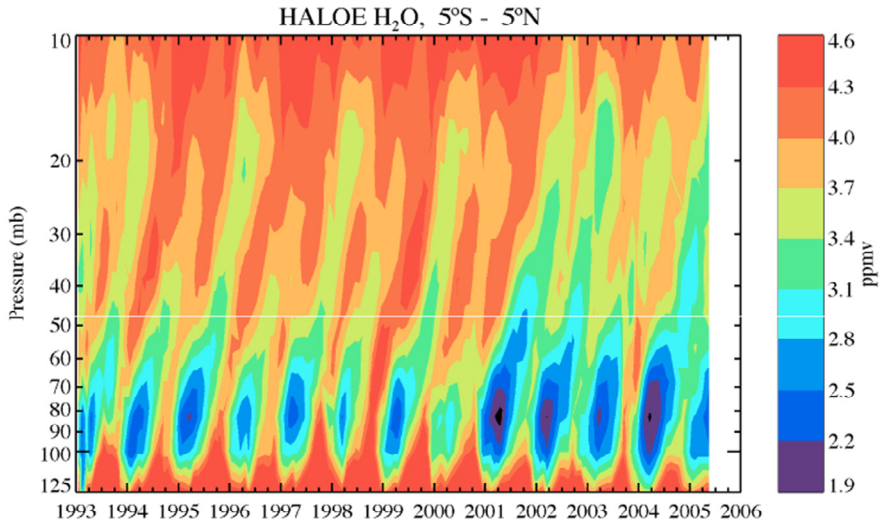


**Figure 2.8**. The "tape recorder" signal in $H_2O$ vapor from HALOE[11] observations (in $ppmv$). Equatorial water vapor concentrations, lower in boreal winter than summer, propagate upward with upwelling. From Rosenlof (2009).

This propagating signal can be used to derive the mean vertical velocity, in particular using the phase lag between different levels (Niwano et al. 2003; Flury et al. 2013). Figure 2.9 shows the results as a function of altitude of this methodology applied to different datasets, including various satellite measurements of $H_2O$ (Schoeberl et al. 2008a). The estimates agree reasonably, showing values smaller than 0.5 $mm \cdot s^{-1}$ everywhere below ~26 km and minimizing around ~20 km. These values agree with the previous estimates by Rosenlof (1995) based on the TEM equations.

Yang et al. (2008) used an accurate radiative transfer scheme, with input of tracer and cloud vertical profiles from observations, to compute radiative heating rates and estimate upwelling from them using a

[11] HAlogen Occultation Experiment.

simplified thermodynamic equation. Their results show an overall similar vertical structure of upwelling as that shown in Figure 2.9. Furthermore, Yang et al. (2010) evaluated the net effect of the clouds on the tropical mean radiative heating rates in the lower stratosphere, and found a relatively small cooling effect (~0.1 $K \cdot day^{-1}$).

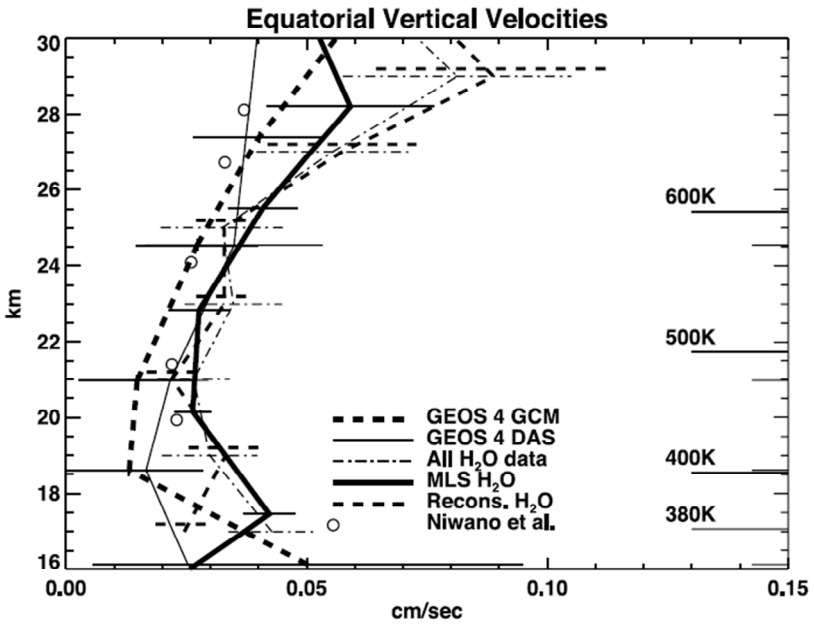


**Figure 2.9**. Estimates of annual mean vertical velocity at the equator from two versions of the GEOS[12] model and from different satellite measurement of $H_2O$ (in $cm \cdot s^{-1}$). From Schoeberl et al. (2008a).

While there is reasonable agreement among different estimates and datasets in the overall annual mean vertical structure of tropical mean upwelling, there is more uncertainty regarding the latitudinal structure. Trace gas and temperature observations suggest a double peak in the annual mean strength of upwelling on both sides of the equator, and weaker ascents over the equator itself. State-of-the-art chemistry-climate models capture this feature, despite the wide spread among models in the

[12] Goddard Earth Observing System.

overall latitudinal structure of upwelling (Butchart et al. 2006). Tracer observations also show a latitudinal seasonal displacement towards the summer pole, suggesting a similar swing of the upwelling region, which has been also found in different estimates (Eluskiewicz et al. 1996, Randel et al. 1998). Figure 2.10 shows the latitude-month climatology of upwelling from the ERA-Interim reanalysis (described in the Data chapter). Both described features are observed in this figure: minimum upwelling at the equator and annual latitudinal displacement. Nevertheless, Fig. 2.10 should not be interpreted as an accurate or realistic upwelling measure, as particular details in the structure can be radically different in other estimates and datasets.

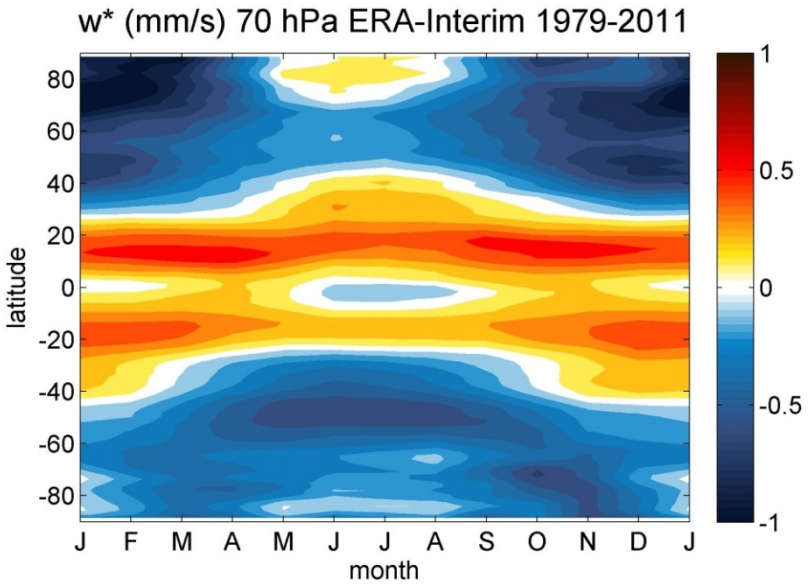


**Figure 2.10**. Vertical component of the residual circulation (Eq. 4b) as a function of latitude and month at 70 hPa computed from ERA-Interim reanalysis daily data.

## • Temporal variability

As follows from the previous Section of this Chapter, quantifying fluctuations in the intensity of upwelling is essential for understanding

changes in tracer concentrations and temperature in the tropical lower stratosphere.

One well-known and important feature of upwelling in the tropical lower stratosphere is the large annual cycle, with tropical mean upwelling in boreal winter (approximately December through March) roughly two times stronger than in summer (June through September). Figure 2.11 shows the seasonality for different upwelling estimates (and two different reanalyses) obtained by Randel et al. (2008).

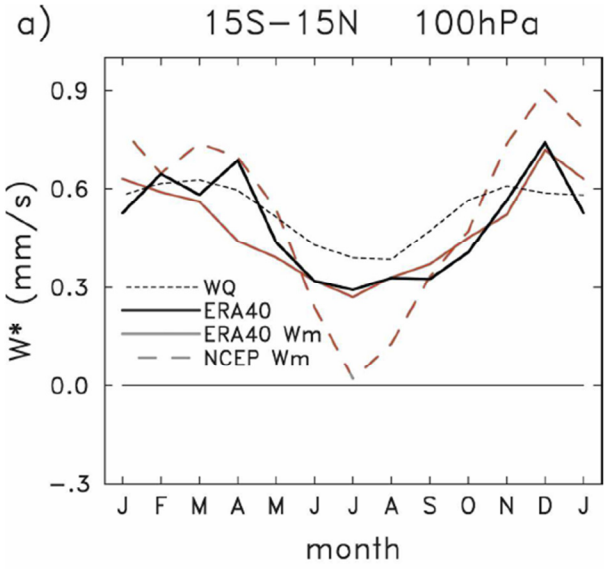


**Figure 2.11**. Mean annual cycle of different estimates of tropical upwelling at 100 hPa averaged over 15°S-15°N (in $mm \cdot s^{-1}$). Upwelling is derived from thermodynamic balance (WQ), from momentum balance (Wm, using ERA-40 and NCEP reanalyses) and computed directly from ERA-40. From Randel et al. (2008).

As a first approximation, the seasonality in upwelling can be thought as resulting from the stronger wave activity in boreal winter as compared to austral counterpart (see end of Section 1c). However, it has been found that this simplified view is not exact, and many other dynamical processes are involved, and the details will be described in the next Section.

The annual cycle in upwelling drives a large annual cycle in temperature just above the tropical tropopause (e.g. Yulaeva et al. 1994). Stronger upwelling of cold air masses from the tropical tropopause in winter as compared to summer leads to the observed seasonality in temperature. As evidenced in Figure 2.12, this seasonality involves around ~6-8 K peak-to-peak annual variations in tropical temperatures, dominating the variability. Furthermore, the annual cycle is localized over a very narrow layer just above the cold point tropopause, while the rest of the tropics shows no annual oscillation (Reed and Vicek 1969, Randel et al. 2007, Fueglistaler et al. 2009a).

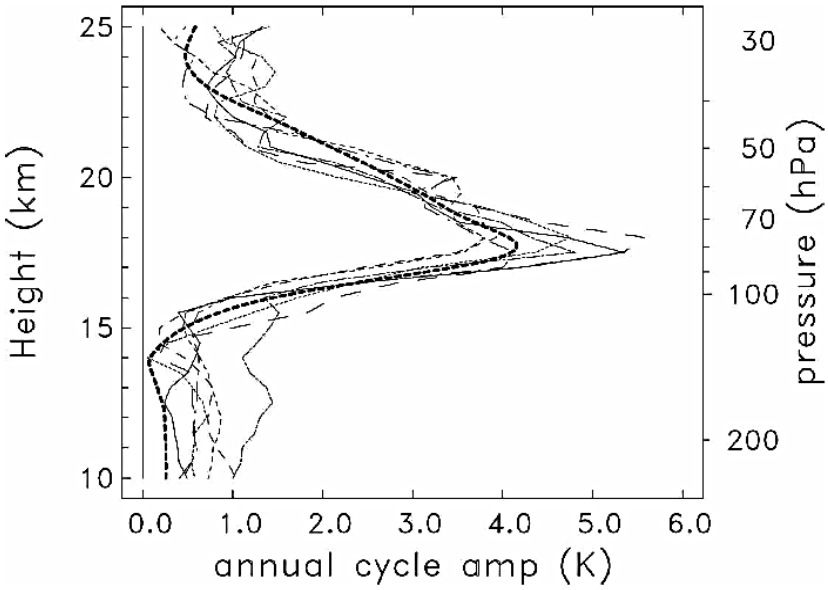


**Figure 2.12**. Tropical temperature annual cycle amplitude as a function of height. Thin lines are radiosonde measurements at different tropical stations and thick dashed line shows GPS tropical mean. From Randel et al. (2007).

It is not obvious why the temperature annual cycle shows the vertical structure in Fig. 2.12, since the seasonality in tropical upwelling is not limited to the range of altitudes of peak amplitude, but is present throughout the stratosphere. Randel et al. (2002) proposed an explanation

for this behavior based on the long radiative timescales in this region. The response in temperature due to changes in upwelling can be reduced to the expression:

$$\frac{T_\sigma}{w_\sigma} = \frac{S}{\sqrt{\alpha^2 + \sigma^2}} \tag{13}$$

where $\sigma$ is the timescale of the fluctuation, e.g. for the annual cycle $\sigma = 2\pi / 365\ day^{-1}$ and $\alpha$ is the radiative damping timescale. Eq. (13) shows that the magnitude of the response is amplified for longer radiative relaxation timescales. Figure 2.13 shows that the vertical structure in temperature seasonality is consistent with the very long radiative timescales (~2-3 months) that are found in this region, as estimated from different methods.

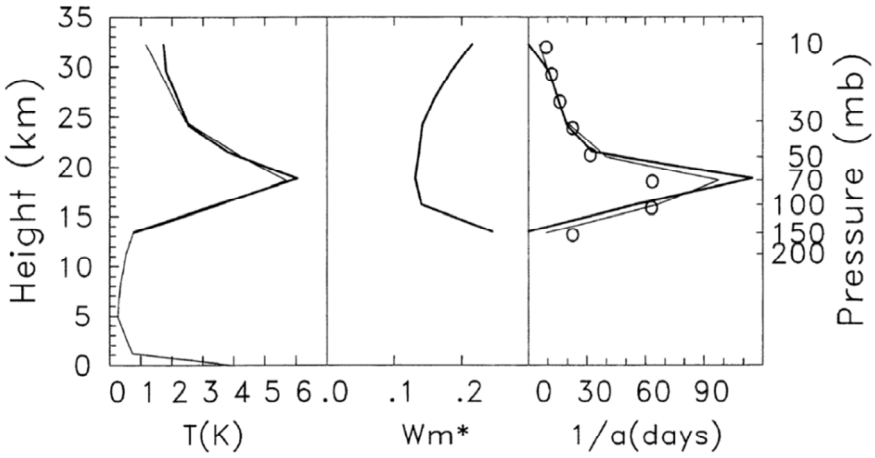


**Figure 2.13**. Vertical structure of the amplitude of the annual cycle in tropical mean temperature (left), upwelling (center) and vertical structure of the radiative relaxation timescale (right). From Randel et al. (2002).

Recent analyses have shown that ozone radiative feedbacks further enhance the amplitude of the temperature annual cycle (Chae and Sherwood 2007, Fueglistaler et al. 2011). Radiative heating rates in the stratosphere can in general be well approximated by a relaxation expression (i.e. Newtonian cooling):

$$\bar{Q} \approx -\alpha(T - T_{eq}) \ , \tag{14}$$

with $\alpha$ an inverse radiative timescale and $T_{eq}$ the equilibrium temperature. From this perspective, ozone concentrations influence temperature seasonality by changing $T_{eq}$, which is a function of the concentration of trace gases (and solar radiation).

In addition to the annual cycle, interannual changes in tropical lower stratospheric temperatures have been linked to climatological fluctuations in upwelling. Temperature in the tropical lower stratosphere is influenced by inter-annual variability such as El Niño-Southern Oscillation (ENSO), the quasi-biennial oscillation (QBO) and large volcanic eruptions (e.g. Calvo et al. 2004, Randel et al. 2009, Calvo et al 2010). It has been shown that ENSO-related changes in temperature can be associated with fluctuations induced in upwelling (Randel et al. 2009, Calvo et al. 2010). Long-term trends in upwelling due to increase in GHG emissions have also been found in model studies, leading to faster ascents and cooler tropical lower stratosphere (e.g. CCMVal 2010, Chapter 4). Despite its consistency across the different models (see Figure 2.13), this result has not been unequivocally confirmed by observations (Engel et al. 2009, Ray et al. 2010, Stiller et al. 2012). More specifically, these observational works do not refer directly to tropical upwelling, but to measurements of stratospheric *age of air*, a transport diagnostic which accounts for both advection and mixing (Waugh and Hall 2002). This quantity can be approximately estimated from measurements of quasi-passive tracers with near-constant growth.

On the other hand, Garcia et al. (2011) argue that the large uncertainties and sparseness of the available measurements used to infer transport strength does not allow accurately determining the trends from observations. In addition, in this work it is proven that relevant differences need to be taken into account when computing age of air from tracers with non-linearly increasing sources.

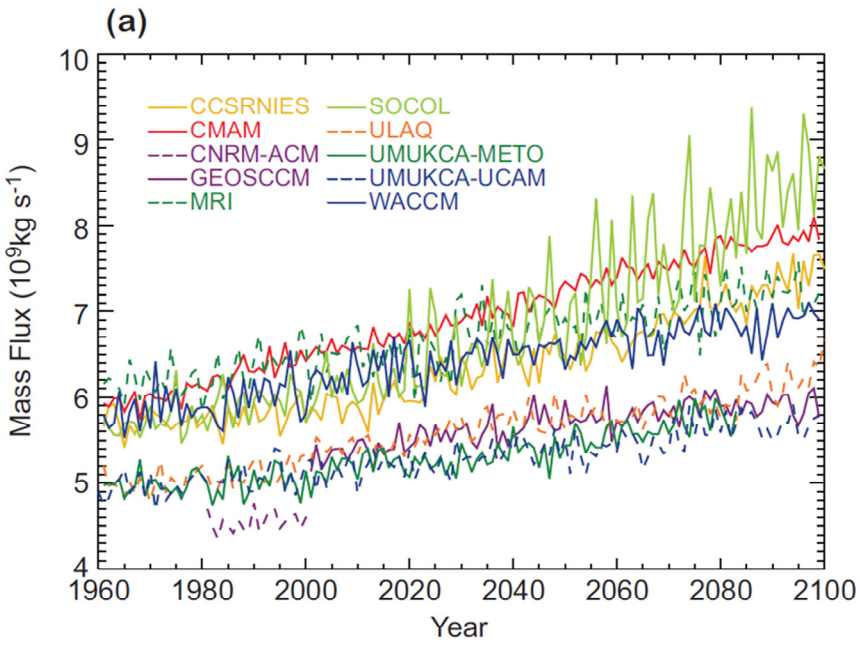


**Figure 2.14**. Timeseries for the REF-B2 scenario of the annual mean upward mass flux at 70 hPa. From CCMVal Report (2010), Chapter 4.

Transient fluctuations in upwelling have been observed during *sudden stratospheric warming* events (i.e. the abrupt breakdown of the polar vortex in midwinter prompted by bursts of planetary wave activity injected in the extratropical stratosphere, e.g. Andrews et al. 1987). These events involve intense polar warming associated with the rapid wind decrease, and some works have shown evidence of corresponding cooling of the tropical lower stratosphere (e.g. Yoshida and Yamazaki 2011). Apart from these dramatic events, upwelling variability on timescales shorter than the annual cycle has received little attention. Randel et al. (2002) showed that temperatures near the tropical tropopause reflect fluctuations in winter extratropical wave activity. This Thesis partly focuses on upwelling sub-seasonal fluctuations, and some novel results are obtained on this topic.

## b. *Dynamical drivers of upwelling*

The general dynamical mechanism driving the BDC was described in Section 1c of the Introduction. Here, the specific dynamical forcings of tropical upwelling are presented in more detail, emphasizing the currently open questions. Theoretical aspects are followed by a revision of the state-of-the-art from both observational and model studies.

### • Theoretical aspects

In Section 1c it was shown that planetary wave breaking leads to wave drag in the winter middle latitudes, which in turn induces poleward mass flux. Such meridional transport occurs across angular momentum isolines (see Figure 2.6), and thus is only allowed at the location of the forcing (in the stationary case, see Eq. 12 and related discussion). Consequently, the vertical motions induced by continuity are also limited to the edges of the forcing region. Haynes et al. (1991) referred to this constraint as the "downward control" principle, by which vertical velocity at a given latitude and height is determined exclusively by the stationary wave drag at that same latitude at that level and above.

Note that angular momentum meridional gradient becomes small (or null) in the tropics in Fig. 2.6. Thus, the wave forcing cannot drive a meridional circulation, and must rather change the zonal mean flow (see Eq. 12). Consequently, at such low latitudes the primary response to a wave drag is an acceleration of the zonal flow and not vertical motion (i.e., nonlinear interactions between wave forcing and zonal flow are relevant). Hence, the "downward control" principle does not apply near the tropics (Holton et al. 1995, Plumb and Eluskiewicz 1999, Haynes 2005).

In the extratropics, the "downward control" holds only in the particular case in which the wave forcing is stationary. In every other case, the force exerts a nonlocal control of the circulation (Holton 1995). For a time-dependent forcing the induced circulation extends further in latitude, such that extratropical wave drag can drive upwelling in the tropics through nonlocal effects (Dickinson et al. 1968, Garcia 1987, Haynes et al.

1991). The remote connection between high and low latitudes results from the coupled response of the atmospheric zonal wind, temperature and meridional circulation to a transient wave drag (e.g. Garcia 1987).

The meridional circulation induced by an extra-tropical wave drag is strongly dependent on the timescale of the forcing ($\sigma$) in relation to the radiative relaxation timescale ($\alpha$) (Haynes et al. 1991, Holton 1995, Haynes 2005). The spatial structure of the response can be expressed in terms of the ratio $\sigma / \alpha$. Figure 2.15 illustrates the spatial structure of the circulation response to a localized westward force as a function of the timescales involved (original figure from Haynes et al. 1991, reproduced by Holton et al. 1995). The "downward control" situation is shown in Fig. 2.15c, corresponding to the steady state ($\sigma / \alpha \to 0$). The induced circulation is limited to the latitudinal extent of the forcing. In contrast, Fig. 2.15a shows the transient or adiabatic case ($\sigma / \alpha \to \infty$), where the thermal relaxation is negligible compared to the timescale of the forcing (i.e. adiabatic case, described by Eliassen 1951 and Plumb 1982). In this case the circulation is able to extend laterally out of the forcing region, and the ratio between the vertical and latitudinal extension of the induced circulation is smaller in Fig. 2.15a than in the stationary case. The transition between these two regimes takes place at different timescales on different regions of the atmosphere. In the tropics, very slow timescales are necessary to reach the stationary case such that, in practice, "downward control" is not relevant in this region. This last statement is in agreement with the argument based on the vanishing meridional gradients in angular momentum exposed above. The case in which the forcing has an annual cycle is represented in Fig. 2.15b, considering $\alpha = (20 days)^{-1}$ (hence $\sigma / \alpha \approx 0.34$). It shows an intermediate situation, where the induced circulation presents deeper vertical extension compared than in the adiabatic case, and upwelling extends across the tropics.

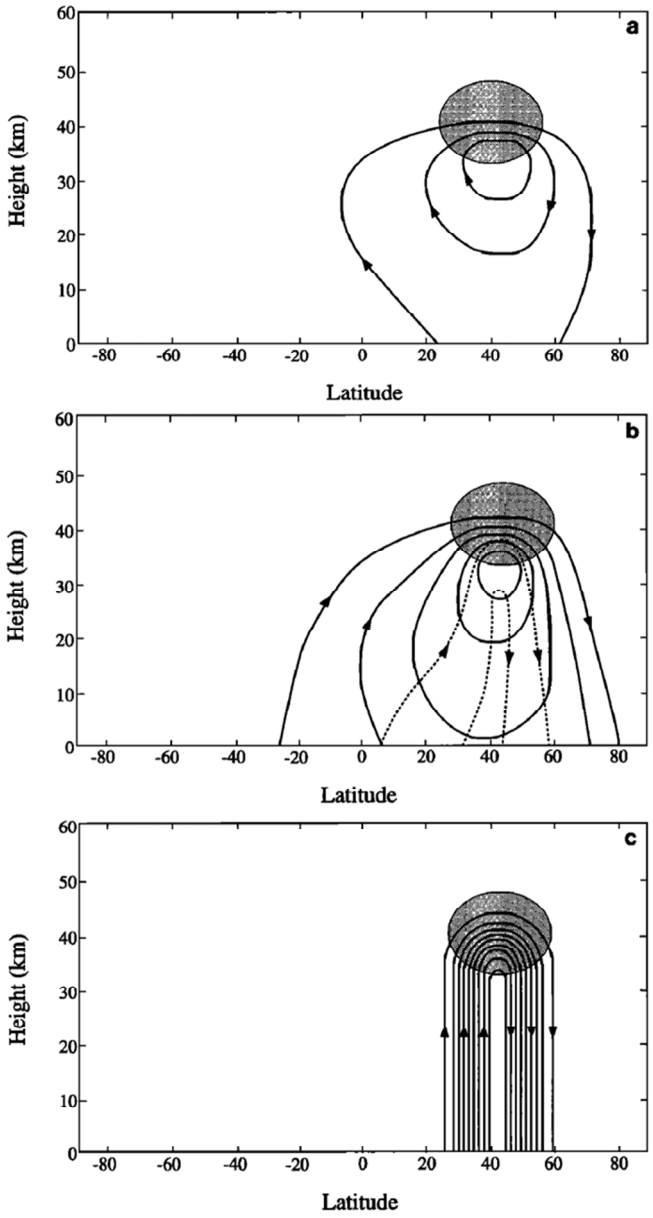


**Figure 2.15**. Numerical idealized experiment of the circulation response to a westward wave drag applied in the shaded region. a) Adiabatic transient case, b) annual cycle (dashed contours show the response) c) stationary case. From Holton et al. (1995).

Holton et al. (1995) observed that wave drag should be located in the subtropics in order to effectively drive upwelling in the tropics. Plumb and Eluskiewicz (1999) further explored the dynamics of upwelling using a numerical linear model, and concluded that seasonally-dependent planetary wave breaking in the extratropics in both hemispheres could not account for maintained annual-mean tropical upwelling. In order to produce a reasonable annual mean rate of upwelling distributed across the tropics they had to place the wave drag within 20° of the equator. In addition, they found that viscosity was needed in the model to obtain a qualitatively realistic latitudinal distribution (i.e., with upwelling displaced towards the summer hemisphere). Semeniuk and Shepherd (2001) showed that subtropical wave drag drive upwelling through nonlinear mechanisms, and no viscosity is required when nonlinearity is included. However, the annual mean upwelling obtained for a realistic amount of forcing situated near 15° latitude was too weak compared to the ascent rates deduced from observations. The role of the stratospheric Hadley circulation has been discussed in several works, and the results suggest that such radiation-driven circulation is important for explaining the latitudinal distribution of upwelling in the upper stratosphere, but its influence does not extend to the lower stratosphere (Dunkerton 1989, Semeniuk and Shepherd 2001, Zhou et al. 2006). The open questions highlighted by these studies call for further research on the dynamical sources of variability in upwelling.

- ## Observational and climate model results

As briefly mentioned in the previous Section 2a, the enhanced wave activity in boreal (as compared to austral) winter does not entirely explain the annual cycle in tropical upwelling. A number of model and observational studies have focused in the last decade in understanding which waves are mainly responsible for the large annual cycle observed in upwelling, which in turn mainly drives the tropical lower stratosphere temperature seasonality (e.g. Yulaeva et al. 1994, Bohem and Lee 2003,

Kerr-Munslow and Norton 2006, Norton 2006, Randel et al. 2008, Ueyama and Wallace 2010). However, the causality chain is particularly difficult to disentangle for the annual cycle, as most of the atmospheric processes exhibit similar seasonal variations. Different studies have emphasized the role of different regions of forcing and types of waves influencing upwelling seasonality.

There are empirical evidences of a connection between the temperatures of the tropical and extratropical lower stratosphere (Yulaeva et al. 1994, Fueglistaler et al. 2011). Based on these coherent fluctuations, some works have proposed a primary role of the extratropical planetary waves on annual temperature variations in the tropics, out of phase with those in the extratropics (Yulaeva et al. 1994, Ueyama and Wallace 2010). However, as argued above, the forcing needs to reach closer to the tropics in order to drive realistic upwelling (Plumb and Eluskiewicz 1999). Ueyama et al. (2013) recently suggested that the influence of the extratropical wave drag on upwelling can be reduced to a downward control situation, taking account of the latitudinal progression of the extratropical wave drag towards the tropics on timescales of ~10 days.

On the other hand, several works have pointed out the crucial role of planetary equatorial waves forced by convection in shaping the seasonality in upwelling around the tropical tropopause (Bohem and Lee 2003, Kerr-Munslow and Norton 2006, Randel et al. 2008, Ryu and Lee 2010, Ortland and Alexander, 2013). Randel et al. (2008) highlighted the primary role of the seasonally-dependent horizontal momentum flux convergence in the subtropics for upwelling seasonality. Such seasonality results from the enhanced equatorward propagation in the subtropics of extratropical waves combined with poleward propagation of equatorial planetary waves during winter in each hemisphere (see Figure 2.7).

The importance of wave drag in the subtropics for upwelling has also been evidenced in relation with the long-term trends in upwelling predicted by models (Butchart et al. 2006, Garcia and Randel 2008, Calvo and Garcia 2009, Garny et al. 2011, Shepherd and McLandress 2011). These model studies show that the mechanism for the predicted increase

in upwelling is mainly a change in the dynamical background structure due to increased GHG emissions. Cooling of the stratosphere and warming of the troposphere lead to increased meridional gradients across the tropopause in the subtropics. Garcia and Randel (2008) and Shepherd and McLandress (2011) argued that thermal wind balance implies an associated strengthening of the upward flank of the subtropical jets, shifting the critical lines to higher levels and thus allowing waves to penetrate further up in the subtropics. Figure 2.16 from that work shows the dynamical changes due to increased GHG emissions: there is enhanced equatorward wave propagation (EP flux) in the subtropics associated with stronger winds in the subtropical lower stratosphere (i.e., higher critical lines).

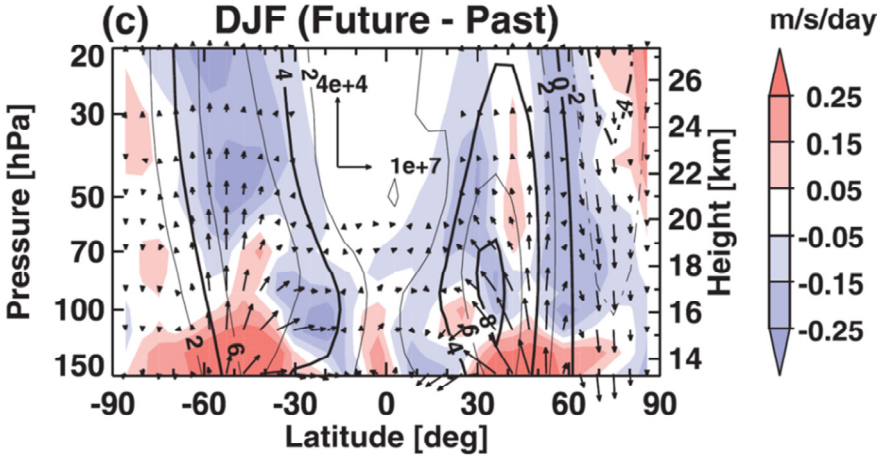


**Figure 2.16**. Difference future minus past of EP flux (arrows), EP flux divergence (shading, in $m \cdot s^{-1} day^{-1}$) and zonal mean winds (contours, in $m \cdot s^{-1}$) for boreal winter. From Shepherd and McLandress (2011).

Recently, Zhou et al. (2012) emphasized the importance of including transient variability for determining the specific wave forcing latitudes relevant for upwelling. Using high-vertical resolution GPS temperature measurements, Grise and Thompson (2013) analyzed the role of four different forcing regions in driving transient variability in upwelling (tropics, extratropics stratosphere, subtropical stratosphere and

subtropical tropopsphere). They found that planetary waves in the extratropical and subtropical stratosphere mainly drive transient upwelling in the lower stratosphere (above ~70 hPa), while equatorial planetary waves and drag in the subtropical troposphere are important for upwelling around the tropopause.

The different dynamical forcing associated with the deep and shallow branches of the BDC (see Figure 2.3), has been highlighted in several works (Garny et al. 2011, Bönish et al. 2011, Chen and Sun 2011, Gerber 2012). The picture arises that upwelling close to the tropopause (e.g. ~100-70 hPa) is mostly related to the variability in the shallow branch of the circulation, associated with wave drag in the subtropics and tropics, while at higher levels (e.g. above 70 hPa) the deep branch is driven mostly by wave activity in the extratropical stratosphere. However, these differences are yet not well established. Overall, more studies are required to understand the specific forcing of upwelling at different levels and on a range of timescales.

# 3 Transport in the tropical lower stratosphere

In Section 1 of this chapter, the general characteristics of the stratospheric circulation have been presented, in close relation with the global thermal structure and tracer distribution. Section 2 has focused on tropical upwelling, describing the main known features and the issues that are currently under debate or poorly understood. The present Section 3 is dedicated to tracer transport in the region near and above the tropical tropopause. To start, Section 3a briefly describes this region of interest. Sections 3b and 3c present an overview of the current state of-the-art regarding tracer transport processes in this region. Section 3d establishes the starting point for the analyses included in this Thesis, in connection with the state-of-the-art presented in this Section.

## a. *The tropical tropopause layer*

The UTLS transition region in the tropics, denoted Tropical Tropopause Layer (TTL), is particularly interesting for several reasons, as briefly outlined in the Motivation and further detailed below. Figure 2.17 shows a schematic of clouds, transport and dynamical processes in the TTL, from Fueglistaler et al. (2009a).

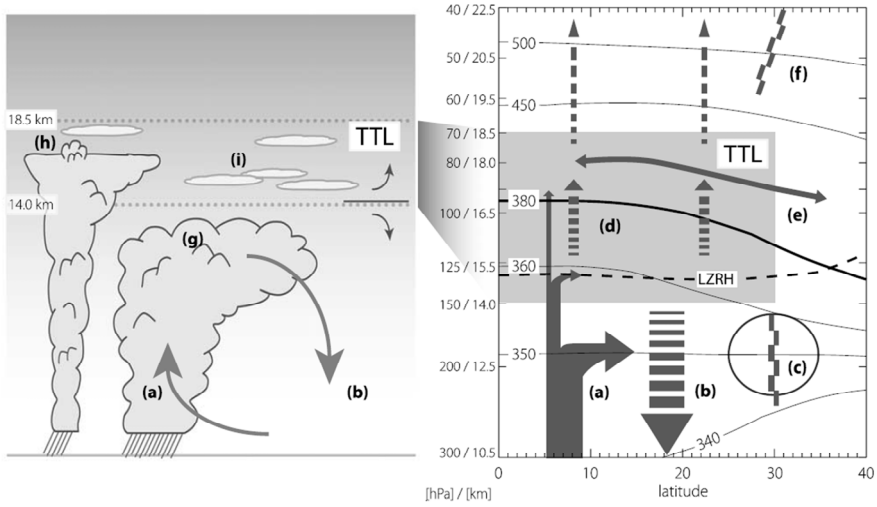


**Figure 2.17**. Schematic of the TTL cloud processes (left panel) and zonal mean transport processes (right). Most relevant features include: deep convection and main outflow below the TTL, with rare penetrations above the tropopause leading to fast transport of tracers from the boundary layer into the TTL (letter a). Radiative cooling by subsidence in clear-sky regions (letter b). Subtropical jets constituting barriers for tropics and the extra-tropics and troposphere-stratosphere quasi-isentropic transport (letter c). Radiative heating above the level of zero radiative heating (indicated as LZRH) driving ascent (letter d). Rapid meridional transport and mixing (letter). Tropical reservoir in the lower stratosphere, i.e., partial isolation of the tropics from the extratropics, characterized by large stirring (letter f). Isolines in the right panel indicate isentropes (in K). For further details refer to the original Figure 2.in Fueglistaler et al. 2009a.

Deep convection is frequent in the tropics, with convective could tops typically reaching ~12 km altitude. Some of these convective clouds overshoot the tropopause, rapidly transporting air masses from near the surface into the TTL in timescales of hours. In addition to strong convective clouds, which cover approximately ~10% of the tropics, high thin cirrus clouds are widespread in the TTL; they strongly impact radiation balances and are relevant for stratospheric water vapor concentrations (e.g. Randel and Jensen 2013). Outside the clouds, the air is subsiding and radiatively cooling below the level of zero radiative heating, denoted LZRH in Fig. 2.17.

Above that level, slow upwelling and radiative heating is observed under all sky conditions.

The radiative balance of the TTL is mainly between cooling by water vapor (strongly decreasing with height) and warming by ozone and $CO_2$ (Thuburn and Craig 2000, Gettelman et al. 2004, Fueglistaler et al. 2009a). The radiative forcing by clouds is a relatively small term in the TTL balance (Gettelman et al. 2004). Yang et al. (2010) accurately estimated the net cloud radiative forcing from observations, and obtained a change in sign near 100 hPa, with heating below (reaching ~+0.3 K/day near 200 hPa) and relatively small cooling above (~-0.1 K/day). It is important to keep in mind that, although the overall thermal structure of the TTL is captured by chemistry-climate models, there are large uncertainties in the TTL heating rates (Fueglistaler et al. 2009b, Randel and Jensen 2013). This could be linked to parameterizations of unresolved processes (such as convection, cloud microphysics or small-scale waves), which both depend on and affect temperature structure and water vapor concentrations.

A key variable strongly linking radiation, dynamics, convection and chemical reactions in the TTL is the temperature (Fueglistaler et al. 2009a). In the zonal mean stratospheric temperature structure (Fig. 2.1) the extremely cold temperatures in this region are an outstanding feature. The 380 K isentrope, highlighted in Fig. 2.17, indicates the approximate altitude of the annual mean cold point tropopause (~100 hPa, ~16.5 km). As shown in Figure 2.18, there is a large spread (~5-10 K) among different models in the exact value of coldest temperatures (Gettelman et al. 2010, CCMVal 2010, Chapter 7, Randel and Jensen 2013). Upwelling transports air masses across and out of this region into the stratosphere, constituting the main pathway to enter the stratosphere. Hence, the thermal and chemical characteristics of the TTL strongly influence those of the stratosphere, and it is thus crucial to understand the physical and chemical processes determining the TTL structure.

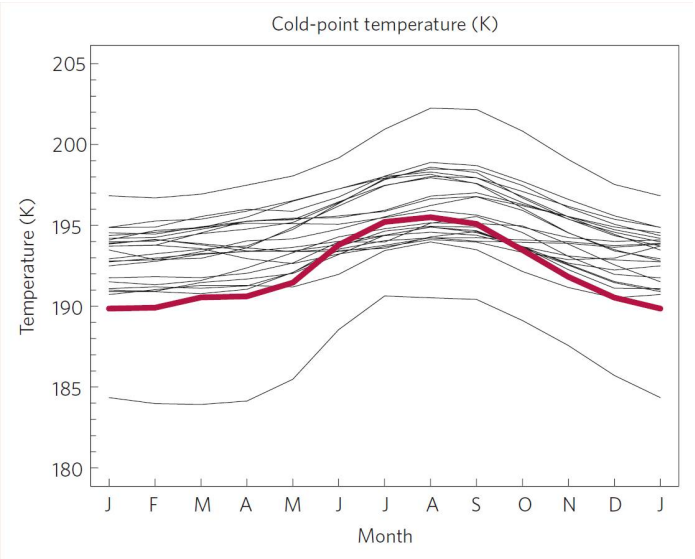


**Figure 2.18**. Annual cycle of the temperature at the cold-point tropopause from the latest generation of chemistry-climate models (CMIP-5), in black, and from GPS observations, in red. From Randel and Jensen (2013).

The lower boundary of the TTL is usually located above the level of maximum convective outflow (i.e., ~14 km, ~150 hPa, 355 K), and the upper limit at ~70hPa (~18.5 km, ~420 K). In the lower part of the TTL, cloud processes dominate transport, in particular rapid ascents by convection and convective detrainment. If cloud tops overshoot the LZRH, the detrained air will not subside but remain in the TTL, with high probability of affecting stratospheric composition. Observations have shown direct injection of high water vapor concentrations into the stratosphere by convective overshooting (e.g. Corti et al. 2008). However, the global-scale contribution of this transport process as opposed to dehydration during slow ascent through the cold point is not well understood (Randel and Jensen 2013).

The region of interest for the present Thesis is the upper part of the TTL, above the cold point tropopause (i.e., the “stratospheric part” of the TTL), extending into the lower tropical stratosphere (i.e., roughly the layer between ~100-50 hPa, or ~16-20 km). In this Thesis, the region including

the upper part of the TTL and tropical lower stratosphere will be in general referred to simply as the tropical lower stratosphere.

As highlighted in Fig. 2.17, the main transport processes in tropical lower stratosphere affecting tracer concentrations are 1) upwelling throughout the tropics, across the whole depth of the TTL and above, and 2) quasi-horizontal transport and mixing across the tropical boundaries near the cold point tropopause. However, the relative roles of these two different mechanisms of transport on tracer distribution and variability in the tropical lower stratosphere are not fully understood, and there is growing interest in quantifying these processes.

In the following sections the effect of these two transport processes (vertical and quasi-horizontal) on tracer concentrations in the tropical lower stratosphere is reviewed.

## b. *Transport by upwelling*

- ### Vertical gradients of tracers

The TTL and lower tropical stratosphere are characterized by sharp vertical gradients in several tracers over a narrow layer of ~5 km thickness. Figure 2.19 shows the annual mean latitude-height cross-section of ozone and carbon monoxide (CO) measurements from the MLS satellite instrument, described in the Data Chapter.

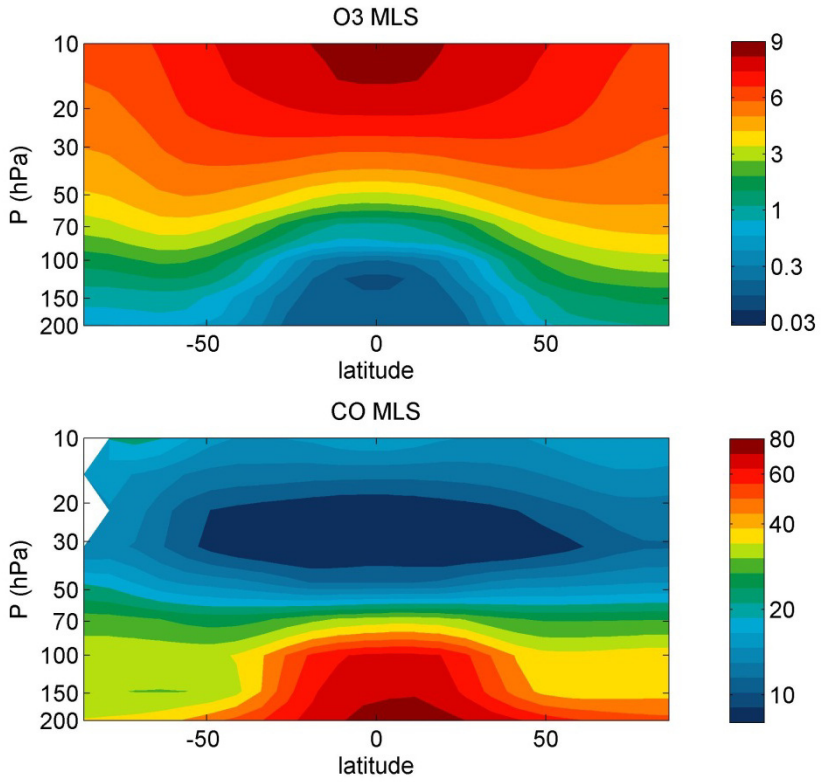


**Figure 2.19**. Annual mean cross-sections of ozone (ppmv) and CO (ppbv) from MLS measurements over 2005-2010. Note that the color scale is logarithmic, due to the very wide range of values existing in this region.

These tracers present large differences between their tropospheric and stratospheric concentrations, determined by chemical sources and sinks. This contrast, together with the fact that the mean lifetimes are similar to the mean transport timescales in this region, makes these tracers particularly interesting for transport studies. Ozone concentrations are low in the troposphere and high in the stratosphere, particularly in the tropics, where it is mainly produced by rapid photochemical reactions. On the other hand, CO is emitted in the troposphere, mainly from biomass burning, and it is photochemically destroyed in the stratosphere, with an approximate lifetime of 3-5 months. Note that the concentrations are expressed in volume mixing ratio in Fig. 2.19 (and throughout the Thesis).

This measure of chemical abundance (which gives the number of molecules of a given compound relative to the total number of air molecules) is particularly useful in the atmosphere because mixing ratio is conserved under changes of pressure or temperature.

Figure 2.19 shows very strong vertical gradients (note the logarithmic scale) in both tracers just above the tropical tropopause. Vertical motion across this region of enhanced gradients has potentially a large impact on such tracers in the tropical lower stratosphere (Randel et al. 2007). This is a key observation that largely motivates this Thesis.

- ## Annual cycle in tracers

High-vertical resolution observations in the lower stratosphere reveal a large annual cycle in ozone in the tropical lower stratosphere over a narrow vertical layer (Logan 1999, Folkins et al. 2006, Randel et al. 2007). Figure 2.20 shows the annual cycle in ozone together with the seasonality in temperature at the same pressure level above the tropical tropopause. The cycle in ozone is almost in phase with temperature. Upwelling seasonality is also shown in Fig. 2.20. Lower ozone is observed during boreal winter as compared to summer, in correspondence with lower temperatures and stronger upwelling. In Section 2a it was shown that the annual cycle in temperature in the tropical lower stratosphere is mainly driven by the seasonality in tropical upwelling. Randel et al. (2007) argue that the annual cycle in ozone also results from the seasonality in upwelling, acting on the strong ozone background vertical gradients in this region (shown in Figure 2.19).

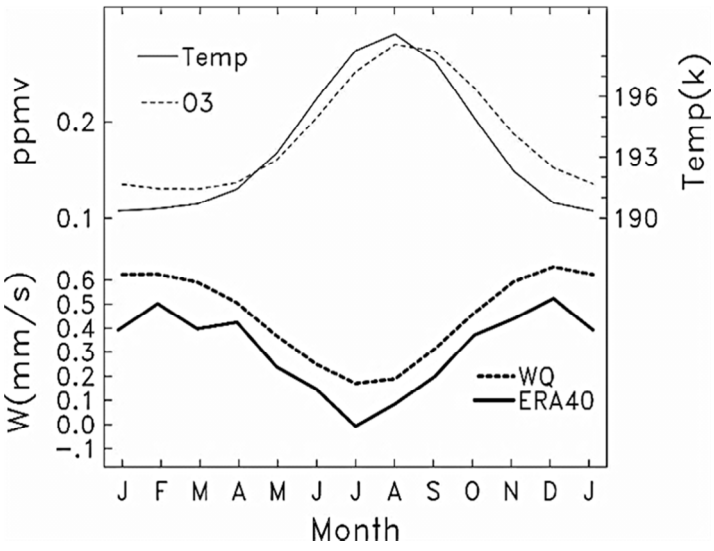


**Figure 2.20**. Annual cycle in tropical mean temperature (from GPS measurements), ozone (from SHADOZ measurements) and upwelling (derived from thermodynamic balance, WQ, and computed from ERA-40) above the tropical tropopause (17.5 km, ~80 hPa). From Randel et al. 2007.

Figure 2.21 shows the vertical structure of the ozone relative annual cycle amplitude (left panel), which peaks just above the tropical tropopause, similar to the structure seen for temperature (Fig. 2.12). The vertical structure of the relative vertical gradient in tropical mean ozone ( $\partial \ln O_3 / \partial z$ ), shown in the right panel of Figure 2.21, also exhibits a sharp peak just above the tropical tropopause. The coherence between the vertical structure of the gradient and the annual cycle highlighted in Figure 2.20 strongly suggests that the annual cycle in ozone follows the upwelling seasonality, enhanced by the large background vertical gradients (Fig.21). Randel et al. (2007) further show that the timing and amplitude of the ozone seasonality are consistent with this forcing mechanism.

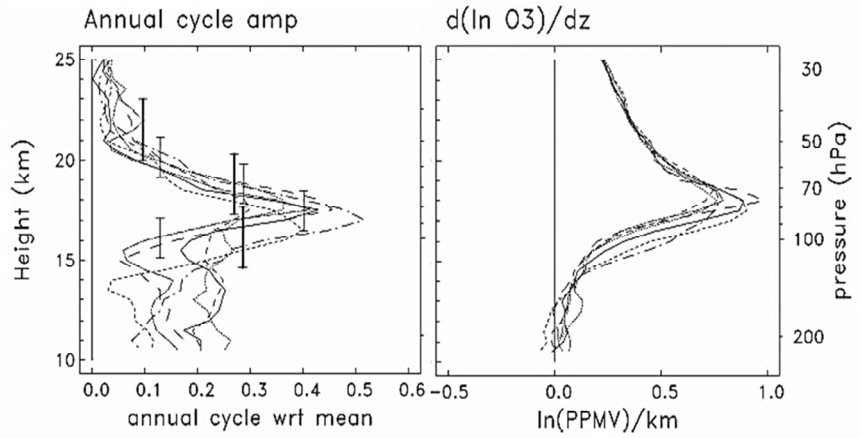


**Figure 2.21**. Vertical structure of tropical mean ozone relative annual cycle amplitude (left) and relative vertical gradient (right) from measurements. Profiles correspond to SHADOZ and longer error bars to MLS satellite measurements (both described in Data section). From Randel et al. 2007.

Other works have obtained similar results. For instance, Folkins et al. (2006) reproduced quite successfully the observed annual cycle in ozone with a simple model that included only seasonal variations in tropical upwelling and in high-altitude convective outflow. Using satellite observations, Schoeberl et al. (2008b) analyzed the vertical transport of ozone and concluded that there is almost no phase shift in the propagation of the annual cycle in ozone in the lower tropical stratosphere. This result is consistent with seasonal variations in upwelling driving annual variations in ozone (since upwelling seasonality is in-phase across different vertical levels).

In addition to the annual cycle in ozone, Folkins et al. (2006), Randel et al. (2007) and Schoeberl et al. (2008b) analyzed the annual cycle in carbon monoxide (CO) observed in this region. The seasonality of CO shows opposite phase to that in temperature and ozone, with higher CO concentrations in boreal winter and vice-versa. Schoeberl et al. (2006) noticed a tape recorder signal in CO satellite observations (similar to that in water vapor, Fig. 2.8). This behavior implies a phase shift in the annual cycle with height, and thus a vertical propagation of the anomalies towards higher levels (by nearly constant upwelling). However, Schoeberl et al.

(2008b) found that the tape recorder-like behavior is observed only above ~70 hPa, where vertical CO gradients are smaller, while below this level the seasonality in upwelling drives the seasonality in CO, and vertical gradients are nearly constant (as for ozone). More measurements of CO with higher vertical resolution and high sensitivity (CO concentrations are very small above ~70 hPa) are necessary in order to better understand CO vertical propagation. Nevertheless, the available measurements of CO show that both the relative amplitude and the background gradients present a peaked vertical structure, similar to those for ozone shown in Fig. 2.21 (Randel et al. 2007). This strongly suggests that the cycle CO is driven by upwelling annual variations acting on the background gradients also for this tracer.

## c. *Horizontal transport*

In the previous Section 3b, evidences have been shown that ozone and CO seasonal cycles are mainly driven by tropical upwelling. In contrast, a number of works have recently proposed a different perspective, which points towards horizontal transport as the main responsible for ozone seasonality above the tropical tropopause (Konopka et al. 2009, 2010, Ploeger et al. 2012). As mentioned in Section 3a, transport in the tropical lower stratosphere is linked not only to upwelling, but also to quasi-horizontal transport and mixing across the tropical boundaries, leading to air exchange between the tropics and the extra-tropics. Note that these two distinct transport processes are in fact related, as they both arise from wave dissipation.

While the tropical lower stratosphere above ~20 km is known to act as a reservoir, in which tracer transport is dominated by large-scale ascent and chemical species are isolated from the extratropics by transport barriers (e.g. Shepherd 2007; see Figures 2.4 and 2.17), horizontal transport is most frequently observed in the TTL near the tropopause. Quasi-horizontal transport and exchange with the extratropics occurs in the region ~15-20 km (~360-450 K), as shown in the schematics in Figs. 2.4

and 2.17, and occurs approximately along the isentropes. Evidence of rapid meridional transport in the layer ~15-20 km has been observed for water vapor (Rosenlof et al. 1997) and other tracers (Santee et al. 2011). However, the temporal variability and vertical structure of quasi-horizontal transport and the corresponding effects on tracer concentrations are subjects of active research.

- ## The Asian monsoon anticyclone

The Asian monsoon upper-level anticyclone is a dominant feature of the boreal summer UTLS circulation, which has important effects on tracer transport in this region (e.g. Randel and Jensen 2013). The monsoon stands out as a patch of troposphere-like values of tracer concentrations (e.g. low ozone, high CO and water vapor), contrasting with the surrounding TTL concentrations. This results from the rapid lifting of boundary-layer air masses by convection (e.g. Fueglistaler et al. 2009a). In addition, the anticyclonic circulation has been found to effectively transport air masses quasi-horizontally from the extra-tropics into the tropics, directly affecting TTL tracer concentrations (Konopka et al. 2009, 2010 and Ploeger et al. 2012).

Using global model simulations with the Chemical Lagrangian Model of the Stratosphere (CLaMS; McKenna et al., 2002), Konopka et al. (2009, 2010) found a large annual cycle in quasi-horizontal transport, in-phase with ozone concentrations, associated with the Asian monsoon upper-level circulation. It is important to note that these analyses are based on isentropic coordinates, and these surfaces undergo a large annual cycle, which is nearly in-phase with ozone, such that the seasonality in ozone is much reduced as compared to that on log-pressure altitudes (Konopka et al. 2009). In contrast with the results presented in Section 3a, these works suggested that isentropic transport played a primary role in causing the ozone seasonality. Figure 2.22 shows the enhanced isentropic transport of ozone from the northern extra-tropics (in-mixing) associated with the summer monsoons (Asian and American) at the isentropic level of 380 K (near the tropopause, see Fig. 2.19). The model ozone concentrations in

Fig. 2.22 are similar to the observations (Konopka et al. 2010, Randel and Jensen 2013). The anticyclonic circulation transports air masses from the extratropics, with very high ozone concentrations, into the tropics, increasing ozone in the boreal summer TTL.

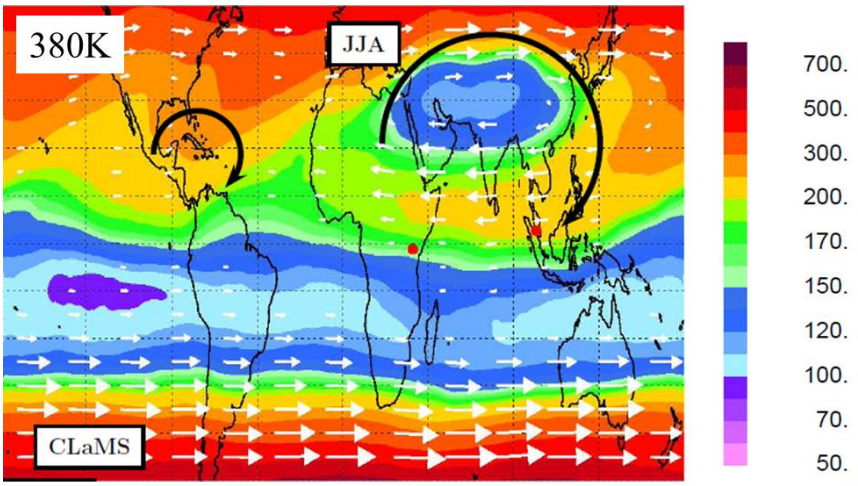


**Figure 2.22**. Ozone concentration at 380 K for boreal summer climatology from the CLaMS model (ppmv). From Konopka et al. (2010).

Finally this mechanism was supported by the results of Ploeger et al. (2012), obtained using a one-dimensional Lagrangian conceptual model with explicitly included in-mixing rates from middle-latitudes from CLaMS. They proved that the ozone annual cycle above the tropical tropopause entirely disappeared in this model if in-mixing was inhibited. Figure 2.23 from that work shows the seasonality of tropical mean ozone (from the Lagrangian model and from observations), and the various reconstructions obtained running the conceptual model including separately transport 1) only from the NH, 2) only from the SH and 3) only from within the tropics. This Figure 2.23 shows that a large seasonality in ozone is obtained when considering only in-mixing from the NH (although the annual mean value is largely underestimated). On the contrary, no annual cycle is observed at 400 K if only trajectories which had stayed within the tropical boundaries during the entire integration time are included in the integration.

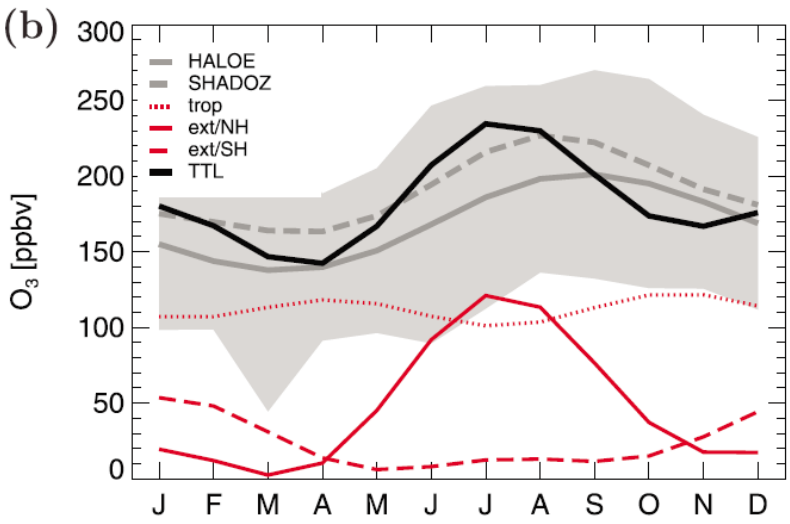


**Figure 2.23**. Annual cycle in tropical mean ozone at 400 K from the one-dimensional Lagrangian model (black line) and from observations (gray lines; gray shading shows standard deviation of the measurements). Red lines show the cycle obtained considering only transport from the NH (solid), the SH (dashed) and within the tropics (dotted). From Ploeger et al. (2012).

Consequently, from these studies, in-mixing of middle-latitude air into the tropics appeared essential to explain tropical ozone seasonality. This is in contrast with upwelling having a dominant role in driving the annual cycle in ozone, as argued by previous works (e.g. Randel et al. 2007). This controversy evidences a lack of understanding regarding the primary forcing mechanism of the ozone seasonality in the tropical lower stratosphere, which helps motivate the analyses performed in the present Thesis.

### d. *Outlook*

As follows from the above description of the state-of-the-art, there is no consensus on the relative importance of different transport processes for driving tracer variability in the tropical lower stratosphere. In particular,

the main cause for the existence of the large annual cycle in ozone above the tropical tropopause is under debate.

As pointed out in the first Section of this Chapter, the advent of satellite scientific platforms (starting in 1979) opened the doors to exploring the global distribution of tracers in the stratosphere. This in turn prompted the advance in our understanding of the general stratospheric circulation and the different transport processes that control tracer distribution and variability. Moreover, in the last ten years, multiple platforms carrying instruments for tracer detection (such as MLS, HIRDLS[13], ACE[14], SMILES[15], EUMETSAT[16] and others; Gettelman et al. 2013) have provided continued observations in the tropical lower stratosphere. These satellite measurements are extremely valuable tools for the comprehensive investigation of tracer distribution, temporal variability and ultimately chemical and transport processes in this region (e.g. Santee et al. 2011). The relatively large amount of data available from different remote sensing instruments, in combination with additional in-situ observations, allows inter-comparison and validation of the measurements.

Figure 2.24 shows daily time series of ozone and carbon monoxide (CO) concentrations near and just above the tropical tropopause, measured by the MLS instrument aboard NASA's Aura satellite (described in the Data Chapter).

The large annual cycles described above, out of phase between ozone and CO, are evident in these series. In addition, there is substantial variability on shorter timescales in both tracers. The accuracy of these tracer measurements allows investigating the transport processes driving the observed detailed fluctuations in the daily time series. The linear correlations between the observed concentrations are highly significant, suggesting that both tracers respond to a common forcing mechanism.

[13] HIgh Resolution Dynamics Limb Sounder.
[14] Advanced Composition Explorer.
[15] Superconducting Submillimeter-Wave Limb-Emission Sounder.
[16] European Organisation for the Exploitation of Meteorological Satellites.

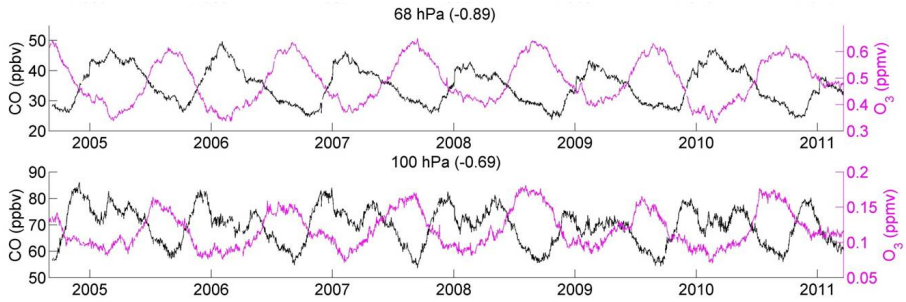


**Figure 2.24**. Time series of ozone and carbon monoxide (CO) from MLS measurements at 100 hPa and 68 hPa. Linear correlations between the series are also indicated. MLS observations used for this Figure 2.are described in the Data Chapter.

One plausible responsible for driving common fluctuations in these two tracers with strong background vertical gradients near the tropical tropopause is upwelling. However, other transport processes, such as isentropic transport and mixing, could contribute to the observed variability in tropical mean tracer concentrations, as seen above. Understanding the origin of the variability in Fig. 2.24 represents a relevant contribution to the current state of knowledge on tracer transport in the lower tropical stratosphere. The time series in Fig. 2.24 contribute to motivate the present Thesis, and constitute the starting point for the studies carried out.

# 3. Objectives

In view of the state of the art described in the previous Chapter, **the general objective of the present Thesis is to investigate upwelling near the tropical tropopause, including the variability on different timescales, the impact on temperature and tracer concentrations in the tropical lower stratosphere and the specific sources of variability**.

This general objective is divided into the following four specific goals:

1. **To quantify tropical upwelling and its uncertainty across the tropical tropopause by computing three independent estimates.**

Three independent estimates of tropical upwelling are computed using ERA-Interim reanalysis data of temperature and wind fields. Upwelling is computed from the reanalysis vertical velocity and also indirectly from thermodynamic balance and momentum balance. The estimates obtained by these calculations are then compared to quantify the degree of uncertainty. The resulting daily time series constitute updated quasi-observational estimates of tropical upwelling, based on state-of-the-art reanalysis data. This specific objective is addressed in **Section 1 of the Results Chapter (Chapter 6)**.

2. **To investigate the links between upwelling and temperature/tracers variability in the tropical lower stratosphere.**

The role of upwelling in driving the common variability between temperature and tracers observed in this region is investigated, focusing on seasonal and sub-seasonal timescales. The analyses are based on temperature and tracer budget calculations using the thermodynamic and

continuity TEM equations, respectively. Two types of data are used for this aim:

- **Observations (Section 1 of Chapter 6)**. For the observational analysis, satellite measurements of tracers (ozone and carbon monoxide, CO) are combined with the time series of upwelling derived for the above objective. Variability on seasonal and sub-seasonal timescales in the tracers and temperature measurements is examined and compared to the fluctuations in the upwelling estimates. Because the tracer measurements are completely independent from the reanalysis data, the comparison further provides a test for the quality of the upwelling estimates.

- **Chemistry-Climate Model output (Section 2 of Chapter 6)**. A similar analysis is performed from a model perspective, using output from the Whole Atmosphere Community Climate Model (WACCM). The ability of the model to represent realistically the region of interest is first evaluated, by comparing temperature and tracer structure and variability to satellite and ground-based observations.

3. **To evaluate the effects of other transport mechanisms on tracer concentrations in the tropical lower stratosphere.**

WACCM output from the previous objective allows explicitly evaluating all transport processes, even those that are not well resolved by the coarser-spatial resolution satellite observations. In **Section 2 of Chapter 6**, the complete TEM tracer budgets computed from WACCM data are analyzed for seasonal and sub-seasonal timescales. The role of vertical advection by tropical upwelling (previous objective) is compared to the other transport terms contributing to change tracer concentrations. Furthermore, in **Section 3 of Chapter 6**, WACCM ozone budget is contrasted with the results of a Lagrangian one-dimensional transport model (the same used in Ploeger et al. 2012). The comparison of the results from these two very different models (Eulerian and Lagrangian)

allows a more comprehensive understanding of the transport processes in the region of interest.

4. **To explore the specific dynamical forcing of tropical upwelling variability on sub-seasonal timescales.**

For this aim, the daily time series of the momentum balance estimate of upwelling computed for the first specific objective are used. The dynamical drivers of the sub-seasonal variability in upwelling are investigated by doing linear regression and composite analyses of the forcing field (i.e. the EP flux divergence) and the response in the zonal mean wind to this forcing, which can also affect upwelling variability. This specific objective is addressed in **Section 4 of Chapter 6**.

The presentation of the Results in this Thesis is organized as a collection of four articles, each one constituting one Section of Chapter 6:

- **Section 1**: *Variability in upwelling across the tropical tropopause and correlations with tracers in the lower stratosphere* (Abalos et al. 2012, ACP).

- **Section 2**: *Quantifying tracer transport in the tropical lower stratosphere using WACCM* (Abalos et al. 2013a, accepted for ACP).

- **Section 3**: *Ozone seasonality above the tropical tropopause: reconciling Eulerian and Lagrangian perspectives of transport* (Abalos et al. 2013b, ACPD).

- **Section 4**: *Dynamical forcing of sub-seasonal variability in the tropical Brewer-Dobson circulation* (Abalos et al. in preparation).

# 4. Data

In this Chapter the different data sets used in the Thesis are described including relevant references. Observational, model and reanalysis data are presented in Sections 1, 2 and 3 respectively.

## 1 Observational data

Three different observational datasets are used: two of them from satellite instruments (MLS[1] and COSMIC[2]) and one balloon-borne observational system (SHADOZ[3]). In particular, the measurements used in this Thesis correspond to ozone from MLS and SHADOZ, carbon monoxide (CO) from MLS and temperature from COSMIC.

### a. *Microwave Limb Sounder (MLS)*

The Earth Observing System Microwave Limb Sounder (EOS MLS) instrument onboard the Aura satellite from the National Aeronautics and Space Administration (NASA) is described in Waters et al. (2006). The Aura satellite was launched on July 15, 2004, and measures several chemical species and other variables using the corresponding radiation emission on the millimeter and sub-millimeter wavelength scale. It retrieves vertical profiles every 165 km along the suborbital track, shown in Figure 4.1, covering the latitudinal range 82°S-82°N. It constitutes an advanced version of the MLS instrument on the UARS[4] satellite, launched in 1991 to investigate the enhanced destruction of ozone in the stratosphere by Chloroflourocarbons (CFCs). One of the main improvements in the EOS MLS respect to its predecessor is that it provides measurements in the

[1] Microwave Limb Sounder.
[2] Constellation Observing System for Meteorology Ionosphere and Climate.
[3] Southern Hemisphere ADditional OZonesondes.
[4] Upper Atmosphere Research Satellite.

UTLS region. Ozone and CO measurements have been evaluated against other satellite and balloon-borne measurements (Waters et al. 2006, Froidevaux et al. 2006, 2008, Livesey et al. 2007, 2008). The precision of MLS measurements in the UTLS has been quantified for ozone (~5-10%) and CO (~30%) on pressure levels between 68 and 147 hPa (Livesey et al. 2007, Froidevaux et al. 2008). CO measurements at and above 46 hPa have large uncertainties, as compared with other satellite measurements (Pumphrey et al. 2007). Ozone at these higher levels has small uncertainties below 5% (Froidevaux et al. 2008).

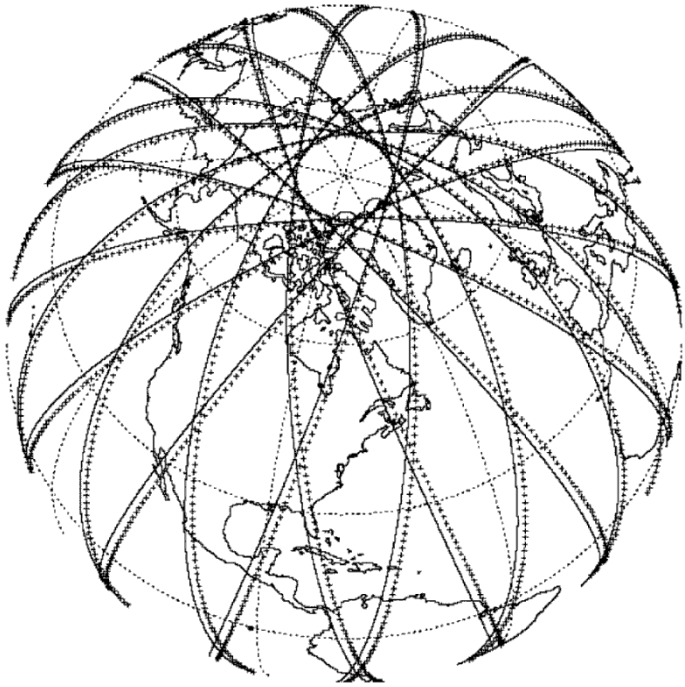

**Figure 4.1**. EOS MLS measurement locations (crosses) and sub-orbital track (solid lines) for a 24-hours period. From Waters et al. (2006).

In this Thesis, zonal mean daily-averaged measurements of ozone and CO for the period September 2004 to December 2010 are used. The data, previously gridded on a 7.5° latitude grid by Mijeong Park (NCAR), was averaged over the latitude band 18.75°S-18.75°N to construct the

tropical-mean time series. This band is representative of the width of the tropics in the lowermost stratosphere, based on the autocorrelations of temperature, upwelling and tracers near the equator with other latitudes (not shown). There are three pressure levels within the tropical tropopause layer at which MLS measures carbon monoxide (147, 100 and 68 hPa) and five for ozone (147, 121, 100, 83 and 68 hPa). The vertical resolution of MLS ozone is approximately 3 km (Froidevaux et al., 2006), while the resolution for CO is ~4.5 km (Livesey et al., 2008). The present study focuses on the effect of tropical upwelling at and above the tropical tropopause, so only the levels of 100 hPa and above are considered. MLS tracer observations are particularly useful for studies of global tracer distribution and variability in the lower stratosphere (e.g. Santee et al. 2011).

### b. *SHADOZ*

Tropical ozonesonde measurements from the SHADOZ (Southern Hemisphere ADditional OZonesondes) network are described in Thompson et al. (2007, 2012) and references therein. SHADOZ is a tropical radiosonde-ozonesonde observational network, with sondes lauched on a weekly basis from currently 12 stations spanning the tropics since 1998 (as shown in Figure 4.2). The SHADOZ project coordinates the measurements in all the sations with and provides additional ozonesondes if necessary.

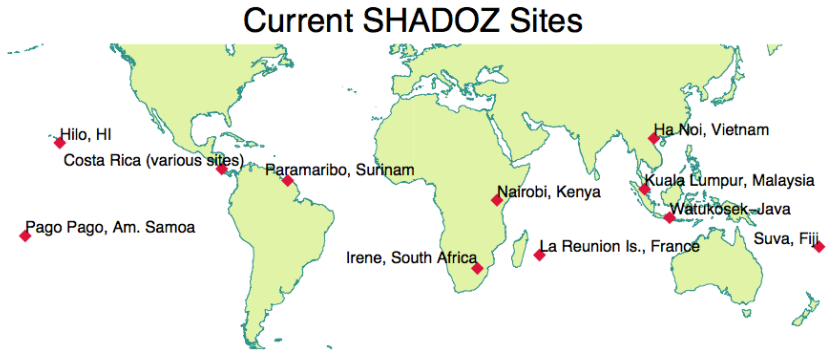

**Figure 4.2**. Location of the current SHADOZ stations (http://croc.gsfc.nasa.gov/shadoz/).

In the present Thesis, ozone measurements from a subset of 7 near-equatorial stations are used for the period 1998-2006, including Nairobi, Kenya (1°S), Kuala Lumpur, Malaysia (3°N), San Cristobal Island (1°S), Ascension Island (8°S); Wautesok, Java (8°S), Malindi, Kenya (3°S), and Paramaribo, Suriname (6°N). The profiles span the range of altitude 0.5 km to 40 km with a vertical resolution of 0.5 km. This is the same data subset used and described in Randel et al. (2007).

### c. *COSMIC GPS*

Temperature observations are taken from the Constellation Observing System for Meteorology Ionosphere and Climate (COSMIC) satellite mission (Anthes et al. 2008). These data are obtained with the global positioning system (GPS) radio-occultation (RO) technique. Six micro-satellites were launched in April 2006 to orbit at an altitude near 500 km for the COSMIC mission. These satellites carry receivers to measure bending angle from other GPS satellites signals. Currently, around 2000 high-quality vertical profiles are retrieved daily from this mission.

COSMIC daily data for the period January 2007 to December 2010 is used in this Thesis. The time series were constructed averaging zonal mean data (which had been previously gridded by Fei Wu, NCAR on a 5° latitude x 20° longitude lattice) over the tropical latitudinal band 20°S-20°N. The vertical levels span the range of altitude 10 km to 25 km with a vertical resolution of 0.2 km.

## 2 Model data

In addition to the observational results, this Thesis includes results based on model data from one WACCM simulation run by Doug Kinnison (NCAR). The chemistry-climate model is briefly described in Section 2a. In

addition, WACCM output is compared with a simple conceptual one-dimensional Lagrangian model, described in Section 2b. Finally, a short description of a simple radiative transfer model used to estimate heating rates from observations of temperature and tracers is given in Section 3c.

## a. *Whole Atmosphere Community Climate Model (WACCM)*

The Whole Atmosphere Community-Climate Model, Version 4 (WACCM4) is the atmospheric component of the coupled climate system model CESM1 (Community Earth System Model, Version 1), extended to cover the altitude range from the surface to the lower thermosphere. Garcia et al. (2007) discuss the processes and parameterizations that are unique to WACCM4. There are 66 vertical levels from the ground to 180 km, with a vertical resolution of 1.1 – 1.4 km in the UTLS in this simulation. The horizontal resolution is 1.9°x2.5° (latitude x longitude). The chemical module of WACCM4 is based on the 3-D chemical transport Model of OZone and Related Tracers, Version 3 (MOZART-3) (Kinnison et al. 2007), incorporating a realistic representation of stratospheric and tropospheric chemistry (in particular, for ozone and CO). The data used in this Thesis corresponds to a 50-year transient run from 1960 to 2010, similar to the REF-B1 simulation used in CCMVal (CCMVal 2010, Chapter 2). It includes anthropogenic and natural forcing from observations (such as trace gases emissions, quasi-biennial oscillation (QBO) or sea surface temperatures), mostly identical to those used by CCMVal (2010) for REF-B1. It is a fully-interactive simulation, with radiatively active gases (such as CO2, H2O, N2O, CH4, CFCs, NO and O3) influencing the radiative heating rates and therefore the dynamics.

WACCM computes tracer transport using a finite-volume dynamical core with a Lagrangian control-volume vertical discretization (Lin, 2004). In this technique, the vertical coordinates are material surfaces, which evolve following hydrostatic dynamics. The finite volumes bounded by two neighboring Lagrangian surfaces can therefore float, be compressed or

expanded. In particular, the presence of diabatic heating/cooling deforms the surfaces, which must be frequently remapped to hydrostatic pressure coordinates. The remapping process involves vertically redistributing tracer mixing ratios from the Lagrangian control volume to the Eulerian framework. Therefore, the vertical velocity (omega) in the model is indirectly derived from considering the pressure change implied by the remapping, and is not used for transport.

Daily data for six years (2004-2009) of output was stored for the present Thesis. The variables used include temperature, ozone, CO, heating rates (including net short and long wave radiative heating), chemical net tendency and three-dimensional winds.

## b. *1-D Lagrangian model*

Part of the results of this Thesis are based on the conceptual Lagrangian one-dimensional tropical tracer model (termed '1D-model' in the following), introduced by Ploeger et al. (2012). In particular, transport of tropical mean ozone is analyzed using this 1D-model (run by Felix Ploeger from Jülich Forschungszentrum), and compared to the tropical mean (Eulerian) results from WACCM4. In the 1D-model, air parcels representing the entire width of the tropics are transported upwards across the isentropes, with ascent rates given by ERA-Interim heating rates corrected multiplying by 0.6, as discussed in Ploeger et al. (2012). The model is based on CLaMS (the Chemistry Lagrangian Model of the Stratosphere, McKenna et al. 2002). During the ascent, photochemical reactions given by CLaMS lead to ozone production along the trajectories. In addition, lateral in-mixing from the extratropics affects tropical mean ozone concentrations. In-mixing rates of ozone are obtained from CLaMS as the number of parcels in the TTL whose (3D) back-trajectories crossed a certain tropical boundary limit (50° equivalent latitude) in the last five months (Ploeger et al. 2012). In this Thesis, in-mixing rates are given as a function of month and isentropic levels (the lowest level in the model is 360 K, where a climatology based on satellite data is imposed as boundary

condition for ozone concentrations). The results of this Lagrangian model are transformed into an Eulerian perspective in order to compare them with WACCM calculations.

### c. *NCAR-Column Radiation Model*

The radiative heating rates used in Section 1 of Chapter 6 were obtained from the NCAR-Column Radiation Model (freely available online, http://dust.ess.uci.edu/crm/) run by Fei Wu (NCAR). The Column Radiation Model, or CRM, is a standalone version of the radiation transfer model used in the NCAR Community Climate Model. In this Thesis zonal mean values of ozone from MLS and temperature from ERA-Interim were given as an input to compute the monthly-mean net radiative heating rates for January 2005-December 2010. Climatological values derived from observations were used for the rest of the tracers (such as water vapor and $CO_2$). One caveat of this accurate radiative transfer model is that the radiative effects of clouds are not included in the heating rate calculations. Nevertheless, as mentioned in the Introduction (Section 2a), Yang et al. (2010) estimated the net effect of cirrus clouds in the TTL to be relatively small.

## 3 Reanalysis data

Reanalysis is the assimilation of long time series of observations with an unvarying assimilating system, developed to produce homogeneous data sets for climate study purposes (Rood 2003). Reanalyses constitute a valuable and widely used tool for atmospheric studies, as they provide a comprehensive and consistent record of weather and climate over time. By combining observations over the globe with a numerical model, reanalyses generate an estimate of the state of the atmosphere that, lacking the spatio-temporal limitations of the observations, is more realistic than free-running models. However, it is important to keep in mind the limitations of reanalyzed data and that results should not be interpreted as observations.

That being said, note that sometimes reanalysis results are referred to as observational, as opposed to purely model results.

### a. *ERA-Interim*

ERA-Interim is the third-generation[5] reanalysis produced at the European Centre for Medium-Range Weather Forecasts (ECMWF), and it is considered to provide one of the most accurate representations of the stratosphere (e.g. Dee et al. 2011). ERA-Interim was initiated in 2006 as an 'interim' reanalysis to prepare for the next-generation extended reanalysis to replace ERA-40, namely ERA-20C[6], which recently started to be produced and will cover the 20$^{th}$ century (Dee 2013). ERA-Interim database starts in January 1979, and is maintained up to date and archived on a monthly basis (Berrisford et al. 2009). The period covered by ERA-Interim coincides with the so-called data-rich period, for which satellite observations are available. The horizontal spectral resolution is T255, (~80 km) and there are 60 vertical levels, with the model top at 0.1 hPa and 25 levels above 100 hPa. The ERA-Interim atmospheric model and reanalysis system uses cycle 31r2 of ECMWF's Integrated Forecast System (IFS), which was introduced operationally in September 2006. Further details on ERA-Interim can be found in Simmons et al. (2006), Dee et al. (2011) and in the webpage http://www.ecmwf.int/research/era/do/get/era-interim.

Several errors detected in ERA-40 were corrected in ERA-Interim, in particular the excessive precipitation in the tropical oceans (hence the hydrological cycle) and the strength of the Brewer-Dobson circulation in the stratosphere. Although some discontinuities in upper stratospheric temperatures have been recently identified, these do not affect the UTLS (McLandress et al. 2013). Figure 4.3 shows the tape recorder signal in stratospheric water vapor in both reanalyses. In ERA-40 alternate dry and moist phases ascend too rapidly as compared to observations (e.g. Fig. 2.8), while ERA-Interim shows much slower ascent rates.

[5] The former versions were ERA-15 and ERA-40.

[6] ERA-20C is an ensemble of 10-member ensemble of data assimilations covering 1900-2010, with a spectral resolution of T159 (~125 km) and 91 vertical levels.

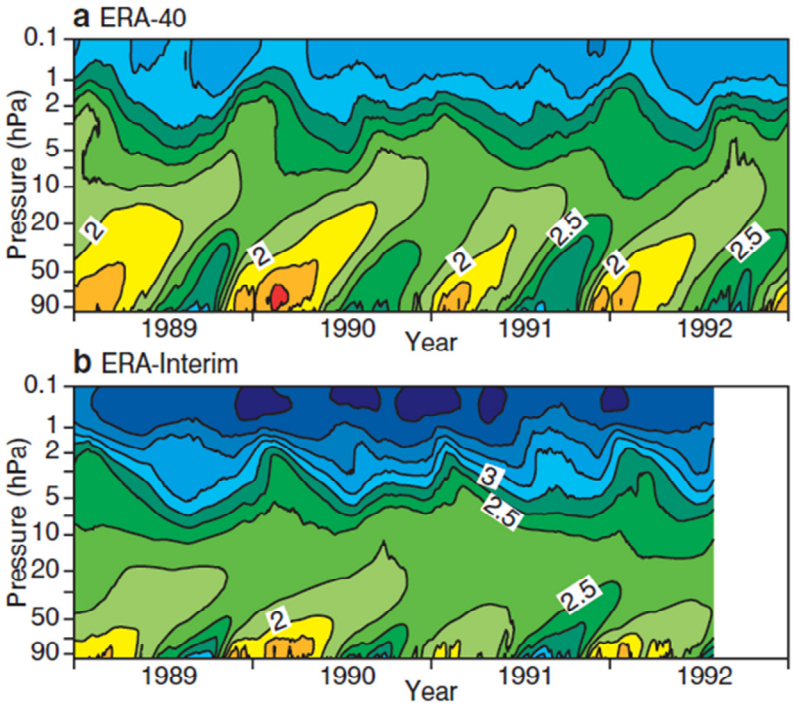


**Figure 4.3**. Tape recorder signal in (a) ERA-40 and (b) ERA-Interim specific humidity averaged over 10°S-10°N ($mg \cdot kg^{-1}$). From Simmons et al. (2006).

An extensive description of the main improvements in data assimilation techniques, bias correction and modeling in ERA-Interim is found in Simmons et al. (2006). Particularly relevant is the introduction of the 4D-Var assimilation method (performed every 12 hours), which interpolates the variables statistically both in space and time. Also, a new scheme of variational bias correction of satellite data is applied in ERA-Interim, which shows a better performance than previous bias handling. New humidity analysis and improved model physics had a positive effect on tropical precipitation (Uppala et al. 2008).

Several works have further confirmed the improved representation of the stratospheric Brewer-Dobson circulation and age of air in the ERA-Interim reanalysis as compared to ERA-40 (Monge-Sanz et al. 2007,

Fueglistaler et al. 2009b). However, it is estimated that ERA-Interim ascent rates are still approximately twice the real values (Dee et al. 2011). On the other hand, Iwasaki et al. (2009) and Seviour et al. (2011) have shown that ERA-Interim yields less noisy vertical velocities compared to other reanalyses.

In this Thesis, archived meteorological data with a horizontal resolution of 1.5°x1.5° on all the 60 archived pressure levels is used. Daily means are computed averaging original 6-hourly data. The data period used depends on the specific objective (September 2004 to December 2010 in the objectives 1 and 2, January 1979 to December 2011 in the objective 4). The ERA-Interim data has been partly downloaded from the ECMWF data server (http://data-portal.ecmwf.int/) and partly provided by Cameron Homeyer (NCAR).

# 5. Methodology

In this chapter the main dynamical analyses carried out in this Thesis are described, as well as the statistical, spectral and numerical methods applied.

## 1 Dynamical analyses

### a. *Estimates of tropical upwelling*

As mentioned in Section 2 of the Introduction chapter, there are no direct measurements of tropical upwelling in the tropical lower stratosphere, thus it needs to be estimated indirectly. One possibility, as described in the Introduction, is to use satellite observations of tracers with seasonally dependent concentrations near the tropical tropopause (such as water vapor) and compute the phase difference between consecutive levels. Alternatively, dynamical methods can be used to infer upwelling. In this Thesis three different estimates are computed, as described below, one directly dependent on the vertical velocity from the reanalysis and two indirect estimates. ERA-Interim temperature and wind fields are used in the calculations.

- Residual circulation

The first estimate of upwelling ($\overline{w}^*$) is obtained simply from the definition of the vertical component of the residual circulation (Eq. 4b in Chapter 2)[1]:

[1] The prime in the equation label indicates that it is a duplicate of an equation found in a previous chapter.

$$\overline{w}^* \equiv \overline{w} + \frac{1}{a\cos\phi}\left(\cos\phi \frac{\overline{v'T'}}{S}\right)_\phi \qquad (4b')$$

This upwelling estimate is mainly dependent on the zonal mean vertical velocity from the reanalysis ($\overline{w}$) in the tropics, where the eddy heat flux ($\overline{v'T'}$) is negligible. Vertical velocity is not constrained by observations in the reanalysis, but derived from mass continuity from the horizontal wind field. Thus, $\overline{w}$ is a small magnitude with large uncertainties associated. As mentioned in the Data chapter, ERA-Interim ascent rates have been shown to be more realistic than the previous ECMWF reanalysis velocities (i.e. ERA-40), but there are still important errors in this field, especially near the tropical tropopause.

- ## Momentum balance

A second estimate of upwelling ($\overline{w}^*_m$) can be derived combining the momentum and continuity TEM equations (as in Randel et al. 2002, based on previous results by Haynes et al. 1991 and Rosenlof 1995 for the stationary case):

$$\overline{u}_t - \hat{f}\overline{v}^* + \overline{w}^* \overline{u}_z = DF \qquad (7')$$

$$(a\cos\phi)^{-1}(\overline{v}^*\cos\phi)_\phi + e^{z/H}(e^{-z/H}\overline{w}^*)_z = 0 \qquad (10')$$

Defining the residual streamfunction, $\Psi^*$, such that:

$$(\overline{v}^*, \overline{w}^*) = \frac{e^{z/H}}{\cos\phi}(-\Psi^*_z, \frac{1}{a}\Psi^*_\phi) \qquad (15)$$

and substituting (15) into (7') and (10'), the following expression can be derived for the residual streamfunction:

$$\Psi^*(\phi,z)=\int_z^{\infty}\frac{-\cos\phi}{\hat{f}}\left[DF(\phi,z')-\overline{u}_t(\phi,z')\right]_{\overline{m}}e^{-z'/H}dz' \tag{16}$$

Considering Eq. (15), this expression can be integrated over a range of latitudes to give tropical mean upwelling at a fixed pressure level (or log-pressure altitude, $z$) over a latitudinal band ($\pm\phi_0$):

$$\left\langle \overline{w}_m^* \right\rangle(z)=\frac{-e^{z/H}}{\int_{-\phi_0}^{\phi_0}a\cos\phi d\phi}\left\{\int_z^{\infty}\frac{e^{-z'/H}\cos\phi}{\hat{f}(\phi,z')}\left[DF(\phi,z')-\overline{u}_t(\phi,z')\right]_{\overline{m}}dz'\right\}_{-\phi_0}^{\phi_0} \tag{17}$$

All the variables in Eq. (17) are defined in Section 1c of the Introduction. The subscript in $\overline{w}_m^*$ indicates that upwelling is estimated from momentum balance. To simplify the calculations, the integrand is computed on constant latitudes instead of along constant zonal mean angular momentum ($\overline{m}$) isolines since these are approximately vertical at the latitudinal boundaries we use (18°S-18°N) (e.g. Fig. 2.6).

As seen in Section 1c of the Introduction, the scaled divergence of the EP flux ($DF$) includes heat and momentum meridional eddy fluxes, which are calculated from the three-dimensional temperature and wind fields from the reanalysis. Consequently, a key uncertainty in this calculation of upwelling is associated with the unresolved waves, which are parameterized in the reanalysis model. As a note, the model simulations in Garcia and Randel (2008) and Calvo and Garcia (2009) suggest that, for the range of latitude/altitude considered in this Thesis, resolved waves explain most of the upwelling.

The expression (17) gives the tropical mean upwelling at a given log-pressure altitude $z$ that is in balance with the applied eddy forcing ($DF$) and corresponding zonal wind tendency ($\overline{u}_t$). Note that the integral is

taken from the altitude where upwelling is computed and to the highest level, and the result is evaluated only at the boundaries of the latitudinal interval. In the stationary case $\overline{u}_t = 0$, and tropical upwelling is determined exclusively by the wave drag ($DF$) just at the boundaries of the tropics and at levels above $z$. This is the "downward control" principle (Haynes et al. 1991) introduced in the Introduction chapter (Section 2b). In contrast, in the transient case the term $\overline{u}_t$ includes nonlocal effects of wave drag at other latitudes. The importance of this nonlocal influence for transient variability in upwelling is highlighted in Section 4 of Chapter 6 (Abalos et al., in preparation).

- ## Thermodynamic balance

The last estimate of upwelling computed in this Thesis ($\overline{w}^*_Q$) is based on thermodynamic balance (Rolsenlof 1995). The TEM thermodynamic and mass continuity equations are:

$$\overline{T}_t = -\overline{v}^* \overline{T}_y - \overline{w}^* S + \overline{Q} - e^{z/H}\left[e^{-z/H}\left(\overline{v'T'}\frac{\overline{T}_y}{S} + \overline{w'T'}\right)\right]_z \qquad (8')$$

$$(a\cos\phi)^{-1}(\overline{v}^*\cos\phi)_\phi + e^{z/H}(e^{-z/H}\overline{w}^*)_z = 0 \qquad (10'')$$

In this work, $Q$ is computed from the NCAR-CRM radiative transfer model (Data chapter, Section 2c), with input of daily mean zonal mean ERA-Interim temperatures and MLS ozone concentrations. Neglecting the eddy term (last term on the right hand side of (8')) and substituting $\overline{v}^* = 0$, a first estimate of residual vertical velocity can be obtained from the thermodynamic equation. Due to uncertainties in the independently computed heating rates, this estimate must be corrected to ensure that mass continuity is satisfied on a pressure surface, implying that $\overline{w}^*$ integrated over latitude must be zero. After applying this correction, the resulting $\overline{w}^*$ is then inserted in Eq. (10'') to compute a new estimate of

$\overline{v}^*$, which is subsequently substituted in (8'). After a few iterations, the method converges and gives an estimate of upwelling, referred to as the thermodynamic estimate $\overline{w}^*_Q$. The subscript $Q$ indicates that this estimate is mainly a function of the heating rates (which in turn depend largely on temperature). There are two main sources of uncertainty in this estimate of upwelling, which include a possible non-negligible contribution of the eddy term plus inaccuracies in the calculations of the heating rates ($Q$) (see Section 2c of the Data chapter).

## b. *Tracer budget analysis*

The analyses in Sections 1, 2 and 3 of the Results Chapter (Abalos et al. 2012, 2013a and 2013b, respectively) are based on the zonal mean ozone and CO budgets in the tropical lower stratosphere. Two different formulations of these balances are used in the present Thesis, namely the TEM and the isentropic formulations.

### • The TEM tracer continuity equation

The continuity equation for tracer concentration can be expressed in the following way in the TEM formalism (Eq. 9.4.13 of Andrews et al. 1987):

$$\overline{\chi}_t = -\frac{\overline{v}^*}{a}\overline{\chi}_\phi - \overline{w}^*\overline{\chi}_z + e^{z/H}\nabla\cdot\mathbf{M} + P - L \qquad (18)$$

This equation states that local changes in zonal mean tracer concentration ($\overline{\chi}$) are given by transport processes, including not only advection by the residual circulation $(\overline{v}^*, \overline{w}^*)$ but also eddy transport ($e^{z/H}\nabla\cdot\mathbf{M}$), plus net chemical production minus loss ($P-L$). The eddy transport term is formulated as the inverse of density times the divergence

of the eddy transport vector, $\mathbf{M}$, with components defined as (Eq. 9A.3 of Andrews et al. 1987):

$$M^{(\phi)} = -e^{-z/H}\left(\overline{v'\chi'} - \frac{\overline{v'T'}}{S}\overline{\chi}_z\right) \tag{19a}$$

$$M^{(z)} = -e^{-z/H}\left(\overline{w'\chi'} + \frac{\overline{v'T'}}{S}\frac{1}{a}\overline{\chi}_\phi\right) \tag{19b}$$

Hence, the components of the eddy transport vector ($\mathbf{M}$) are a function of the meridional and vertical eddy fluxes of tracer concentration ( $\overline{v'\chi'}$ and $\overline{w'\chi'}$, respectively). Note that there are other terms in addition to the eddy fluxes in Eqs. (19). Recalling that $\nabla\cdot\mathbf{M} \equiv (a\cos\phi)^{-1}(M^{(\phi)}\cos\phi)_\phi + (M^{(z)})_z$, and given the definition of the residual circulation:

$$\overline{v}^* \equiv \overline{v} - e^{z/H}\left(e^{-z/H}\frac{\overline{v'T'}}{S}\right)_z \tag{4a'}$$

$$\overline{w}^* \equiv \overline{w} + \frac{1}{a\cos\phi}\left(\cos\phi\frac{\overline{v'T'}}{S}\right)_\phi \tag{4b''}$$

it can be seen that the TEM definition of *eddy transport* (Eq. 19) is not completely independent from the *advective transport* by $(\overline{v}^*, \overline{w}^*)$. However, the TEM tracer continuity equation (Eq. 18) is one possible and convenient way of separating the contribution from the zonal mean overturning (Brewer-Dobson) circulation, characterized by upwelling in the tropics and downwelling at high latitudes, from the predominantly horizontal eddy transport (cf. schematic of transport in Fig. 2.3 of the Introduction).

- ## Isentropic formulation

Alternatively, the tracer continuity equation can be formulated in isentropic coordinates (Eq. 9.4.21 of Andrews et al. 1987):

$$\bar{\chi}_t = -\frac{\bar{v}^*}{a}\bar{\chi}_\phi - \bar{Q}^*\bar{\chi}_\theta + \left\{-(a\bar{\sigma})^{-1}\left[\overline{(\sigma v)'\chi'}\right]_\phi - \bar{\sigma}^{-1}\left[\overline{(\sigma Q)'\chi'}\right]_\theta\right\} + \bar{P}^* - \bar{L}^* \tag{20}$$

where the mass-weighted variables with a bar and a star are defined as mass-weighted zonal-mean variables:

$$\bar{A}^* \equiv \frac{\left(\overline{\sigma A}\right)}{\bar{\sigma}} \tag{21}$$

with the "density" on isentropes defined as:

$$\sigma \equiv -\frac{1}{g}\frac{\partial p}{\partial \theta} \tag{22}$$

Note that the transient term: $-\bar{\sigma}^{-1}\left(\overline{\sigma'\chi'}\right)_t$ is omitted in Eq. (20), as it is negligible for ozone and CO budgets in our region of interest. To highlight the analogy with the TEM equation (Eq. 18), the isentropic formulation (Eq. 20) is presented in the same order. The tendency in zonal mean tracer concentration on a given isentrope is determined by transport processes, including advection by the mean isentropic and cross-isentropic circulation $(\bar{v}^*, \bar{Q}^*)$ and eddy transport (bracketed term on the right hand side), plus chemical sources and sinks. Note that, in this case, the eddy transport term is a function exclusively of the divergence of the (meridional and cross-isentropic) tracer eddy fluxes.

Isentropic coordinates are widely used in stratospheric transport studies, because they provide a simplified framework for adiabatic

processes (e.g. Plumb 2002). In regions where diabatic motions are negligible, air parcels tend to stay on isentropes in timescales of tens of days (Andrews et al. 1987). Isentropic coordinates have been proven particularly advantageous, for instance, in Lagrangian modeling of air parcel trajectories (e.g. Ploeger et al. 2010), and also for representing episodes of wave breaking and subsequent stirring in the middle latitudes, dominated by quasi-horizontal motions (e.g. McIntyre and Palmer 1983, Holton et al. 1995, Plumb 2002).

In the region under study in this Thesis (the tropical lower stratosphere) the differences between isentropic and log-pressure coordinates are particularly important, because vertical motions are dominant and diabatic transport is not negligible (i.e., tracers do not travel on constant isentropic surfaces). In addition, isentropes suffer large vertical displacements in this region of the atmosphere; in particular there is a large annual cycle in potential temperature just above the tropical tropopause (see Introduction, Section 2a).

# 2 Mathematical tools

In this Section the different mathematical methods and techniques used in the Thesis are presented. Section 2a introduces the statistical methods applied, Section 2b explains the spectral analyses performed and finally Section 2c briefly describes the basic numerical computation methods used in this Thesis.

## a. *Statistical methods*

The statistical methods used in the present work include analysis of linear relationships between two variables, statistical testing of hypothesis and graphical representation (in latitude-height cross sections) of linear projections and composites.

## • Linear regression

Statistical analysis provides the tools to objectively determine if the temporal evolution of two variables X and Y is related or not, and if it is, to what extent. As a first step, it is extremely useful to visualize the data on a scatter diagram (Y versus X). If the time series of X(t) and Y(t) tend to co-vary (i.e., one increases when the other one increases or decreases), the points on the scatter plot will tend to align on a straight line[2]. Two time series can co-vary for two reasons: because changes in one of them lead to changes in the other or because both variables share a common source of variability. This is undistinguishable from a statistical point of view, and physical interpretation is required to determine whether there is a causal relationship between two variables or not. In the first case, the *independent* variable causes the changes in the *dependent* variable. If the independent variable (X) is known, the dependent field (Y) can be estimated by a function g(X). The mean squared error gives a reasonable estimate of the accuracy of this approximation:

$$< (Y - g(X))^2 > \tag{23}$$

where < A > indicates the expectation value of A. This error (Eq. 23) can be minimized to obtain the function g(X) that best approximates Y. In the case that g(X) is forced to be linear, it can be shown that (von Storch and Zwiers 1999):

$$g(X) = \mu_Y + \frac{\sigma_Y}{\sigma_X} \rho_{XY} (X - \mu_X) \tag{24}$$

with $\sigma_X$ and $\sigma_Y$ the standard deviation and $\mu_X$, $\mu_Y$ the mean of each variable:

[2] Only the case of linear relations is relevant for this Thesis.

$$\rho_{XY} = \frac{<(X-\mu_X)(Y-\mu_Y)>}{\sigma_X \sigma_Y} \tag{25}$$

is the correlation coefficient. Using the expression (24), the mean squared error (Eq. 23) is $\sigma_Y^2(1-\rho_{XY}^2)$. Hence, the error is zero when the correlation coefficient is one. In this case the dependent variable Y can be predicted from the independent variable X by $Y = \mu_Y + \frac{\sigma_Y}{\sigma_X}(X-\mu_X)$ with probability one. It can be shown that the correlation coefficient $\rho_{XY}$ is also a measure of the fraction of variance of Y that can be explained from X using a linear model (von Storch and Zwiers 1999).

In the case of a limited sample with n observations $(x_i, y_i)$, (i=1, …, n), the correlation coefficient can be estimated as:

$$r_{XY} = \frac{\sum_{i=1}^{n}(x_i-\overline{x})(y_i-\overline{y})}{\sqrt{\sum_{i=1}^{n}(x_i-\overline{x})^2(y_i-\overline{y})^2}} \tag{26}$$

with $(\overline{x}, \overline{y})$ the mean of the observed sample corresponding to the variables $(X, Y)$.

The value of $r_{XY}$ indicates the degree of accuracy of the linear regression model to represent the points in the scatter diagram (i.e., a straight line has $r_{XY} = \pm 1$ depending on the sign of the slope, and a circular distribution implies $r_{XY} = 0$).

A simple linear regression model can be estimated by least squares given n pairs of observations $(x_i, y_i)$. The observation $y_i$ can be obtained from $x_i$ with a linear model plus the error $e_i$ associated to the linear estimate corresponding to the observation $x_i$:

$$y_i = a_0 + a_1 x_i + e_i \tag{27}$$

If $\hat{a}_0$ and $\hat{a}_1$ are estimates of the regression coefficients in Eq. (27), the error can be estimated as $\hat{e}_i = y_i - \hat{a}_0 - \hat{a}_1 x_i$, and the sum of squared errors is:

$$\sum_{i=1}^{n} (y_i - \hat{a}_0 - \hat{a}_1 x_i)^2 \tag{28}$$

Minimizing this function (28) respect to $\hat{a}_0$ and $\hat{a}_1$ (i.e., forcing the partial derivatives to be zero), the following expressions are obtained for the regression parameters (intercept and slope):

$$\hat{a}_0 = \overline{y} - \hat{a}_1 \overline{x} \tag{29a}$$

$$\hat{a}_1 = \frac{\sum_{i=1}^{n} x_i y_i - n \cdot \overline{x} \cdot \overline{y}}{\sum_{i=1}^{n} x_i^2 - n \cdot \overline{x}^2} = \frac{S_{XY}}{S_{XX}} \tag{29b}$$

with

$$S_{XY} = \sum_{i=1}^{n} x_i y_i - n \cdot \overline{x} \cdot \overline{y} \tag{30a}$$

$$S_{XX} = \sum_{i=1}^{n} x_i^2 - n \cdot \overline{x}^2 \tag{30b}$$

Although there are several other methods to estimate the parameters of a linear regression (e.g. Bartlett, EOF …), the least squares is a robust estimate when the errors are normally distributed and independent (Montgomery and Peck 1982, von Storch and Zwiers 1999).

## • Statistical significance tests

Statistical tests allow inferring general conclusions for an entire population from a limited random data sample. This is done using the statistical procedure of *hypothesis testing*, which consists in proposing an initial hypothesis (null hypothesis, H0) and deciding if it is rejected or not for a given *significance level* (i.e., the probability of rejecting H0 being true). A statistic, distributed following a given probability function if H0 is true, is computed from the sample data and placed in the corresponding distribution. The *significance level* (α) determines if the sample statistic falls into the non-rejection region (Fig. 5.1). If the statistic falls outside the non-rejection region the null hypothesis is rejected and the alternative hypothesis (H1) is accepted with a significance level of α. Depending on the aim, the interest of the user will be to reject or accept H0, and this drives the choice of the value of α.

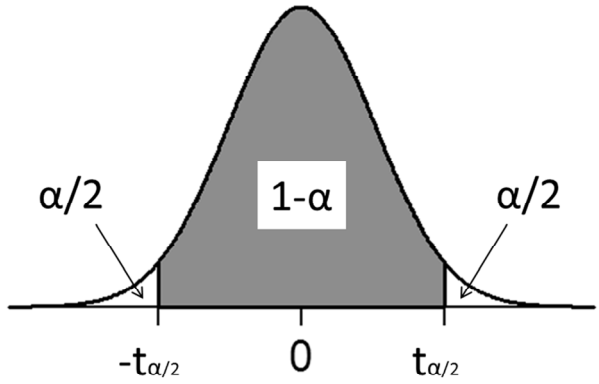


**Figure 5.1**. Probability density function of a statistic in the case of a two-tailed test. If the statistic falls under the shaded area (non-rejection region), H0 cannot be rejected with probability 1-α.

Three statistical parametric tests are used in this Thesis, described below.

i. *Test for the difference of means*.

In this test the null hypothesis is that the mean of two variables is equal (H0: $\mu_X = \mu_Y$). The statistic of this test for sample sizes $n_X \cong n_Y$ and $n_X + n_Y \geq 30$) follows a normal distribution, and H0 is rejected with significance level $\alpha$ if:

$$\frac{\left|\overline{x} - \overline{y}\right|}{\sqrt{\frac{S_{XX}^2}{n_X} + \frac{S_{YY}^2}{n_Y}}} > z_{\alpha/2} \tag{31}$$

where $S_{YY} = \sum_{i=1}^{n} y_i^2 - n \cdot \overline{y}^2$ and the other variables are defined above.

*ii. Student's t test for the correlation coefficient*

In order to determine if two variables are linearly correlated (even if the samples satisfy $r_{XY} \neq 0$) a statistical test must be performed, with the null hypothesis that the correlation coefficient is zero (H0: $\rho_{XY} = 0$), i.e., the variables X and Y are independent. The statistic is:

$$t = \left|r_{XY}\right| \sqrt{\frac{n-2}{1-r_{XY}^2}} \tag{32}$$

and follows a Student's t distribution with n-2 degrees of freedom. The null hypothesis is rejected, with significance level of $\alpha$, in the case $t > t_{\alpha/2}$.

*iii. Confidence interval for the linear regression slope*

A confidence interval for a given statistical significance level (α) can be defined for the linear regression slope estimate in Eq. (29b). The

confidence interval for the linear regression slope, with level of confidence of 1-$\alpha$, is given by:

$$\hat{a}_1 \pm t_{\alpha/2}\sqrt{\frac{S_{YY}-\frac{S_{XY}^2}{S_{XX}}}{S_{XX}(n-2)}} \qquad (33)$$

where $S_{XY}$, $S_{XX}$ and $S_{YY}$ are defined above.

In this Thesis the level of significance is chosen as α=0.01, that is, the level of confidence is 1- α=0.99 (the probability of accepting H0 being true).

## • Projections and extreme composites

The Objective 4 pursued in this Thesis (Section 4 of the Results) is to identify the main drivers of upwelling variability on sub-seasonal timescales. For this aim, it is useful to visualize the linear correlations of the time series of tropical upwelling with the series of the forcing field at each spatial point on a latitude-height plane. Such spatial representation of the correlations allows identifying the regions where the dynamical field is significantly correlated with the upwelling time series. It is common to combine this information with the projection in the latitude-height cross-sections. The projection of a field (with both spatial and temporal dimensions) onto a time series is obtained by multiplying the temporal anomalies of the field (that is the value at each time minus the temporal mean) by the standardized time series (i.e., the series divided by its standard deviation). The resulting representation has the units of the field per unit standard deviation in the series. Hence, the projections inform of the magnitude of the response, and are only relevant in regions where the correlations are statistically significant.

Finally, composite cross-sections are constructed by averaging a field for all the times at which a given condition is reached. The spatial structure corresponding to the extreme events (namely, strong and weak upwelling)

is then proven to be statistically different from the seasonal mean state using the Student's *t* test for the difference of means described above.

## b. *Spectral analyses*

Spectral analysis of a time series allows identifying the timescales on which the variance of a time series is concentrated. The basic concepts of this methodology are described below, as well as the application to perform spectral filters of time series as used in this Thesis. In addition, space-time cross-spectral analysis is described, as carried out in this Thesis.

### • Fourier transform and spectral filters

A time series of finite length $NT$ can be expanded into a finite series of sine and cosine functions (e.g., Bloomfield 2000):

$$x(t) = A_0 + \left\{ 2 \sum_{0<j<NT/2} \left[ A_j \cos(\omega_j t) + B_j \sin(\omega_j t) \right] \right\} + A_{NT/2} \cos(\omega_{NT/2} t), \quad \text{with } t = 0,1,\ldots,NT-1 \tag{34}$$

where the discrete angular frequencies are $\omega_j = 2\pi j / NT$, with $j = 1,2,\ldots,(NT-1)/2$, and the last term in Eq. (34) is included only if $NT$ is even. The coefficients in (34) are defined as:

$$A_0 = \frac{2}{NT} \sum_{t=0}^{NT-1} x(t) \tag{35a}$$

$$A_j = \frac{2}{NT} \sum_{t=0}^{NT-1} x(t) \cos(\omega_j t) \tag{35b}$$

$$B_j = \frac{2}{NT} \sum_{t=0}^{NT-1} x(t) \sin(\omega_j t) \tag{35c}$$

Making use of the Euler relation $e^{ix} = \cos x + i \sin x$, the sinusoids can be transformed into exponentials ($\cos x = (e^{ix} + e^{-ix})/2$, $\sin x = (e^{ix} - e^{-ix})/2$) and Eq. (34) can be expressed more compactly as:

$$x(t) = \sum_j X(\omega_j) e^{i\omega_j t} \tag{36}$$

The coefficients of the discrete Fourier transform (Eqs. 35) in this notation are:

$$X(\omega_j) = \frac{1}{NT} \sum_{t=0}^{NT-1} x(t) e^{-i\omega_j t} \tag{37}$$

These coefficients are complex numbers corresponding to:

$$X(\omega_j) = \frac{1}{2}\left( A_j - iB_j \right) \tag{38}$$

The periodogram shows how the variance of a time series is distributed across the different frequencies $\omega_j$, and is given by:

$$I_j = \frac{NT}{4}(A_j^2 + B_j^2) = NT \left| X(\omega_j) \right|^2 \tag{39}$$

The total variance of the time series is obtained integrating the periodogram for all the components:

$$\frac{1}{NT}\sum_{t=0}^{NT-1}\left(x(t)-\overline{x}\right)^2=\frac{1}{4}\sum_j\left(A_j^2+B_j^2\right)=\sum_j\left|X(\omega_j)\right|^2=\frac{1}{NT}\sum_j I_j \tag{40}$$

In the present Thesis the periodogram is computed using the Fast Fourier Transform (FFT) algorithm implemented in MATLAB[3]. The output of MATLAB's function FFT gives $NT$ coefficients, corresponding to the frequencies $f=\left(0,\frac{1}{NT},\frac{2}{NT},...,\frac{1}{2}-\frac{1}{NT},\frac{1}{2},-\frac{1}{2}-\frac{1}{NT},...,-\frac{1}{NT}\right)$, assuming $fs=1$. The co-spectrum between two series $x(t)$ and $y(t)$ can be computed from the Fourier transform coefficients of each of the series ( $X(\omega_j)$ and $Y(\omega_j)$ ) as:

$$CO(\omega_j)=\mathrm{Re}\left\langle X(\omega_j)\cdot Y(\omega_j)^*\right\rangle. \tag{41}$$

where the asterisk denotes the complex conjugate.

Spectral filters are commonly used to select or eliminate the variability corresponding to a given range of timescales from a signal. High-pass, low-pass and band-pass spectral filters are applied in this Thesis. In all cases, spectrally filtered time series are obtained following the steps:

1) Compute the FFT coefficients of the time series (Eq. 37).
2) Set to zero the FFT coefficients corresponding to the frequencies to be removed from the series (e.g. for high-pass filter remove all frequencies lower than a given threshold). That is, multiply the FFT output by the filtering vector $F(k)$, which takes values 0 or 1 $X_f(k)=X(k)*F(k)$.

[3] MATLAB's FFT coefficients are:

$$FFT(\omega_j)=\sum_{t=0}^{NT-1}x(t)e^{-i\omega_j t}=NT\cdot X(\omega_j).$$

3) Compute the inverse FFT of the result of step 2 (Eq. 36).

## • Space-time cross-spectrum calculations

In order to analyze the characteristics of zonally propagating waves, it is convenient to perform a space-time spectral decomposition of the fluctuating fields. Space-time spectral analysis allows representing the variance of the signal (initially expressed in terms of longitude and time) as a function of frequency (or period) and wavenumber. The technique for estimating the two-dimensional spectrum consists in performing two consecutive Fourier transforms, one in longitude and one in time (Hayashi 1982, Wheeler and Kiladis 1999). Following Welch (1967), the temporal dimension of the field is divided in segments of desired length depending on the timescales of interest, which can overlap. Each of the segments is weighted with a window function, with zero values at the extremes of the interval, and the overlapping helps minimizing the loss of data in the extremes. The periodogram is computed for each modified segment and then averaged together to obtain an estimate of the power spectrum. On the longitudinal dimension this procedure is not necessary because the periodicity is satisfied. The space-time field can be decomposed as a function of wavenumber $k$ and frequency $\omega$ (Hayashi 1982):

$$x(\lambda,t) = \mathrm{Re}\sum_{k}\sum_{\omega}\left[X(k,\omega)e^{i(k\lambda-\omega t)} + X(k,-\omega)e^{i(k\lambda-\omega t)}\right] \qquad (39)$$

where $\mathrm{Re}$ indicates the real value, $\lambda$ is the longitude and westward/eastward propagating waves are separated by taking positive and negative values of the frequency. The coefficients in (39) are given by:

$$X_{k\omega} = \frac{1}{2\pi NT}\sum_{t=0}^{NT-1}\sum_{\lambda=0}^{2\pi} x(\lambda,t)e^{-i(k\lambda+\omega t)}\,. \qquad (40)$$

The space-time power spectrum is the variance for each frequency and wavenumber, obtained averaging all segments:

$$P_{k,\omega} = \frac{1}{2}\left\langle \left| X_{k\omega} \right|^2 \right\rangle \tag{41}$$

where the angle brackets denote average over several calculations of $X_{k\omega}$ (for instance over several temporal segments).

In addition to decomposing one field into its spectral components, the space-time cross-spectrum can be computed between two fields. In this Thesis, eddy fluxes (i.e., the product of the zonal anomalies of two fields) are decomposed into contributions from different wavenumbers and phase-speeds. For this, the co-spectrum is first estimated as a function of wavenumber $k$ and frequency $\omega$, and then interpolated into a grid of phase-speeds ($c = \omega/(k/a\cos\phi)$), as described by Randel and Held (1991). Westward and eastward propagating waves are taken in this case as negative and positive phase speeds, respectively. The steps followed in this Thesis to compute the cross-spectral decomposition of the eddy flux $\overline{x'y'}$, with $x = x(\lambda,t)$ and $y = y(\lambda,t)$, are:

1) Select the extended winter season (DJFM) of each year from $x(\lambda,t)$, remove the mean and trend of each segment and apply a rectangular window of the size of the interval.
2) Compute the FFT for each of the temporal segments at each spatial location.
3) Compute the spatial FFT of the results from the previous step.
4) Average the result of 3) for all years to obtain an estimate of the Fourier transform.
5) Repeat steps 1-4 with the other field $x(\lambda,t)$.
6) Obtain the wavenumber-frequency co-spectrum as:

$$CO_{k\omega} = 2\left\langle \mathrm{Re}(X_{k\omega} \cdot Y^*_{k\omega}) \right\rangle \tag{41}$$

where the angle brackets indicate smoothing in frequency. Transform to co-spectra power density dividing by $\Delta\omega$.

7) Transform $CO_{k\omega}$ to wavenumber versus phase-speed co-spectrum ($CO_{kc}$), interpolating $CO_{k\omega}$ to a predefined phase-speed grid. In order to conserve total power, the interpolated data must be scaled:

$$CO_{k\omega} = CO_{kc} \cdot \frac{k}{a\cos\phi}, \tag{42}$$

8) The resulting co-spectral power density has units of the flux divided by $\Delta c = 1 m/s$. In Section 2 of the Results the co-spectrum is finally summed for all the wavenumbers and represented as a function of phase-speed and latitude (Abalos et al. 2013a).

## c. *Numerical tools*

**Derivatives** are computed in this Thesis using finite differences, combining centered differences with forward and backward differences at the extremes of the interval. The derivative of the function $f$ at one grid point $i$ is estimated from the neighboring points, which can be centered (c), backward (b) and forward (f) depending on the needs:

$$\left.\frac{df(x_i)}{dx}\right|_c \approx \frac{f(x_{i+1}) - f(x_{i-1})}{x_{i+1} - x_{i-1}} \tag{43a}$$

$$\left.\frac{df(x_i)}{dx}\right|_f \approx \frac{f(x_{i+1}) - f(x_i)}{x_{i+1} - x_i} \tag{43b}$$

$$\left.\frac{df(x_i)}{dx}\right|_b \approx \frac{f(x_i) - f(x_{i-1})}{x_i - x_{i-1}}. \tag{43c}$$

**Integrals** are computed using the trapezoidal rule. The area enclosed by the function $f$ between the points $a$ and $b$ can be approximated by the discrete sum of $N$ trapezoids:

$$\int_a^b f(x) \approx \frac{1}{2}\sum_{i=1}^{N}(x_{i+1}-x_i)(f(x_{i+1})+f(x_i)) \tag{44}$$

Finally, **linear interpolation** is performed to re-grid the data onto a different lattice. Assuming linear behavior between two consecutive grid points $(x_0, y_0)$ and $(x_1, y_1)$ the value of the function $y$ is deduced at an intermediate position $x$ as:

$$y = y_0 + (y_1 - y_0)\frac{x - x_0}{x_1 - x_0}. \tag{45}$$

# 6. Results

The Results Chapter is divided in four Sections, each one corresponding to one article written during the Thesis.

# 1 Variability in upwelling across the tropical tropopause and correlations with tracers in the lower stratosphere.

*Abalos, M., Randel, W. J. and Serrano, E., Atmos. Chem. Phys., 12, 11505–11517, doi:10.5194/acp-12-11505-2012, 2012.*

Atmos. Chem. Phys., 12, 11505–11517, 2012
www.atmos-chem-phys.net/12/11505/2012/
doi:10.5194/acp-12-11505-2012


Atmospheric Chemistry and Physics

# Variability in upwelling across the tropical tropopause and correlations with tracers in the lower stratosphere

**M. Abalos[1], W. J. Randel[2], and E. Serrano[1]**

[1]Depto. de Geofísica y Meteorología, Universidad Complutense de Madrid, Madrid, Spain
[2]National Center for Atmospheric Research, Boulder, Colorado, USA

*Correspondence to:* M. Abalos (mabalosa@fis.ucm.es)

Received: 12 July 2012 – Published in Atmos. Chem. Phys. Discuss.: 31 July 2012
Revised: 12 October 2012 – Accepted: 19 November 2012 – Published: 4 December 2012

**Abstract.** Temporal variability of the upwelling near the tropical tropopause on daily to annual timescales is investigated using three different estimates computed from the ERA-Interim reanalysis. These include upwelling archived by the reanalysis, plus estimates derived from thermodynamic and momentum balance calculations. Substantial variability in upwelling is observed on both seasonal and subseasonal timescales, and the three estimates show reasonably good agreement. Tropical upwelling should exert strong influence on temperatures and on tracers with large vertical gradients in the lower stratosphere. We test this behavior by comparing the calculated upwelling estimates with observed temperatures in the tropical lower stratosphere, and with measurements of ozone and carbon monoxide (CO) from the Aura Microwave Limb Sounder (MLS) satellite instrument. Time series of temperature, ozone and CO are well correlated in the tropical lower stratosphere, and we quantify the influence of tropical upwelling on this joint variability. Strong coherent annual cycles observed in each quantity are found to reflect the seasonal cycle in upwelling. Statistically significant correlations between upwelling, temperatures and tracers are also found for sub-seasonal timescales, demonstrating the importance of upwelling in forcing transient variability in the lower tropical stratosphere.

## 1 Introduction

The mean circulation in the tropical lower stratosphere is characterized by upwelling, which transports air masses across the tropical tropopause into the lower stratosphere. This constitutes the ascending branch of the global mean stratospheric circulation, which is completed by poleward flow in each hemisphere and subsidence at high latitudes (i.e. the so-called Brewer-Dobson circulation, Brewer, 1949; Dobson, 1956). This wave-driven circulation strongly influences the chemical composition and thermodynamic balance of the global stratosphere (e.g. Andrews et al., 1987). Despite the key role of tropical upwelling in the stratospheric circulation, there are significant uncertainties regarding its intensity and variability and the associated forcing mechanisms. Due to its small magnitude ($\sim 10^{-4}$ m s$^{-1}$) and the lack of direct measurements, lower stratospheric tropical upwelling is poorly constrained in current meteorological analysis systems; for example, Iwasaki et al. (2009) show substantial discrepancies in upwelling among different reanalysis data sets. Alternatively, the tropical upwelling has been estimated indirectly using thermodynamic balance (Gille et al., 1987; Rosenlof, 1995), momentum balance (Randel et al., 2002), and via variations in tracer concentration such as water vapor (e.g. Mote et al., 1996; Niwano et al., 2006; Schoeberl et al., 2008b). Observations show that fluctuations in tropical upwelling have an impact on the thermal and chemical behavior of the tropical tropopause layer (TTL), a transition region characterized by strong dynamical and chemical vertical gradients (Fueglistaler et al., 2009a). For instance, the strong annual cycle in temperature observed above the tropical tropopause is linked to the seasonality of the Brewer-Dobson circulation (Reed and Vlcek, 1969; Yulaeva et al., 1994). Randel et al. (2002) show that the vertical structure of the amplitude of the temperature annual cycle (peaking near 70 hPa) is consistent with the long radiative timescales in this region. They also highlight that sub-seasonal variations in temperature and tropical upwelling are closely coupled.

**Published by Copernicus Publications on behalf of the European Geosciences Union.**

High vertical resolution observations in the lower stratosphere also reveal a large annual cycle in ozone confined to a narrow region above the tropical tropopause (Logan, 1999; Folkins et al., 2006; Randel et al., 2007). Folkins et al. (2006) reproduce quite successfully the observed annual cycle by using a simple model including seasonal variations in tropical upwelling and in high altitude convective outflow. Using ozonesonde and satellite observations Randel et al. (2007) show that the temporal phasing and vertical structure of the ozone seasonal cycle can be explained by the seasonality in tropical upwelling acting on the strong background ozone vertical gradient. They also note that the seasonal cycle in ozone is approximately in phase with the temperature cycle, and both amplitudes show a very similar vertical structure. Schoeberl et al. (2008a) observe that there is almost no phase shift of the annual cycle in ozone with height in the lower tropical stratosphere, and this is consistent with seasonal variations in upwelling driving annual variations in ozone. In addition, Folkins et al. (2006), Randel et al. (2007) and Schoeberl et al. (2008a) analyze the annual cycle in carbon monoxide (CO) observed in this region, and conclude that the upwelling also has a dominant role in forcing this cycle (because of the strong background vertical gradient above the tropopause). Furthermore, it has been suggested that a comprehensive understanding of thermal behavior in this region must include a feedback of the ozone radiative effects on temperature (Chae and Sherwood, 2007; Fueglistaler et al., 2011). While there is general agreement on the origin of the annual cycle in temperature above the tropical tropopause, there is still controversy on the primary forcing mechanism(s) of the observed annual cycle in tracer concentrations (ozone and CO). For instance, Konopka et al. (2010) and Ploeger et al. (2012) suggest that in-mixing of air from the extra-tropics into the TTL makes a major contribution to the seasonal cycle in ozone concentration above the tropical tropopause. In particular, they propose that horizontal transport associated with the upper-level circulation of the Asian monsoon plays a dominant role in building the ozone maximum observed in boreal summer. This result, based on trajectory calculations using the Chemistry Lagrangian Transport Model of the Stratosphere (CLaMS), is in contrast with the view that the seasonal cycle in ozone is mainly forced by tropical upwelling (e.g. Randel et al., 2007). In addition to the seasonal cycle, high-temporal resolution satellite measurements of ozone and CO reveal variability on subseasonal timescales in this region. The analysis of these faster variations can provide complementary information on the relative roles of the different forcing mechanisms.

The aim of the present study is to investigate the relationships between tropical upwelling variability and the fluctuations in temperature and the concentrations of ozone and CO just above the tropical tropopause across a broad range of timescales. We seek to understand and quantify uncertainties in tropical upwelling by calculating three different estimates from reanalysis data. We then combine the meteorological data with satellite observations of tracer concentrations and examine correlated variability among temperature, ozone and CO in terms of coherence with upwelling, focusing separately on seasonal and sub-seasonal timescales.

## 2 Data and upwelling calculations

### 2.1 Satellite and meteorological data

Observations from the Microwave Limb Sounder (MLS) onboard the Aura satellite (Waters et al., 2006) cover now more than eight years (starting September 2004). We use zonal mean daily averaged measurements of ozone and CO for the period September 2004 to December 2010 on a 7.5° latitude grid, and analyze the time series averaged over the latitude band 18.75° N–S. This band is representative of the width of the tropics in the lowermost stratosphere, based on the autocorrelations of temperature, upwelling and tracers near the equator with other latitudes. There are three pressure levels within the tropical tropopause layer at which MLS measures carbon monoxide (147, 100 and 68 hPa) and five for ozone (147, 121, 100, 83 and 68 hPa). The vertical resolution of MLS ozone is approximately 3 km (Froidevaux et al., 2006), while the resolution for CO is 4.5 km (Livesey et al., 2008). The present study focuses on the effect of tropical upwelling at and above the tropical tropopause, so only the levels of 100 hPa and above are considered. As a note, water vapor is not included in this analysis because it is largely affected by dehydration near the cold point tropopause, and is less influenced by transport.

Upwelling estimates are derived from temperature and wind fields from the ERA-Interim reanalysis (Dee et al., 2011) generated at the European Centre for Medium-Range Weather Forecasts (ECMWF), with calculations described below. In view of the results of Seviour et al. (2011), who show large diurnal variability in ERA-Interim upwelling results, we compute daily averages from 6-hourly data. The meteorological data is archived on 60 vertical levels, with a horizontal resolution of $1.5° \times 1.5°$. The ERA-Interim reanalysis has been shown to provide an improved representation of the stratospheric Brewer-Dobson circulation and age of air compared to the previous ECMWF reanalysis, ERA-40 (Monge-Sanz et al., 2007; Fueglistaler et al., 2009b). Iwasaki et al. (2009) and Seviour et al. (2011) show that ERA-Interim yields less noisy vertical velocities compared to other reanalyses. We choose pressure levels for this analysis of 100, 80 and 70 hPa, to nearly match the levels of constituent observations (broad layers centered at 100, 83 and 68 hPa).

Time series of tropical zonal mean temperatures in the lower stratosphere from the ERA-Interim data are shown in Fig. 1 (averaged over 18° N–S), together with ozone and CO concentrations from MLS as described above. Each of the time series in Fig. 1 is standardized to unit variance, and CO is plotted on an inverted scale. The results in Fig. 1 show

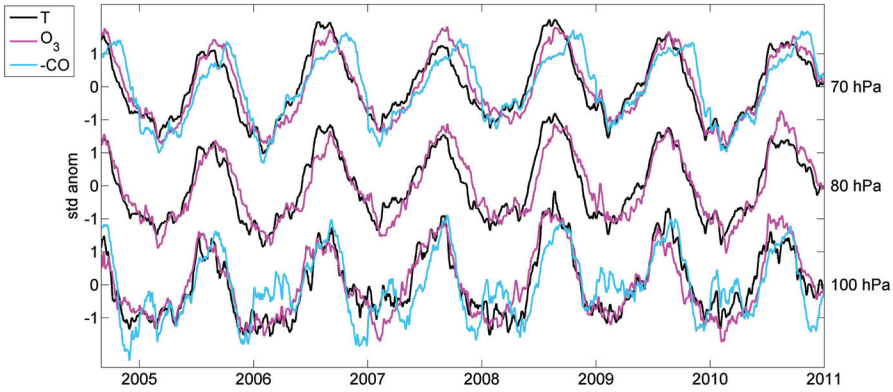


**Fig. 1.** Time series of standardized anomalies of daily temperatures from ERA-Interim and ozone and CO mixing ratio measurements from MLS averaged over 18° N–S at three pressure levels across the tropical tropopause (70, 80 and 100 hPa from top to bottom; levels shown for MLS are 68, 83 and 100 hPa). 3-days running means are applied to the daily series. CO concentrations are plotted on a reversed scale in order to highlight the common fluctuations.

coherence among the time series of reanalysis temperatures and the completely independent satellite constituent observations. The common variability is especially evident in the large annual cycles, which are approximately in phase over the three pressure levels (with the -inverted- minimum in CO having a time lag of ∼2 months compared to the maxima in temperature and ozone at 70 hPa). There is an additional semi-annual component evident for CO at 100 hPa, related to seasonally dependent tropospheric sources and convective transport, as discussed further in Sect. 3. There is also evidence for correlated sub-seasonal variability in Fig. 1, suggesting that these variations share a common forcing. In this study we examine the role of the tropical upwelling variability in forcing these joint fluctuations of temperature, ozone and CO.

### 2.2 Upwelling calculations

Three different estimates of zonal average tropical upwelling are obtained using the temperature and wind fields from ERA-Interim, including direct upwelling from the reanalysis, and estimates calculated from thermodynamic and momentum balances. The details of these latter calculations can be found in Randel et al. (2002); here we focus on highlighting the main uncertainties associated with each estimate. The first, which will be referred to as $\overline{w}^*$, is the vertical component of the residual circulation in the Transformed Eulerian Mean (TEM) formulation in log-pressure coordinates as defined in Andrews et al. (1987):

$$\overline{w}^* \equiv \overline{w} + \frac{1}{a\cos\phi}\frac{\partial}{\partial\phi}\left(\cos\phi\frac{\overline{v'T'}}{S}\right) \quad (1)$$

where $S$ is the static stability parameter, $S = HN^2/R$, a function of the Brunt-Väisälä frequency ($N$), with $H = 7$ km and $R = 287\,\mathrm{m^2\,s^{-2}\,K^{-1}}$, and the rest of the notation is the same as in Andrews et al. (1987). In the tropics the $\overline{v'T'}$ term in Eq. (1) is small, so that $\overline{w}^*$ primarily depends on the reanalysis zonal mean vertical velocity ($\overline{w}$). Although one of the major improvements in this third-generation reanalysis compared to its predecessor ERA-40 is the weaker and hence more realistic stratospheric circulation (Dee et al., 2011), there are still large uncertainties in this magnitude, especially near the tropical tropopause.

The second estimate is calculated from the momentum balance using the expression (11) in Randel et al. (2002), obtained combining the TEM momentum and continuity equations:

$$\langle\overline{w}^*_m\rangle(z) = \quad (2)$$
$$\frac{-e^{z/H}}{\int_{-\phi_0}^{\phi_0} a\cos\phi d\phi}\left\{\int_z^\infty \frac{e^{-z'/H}\cos\phi}{\hat{f}(\phi,z')}\left[DF(\phi,z') - \overline{u}_t(\phi,z')\right]_{\overline{m}} dz'\right\}_{-\phi_0}^{\phi_0}$$

Here $DF$ is the scaled Eliassen-Palm flux divergence, $\hat{f} = f - (1/a\cos\phi)(\partial/\partial\phi)(\overline{u}\cos\phi)$, where $f$ is the Coriolis parameter, and $\overline{u}_t$ is the zonal mean zonal wind tendency. This expression gives the tropical upwelling at a fixed pressure level and averaged over a latitudinal band ($\pm\phi_0$) which is in balance with the circulation and eddy forcing calculated from the reanalysis. To simplify the calculations, the integrand is computed on constant latitudes instead of along isolines of constant zonal mean angular momentum, since at the latitudinal boundaries we use (±18° ) these isolines are approximately vertical. The divergence of the Eliassen-Palm flux includes eddy fluxes calculated from the three-dimensional temperature and wind fields from the reanalysis, such that a key uncertainty in the calculation of $\overline{w}^*_m$ is associated with the unresolved waves that are not taken into account in these

fluxes. As a note, the model simulations in Garcia and Randel (2008) and Calvo and Garcia (2009) suggest that, for the range of latitude/altitude considered here, resolved waves explain most of the upwelling.

The third estimate of upwelling is derived by iteratively solving the TEM thermodynamic equation (Eq. (4) below) neglecting the eddy transport term (last term on the right hand side in Eq. (4)) and the TEM continuity equation:

$$\frac{1}{a\cos\phi}\frac{\partial}{\partial\phi}\left(\overline{v}^*\cos\phi\right)+e^{z/H}\frac{\partial}{\partial z}\left(\overline{w}^*e^{-z/H}\right)=0 \qquad (3)$$

following the procedures described in Rosenlof (1995). In this calculation one relevant source of uncertainty is associated with the heating rates ($Q$) in the thermodynamic equation. For levels at and above 100 hPa, radiative heating is the primary diabatic forcing, and hence $\overline{w}^*_Q$ can be estimated using an accurate radiative heating code. We use the heating rates from the National Center for Atmospheric Research Column Radiation Model (NCAR-CRM; Gettelman et al., 2004) with input of daily ERA-Interim temperatures and MLS ozone. The annual mean heating rates provided by this model agree reasonably well with other estimates near the tropical tropopause in terms of the magnitude and the vertical structure (Gettelman et al., 2004). Also the seasonality in our calculations is consistent with that shown in Yang et al. (2008), with highest values in DJF and lowest in JJA. Our results are ∼0.1 K day$^{-1}$ higher in the annual mean compared to Yang et al. (2008), but this difference is within the range of uncertainty defined by the spread of a set of five different estimates shown in Gettelman et al. (2004). A more relevant difference is that our calculations do not result in near-zero heating rates during NH summer across ∼70 to 50 hPa, as shown in Yang et al. (2008). As a consequence, the amplitude of the seasonal cycle in our heating rates over these levels (∼0.1 K day$^{-1}$) is approximately half of theirs. Nevertheless, the interpretation of the near-zero heating rates in Yang et al. (2008) is not clear to us, as they imply near-zero downward net mass flux outside the tropics in order to satisfy mass continuity. Finally, we note that our calculations do not include the effects of clouds on the radiative balance. However, according to Yang et al. (2010), the net effect of clouds on the zonal mean heating rates in the tropics is relatively small ($\leq -0.05$ K day$^{-1}$) at and above the tropical tropopause.

One aspect of the $\overline{w}^*_Q$ calculations is that the computed vertical velocities may not satisfy the constraint of zero net mass flux across a pressure surface (Rosenlof, 1995). Hence, the calculated vertical velocities require some adjustment to enforce this constraint, although the method of making this adjustment is arbitrary. Figure 2 shows a comparison of the latitudinal profile of the three estimates of upwelling, for the annual mean of the entire period. Two different calculations of $\overline{w}^*_Q$ are also included, based on making a constant adjustment independent of latitude or only adjusting values over 45° N–S. The different adjustments yield very similar values

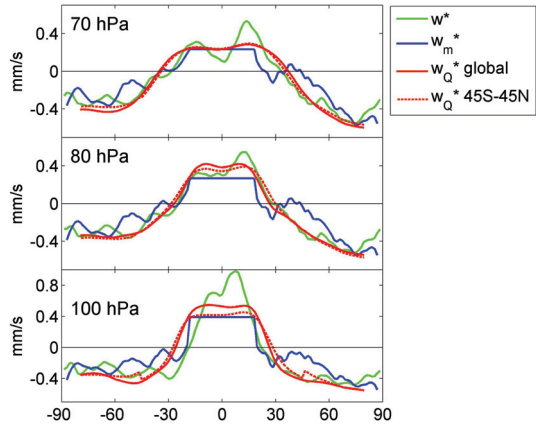


**Fig. 2.** Latitudinal structure of the three upwelling estimates at the indicated pressure levels (70, 80 and 100 hPa from top to bottom). Green: residual circulation ($\overline{w}^*$) blue: momentum balance estimate ($\overline{w}^*_m$), and red: thermodynamic estimate ($\overline{w}^*_Q$). Two red lines are shown: the solid line is the thermodynamic upwelling estimate computed with the global adjustment and the dashed line adjusting only within the range 45° N–S (see text for details) (mm s$^{-1}$).

of $\overline{w}^*_Q$ at 70 hPa, but larger variations are found at lower levels, where the adjustment focused over low latitudes provides smaller values of upwelling. This could be related to the larger contribution of the eddy term in the thermodynamic balance (Eq. 4) at these lower levels, which is confined to low latitudes (results based on analysis of ERA-Interim data, not shown here). The eddy term is neglected in our calculations of $\overline{w}^*_Q$, and this is a source of bias for this estimate (particularly at 80 hPa, where this term is largest), as further discussed in Sect. 3.1. By adjusting $\overline{w}^*_Q$ only in the range 45° N-S we partly account for these larger biases at low latitudes, and this is the $\overline{w}^*_Q$ used throughout the rest of this work. On the other hand, the vertical velocity can be obtained from momentum balance everywhere except in the deep tropics, where $\hat{f} \to 0$, and hence Eq. (2) yields a constant value for $\overline{w}^*_m$ throughout the width of the tropics (18° N-S), as shown in Fig. 2.

### 2.3 Comparisons of upwelling estimates

The time average comparisons in Fig. 2 show overall agreement in the magnitude and latitudinal structure of all the estimates, with the upwelling from reanalysis, $\overline{w}^*$, showing somewhat stronger tropical upwelling compared to $\overline{w}^*_m$ and $\overline{w}^*_Q$, especially at 100 hPa. Note that the magnitude of $\overline{w}^*_Q$ is likely overestimated at 80 hPa in the tropics, as discussed in Sect. 3.1. Time series of each of the upwelling estimates averaged over 18° N-S are shown in Fig. 3 for pressure levels 100, 80 and 70 hPa. This figure also shows corresponding mean seasonal cycles, calculated as monthly averages over

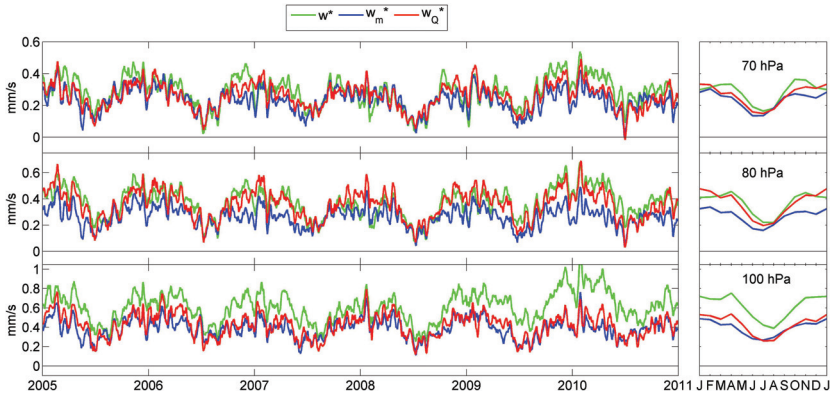


**Fig. 3.** Time series and mean seasonal cycles of the three upwelling estimates averaged over 18° N–S at 70, 80 and 100 hPa (top to bottom panels). Green: residual circulation ($\overline{w}^*$), blue: momentum balance estimate ($\overline{w}^*_m$), and red: thermodynamic estimate ($\overline{w}^*_Q$). 11-days running means are applied to the time series. The annual cycles are calculated as monthly means over 2005–2010 (mm s$^{-1}$).

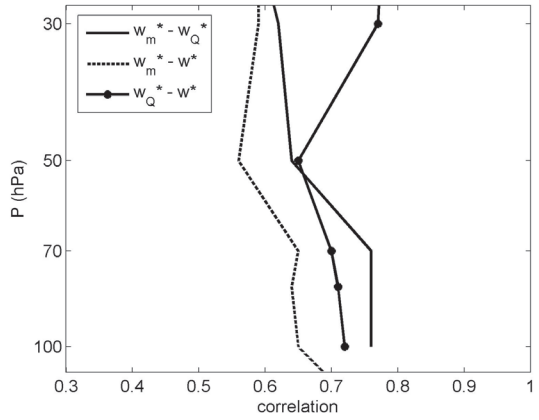


**Fig. 4.** Linear correlations among the time series of the three upwelling estimates as a function of pressure.

the entire data record. Figure 3 shows overall good agreement among the time series and the mean seasonal variation of the three upwelling estimates, especially between $\overline{w}^*_m$ and $\overline{w}^*_Q$. Inspection of the variability in the time series reveals strong similarities among the three estimates, showing numerous common fluctuations on a wide range of timescales. Note that the good agreement between $\overline{w}^*_m$ and $\overline{w}^*_Q$ suggests that $\overline{w}^*_m$ may be accurately calculated from resolved eddy fluxes alone. Correlations between the different estimates are shown in Fig. 4. The correlations among $\overline{w}^*$, $\overline{w}^*_m$ and $\overline{w}^*_Q$, in the tropical lower stratosphere are around 0.64–0.76. These fairly high correlations between the estimates are encouraging, given the uncertainties described above and the very different approaches followed to compute them. The degree of agreement among these estimates reflects a reasonably good understanding of the seasonal and sub-seasonal variability in tropical upwelling.

## 3 Co-variations of upwelling, temperatures and tracers

A simple explanation for the strong correlations between temperatures and tracers in the tropical lower stratosphere (Fig. 1) is that they result primarily from forcing by tropical upwelling. The origin of this coupling can be appreciated by examining the zonal mean thermodynamic and tracer mixing ratio continuity equations in the TEM formalism (Andrews et al., 1987):

$$\frac{\partial \overline{T}}{\partial t} = -\overline{v}^* \frac{1}{a}\frac{\partial \overline{T}}{\partial \phi} - \overline{w}^* S + \overline{Q} \qquad (4)$$

$$-\frac{1}{e^{-z/H}}\frac{\partial}{\partial z}\left[e^{-z/H}\left(\overline{v'T'}\frac{\partial \overline{T}/\partial \phi}{a \cdot S} + \overline{w'T'}\right)\right]$$

$$\frac{\partial \overline{\chi}}{\partial t} = -\overline{v}^* \frac{1}{a}\frac{\partial \overline{\chi}}{\partial \phi} - \overline{w}^* \frac{\partial \overline{\chi}}{\partial z} + \nabla \cdot \boldsymbol{M} + P - L \qquad (5)$$

In the continuity Eq. (5), $\overline{\chi}$ represents the zonal mean mixing ratio of the tracer, $\nabla \cdot \boldsymbol{M}$ is the eddy transport term (as in Andrews et al., 1987, Eq. 9.4.13) and $P - L$ is the chemical production minus loss rate. Averaging over the tropics and for a given pressure level, these equations state that the changes in tropical mean temperature or tracer concentration arise from the combined effects of meridional and vertical advection by the residual mean circulation (that is, mean meridional transport to/from the extra-tropics and upwelling acting on the background vertical gradient), eddy transport and diabatic heating in the case of temperature or chemical sources/sinks for tracers. Equations (4) and (5) form the basis for our analysis of temperature and tracer coupling with

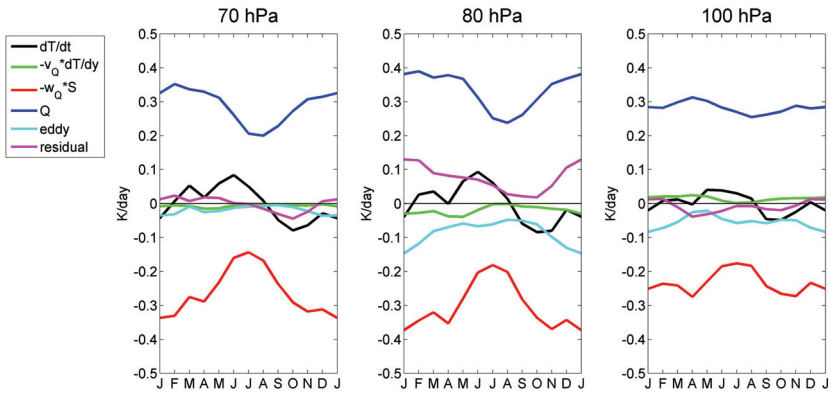


**Fig. 5.** Mean seasonal cycle (monthly means for the period 2005-2010) of the terms in the thermodynamic equation (Eq. 4) averaged over 18° N–S for the three pressure levels indicated. The residual is defined as the difference between the tendency and the sum of all the explicitly evaluated terms (K day$^{-1}$).

mean tropical upwelling, and we focus separately on the seasonal cycle and sub-seasonal variations seen in Figs. 1 and 3.

### 3.1 Seasonal cycles

In order to evaluate the relative contribution of the different forcings to the seasonal cycles of temperature, ozone and CO, we analyze the monthly means for the entire period (2005–2010) of all the terms in Eqs. (4) and (5). Figure 5 shows the seasonal average thermodynamic balance, after averaging Eq. (4) over a latitudinal band of 18° N–S, using the estimate of $\overline{w}^*_Q$ for mean upwelling. $\overline{Q}$ is calculated from the radiative heating code as described in Sect. 2.2.

The primary thermodynamic balance in the tropical lower stratosphere in Fig. 5 is between upwelling (adiabatic cooling) and diabatic heating (i.e. $\overline{w}^*_Q S \sim \overline{Q}$). The temperature tendency is a relatively small component of the balance, and the meridional advection term is negligible. We have included the eddy term in Fig. 5 (derived from the ERA-Interim eddy fields), even though it is not used to compute $\overline{w}^*_Q$, as explained in Sect. 2.2. This term shows a maximum in the tropics near 80 hPa, which is mainly associated with the vertical convergence of the vertical eddy heat flux ($\overline{w'T'}$) in Eq. (4). There are small residuals in Fig. 5 at 70 hPa (where the eddy term is almost zero) and 100 hPa, indicating that the magnitude and seasonality of the computed estimate $\overline{w}^*_Q$ are consistent with the total thermodynamic balance at these levels. On the other hand, at 80 hPa the residual approximately mirrors the relatively large negative eddy term. This implies that, as a result of neglecting the eddies in the thermodynamic equation, the magnitude of the computed upwelling is overestimated at 80 hPa (by about $\sim$0.15 mm s$^{-1}$ in the annual mean). Nevertheless, it should be borne in mind that the vertical eddy heat flux ($\overline{w'T'}$) in Fig. 5 is likely subject to large uncertainties associated with the reanalysis eddy vertical velocity anomalies. The overall balances are similar if $\overline{w}^*_m$ or $\overline{w}^*$ are used instead of $\overline{w}^*_Q$, although larger residuals are derived when using $\overline{w}^*$ (especially at 100 hPa). The interpretation of the $\overline{w}^*_Q S \sim \overline{Q}$ balance is that upwelling forces tropical temperatures below radiative equilibrium ($\overline{T}_{\rm eq}$), and the atmosphere responds locally by longwave radiative heating. This radiative heating is due primarily to the effects of longwave forcing by ozone and $CO_2$ (e.g. Thuburn and Craig, 2000; Gettelman et al., 2004), and $\overline{Q}$ can be reasonably approximated in this region by Newtonian cooling: $\overline{Q} \sim -\alpha_{\rm rad}\left(\overline{T} - \overline{T}_{\rm eq}\right)$, where $\alpha_{\rm rad}$ is an inverse radiative relaxation timescale and $\overline{T}_{\rm eq}$ is a background radiative equilibrium temperature. The seasonal variations in upwelling are echoed in approximately mirror image variations in $\overline{Q}$ at 70 and 80 hPa in Fig. 5: weaker NH summer upwelling results in warmer temperatures and weaker radiative heating, and there is a slight delay in $\overline{Q}$ compared to $\overline{w}^*$ because of the $\sim$1–2 month radiative relaxation timescale in the lower stratosphere. The longer relaxation timescales (smaller $\alpha_{\rm rad}$) also result in relatively larger temperature variations for these pressure levels (cf. Randel et al., 2002). Although the seasonal variation in upwelling at 100 hPa is around a factor of 2–2.5 (Fig. 3), the upwelling transport term in Fig. 5 at this level varies only $\sim$1.5. This is because there is a seasonal cycle in static stability $S$ at 100 hPa (with NH summer values $\sim$1.5 times larger than winter), so that the quantity $\overline{w}^*_Q S$ varies much less than $\overline{w}^*_Q$ alone. This partial compensation results in smaller seasonal variations in $\overline{Q}$ and $\partial\overline{T}/\partial t$ at 100 hPa compared to higher levels.

Figure 6 shows the analogous calculations for the zonal average ozone continuity equation (Eq. (5)), where the explicitly evaluated terms include the tendency of the ozone mixing ratio, the meridional advection, and the upwelling forcing. We have also included an ozone photochemical production

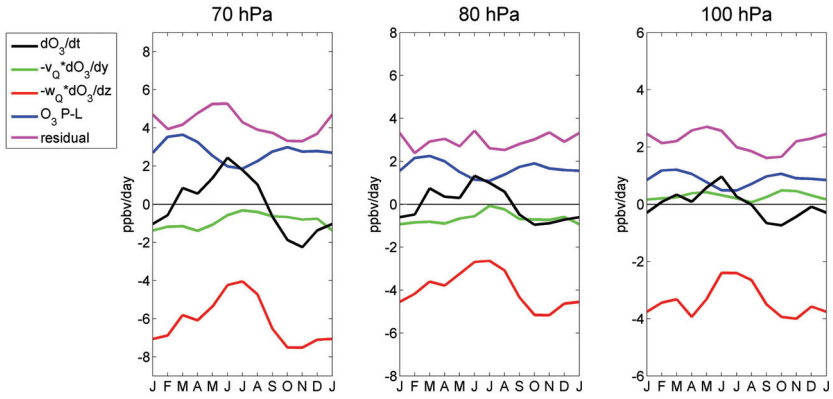


**Fig. 6.** Mean seasonal cycle for the period 2005–2010 of the terms in the continuity equation for ozone concentration (Eq. 5) averaged over 18° N–S at the indicated levels (ppbv day$^{-1}$).

minus loss term ($P-L$ in Eq. (5)), obtained from a long-term simulation using the WACCM (Whole Atmosphere Community Climate Model) chemistry-climate model (Doug Kinnison 2011, personal communication). The photochemical production in Fig. 6 shows a weak semi-annual cycle, following the solar declination in the tropics. Figure 6 also shows the residual of the calculated balance, which is a relatively large positive term at each level (∼4–5 ppbv day$^{-1}$ at 70 hPa), and represents eddy transport terms (not explicitly computed in these calculations due to the coarse horizontal resolution of the tracer observations) plus uncertainties in the rest of the terms. The presence of a significant residual in these calculations is consistent with the importance of eddy transport into the tropics for the ozone budget, as suggested previously by Konopka et al. (2010) using a three-dimensional Lagrangian transport model. We note that the residuals in Fig. 6 do not show large annual variations and, particularly at 70 hPa, the seasonality in the upwelling term is dominant.

The overall seasonal behavior of the ozone budget (Fig. 6) highlights tropical upwelling as a primary forcing term, with the ozone tendency closely following the upwelling term. There is strong similarity to the seasonal thermodynamic balance (Fig. 5), and the dominant role of upwelling in both balances suggests that the in-phase annual cycles in ozone and temperature seen in Fig. 1 are linked as a response to the seasonal variation in upwelling. As in the case of temperature, the upwelling forcing on ozone has a smaller seasonal cycle at 100 hPa compared to the higher levels due to the partial cancellation between the annual cycles of tropical upwelling (largest during NH winter) and ozone vertical gradient (smallest during NH winter; result not shown). In fact, the latter is very similar to the seasonal cycle of the static stability at this level.

The seasonal balance for zonal average CO at 70 hPa is shown in Fig. 7. This is the level where the relative vertical gradient in background CO is largest, and so it is anticipated that the vertical transport has a large influence on observed variability. In these budget calculations we have also included a chemical production minus loss term in Eq. (5) for CO; the loss is approximated by $\beta \cdot$CO, with $\beta$ an inverse chemical damping timescale of 100 days (estimated from WACCM data), and a small chemical production term is also obtained from WACCM. The time average budget in Fig. 7 reflects a balance between CO increase due to vertical transport and decrease due to photochemical loss. A seasonal variation of approximately a factor of 2 is found for the contribution of upwelling to the CO budget in Fig. 7 (which simply follows the annual cycle in upwelling), and the observed CO tendency closely follows this seasonality. The photochemical loss approximately mirrors the upwelling

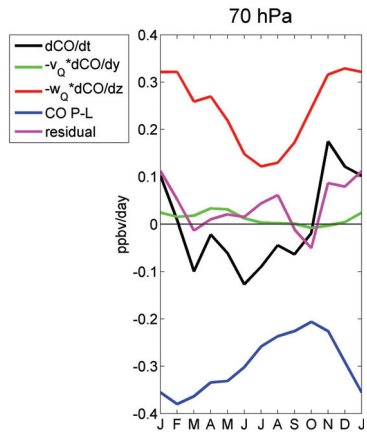


**Fig. 7.** Mean seasonal cycle (2005–2010) of the terms in the CO continuity equation at 70 hPa averaged over 18° N–S (ppbv day$^{-1}$).

tendency, with a time lag of several months. The calculated residual is a relatively small component of the CO balance for most months, suggesting a relatively simple balance for CO in the tropical lower stratosphere. There is a larger residual during November–January in Fig. 7, which may be due to unresolved eddy transport effects or to uncertainties in calculations for the resolved terms. The seasonal CO budget at 100 hPa (not shown) is dominated by the semi-annual cycle in CO concentrations seen in Fig. 1, and is somewhat more complicated than the 70 hPa results in Fig. 7. The characteristic double peak in CO in the tropical upper troposphere (seen for 100 hPa data in Fig. 1) is associated with emissions from biomass burning before the rain seasons, coupled with the semi-annual cycle in near-equatorial convection (Folkins et al., 2006; Schoeberl et al. 2006; Liu et al, 2007). The overall smaller residuals obtained in the CO balance compared to ozone, suggest that eddy mixing makes a more modest contribution to the CO tropical budget. Reduced horizontal eddy transport for CO is consistent with the relatively smaller meridional gradients in this tracer compared to ozone (as pointed out in Ploeger et al., 2012).

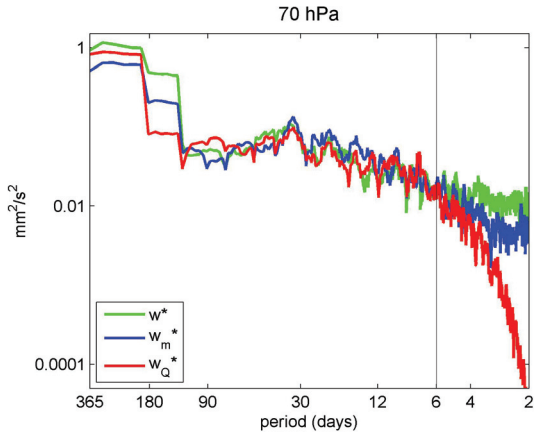


**Fig. 8.** Power spectra of the three upwelling estimates at 70 hPa as a function of log-frequency. An 11-point running mean was applied to the spectra ($mm^2\ s^{-2}$).

### 3.2 Sub-seasonal variability

The time series in Fig. 1 reveal correlated variations between temperatures and tracers at timescales shorter than the annual cycle. Sub-seasonal variations in upwelling (as seen in Fig. 3) are one likely source for such correlated variability, and here we investigate the links between upwelling and tracer variations on sub-seasonal timescales. In these analyses we focus on comparing time tendencies of temperature and tracers (i.e. $\partial\overline{T}/\partial t$, $\partial\overline{O_3}/\partial t$ and $\partial\overline{CO}/\partial t$) with the various estimates of upwelling, following the expected relationships based on Eqs. (4) and (5).

Assuming the idealized case where for transient variations the vertical velocity terms dominate the thermodynamic and continuity equations (i.e. neglecting meridional advection, eddy transport, radiative or chemical forcing terms), Eqs. (4) and (5) reduce to:

$$\frac{\partial\overline{T}}{\partial t} = -\overline{w}^* S \tag{6}$$

$$\frac{\partial\overline{\chi}}{\partial t} = -\overline{w}^* \overline{\chi}_z \tag{7}$$

with $\overline{\chi}_z \equiv \partial\overline{\chi}/\partial z$. These simplified equations directly relate the tendencies to $\overline{w}^*$, and imply that for these idealized conditions (where $\overline{w}^*$ dominates the transport) the temperature and tracer tendencies are closely linked:

$$\left(\frac{\partial\overline{\chi}}{\partial t}\right) \Big/ \left(\frac{\partial\overline{T}}{\partial t}\right) = \overline{\chi}_z / S \sim \text{constant} \tag{8}$$

(and similarly, the ratio of tendencies for different tracers are related by the ratios of their respective background vertical gradients). The ratio $\overline{\chi}_z/S$ can be considered approximately constant, given that the tracer vertical gradients and the static stability are nearly stationary on sub-seasonal timescales. We note that the strong relationships with upwelling are most likely to occur in the region of largest background vertical gradients (i.e., near 70 hPa for ozone and CO).

In the following analyses we focus on sub-seasonal variations associated with timescales shorter than one year and longer than 6 days, isolated by harmonic analysis of the respective time series. The 6-day frequency cutoff is intended to remove the day-to-day variability in the different upwelling estimates, which shows large differences among the different calculations and little coherence with temperatures or tracers. In fact, the correlations in Fig. 4 increase by about ∼0.1 if these high frequencies are filtered out. Figure 8 shows the power spectra of the three upwelling estimates at 70 hPa to illustrate the very different spectral behavior of the data at the highest frequencies, motivating the high frequency (6-day) cutoff. Our detailed results are not sensitive to the exact choice of high frequency cutoff.

Figure 9 shows standardized anomalies of the temperature, ozone and CO tendencies at 70 hPa, together with corresponding time series of upwelling for a period of one year (2010), in order to focus on detailed sub-seasonal behavior. Visual inspection of Fig. 9 shows coherent variations between $\partial\overline{T}/\partial t$ and $\partial\overline{O_3}/\partial t$ at 70 hPa, and somewhat lower agreement of $\partial\overline{CO}/\partial t$ with the other two series. Time series of the upwelling estimates show highly coherent variations, which often show good correspondence with the temperature and tracer tendencies.

The correlations between sub-seasonal variations in upwelling and tendencies of temperature and tracers are shown in Fig. 10 (calculated from data over all years 2005–2010), for altitude levels over 100–30 hPa; these include results for

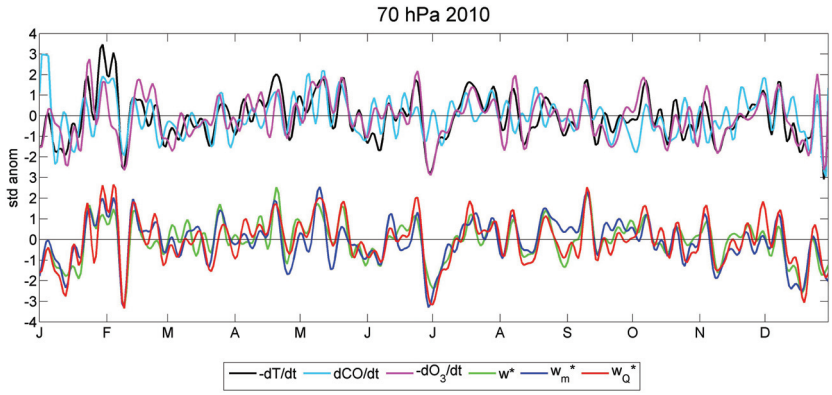


**Fig. 9.** Top curves show time series for the year 2010 of standardized anomalies of temperature (black), ozone (purple) and CO (light blue) tendencies. Bottom curves show the three estimates of upwelling: $\overline{w}^*$ (green), $\overline{w}^*_m$ (blue) and $\overline{w}^*_Q$ (red) at 70 hPa. Temperature and ozone tendencies are plotted on a reversed scale. All series are filtered to remove timescales $\geq 1$ yr and $\leq 6$ days.

each of the three different upwelling estimates. Taking into account the appropriate degrees of freedom for these data, correlations above 0.12 are significant at the 99 % level.

Temperature tendencies (Fig. 10a) show highly significant correlations with each of the upwelling estimates, with small variations with altitude. Very high correlations ($>0.8$) are found for $\overline{w}^*_Q$, and this is expected as $\overline{w}^*_Q$ is calculated using thermodynamic balance with observed $\partial\overline{T}/\partial t$. Correlations of $\partial\overline{T}/\partial t$ with $\overline{w}^*_m$ and $\overline{w}^*$ are somewhat lower but still highly significant ($\sim$0.7), and this enhances confidence in these estimates.

Correlations between ozone tendencies and upwelling (Fig. 10b) show overall significant values, with similar results for the different upwelling estimates. The largest correlations are found at 70 hPa and above, and this is reasonable as the background vertical gradient of ozone is larger at these levels. For CO tendencies (Fig. 10c), the correlations are somewhat lower compared to ozone, with a different vertical structure that shows largest correlations at 100 and 70 hPa and almost zero at 50 hPa. It is important to note that due to the $\sim$4.5 km vertical resolution of MLS CO observations, particular caution should be taken when drawing conclusions based upon the detailed vertical structure of CO. Also, near 50 hPa the absolute values of CO mixing ratio are very small ($\sim$10–20 ppbv) and hence it is likely that measurements at these upper levels are subject to larger relative uncertainties. Note that MLS measurements currently constitute the only available observational dataset of CO with daily temporal resolution in this region.

Further confirmation that sub-seasonal variations in upwelling make an important contribution to sub-seasonal variability in the tracer fields is provided by comparing the observed ratios of tracer versus temperature tendencies to the theoretical estimate (i.e. time-mean $\overline{\chi_z}/S$, Eq. 8). Figure 11a shows a scatter diagram of $\partial\overline{T}/\partial t$ versus $\partial\overline{O_3}/\partial t$ for the 70 hPa data (as shown in Fig. 9 but for the entire period), showing a significantly correlated distribution ($r = 0.63$) with a linear slope of $20.4 \pm 1.9$ ppbv K$^{-1}$ (estimated using least squares linear regression, including a 2-sigma uncertainty level). This observed slope compares quite well with the theoretical value $\overline{\chi}/S = 23.4$ ppbv K$^{-1}$ at 70 hPa, indicating that the observed variations are not too far from the case of variability controlled by upwelling via Eqs. (6)–(8). Figure 11b shows a similar diagram for $\partial\overline{T}/\partial t$ versus $\partial\overline{CO}/\partial t$ statistics at 70 hPa. In this case there is a larger dispersion of the scattered points and the correlation is lower ($r = -0.47$). This could be at least partly related to the coarser vertical resolution of CO observations discussed above. The slope given by Eq. (8) for this tracer is $-0.90$ ppbv K$^{-1}$, and the linear regression gives a similar slope of $-1.14 \pm 0.16$ ppbv K$^{-1}$. Overall the observed slopes for both ozone and CO in Fig. 11 are reasonably similar to calculations based on the highly idealized situation where upwelling is the dominant forcing mechanism for sub-seasonal variability (although the theoretical slopes lie outside of the 2-sigma (95 %) bounds of the regression slopes in both cases, which could result from data uncertainties or additional forcing mechanisms). These results are consistent with the coherent fluctuations observed between upwelling and tracer tendencies in Figs. 9 and 10.

It is worth noting that the lines in Fig. 11 have a smaller slope than what a visual examination of the scattered data points suggests. A simple analysis with synthetic data was made to understand this discrepancy. We constructed two linearly related variables (y = mx) and added some noise (normally distributed random variations) to each variable independently. Inspection of the scatter diagrams for different noise levels revealed that the actual slope (=m by construction) coincides with the visual slope only if the amount of

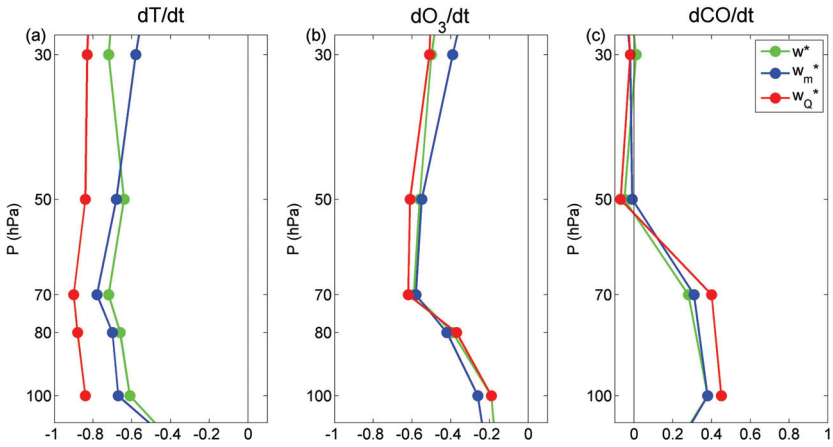


**Fig. 10.** Linear correlations as a function of pressure between the upwelling estimates and temperature **(a)**, ozone **(b)** and CO **(c)** tendencies. Results are shown for the three estimates ($\overline{w}^*$ in green, $\overline{w}^*_m$ in blue and $\overline{w}^*_Q$ in red). The correlations are calculated between the sub-seasonal time series (6 days < periods < 1 yr) as shown in Fig. 10 but for the 6-yr long (2005–2010) time series. The 99 % significance level is $\alpha \sim 0.12$.

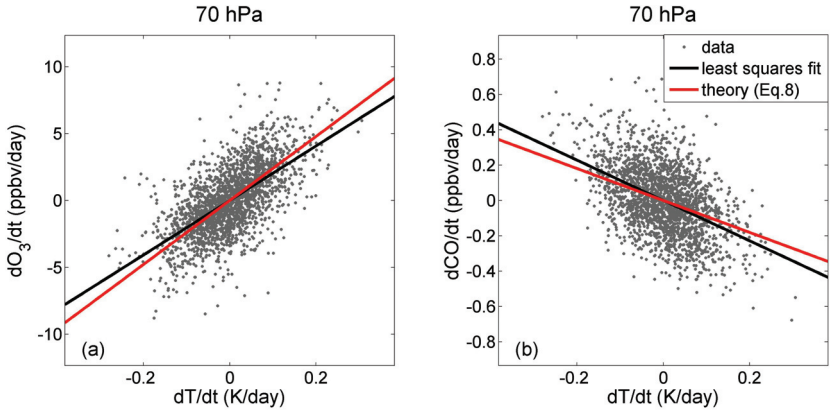


**Fig. 11.** Scatter diagrams of **(a)** ozone and **(b)** CO tendency versus temperature tendency at 70 hPa. The dots correspond to sub-seasonal filtered data as in Figs. 9 and 10. The black line is the least squares linear fitting of the data and the red line is the estimated slope using the simplified relation ($\overline{\chi}_z/S$) from Eq. (8).

noise in both variables is comparable; the actual slope is smaller (larger) than the visual slope if the noise is larger (smaller) in y than in x. Accordingly, the discrepancy in Fig. 11 can be understood if there are larger uncertainties in MLS tracer tendencies (y axis) than in ERA-Interim temperature tendencies (x-axis). Furthermore, this exercise proved that, under this assumption, the slope given by the least squares regression of $\partial\overline{\chi}/\partial t$ onto $\partial\overline{T}/\partial t$ (as shown in Fig. 11) is an accurate estimate of the actual slope of the data.

Note that less than 50% of variance in the tendencies is explained by upwelling for both tracers, so that it is not possible to state that upwelling is the dominant control mechanism of sub-seasonal tracer variability. Instead, the results should be interpreted as a statistical proof that the suggested physical mechanism accounts for a significant fraction of the observed tracer variability. Overall, the observed statistically significant correlations of tropical upwelling with temperature and tracer tendencies, together with the reasonable agreement between the slope of the tracer versus temperature tendencies and predictions from the idealized balance in Eqs. (6)–(8), are strong evidence that sub-seasonal variations in upwelling make an important contribution to corresponding variability in temperature, ozone and CO in the tropical

lower stratosphere, in particular at the levels where vertical gradients are larger.

## 4 Summary and discussion

Tropical upwelling is a key aspect of the global stratospheric circulation, but fundamental aspects such as forcing mechanisms and temporal variability are poorly understood. In this study we evaluated the variability and quality of zonal average tropical upwelling estimates derived from different techniques ($\overline{w}^*$, $\overline{w}^*_m$ and $\overline{w}^*_Q$). Overall there is good agreement among the three (independent) estimates, although the magnitude of $\overline{w}^*$ from ERA-Interim is somewhat larger than the other estimates, especially at 100 hPa. This consistency, particularly between $\overline{w}^*_m$ and $\overline{w}^*_Q$, reflected in Figs. 3 and 4, is the primary evidence of the accuracy of the estimates. Furthermore, sub-seasonal variations are correlated with both temperatures and tracer concentrations in the tropical lower stratosphere. This result implies that sub-seasonal variations in the upwelling estimates reflect - at least to the extent quantified by the correlations in Figs. 4 and 10 - actual fluctuations in the atmosphere, and hence gives further confidence in the variability of the indirect upwelling estimates on fast timescales. For instance, the reasonable agreement of $\overline{w}^*_m$ with the other estimates suggests the possibility of analyzing the terms in the momentum balance to understand dynamical forcing mechanisms of tropical upwelling at sub-seasonal timescales.

Time series for 2005–2010 in Fig. 1 show coherence among temperature, ozone and CO in the tropical lower stratosphere, for both seasonal and sub-seasonal timescales. Because ozone, CO and (potential) temperature all exhibit enhanced vertical gradients in the tropical lower stratosphere, the observed relationships suggest that upwelling plays a central role in producing this coherent behavior. We have evaluated explicitly the zonal mean thermodynamic and tracer continuity equations to quantify the influence of upwelling, focusing separately on seasonal and sub-seasonal timescales. The seasonal calculations (based on monthly averaged data) show that upwelling is a dominant term in all cases (Figs. 5, 6 and 7), so that the seasonal cycle in upwelling (maximum during NH winter) is a simple mechanism responsible for the coupled seasonal variations in temperature, ozone and CO. This summary statement is most applicable for altitudes where the background gradients are strongest (i.e. near 70 hPa for ozone and CO).

An important caveat is that the seasonal ozone and CO budgets in our calculations (Figs. 6 and 7) have significant residuals, which are likely due to eddy transport not resolved in our analyses plus uncertainties in the resolved terms. The importance of eddy transport for ozone in the tropical lower stratosphere has been suggested by Konopka et al. (2009, 2010) and Ploeger et al. (2012), hereafter KP. The results of KP deserve further discussion. Their calculations, based on analysis of Lagrangian trajectories on isentropic levels, suggest that the seasonal cycle of ozone in the tropical lower stratosphere is primarily a response to horizontal transport (in-mixing), rather than upwelling. Our results, based on TEM budget calculations on altitude (log-pressure) surfaces (Fig. 6), clearly highlight the dominance of vertical transport for the ozone seasonal cycle. Understanding the very different results from these distinct calculations will require further analysis, and here we just briefly discuss some of the possible reasons for this discrepancy. One relevant difference between KP and the present work is the choice of the vertical coordinate. Konopka et al. (2009) show that the amplitude of the seasonal cycle in ozone is reduced by more than 50 % when analyzed on isentropic levels. This is because of the strong correlation between temperature and ozone (see Fig. 1), so that the annual cycle in potential temperature in this region is almost in phase with ozone. However, it is precisely this common variability between tracers and temperature that we are interested in, which we argue arises mainly from the effect of tropical upwelling. Because the seasonal variation in the isentropes is a response to upwelling (combined with corresponding diabatic forcing), understanding the movement of the isentropes is an integral part of the coupled problem. Another fundamental difference between KP and our analyses is the Lagrangian versus TEM approach. In the present work the TEM framework is used to investigate the origin of the seasonality in ozone as revealed by (Eulerian) observations. On the other hand, Lagrangian calculations provide values of ozone concentrations from material derivatives integrated along parcel trajectories. It is possible that the results are only apparently contrasting because of the different perspective (e.g. high-ozone air in-mixed at lower levels and then transported upward by tropical upwelling will be considered horizontal transport in the Lagrangian view and vertical advection in the TEM calculations). Ploeger et al. (2012) point out that because of these differences the comparison is not straight-forward, and we remark here the importance of bearing in mind the characteristics of each analysis when interpreting the results. Indeed, these constitute very interesting issues to be explored in future studies in order to improve our understanding of tracer variability and transport processes in the tropical lower stratosphere.

Finally, sub-seasonal variations in upwelling show statistically significant correlations with temperature and tracer tendencies. In addition, the slopes of the observed ratios of temperature versus ozone and CO tendencies (Fig. 11) are relatively close to the idealized situation where variability is primarily controlled by fluctuations in upwelling (Eqs. 6–8). This proves that variability in upwelling explains a significant fraction of the transient fluctuations in ozone and CO at levels with large vertical gradients above the tropical tropopause. These results for sub-seasonal timescales are also consistent with our findings for the respective seasonal cycles, and highlight the important role of tropical

upwelling in forcing tracer variability across a broad range of timescales.

*Acknowledgements.* We thank Mijeong Park for providing MLS data, Fei Wu for calculating the radiative heating rates and Doug Kinnison for providing the chemical production and loss rates for ozone and CO from WACCM. The ECMWF provided the ERA-Interim data used in this work. We thank John Bergman and Rolando R. Garcia for constructive comments on the manuscript. We also thank four anonymous referees for their helpful reviews. This work was partially supported under the NASA Aura Science Program. Most of the work has been carried out at NCAR during visits of Marta Abalos funded by the FPI program from the Spanish Ministry of Science and Innovation. The National Center for Atmospheric Research is operated by the University Corporation for Atmospheric Research, under sponsorship of the National Science Foundation.

Edited by: P. Haynes

## References

Andrews, D. G., Holton, J. R., and Leovy, C. B.: Middle Atmosphere Dynamics, Academic Press, Orlando, Florida, 489 pp., 1987.

Bernath, P. F., McElroy, C. T., Abrams, M. C., Boone, C. D., Butler, M., Camy-Peyret, C., Carleer, M., Clerbaux, C., Coheur, P. F., Colin, R., DeCola, P., DeMazière, M., Drummond, J. R., Dufour, D., Evans, W. F. J., Fast, H., Fussen, D., Gilbert, K., Jennings, D. E., Llewellyn, E. J., Lowe, R. P., Mahieu, E., McConnell, J. C., McHugh, M., McLeod, S. D., Michaud, R., Midwinter, C., Nassar, R., Nichitiu, F., Nowlan, C., Rinsland, C. P., Rochon, Y. J., Rowlands, N., Semeniuk, K., Simon, P., Skelton, R., Sloan, J. J., Soucy, M.-A., Strong, K., Tremblay, P., Turnbull, D., Walker, K. A., Walkty, I., Wardle, D. A., Wehrle, V., Zander, R., and Zou, J.: Atmospheric Chemistry Experiment (ACE): Mission overview, Geophys. Res. Lett., 32, L15S01, doi:10.1029/2005GL022386, 2005.

Brewer, A. W.: Evidence for a world circulation provided by the measurements of helium and water vapour distribution in the stratosphere, Q. J. Roy. Meteor. Soc., 75, 351–363, 1949.

Calvo, N. and Garcia, R. R.: Wave forcing of the tropical upwelling in the lower stratosphere under increasing concentrations of greenhouse gases, J. Atmos. Sci., 66, 3184–3196, 2009.

Chae, J. H. and Sherwood, S. C.: Annual temperature cycle of the tropical tropopause: A simple model study, J. Geophys. Res., 112, D19111, doi:10.1029/2006JD007956, 2007.

Dee, D. P., Uppala, S. M., Simmons, A. J., Berrisford, P., Poli, P., Kobayashi, S., Andrae, U., Balmaseda, M. A., Balsamo, G., Bauer, P., Bechtold, P., Beljaars, A. C. M., van de Berg, L., Bidlot, J., Bormann, N., Delsol, C., Dragani, R., Fuentes, M., Geer, A. J., Haimberger, L., Healy, S. B., Hersbach, H., Hólm, E. V., Isaksen, L., Kållberg, P., Köhler, M., Matricardi, M., McNally, A. P., Monge-Sanz, B. M., Morcrette, J.-J., Park, B.-K., Peubey, C., de Rosnay, P., Tavolato, C., Thépaut, J.-N., and Vitart, F.: The ERA-interim reanalysis: configuration and performance of the data assimilation system, Q. J. Roy. Meteor. Soc., 137, 553–597, doi:10.1002/qj.828, 2011.

Dobson, G. M. B.: Origin and distribution of the polyatomic molecules in the atmosphere, Proc. R. Soc. A, 236, 187–193, doi:10.1098/rspa.1956.0127, 1956.

Folkins, I., Bernath, P., Boone, C., Lesins, G., Livesey, N., Thompson, A. M., Walker, K., and Witte, J. C.: Seasonal cycles of $O_3$, CO, and convective outflow at the tropical tropopause, Geophys. Res. Lett., 33, L16802, doi:10.1029/2006GL026602, 2006.

Froidevaux, L., Livesey, N. J., Read, W. G., Jiang, Y. B., Jimenez, C., Filipiak, M. J., Schwartz, M. J., Santee, M. L., Pumphrey, H. C., Jiang, J. H., Wu, D. L., Manney, G. L., Drouin, B. J., Waters, J. W., Fetzer, E. J., Bernath, P. F., Boone, C. D., Walker, K. A., Jucks, K. W., Toon, G. C., Margitan, J.,J., Sen, B., Webster, C. R., Christensen, L. E., Elkins, J. W., Atlas, E., Lueb, R. A., and Hendershot, R.: Early validation analyses of atmospheric profiles from EOS MLS on the Aura satellite, IEEE Trans. Geosci. Remote Sens., 44, 1106–1121, 2006.

Fueglistaler, S., Dessler, A. E., Dunkerton, T. J., Folkins, I., Fu, Q., and Mote, P. W.: Tropical tropopause layer, Rev. Geophys., 47, RG1004, doi:10.1029/2008RG000267, 2009a.

Fueglistaler, S., Legras, B., Beljaars, A., Morcrette, J. J., Simmons, A., Tompkins, A. M., and Uppala, S.: The diabatic heat budget of the upper troposphere and lower/mid stratosphere in ECMWF reanalysis, Q. J. Roy. Meteor. Soc., 135, 21–37, doi:10.1002/qj.361, 2009b.

Fueglistaler, S., Haynes, P. H., and Forster, P. M.: The annual cycle in lower stratospheric temperatures revisited, Atmos. Chem. Phys., 11, 3701–3711, doi:10.5194/acp-11-3701-2011, 2011.

Garcia, R. R. and Randel, W. J.: Acceleration of the Brewer-Dobson circulation due to increases in greenhouse gases, J. Atmos. Sci., 65, 2731–2739, 2008.

Gettelman, A., Forster, P., Fujiwara, M., Fu, Q., Vömel, H., Gohar, L., Johason, C., and Ammerman, M.: The radiation balance of the tropical tropopause layer, J. Geophys. Res., 109, D07103, doi:10.1029/2003JD004190, 2004.

Gille, J. C., Lyjak, L. V., and Smith, A. K.: The global residual mean circulation in the middle atmosphere for the northern winter period, J. Atmos. Sci., 44, 1437–1452, 1987.

Iwasaki, T., Hamada, H., and Miyazaki, K.: Comparisons of Brewer-Dobson circulations diagnosed from reanalyses, J. Meteor. Soc. Jpn., 87, 997–1006, 2009.

Konopka, P., Grooß, J.-U., Ploeger, F., and Müller, R.: Annual cycle of horizontal in-mixing into the lower tropical stratosphere, J. Geophys. Res., 114, D19111, doi:10.1029/2009JD011955, 2009.

Konopka, P., Grooß, J.-U., Günther, G., Ploeger, F., Pommrich, R., Müller, R. and Livesey, N.: Annual cycle of ozone at and above the tropical tropopause: observations versus simulations with the Chemical Lagrangian Model of the Stratosphere (CLaMS), Atmos. Chem. Phys., 10, 121–132, doi:10.5194/acp-10-121-2010, 2010.

Liu, C., Zipser, E., Garrett, T., Jiang, J. H., and Su, H.: How do the water vapor and carbon monoxide "tape recorders" start near the tropical tropopause?, Geophys. Res. Lett., 34, L09804, doi:10.1029/2006GL029234, 2007.

Livesey, N. J., Filipiak, M. J., Froidevaux, L., Read, W. G., Lambert, A., Santee, M. L., Jiang, J. H., Pumphrey, H. C., Waters, J. W., Cofield, R. E., Cuddy, D. T., Daffer, W. H., Drouin, B. J., Fuller, R. A., Jarnot, R. F., Jiang, Y. B., Knosp, B. W., Li, Q. B., Perun, V. S., Schwartz, M. J., Snyder, W. V., Stek, P. C., Thurstans, R. P., Wagner, P. A., Avery, M., Browell, E. V., Cam-

mas, J.-P., E. Christensen, L., Diskin, G. S., Gao, R.-S., Jost, H.-J., Loewenstein, M., Lopez, J. D., Nedelec, P., Osterman, G. B., Sachse, G. W., and Webster, C. R.: Validation of Aura Microwave Limb Sounder $O_3$ and CO observations in the upper troposphere and lower stratosphere, J. Geophys. Res., 113, D15S02, doi:10.1029/2007JD008805, 2008.

Logan, J. A.: An analysis of ozonesonde data for the lower stratosphere: Recommendations for testing models, J. Geophys. Res., 104, 16151–16170, 1999.

Monge-Sanz B. M., Chipperfield M. P., Simmons A. J., Uppala S. M.: Mean age of air and transport in a CTM: Comparison of different ECMWF analyses, Geophys. Res. Lett., 34, L04801, doi:10.1029/2006GL028515, 2007.

Mote, P. W., Rosenlof, K. H., Mclntyre, M. E., Carr, E. S., Gille, J. C., Holton, J. R., Kinnersley, J. S., Pumphrey, H. C., Russell III, J. M., and Waters, J. W.: An atmospheric tape recorder: The imprint of tropical tropopause temperatures on stratospheric water vapor, J. Geophys. Res., 101, 3989–4006, 1996.

Niwano, M., Yamazaki, K., and Shiotani, M.: Seasonal and QBO variations in ascent rate in the tropical lower stratosphere as inferred from UARS HALOE trace gas data, J. Geophys. Res., 108, 4794, doi:10.1029/2003JD003871, 2003.

Ploeger, F., Konopka, P., Müller, R., Fueglistaler, S., Schmidt, T., Manners, J., Grooß, J.-U., Günther, G., de Forster, P. M., and Riese, M.: Horizontal transport affecting trace gas seasonality in the Tropical Tropopause Layer (TTL), J. Geophys. Res., 117, D09303, doi:10.1029/2011JD017267, 2012.

Randel, W. J., Garcia, R. R., and Wu, F.: Time-dependent upwelling in the tropical lower stratosphere estimated from the zonal-mean momentum budget, J. Atmos. Sci., 59, 2141–2152, 2002.

Randel, W. J., Park, M., Wu, F., and Livesey, N.: A large annual cycle in ozone above the tropical tropopause linked to the Brewer-Dobson circulation, J. Atmos. Sci., 64, 4479–4488, 2007.

Reed, R. J. and Vlcek, C. L.: The annual temperature variation in the lower tropical stratosphere, J. Atmos. Sci., 26, 163–167, 1969.

Rosenlof, K. H.: Seasonal cycle of the residual mean meridional circulation in the stratosphere, J. Geophys. Res., 100, 5173–5191, 1995.

Seviour, W. J. M., Butchart, N., and Hardiman, S. C.: The Brewer–Dobson circulation inferred from ERA-Interim, Q. J. Roy. Meteor. Soc., 138, 878–888, doi:10.1002/qj.966, 2011.

Schoeberl, M. R., Duncan, B. N., Douglass, A. R., Waters, J., Livesey, N., Read, W., and Filipiak, M.: The carbon monoxide tape recorder, Geophys. Res. Lett., 33, L12811, doi:10.1029/2006GL026178, 2006.

Schoeberl, M. R., Douglass, A. R., Newman, P. A., Lait, L. R., Lary, D., Waters, J., Livesey, N., Froidevaux, L., Lambert, A., Read, W., Filipiak, M. J., and Pumphrey, H. C.: QBO and annual cycle variations in tropical lower stratosphere trace gases from HALOE and Aura MLS observations, J. Geophys. Res., 113, D05301, doi:10.1029/2007JD008678, 2008a.

Schoeberl, M. R., Douglass, A. R., Stolarski, R. S., Pawson, S., Strahan, S. E., and Read, W.: Comparison of lower stratospheric tropical mean vertical velocities, J. Geophys. Res., 113, D24109, doi:10.1029/2008JD010221, 2008b.

Thuburn, J. and Craig, G. C.: Stratospheric influence on tropopause height: The radiative constraint, J. Atmos. Sci., 57, 17–28, 2000.

Waters, J. W., Froidevaux, L., Harwood, R. S., Jarnot, R. F., Pickett, H. M., Read, W. G., Siegel, P. H., Cofield, R. E., Filipiak, M. J., Flower, D. A., Holden, J. R., Lau, G. K., Livesey, N. J., Manney, G.L., Pumphrey, H.C., Santee, M. L., Wu, D. L., Cuddy, D. T., Lay, R. R., Loo, M. S., Perun, V. S., Schwartz, M. J., Stek, P. C., Thurstans, R. P., Boyles, M. A., Chandra, K. M., Chavez, M. C., Gun-Shing, C., Chudasama, B. V., Dodge, R., Fuller, R. A., Girard, M. A., Jiang, J. H., Yibo, J., Knosp, B. W., LaBelle, R. C., Lam, J. C., Lee, K. A., Miller, D., Oswald, J. E., Patel, N. C., Pukala, D. M., Quintero, O., Scaff, D. M., Van Snyder, W., Tope, M. C., Wagner, P. A., and Walch, M. J.: The Earth Observing System Microwave Limb Sounder (EOS MLS) on the Aura Satellite, IEEE Trans. Geosci. Remote Sens., 44, 1075–1092, 2006.

Yang, Q., Fu, Q., Austin, J., Gettelman, A., Li, F., and Vömel, H.: Observationally derived and general circulation model simulated tropical stratospheric upward mass fluxes, J. Geophys. Res., 113, D00B07, doi:10.1029/2008JD009945, 2008.

Yang, Q., Fu, Q., and Hu, Y.: Radiative impacts of clouds in the tropical tropopause layer, J. Geophys. Res., 115, D00H12, doi:10.1029/2009JD012393, 2010.

Yulaeva, E., Holton, J. R., and Wallace, J. M.: On the cause of the annual cycle in tropical lower-stratospheric temperature, J. Atmos. Sci., 51, 169–174, 1994.

# 2 Quantifying tracer transport in the tropical lower stratosphere using WACCM.

*Abalos, M., Randel, W. J., Kinnison, D. E., and Serrano, E., Atmos. Chem. Phys., 13, 10591-10607, doi:10.5194/acp-13-10591-2013, 2013a.*

Atmos. Chem. Phys., 13, 10591–10607, 2013
www.atmos-chem-phys.net/13/10591/2013/
doi:10.5194/acp-13-10591-2013


Atmospheric Chemistry and Physics Open Access

# Quantifying tracer transport in the tropical lower stratosphere using WACCM

**M. Abalos[1], W. J. Randel[2], D. E. Kinnison[2], and E. Serrano[1]**

[1]Universidad Complutense de Madrid, Depto. de Meteorología y Geofísica, Madrid, Spain
[2]National Center for Atmospheric Research, Boulder, Colorado, USA

*Correspondence to:* M. Abalos (mabalosa@fis.ucm.es)

Received: 24 April 2013 – Published in Atmos. Chem. Phys. Discuss.: 21 May 2013
Revised: 3 October 2013 – Accepted: 5 October 2013 – Published: 1 November 2013

**Abstract.** The zonal mean transport of ozone and carbon monoxide (CO) near the tropical tropopause is investigated using the Whole-Atmosphere Community Climate Model version 4 (WACCM4). The variability in temperature, ozone and CO in the model shows good agreement with satellite and balloon observations. Modeled temperature and tracers exhibit large and closely coupled annual cycles in the tropical lower stratosphere, as in the observations. The thermodynamic and tracer budgets in the model are analyzed based on the Transformed Eulerian Mean (TEM) framework on log-pressure coordinates and also using the isentropic formulation. Results show that the coupled seasonal cycles are mainly forced by tropical upwelling over altitudes with large vertical tracer gradients, in agreement with previous observational studies. The model also allows explicit calculation of eddy transport terms, which make an important contribution to ozone tendencies in the tropical lower stratosphere. The character of the eddy fluxes changes with altitude. At higher levels (∼ 2 km above the cold point tropopause), isentropic eddy transport occurs during winter and spring in each hemisphere in the sub-tropics, associated with transient Rossby waves acting on strong background latitudinal gradients. At lower altitudes, close to the tropical tropopause, there is a maximum in horizontal eddy transport during boreal summer associated with the Asian monsoon anticyclone. Subseasonal variability in ozone and CO, tied to fluctuations in temperature, is primarily driven by transient tropical upwelling. In isentropic coordinates, the overall tracer budgets are similar to the log-pressure results, highlighting cross-isentropic advection as the main term in the time-mean balance, with large seasonality above the tropopause. However, in isentropic coordinates the tracer variability is largely reduced on both seasonal and sub-seasonal timescales, because tracer fluctuations are highly correlated with temperature (as a response to upwelling).

## 1 Introduction

The tropical tropopause layer (TTL) acts as a boundary condition for the chemical composition of the stratosphere, such that the temperature and tracer concentrations of the air just above the tropical tropopause affect the composition of the entire stratosphere (e.g. Fueglistaler et al., 2009). In addition, concentrations of radiatively active trace gases in the TTL and the tropical lower stratosphere have a particularly large impact on radiative forcing, influencing surface climate (Riese et al., 2012). Hence, it is crucial for chemistry-climate models to correctly represent tracer behavior in this region in order to simulate present and future climate (Gettelman et al., 2010). The spatial distribution and temporal variability of constituents in the tropical lower stratosphere is mostly determined by transport processes, along with chemical sources and sinks. Some of the key issues regarding tracer transport in this region remain poorly quantified, such as the relative importance of vertical advection by large-scale tropical upwelling and irreversible mass exchange between the tropics and the extra-tropics. Observational and modeling studies suggest that the tropical lower stratosphere above ∼ 20 km acts as a reservoir, in which chemical species are in partial isolation from the extra-tropics (Plumb, 1996). Within this region, tracer transport is dominated by large-scale ascent associated with the Brewer–Dobson circulation (Plumb, 2002; Shepherd, 2007). The barriers separating this

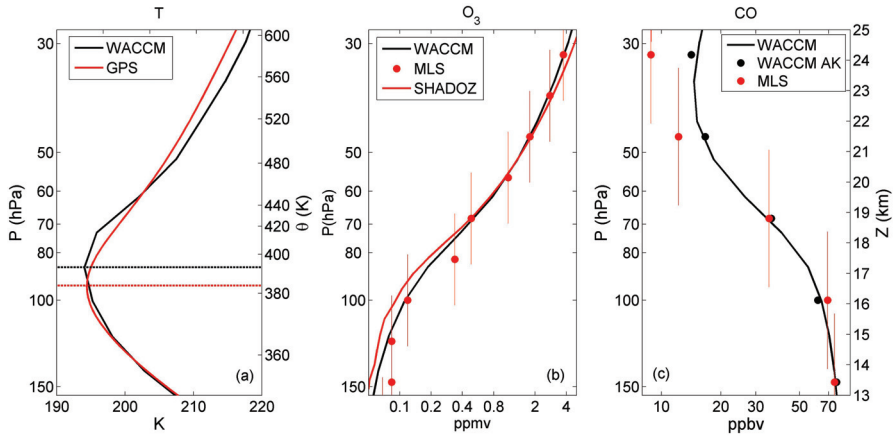


**Fig. 1.** Vertical structure of annual mean temperature **(a)**, ozone **(b)** and CO **(c)** in WACCM and in observations averaged over the tropics (18° S–18° N for WACCM, 18.75° S–18.75° N for MLS and 20° S–20° N for GPS). Solid black line: WACCM, solid red: GPS in **(a)** and SHADOZ in **(b)**, red dots: MLS, black dots in **(c)**: WACCM with MLS CO averaging kernel. The vertical red bars indicate the width of the MLS averaging layers. For reference, the location of annual mean isentropic levels in WACCM is indicated on panel **(a)** and the approximate altitude on panel **(c)**, calculated as $Z = -H \ln(P/P_0)$, with $P_0 = 1000$ hPa and $H = 7$ km. The ozone and CO scales are logarithmic in order to better represent the sharp vertical gradients. Horizontal dashed lines in panel **(a)** indicate the location of the annual mean cold point tropopause in WACCM (black) and in GPS observations (red).

tropical upwelling region from the mid-latitudes, where isentropic mixing dominates over slow poleward advection, are not static but move seasonally towards the summer hemisphere, extending the winter surf zone towards the equator (Haynes and Shuckburgh, 2000a). More rapid horizontal transport and exchange with the extra-tropics occurs in the region ∼ 15–20 km (∼ 360–450 K), as evidenced by water vapor (Rosenlof et al., 1997) and other tracers (Santee et al., 2011). Thus, the composition of the tropical lower stratosphere is influenced by both the mean circulation and eddy transport effects.

Observations of the seasonal cycle of ozone in the tropical lower stratosphere show a large annual cycle with a sharply peaked vertical structure, which is in phase with temperature (Randel et al., 2007). Randel et al. (2007) proposed that this behavior results primarily from vertical transport; seasonal variations in the Brewer–Dobson circulation acting on the strong background vertical gradient in ozone can account for the phase, amplitude and vertical structure of the ozone annual cycle. Similar effects occur for other tracers with strong vertical gradients across the tropopause, including carbon monoxide (CO) (Randel et al., 2007) or tropospheric hydrocarbons such as ethane ($C_2H_6$) (Park et al., 2013). On the other hand, complementary modeling analyses using a Lagrangian transport framework suggest that the large annual cycle in ozone mainly results from horizontal in-mixing, in particular due to transport associated with the Asian summer monsoon anticyclone (Konopka et al., 2009, 2010; Ploeger et al., 2012). These contrasting viewpoints help to motivate the current analysis.

The recent study of Abalos et al. (2012) analyzed the observed budgets of temperature, ozone and CO in the tropical lower stratosphere based on the Transformed Eulerian Mean (TEM) formalism, using three derived estimates of tropical upwelling. These results demonstrated the dominant role of tropical mean upwelling in forcing the observed coherent seasonal cycles in temperature and tracers at levels with large background vertical gradients. However, the eddy components of transport could not be estimated by Abalos et al. (2012) because of the coarse resolution of the satellite ozone and CO measurements; their ozone budget calculations include a relatively large residual, which they argue may be associated with unresolved eddy transport. Here we perform a similar detailed budget analysis using the output of a free-running chemistry-climate model (WACCM4), and explicitly evaluate the effects of mean advection, eddy transport and chemical sources/sinks on ozone and CO in the tropical lower stratosphere. We include TEM (on log-pressure vertical coordinates) and isentropic calculations to contrast the results. Because the seasonal cycles in ozone and CO are strongly correlated with temperature (as a response to variations in upwelling, in turn resulting from variations in wave driving), the variability in tracers is smaller in isentropic coordinates (Konopka et al., 2009), and the two vertical coordinates provide complementary perspectives.

Our analyses first focus on evaluating the behavior of temperature, ozone and CO in the model simulation, with

emphasis on the coupled seasonal variations and the associated vertical structure. We then quantify the thermodynamic and tracer budgets in the model, for both the seasonal cycle and sub-seasonal variability.

## 2 Model and observational data

### 2.1 WACCM data

In this study we use six years (2004–2009) of daily data from a free-running simulation with the Whole-Atmosphere Community Climate Model, Version 4 (WACCM4). WACCM4 is the atmospheric component of the coupled climate system model CESM1 (Community Earth System Model, Version 1), extended to cover the altitude range from the surface to the lower thermosphere. It is a fully interactive model, wherein the radiatively active gases ($CO_2$, $H_2O$, $N_2O$, $CH_4$, CFCs, NO, $O_3$) influence the radiative heating rates and therefore the dynamics. Processes and parameterizations that are unique to WACCM4 are discussed in Garcia et al. (2007). This simulation uses 66 vertical levels from the ground to 180 km, with a vertical resolution of 1.1–1.4 km in the upper troposphere-lower stratosphere (UTLS). The horizontal resolution is $1.9° \times 2.5°$(latitude $\times$ longitude). The chemical module of WACCM4 is based upon the 3-D chemical transport Model of OZone and Related Tracers, Version 3 (MOZART-3) (Kinnison et al., 2007), incorporating a realistic representation of stratospheric and tropospheric chemistry (in particular, for ozone and CO). The simulation used here is a 50 yr transient run from 1960 to 2010, similar to the REF-B1 simulation used in CCMVal-2 (SPARC CCMVal, 2010, Chapter 2). This simulation includes anthropogenic and natural forcings from observations (such as trace gases emissions, quasi-biennial oscillation (QBO) or sea surface temperatures), mostly identical to those used by SPARC CCMVal (2010) for REF-B1.

Tracer transport in WACCM is computed using a finite-volume dynamical core with a Lagrangian control-volume vertical discretization (Lin, 2004). In this technique, the vertical coordinates are material surfaces, which evolve following hydrostatic dynamics. The finite volumes bounded by two neighboring Lagrangian surfaces can therefore float, be compressed or expanded. In particular, the presence of diabatic heating/cooling deforms the surfaces, which must be frequently remapped to hydrostatic pressure coordinates. The remapping process involves vertically redistributing tracer mixing ratios from the Lagrangian control volume to the Eulerian framework. Therefore, the model does not explicitly solve vertical transport and the vertical velocity (omega) is indirectly derived from considering the pressure change implied by the remapping. The possible lack of precise correspondence between the vertical motion implicit in the remapping process and the omega field output by the model (and used in our transport calculations) can lead to small uncertainties in our tracer budgets.

### 2.2 Observations

The temperature, ozone and CO in the tropical lower stratosphere from the model simulation are compared to observations to demonstrate the ability of the model to represent their spatial structure and variability in a realistic manner. We compare WACCM temperatures with GPS radio occultation observations from the Constellation Observing System for Meteorology Ionosphere and Climate (COSMIC) satellite mission (Anthes et al., 2008). Comparisons are based on COSMIC daily data for the period January 2007 to December 2010 averaged zonally and over tropical latitudes (20° S–20° N). WACCM ozone is compared to tropical ozonesonde measurements from the SHADOZ (Southern Hemisphere ADditional OZonesondes) network (Thompson et al., 2007, 2012), using a subset of 7 near-equatorial stations during the period 1998–2006 (the same data described in Randel et al., 2007). We also use both ozone and CO satellite measurements from the Microwave Limb Sounding (MLS) instrument on the Aura satellite (Livesey et al., 2008). In particular we use daily zonal mean data averaged over 18.75° S–18.75° N for the period 2005–2010. The ozone data have a vertical resolution near 3 km, with data on vertical layers centered on the pressure levels of 100, 83, 68, 56 and 46 hPa; CO has a lower vertical resolution of $\sim$ 4.5 km, with data for levels centered at 100, 68 and 46 hPa. Further details of these MLS data can be found in Abalos et al. (2012).

## 3 Comparison of WACCM with observations

### 3.1 Tropical UTLS temperature, ozone and CO

Taguchi (2009) demonstrated that WACCM produces a realistic simulation of the tropical lower stratosphere, including an accurate annual cycle of temperature and circulation. Here we focus more explicitly on comparing the behavior of temperature, ozone and CO in the model with observations. The vertical structure of tropical mean temperature, ozone and CO, averaged over all the available years, is shown in Fig. 1. The annual mean values agree very well with the observations, and the overall vertical structure is well captured by the model. In particular the model accurately simulates the strong vertical gradients in ozone and CO, which are important features of this region. One relevant difference is that the minimum temperature (i.e. the annual mean cold point tropopause) is found at a higher level in WACCM (86 hPa) compared to GPS observations ($\sim$ 95 hPa). Note that if GPS temperature data is sampled at the WACCM pressure levels the cold point is located at 101 hPa, one level below the cold point in the model results.

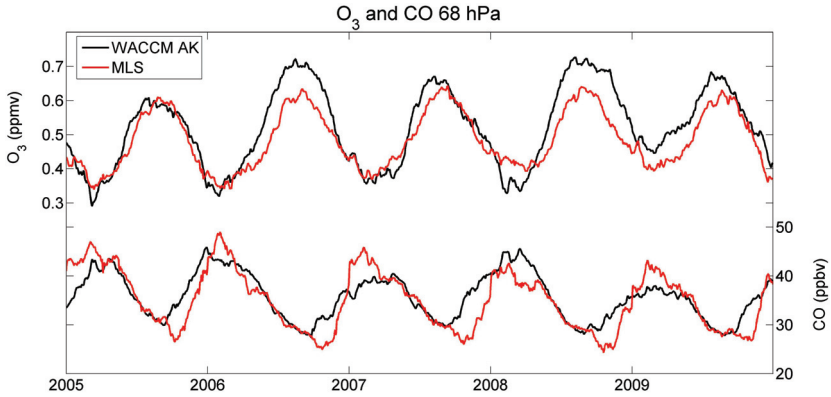


**Fig. 2.** Time series of zonal mean 68 hPa ozone and CO from MLS observations (red lines) and from WACCM (calculated using MLS averaging kernels, black lines). Results are averaged over 18° S–18° N for WACCM and 18.75° S–18.75° N for MLS.

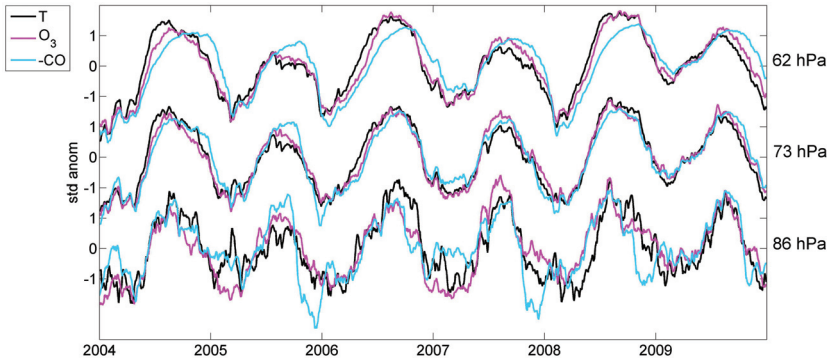


**Fig. 3.** Time series of zonal mean temperature, ozone and CO from WACCM at 62, 73 and 86 hPa averaged over 18° S–18° N. Standardized anomalies are shown for each level, and the anomalies of CO are inverted to highlight correlated behavior.

Time series of ozone and CO from WACCM are compared to five years of MLS observations at 68 hPa (first level above the tropopause where both ozone and CO MLS observations are available) in Fig. 2, with MLS averaging kernels applied to the model results. These time series show the key feature of large annual cycles in ozone and CO, which are approximately out of phase. There is good agreement in the magnitude and phase of the seasonal cycles between the model and the observations for both tracers. Abalos et al. (2012) highlighted the correlated variability between temperature, ozone and CO across the tropical tropopause from observations. Similar coherent behavior is seen in WACCM, both for the seasonal cycles and the sub-seasonal variability (i.e., timescales shorter than the seasonal cycle), as shown in Fig. 3 (compare to Fig. 1 in Abalos et al., 2012). Note that the model realistically produces a semi-annual cycle in CO concentrations near the tropopause (86 hPa), linked to surface emissions (see Abalos et al., 2012).

Randel et al. (2007) pointed out that the annual cycles in temperature, ozone and CO are characterized by a sharply peaked vertical structure above the tropical tropopause. Figure 4 shows that this important feature is reproduced in WACCM with realistic amplitudes, although the relative maxima are shifted to slightly higher altitudes in the model compared to observations for temperature and ozone. The lower resolution of the CO measurements does not allow a similar detailed comparison (note that CO model results weighted with MLS averaging kernels are also shown in Fig. 4). This vertical shift may be related to the higher altitude of the cold point in WACCM compared to observations (Fig. 1a). Despite this difference, WACCM is able to reproduce the characteristic vertical structure of the seasonal cycles; however one should be aware that, in terms of temperature structure and tracer variability near the tropical tropopause, a given vertical level in the model does not correspond exactly to the same level in the observations.

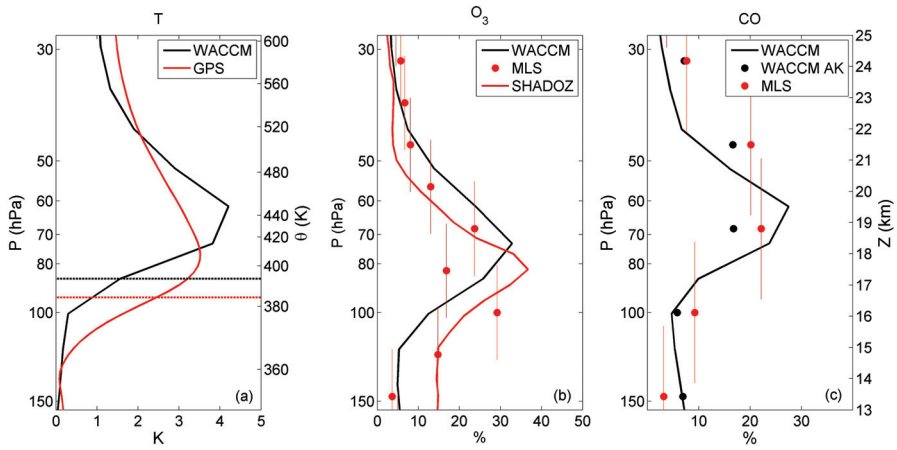


**Fig. 4.** As in Fig. 1 but for the vertical structure of annual cycle amplitude in temperature **(a)**, ozone **(b)** and CO **(c)** in the tropics. The amplitude for the tracers is shown relative to the annual mean concentration.

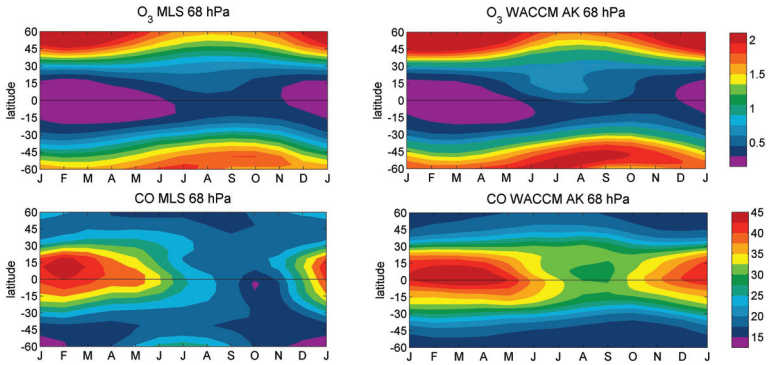


**Fig. 5.** Mean seasonal cycles of ozone (ppmv, upper panels) and CO (ppbv, lower panels) in MLS (left) and WACCM (right) at 68 hPa. MLS averaging kernels have been applied to WACCM data.

Note that the MLS ozone annual amplitude agrees reasonably well with the ozonesonde measurements, except at the 83 hPa level, where the MLS value is too small.

Figure 5 shows the latitudinal structure of the seasonal variation in ozone and CO at 68 hPa in WACCM (with MLS averaging kernels applied) and in MLS. There is good agreement between the model and the observations, and WACCM realistically represents the latitudinal swing of the tropical concentrations towards the summer hemisphere and the meridional gradients, stronger during winter in each hemisphere for both tracers. There is an asymmetry between the hemispheres in the ozone seasonality, with higher ozone concentrations during NH summer in the northern part of the tropics compared to the southern part, which is more pronounced in the model than in the observations. For CO, WACCM slightly overestimates the latitudinal gradients compared with MLS observations and does not show the deep minimum in October–November in the SH tropics seen in MLS, but the overall structure is quite realistic.

In general, WACCM reproduces the key spatial features and temporal variability in temperature, ozone and CO and hence we conclude that the model is a useful tool for the analysis of tracer transport in the tropical UTLS.

### 3.2 Thermodynamic balance

As a background to understanding the seasonality in the tracer budgets, we include the analysis of the model thermodynamic balance in the tropics, based on the TEM formalism (Andrews et al., 1987):

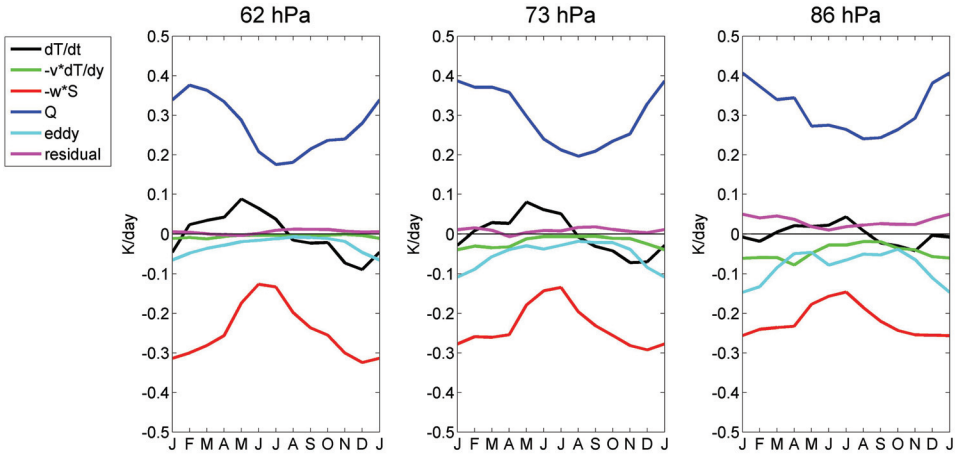


**Fig. 6.** Mean seasonal cycle (monthly means) of all the terms in the thermodynamic balance (Eq. 1) in WACCM computed at three pressure levels and averaged over 18° S–18° N.

$$\bar{T}_{\mathrm{t}} = -\bar{v}^*\bar{T}_y - \bar{w}^* S + \bar{Q} - e^{z/H}\left[e^{-z/H}\left(\overline{v'T'}\frac{\bar{T}_y}{S} + \overline{w'T'}\right)\right]_z . \quad (1)$$

In this equation and in the rest of the manuscript overbars indicate zonal means, primes are deviations from it, and subscripts denote partial derivatives. $\bar{Q}$ is the diabatic heating, $(\bar{v}^*, \bar{w}^*)$ are the components of the residual circulation, $S = H \cdot N^2/R$ with $H = 7\,\mathrm{km}$, $R = 287\,\mathrm{m^2\,s^{-2}\,K^{-1}}$ and $N^2$ is the Brunt–Väisälä frequency. Figure 6 shows the monthly mean budget terms in Eq. (1), evaluated at model levels 86, 73 and 62 hPa averaged over 18° S–18° N. The last term on the right-hand side of Eq. (1) is labeled "eddy" in Fig. 6, and there is a small residual term, which is the difference between the actual tendency ($\bar{T}_{\mathrm{t}}$) and that computed from Eq. (1) (this definition of residual is valid elsewhere in the manuscript). The thermodynamic balance in the tropical lower stratosphere is primarily between cooling by mean upwelling ($-\bar{w}^* S$) and radiative heating ($\bar{Q}$), and these show annual cycles which follow the stronger upwelling during boreal winter. The temperature tendency closely mimics the upwelling. The WACCM thermodynamic balance is similar to quasi-observational estimates based on ERA-Interim reanalysis data by Abalos et al. (2012). At the cold point tropopause level (86 hPa), the eddy term in Eq. (1) is a fairly large term in the balance. This eddy term is mainly associated with the vertical eddy heat flux, $\overline{w'T'}$, which is relatively important only over a narrow vertical layer just around the tropical tropopause. This result from the model shows similar magnitude and seasonality as the ERA-Interim calculation in Abalos et al. (2012). Figure 6 shows that the mechanisms that lead to the large seasonal cycle in WACCM temperature in this region are consistent with the observations, linked primarily to the seasonal cycle in upwelling. This is an important test for the model, and indicates a realistic simulation of dynamical and thermal processes in the tropical lower stratosphere.

## 4 Tracer transport

### 4.1 Time average tracer budgets

The TEM continuity equation for zonal mean tracer concentration gives the local change in tracer concentration as a result of transport processes and chemical sources and sinks (Andrews et al., 1987, Eq. 9.4.13):

$$\bar{\chi}_t = -\bar{v}^*\bar{\chi}_y - \bar{w}^*\bar{\chi}_z + e^{z/H}\nabla\cdot\boldsymbol{M} + P - L, \quad (2)$$

In this equation, transport of the zonal mean tracer concentration ($\bar{\chi}$) occurs via advection by the residual circulation $(\bar{v}^*, \bar{w}^*)$ and eddy effects ($e^{z/H}\nabla\cdot\boldsymbol{M}$), and $P-L$ is the chemical production minus loss rate. The eddy transport term is formulated as the divergence of the eddy transport vector, $\boldsymbol{M}$, with components defined as in Eq. 9A.3 of Andrews et al. (1987):

$$\begin{cases} M_y = -e^{-z/H}\left(\overline{v'\chi'} - \frac{\overline{v'T'}}{S}\bar{\chi}_z\right) \\ M_z = -e^{-z/H}\left(\overline{w'\chi'} + \frac{\overline{v'T'}}{S}\bar{\chi}_y\right) \end{cases} \quad (3)$$

Figure 7 illustrates the effects of residual mean advection and eddy transport on ozone and CO concentrations in the annual mean. Given the sharp vertical gradients in this region, it is convenient to represent changes in ozone and CO relative to

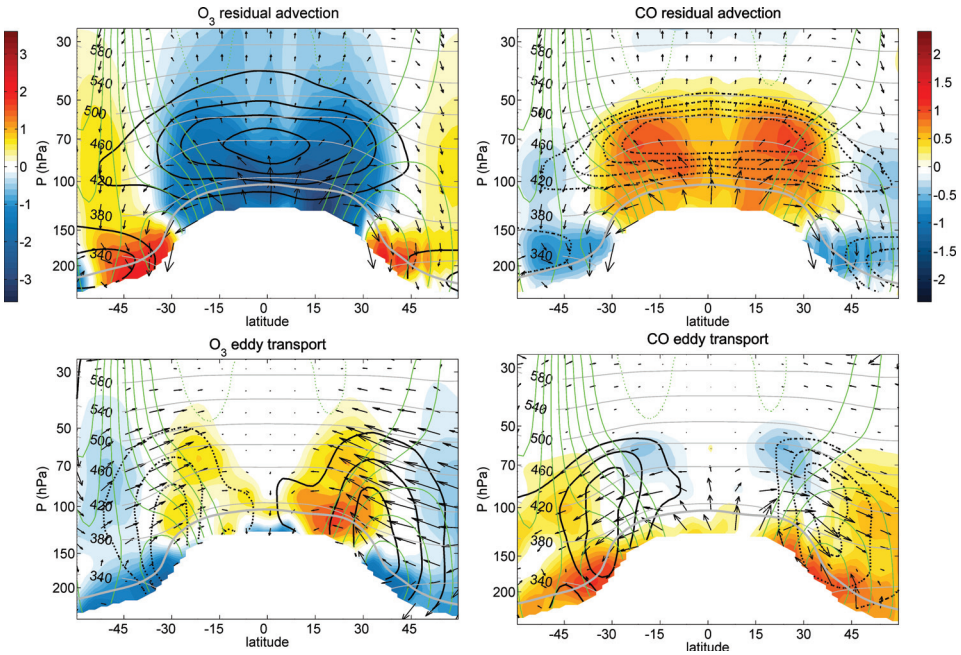


**Fig. 7.** Annual mean of residual advection (upper panels) and eddy transport (lower panels) for ozone (left) and CO (right) in WACCM, formulated in local percentage tendencies, as in Eq. (4). In upper panels, shading: $-\bar{v}^* \ln(\bar{\chi})_y - \bar{w}^* \ln(\bar{\chi})_z$, arrows: $(\bar{v}^*, \bar{w}^*)$, black contours: vertical tracer gradient (dashed: negative, solid: positive). In lower panels, shading: $e^{z/H} \nabla \cdot \boldsymbol{M}/\bar{\chi}$, arrows: $(-M_y, -M_z)$, black contours: meridional tracer gradient. Units of tracer tendency (shading) are (% day$^{-1}$) with respect to the annual mean concentration. Green contours show annual mean zonal wind (contour spacing: 5 m s$^{-1}$). A few annual mean isentropes are shown in gray and labeled. The annual mean lapse rate tropopause is indicated by the thick gray line.

the time mean concentration at each location; thus, the terms in Fig. 7 are expressed as local percentage values. This is equivalent to re-writing Eq. (2) in terms of the logarithm of tracer concentration:

$$\ln(\bar{\chi})_t = -\bar{v}^* \ln(\bar{\chi})_y - \bar{w}^* \ln(\bar{\chi})_z + e^{z/H} \nabla \cdot \boldsymbol{M}/\bar{\chi} + (P - L)/\bar{\chi} \quad (4)$$

and representing the time-mean of this equation. The arrows in Fig. 7 illustrate the components of the mean residual circulation $(\bar{v}^*, \bar{w}^*)$ in the upper panels (corresponding to advective transport), and the components of the vector $\boldsymbol{M}$ with the sign reversed $(-M_y, -M_z)$ in the lower panels (corresponding to eddy transport). Figure 7 shows that, for both tracers, transport in the tropical lower stratosphere is dominated by the advective component, which is mainly due to vertical advection by tropical upwelling (plus a smaller contribution from meridional advection by the shallow branch of the residual circulation below $\sim$ 70 hPa). The eddy component of transport occurs mostly along isentropes in the sub-tropics and middle latitudes. Advection by the residual circulation leads to decrease in ozone (increase in CO) concentrations in the tropics and increase (decrease) in the extra-tropics, and tracer tendencies are largest where the background vertical gradients are enhanced (indicated by the black contours). On the other hand, eddy transport acts to increase ozone (decrease CO) concentrations on the equatorward upper flanks of the subtropical jets, and decrease ozone (increase CO) in the extra-tropics. The largest eddy transport coincides with the regions of large meridional gradients (black contours), near the upper flanks of the subtropical jets.

### 4.2 Seasonal cycles

While the previous section focused on separating mean advection and eddy transport effects, we use a slightly different analysis in the rest of the work, based on separating the vertical and horizontal components of tracer transport. This simplifies the interpretation of the results and is motivated by the fact that, in the tropical lower stratosphere, mean advection is mainly vertical and eddy transport effects are mainly horizontal (cf. Fig. 7). To separate vertical and horizontal transport we simply rearrange Eq. (2):

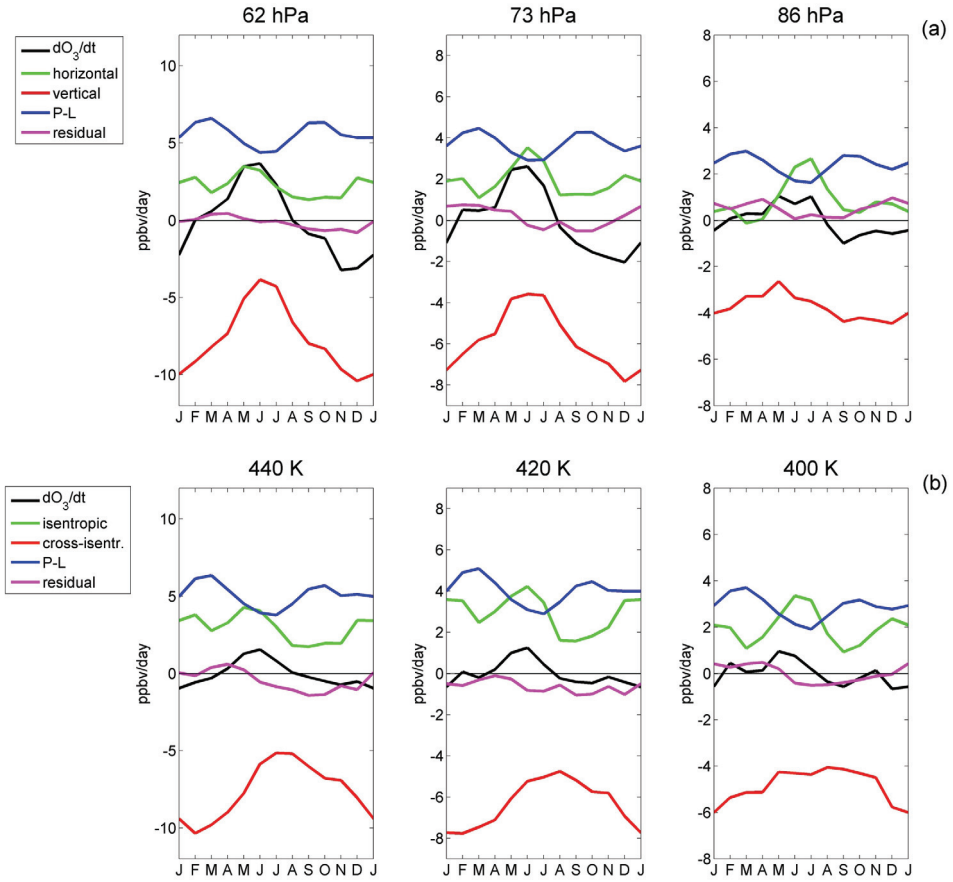


**Fig. 8.** Mean seasonal cycles (monthly means) of terms in the ozone continuity equation averaged over 18° S–18° N on pressure levels (Eq. 5, **a**) and isentropic levels (Eq. 6, **b**).

$$\bar{\chi}_t = \left[-\bar{v}^*\bar{\chi}_y + e^{z/H}(\cos\varphi)^{-1}(M_y\cos\varphi)_y\right] + \left[-\bar{w}^*\bar{\chi}_z + e^{z/H}(M_z)_z\right] + P - L. \quad (5)$$

The complete ozone and CO budgets showing all advective and eddy transport terms separately can be found in the Appendix (Figs. A1 and A2).

The use of isentropic coordinates is common in tracer transport studies, since for negligible diabatic heating rates tracers tend to move on constant potential temperature surfaces. Although this is not the case in the tropical lower stratosphere, where diabatic heating is a dominant term (see Fig. 6), it is enlightening to complement our analyses with analogous calculations on isentropes. In this coordinate system the continuity equation for the tracers is (Eq. 9.4.21 of Andrews et al., 1987):

$$\bar{\chi}_t = \left\{-\bar{v}^*\bar{\chi}_y - \bar{\sigma}^{-1}\left[\overline{(\sigma v)'\chi'}\right]_y\right\} + \left\{-\bar{Q}^*\bar{\chi}_\theta - \bar{\sigma}^{-1}\left[\overline{(\sigma Q)'\chi'}\right]_\theta\right\} + \bar{P}^* - \bar{L}^* \quad (6)$$

where the variables with a star:

$$\bar{A}^* \equiv \frac{\overline{(\sigma A)}}{\bar{\sigma}} \quad (7)$$

represent mass-weighted variables, defining the "density" on isentropes as

$$\sigma \equiv -\frac{1}{g}\frac{\partial p}{\partial\theta}. \quad (8)$$

Note that we have omitted the transient term: $-\bar{\sigma}^{-1}\overline{(\sigma'\chi')}_t$ in Eq. (6), which is negligible for ozone and CO budgets in our region of interest (not shown).

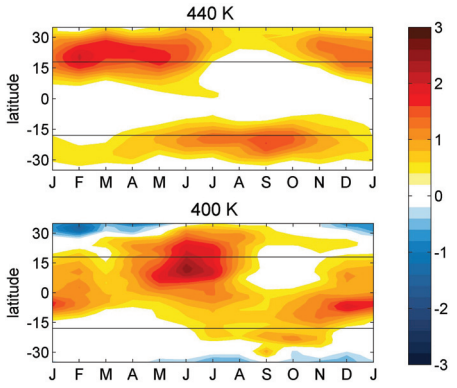


**Fig. 9.** Mean seasonal cycle (monthly means) of ozone relative tendency due to isentropic transport at 440 K and 400 K as a function of latitude. Tendencies are divided by the local annual mean concentration. Horizontal black lines indicate the location of 18° S and 18° N latitudes. Units: (% day$^{-1}$).

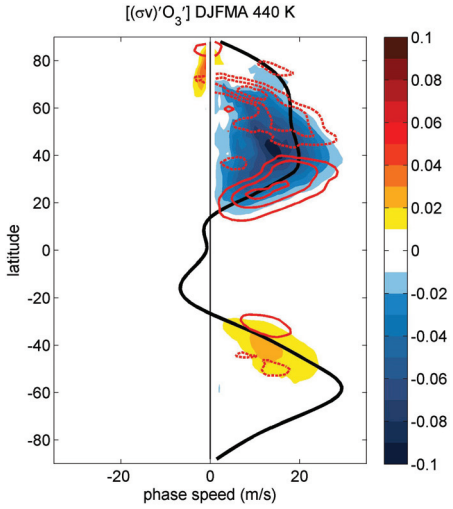


**Fig. 10.** Latitude versus phase-speed representation of the ozone eddy flux co-spectrum at 440 K for the winter-spring season (December through April). The spectrum of the eddy covariance ($\overline{(\sigma v)' O_3'}$) is multiplied by the cosine of latitude to emphasize the behavior in low latitudes. Red contours represent the meridional convergence of the eddy flux (term $-\bar{\sigma}^{-1}\left[\overline{(\sigma v)' O_3'}\right]_y$ in Eq. 6); solid contours indicate convergence of the eddy flux, associated with positive ozone tendencies. The solid black line shows the zonal mean zonal wind. A 9-point running mean in-phase speed is applied to the contours. (Shading units: kg m$^{-1}$ s$^{-1}$ K$^{-1}$ ppmv, contour levels spacing is 0.2 ppbv day$^{-1}$).

Figure 8a shows the terms in the WACCM ozone budget (Eq. 5) on the same pressure levels shown in Fig. 6. There is a large seasonal cycle in ozone at the upper level (62 hPa), which follows closely the seasonality in vertical transport (mainly tied to advection by tropical upwelling, see Fig. A1). There is a small semi-annual cycle in the chemical net production rates, linked to the sun transit over the equator in the equinox seasons. Note that the horizontal transport is a relatively small positive term and shows little seasonal variation at this level. There is also a small near-constant residual in these calculations, which might be related to uncertainties in the numerical calculations. At lower levels the amplitude of the ozone annual cycle decreases, as does the seasonality in the vertical transport term. On the other hand, at the lowest level (86 hPa, near the model tropopause) the seasonality in the horizontal transport term shows a maximum during NH summer, which approximately coincides with the positive ozone tendency. Figure A1 shows that horizontal eddy transport makes the largest contribution to this summer maximum at tropopause level. Overall, the balances in Fig. 8a are consistent with the observationally derived ozone balances in Abalos et al. (2012), especially taking into account the differences in vertical levels discussed above. The WACCM results support their hypothesis that the residual in the observational calculations is mainly associated with eddy transport effects.

Figure 8b shows the terms in the ozone continuity equation on isentropic levels (Eq. 6), combining isentropic (quasi-horizontal) and cross-isentropic (quasi-vertical) terms, as in the analysis on pressure levels. Overall, the ozone budgets are similar in pressure (Fig. 8a) and isentropic (Fig. 8b) coordinates, and in particular the cross-isentropic transport is a dominant term in the budget at each level. However, on isentropic coordinates the amplitude of the annual cycle in ozone is largely reduced, so that the ozone tendency is relatively small at every level compared to the other terms in the balance. This decrease in seasonal cycle amplitude is due to the annual cycle in potential temperature, which is almost in phase with ozone, as previously pointed out by Konopka et al. (2009). The relative amplitude of the annual cycle in ozone is reduced by > 50 % on isentropes compared to the amplitude on pressure levels, and its vertical structure changes as well: the relative maximum amplitude on isentropic coordinates is found at lower levels, close to the tropopause (∼ 380–400 K) (result not shown). The isentropic transport (mainly due to the eddies, see Fig. A1) is similar to the horizontal transport observed on pressure levels, showing a boreal summer maximum near the tropopause (e.g. 400 K) and less seasonality at higher levels.

The change in the seasonality of isentropic transport with height is shown more clearly in the latitude-month sections in Fig. 9; the results are very similar for horizontal transport on nearby pressure levels. At the upper levels (e.g. 440 K) maximum tendencies occur in the sub-tropics during winter and spring in each hemisphere (larger in the NH). This is mainly due to enhanced isentropic eddy transport just

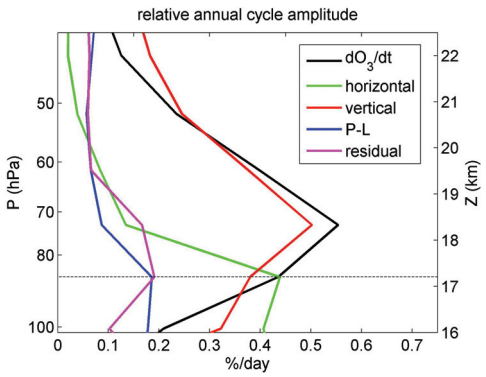


**Fig. 11.** Vertical structure of the annual cycle amplitude of the terms in the TEM continuity equation for ozone concentration (Eq. 5) averaged over 18° S–18° N. Relative amplitudes are obtained dividing by the annual mean concentration. The approximate altitude is calculated as for Fig. 1. The dashed horizontal line indicates the location of the annual mean cold point tropopause in WACCM.

above the sub-tropical jets during these seasons, acting on the strong background meridional gradients in ozone (see Fig. 7). This eddy transport is further characterized in Fig. 10, which shows the ozone eddy flux ($\overline{(\sigma v)' O_3'}$) at 440 K for northern winter and spring (DJFMA) as a function of latitude and phase speed of the eddies. This is calculated based on the space-time co-spectrum of the ozone eddy fluxes, interpolated from frequency to phase-speed space following Randel and Held (1991). The results show a broad region of negative (i.e. equatorward) ozone eddy flux in the NH associated with eastward traveling (Rossby) waves, and there is convergence of the eddy flux in the sub-tropics (term $-\bar{\sigma}^{-1}\left[\overline{(\sigma v)' O_3'}\right]_y$ in Eq. 6), associated with the positive ozone tendencies seen in Fig. 9 (upper panel). This flux convergence in the sub-tropics is mainly due to medium-scale eddies with wavenumbers between ∼ 4–10 (not shown) and phase speeds of ∼ 5–20 m s$^{-1}$. It is interesting to note that the patterns of subtropical eddy flux convergence approximately follow the zonal mean winds ($\bar{u}$) at this level, which is suggestive of critical layer interactions (where the wave phase speed $c$ is close to $\bar{u}$). This behavior is consistent with eddy flux convergences associated with Rossby wave breaking near critical levels as discussed, for example, in Homeyer and Bowman (2013).

At levels closer to the tropopause (such as 400 K) the amplitude of the ozone winter eddies is much smaller, and isentropic (eddy) transport shows a single maximum during NH summer (Fig. 9, lower panel). This enhanced summer horizontal transport of ozone into the tropics is linked to the anticyclonic circulation associated to the Asian (and North American) monsoons, which carry middle-latitude air masses with high ozone concentrations into the tropics (WACCM ozone and horizontal wind climatology for boreal summer is qualitatively similar to Fig. 7 in Konopka et al., 2010). This result is consistent with the works of Konopka et al. (2010) and Ploeger et al. (2012). The present WACCM calculations (e.g. Fig. 9) highlight the finding that the summer monsoon maximum in horizontal transport is primarily a feature found close to the tropopause, while very different seasonal behavior is observed at higher altitudes. This change with altitude in the seasonality of the ozone transport terms is evidenced in Fig. 11, which shows the vertical structure of the relative annual amplitude of each term in the TEM budget. The sharp peak in the seasonality of the ozone tendency in the lower stratosphere (around ∼ 70 hPa) is clearly associated with that in vertical transport (thus in tropical upwelling), while the seasonality in horizontal transport is important at lower levels, near the tropopause. Note that although Fig. 11 shows the amplitude but not the phasing of the annual cycles, Fig. 8a shows clear in-phase behavior between the observed ozone tendency and the largest forcing at each level. We also note that the vertical shift in the tropopause height and the maximum ozone amplitude in WACCM as compared to observations (Fig. 4b) can influence the structure in Fig. 11. In particular, it is not trivial to guess how the different transport terms would change if these biases were removed from the model.

Figure 12 shows the balance of the terms in the CO continuity equation in WACCM. The primary balance is between the increase due to mean upwelling and decrease by photochemical loss, and there is a strong annual cycle in the CO tendency (at 62 and 73 hPa) that follows the upwelling. For CO the horizontal transport is relatively smaller than for ozone, and this is due to the smaller background meridional gradients in CO (as noted by Ploeger et al., 2012). At levels close to the tropopause (86 hPa) a semi-annual cycle in CO is evident, linked to variations in CO sources and near-equatorial deep convection (e.g. Liu et al., 2013; Park et al., 2013). In isentropic coordinates the annual cycle amplitude of CO is reduced by ∼ 30 % with respect to that on pressure levels, but the vertical structure is not significantly changed in this case (not shown). The cross-isentropic (quasi-vertical) transport term is the largest term in the isentropic balance, with a seasonal cycle that is delayed ∼ 1–2 months compared to the cycle in pressure coordinates.

### 4.3 Sub-seasonal variability

The time series of WACCM temperature and tracers in Fig. 3 show correlated variability at timescales shorter than the seasonal cycle. Similar coherent sub-seasonal variability is seen in observations, and Abalos et al. (2012) showed that these were linked to transient variations in tropical upwelling. Using WACCM output we are able to evaluate the contribution from all the transport terms to the sub-seasonal variability in the tracers. We do this by first filtering the time series to isolate sub-seasonal variations (retaining periods < 1 yr), and then examining correlations among the different terms in the

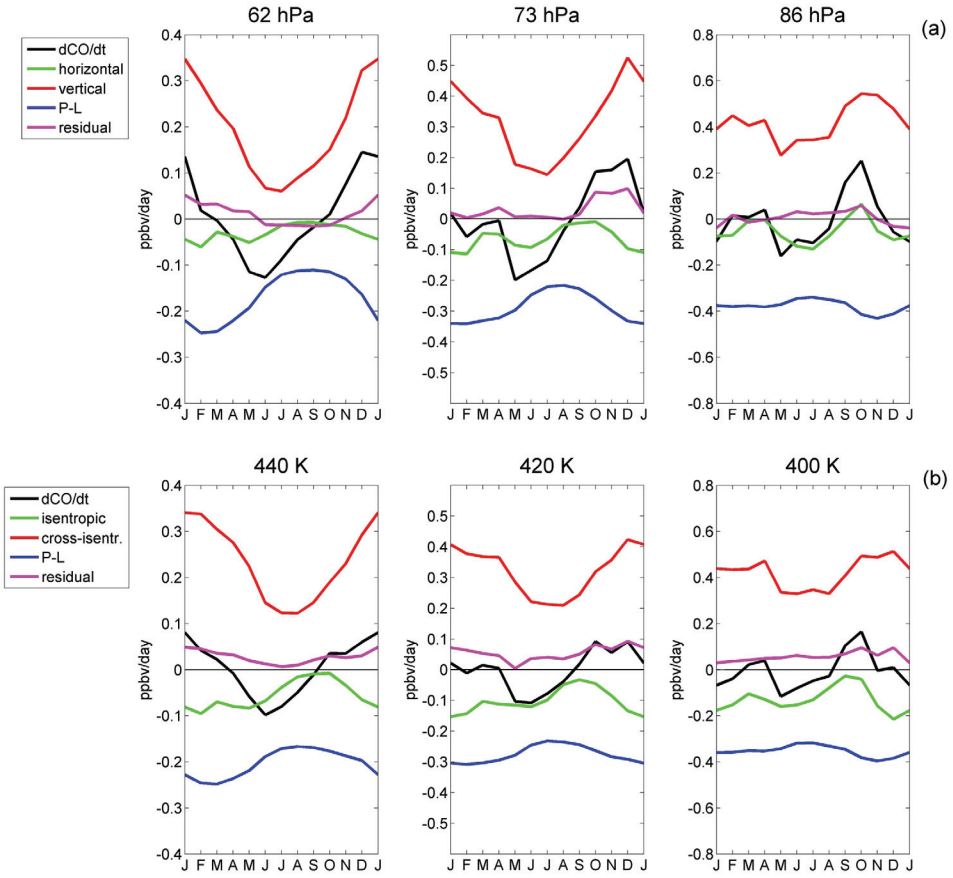


**Fig. 12.** Mean seasonal cycle (monthly means) of the terms in the CO continuity equation averaged over 18° S–18° N on pressure levels (Eq. 5, **a**) and isentropic levels (Eq. 6, **b**).

thermodynamic and tracer continuity equations (Eqs. 1 and 5 respectively). Figure 13a shows the correlation between temperature tendency ($\partial\bar{T}/\partial t$) and vertical advection by tropical upwelling, revealing high correlations ($\sim 0.8$) at and above 73 hPa. At lower levels, near and below the tropopause (86 hPa), the correlations of $\partial\bar{T}/\partial t$ with upwelling decrease and diabatic heating ($\bar{Q}$) gradually becomes the main driver of sub-seasonal variability in temperature. Figure 13b and c show the correlations of the ozone and CO tendencies with vertical and horizontal transport terms. In both cases sub-seasonal tracer fluctuations are most strongly correlated with the vertical transport. There is also a contribution from horizontal transport, particularly at lower levels, which is somewhat more important for ozone than for CO. Tropical upwelling and the eddy term make the primary contributions to the vertical transport and the horizontal transport, respectively, and the correlations of the tracer tendencies with these components are also shown in Fig. 13b and c. Note that for CO at lower levels a large fraction of the correlations with vertical transport are not explained by upwelling, because of an important contribution from vertical eddy transport. This vertical eddy transport in the model is linked to regional positive CO anomalies (originating from localized emissions), which coincide with enhanced vertical velocity anomalies.

As with the seasonal cycle, the variability of tracers on sub-seasonal timescales is reduced in isentropic compared to log-pressure coordinates, because transient upwelling forces correlated variations in temperature and tracers. The fraction of sub-seasonal variability on isentropes compared to that on nearby pressure levels decreases from $\sim 75$ % near 86 hPa to $\sim 30$ % near 62 hPa for ozone and CO. The vertical structure is the mirror image of the correlations between each of the tracers and temperature, i.e., the fraction is low where the tracer-temperature correlations are high. This is consistent

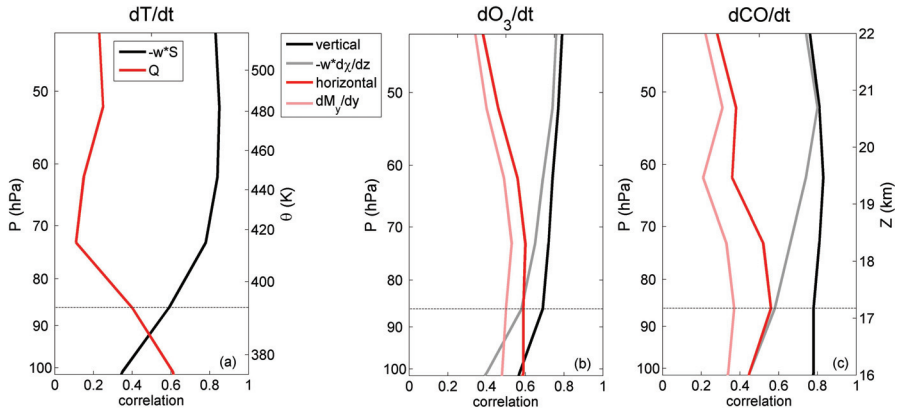


**Fig. 13.** Correlations between tendencies and forcings for tropical sub-seasonal variability in WACCM. **(a)** Correlations between sub-seasonal temperature tendency ($\partial\bar{T}/\partial t$) and vertical advection by tropical upwelling (solid black line). The red line shows correlations of $\partial\bar{T}/\partial t$ with the diabatic heating rates ($\bar{Q}$). **(b)** and **(c)** Correlations of vertical (black) and horizontal (red) components of transport with ozone **(b)** and CO **(c)** tendencies. Lines in the washed colors indicate correlations of the tendency with the component that makes the largest contribution to each transport term (tropical upwelling for vertical transport and eddy term for horizontal transport). All series are filtered to isolate sub-seasonal timescales (that is, periods < 1 yr) before computing the correlations. For reference, the location of annual mean isentropic levels in WACCM is indicated on **(a)** and the approximate altitude on **(c)**, estimated as described in Fig. 1. The dashed horizontal lines indicate the location of the annual mean cold point tropopause in WACCM.

with the fact that on isentropes the fraction of tracer variability that is common with temperature (forced mainly by upwelling) is removed. Because the (relatively large) component of variability tied to the adiabatic component of upwelling is removed in isentropic coordinates, the remaining tracer variability is best correlated with isentropic (quasi-horizontal) eddy transport (results not shown). The contribution of isentropic transport is relatively less important for CO than for ozone (consistent with smaller meridional gradients in CO) and the correlations with cross- and isentropic transport are comparable.

## 5 Summary and discussion

A free-running simulation from WACCM (version 4) is shown to represent the most relevant aspects of temperature, ozone and CO spatial structure and temporal variability near the tropical tropopause. One caveat is that the tropopause is slightly higher in the model and the pressure levels do not correspond to exactly the same levels in the atmosphere in terms of temperature and tracer variability.

The shift in the tropopause height is likely associated with the limited vertical resolution of the model (e.g. Gettelman et al., 2010). We have compared the vertical structure of temperature and tracer mean values and annual amplitudes (Figs. 1 and 4) with results from a high-vertical resolution (∼ 300 m) simulation with WACCM version 3, similar to that used in the last CCMVal report (SPARC CCMVal, 2010). The bias in the annual mean cold point tropopause height practically disappears when the vertical resolution is increased. In addition, the shift in the altitude of maximum annual amplitude is largely reduced, especially for ozone. This comparison (not shown) proves that the model is able to capture the altitude of the tropopause more realistically than it appears when using the usual (coarser) resolution. Furthermore, it suggests that increasing the vertical resolution in the model could help improve the representation of tracer transport processes near the tropical tropopause.

Despite the described shift, the overall vertical structure and annual cycle of the temperature and tracer variability is realistically captured, and the model constitutes a valuable tool for tracer transport studies. We use WACCM results to quantify all the terms in the tracer budgets and analyze the different transport mechanisms determining the mean structure and variability on seasonal and sub-seasonal timescales. The time-mean picture shows that the budget of ozone in the tropical lower stratosphere is a balance of mean vertical advection with photochemical ozone production plus significant positive tendencies from eddy transport from the sub-tropics. These results support the observational analysis of Abalos et al. (2012), demonstrating that the residuals in their tracer budgets are largely associated with unresolved eddy transport terms.

Eddy transport is important for tropical ozone in the lower stratosphere, and has an interesting vertical structure in the model. At higher levels (∼ 440 K) eddy transport occurs in the sub-tropics during winter and spring in each hemisphere, on the upper flanks of the subtropical jets. On the other hand,

at levels closer to the tropopause (∼ 400 K) horizontal transport of ozone is dominated by the Asian monsoon anticyclonic circulation in NH summer. The vertical advection by tropical upwelling shows a large annual cycle at the higher levels (around ∼ 70 hPa, coinciding with stronger vertical gradients), and mainly drives the ozone seasonality at these altitudes. Close to the tropopause, the seasonality in vertical advection is smaller and instead there is a larger annual cycle in horizontal transport (Fig. 11). For CO, vertical transport dominates the seasonal cycle and effects of horizontal transport are less important than for ozone. A semi-annual cycle is observed at the tropopause level, linked to seasonally and spatially dependent CO emissions.

A number of modeling studies have examined the vertical structure and seasonality of quasi-horizontal eddy transport between the tropics and extra-tropics in the lower stratosphere (Chen et al., 1994; Volk et al., 1996; Waugh, 1996). One common conclusion of these studies is that the largest exchange occurs near the tropopause during boreal summer, mainly associated with wave activity linked to monsoonal circulations. Observational studies have also identified the near-tropopause transport associated with the Asian monsoon (e.g. Trepte et al., 1993). Large boreal summer ozone in-mixing rates derived from trajectory calculations in Ploeger et al. (2012) are observed in the layer ∼ 370–420 K. At higher levels the tropics are more isolated and transport events are associated with breaking Rossby waves during the winter season (Waugh, 1996). Haynes and Shuckburgh (2000a, b) presented a detailed analysis of the seasonality and spatial structure of mixing throughout the upper troposphere and the stratosphere, and their results show enhanced mixing in the summer northern tropics below ∼ 400 K. The vertical confinement of the horizontal mixing effect of the summer monsoon anticyclones to levels close to the tropopause obtained with WACCM calculations is in agreement with these previous works. On the other hand, at higher levels (∼ 450 K) Haynes and Shuckburgh (2000a, b) observed a latitudinal displacement of the tropical reservoir (identified as the region with near-zero mixing) towards the summer hemisphere, slightly more pronounced in boreal summer. They argued that this marked seasonality in the location of the subtropical transport barriers is a key issue for understanding spatial and temporal distribution of mixing in the tropical lower stratosphere. A similar seasonal latitudinal displacement of the tropical reservoir (i.e., the region with near-zero eddy transport) can also be identified in our results (see the upper panel of Fig. 9). The picture of tracer transport that arises from the present model analysis is also consistent with the climatology of Rossby wave breaking in the subtropics from the ERA-Interim reanalysis derived by Homeyer and Bowman (2013). Their results show enhanced transport into the tropics during northern summer (associated with the Asian monsoon) limited to levels below ∼ 420 K, and more modest seasonality with slightly more frequent wave breaking during winter and spring above that level.

The choice of isentropic versus log-pressure vertical coordinates influences the detailed budget results, and by using both coordinate systems in this work we are able to quantify these complementary perspectives. As first discussed by Konopka et al. (2009), the amplitude of the seasonal cycle in ozone in isentropic coordinates is reduced by more than 50 % compared to the amplitude on pressure levels. On isentropes, the largest (relative) annual cycle for ozone is found at levels close to the tropopause, where the Asian monsoon makes a major contribution to the summer maximum via eddy transport. At higher altitudes, where the largest annual cycles in temperature and ozone occur, approximately 2/3 of the ozone seasonal variation is removed in isentropic coordinates, and the tendency is a relatively small term in the balance (Fig. 8b). In the case of CO, the seasonal amplitude is also reduced on isentropes but to a smaller degree, the vertical structure is unchanged and the overall balance remains similar (Fig. 12).

Because upwelling forces a large seasonal cycle in temperature at the same altitudes where the cycles in tracers are largest, the log-pressure coordinates allow simple understanding of the coupled seasonal cycles in tracers and temperature. The use of these two different vertical coordinates accounts for part of the existing discrepancy regarding the origin of the ozone seasonality. However, it remains an open question how to reconcile the Eulerian-based results in this study with the Lagrangian transport calculations of Konopka et al. (2009, 2010) and Ploeger et al. (2012).

Finally, the model simulation also reveals variability on sub-seasonal timescales in tropical lower stratosphere tracers, which are strongly correlated with temperature for ozone and anti-correlated for CO. These coupled variations mainly result from the corresponding transient fluctuations in upwelling (Fig. 13). At levels close to the tropopause, there is also an important contribution from horizontal eddy transport for ozone and from vertical eddy transport for CO. The variability linked to adiabatic tropical upwelling is removed on isentropic coordinates, and the (considerably smaller) subseasonal fluctuations in the tracers are mostly due to eddy quasi-horizontal (isentropic) transport events, especially for ozone.

**Appendix A**

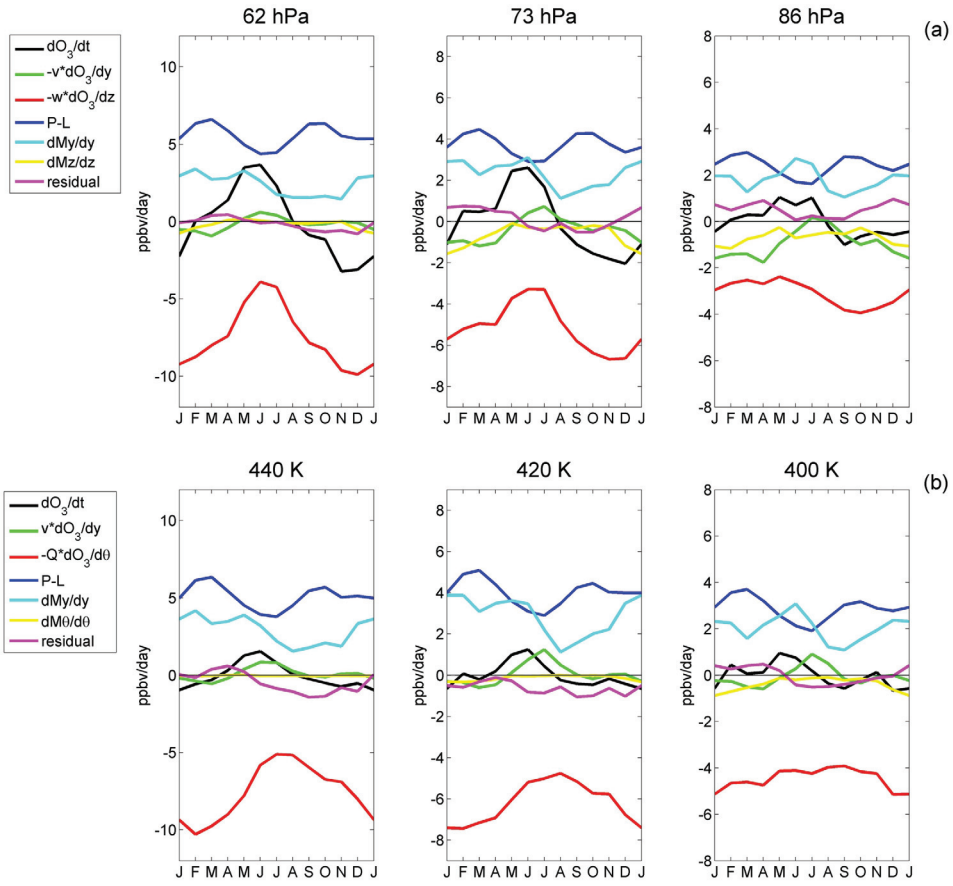


**Fig. A1.** Mean seasonal cycle (monthly means) of the terms in the ozone continuity equation averaged over 18° S–18° N on pressure levels (Eq. 2, **a**) and isentropic levels (Eq. 6, **b**).

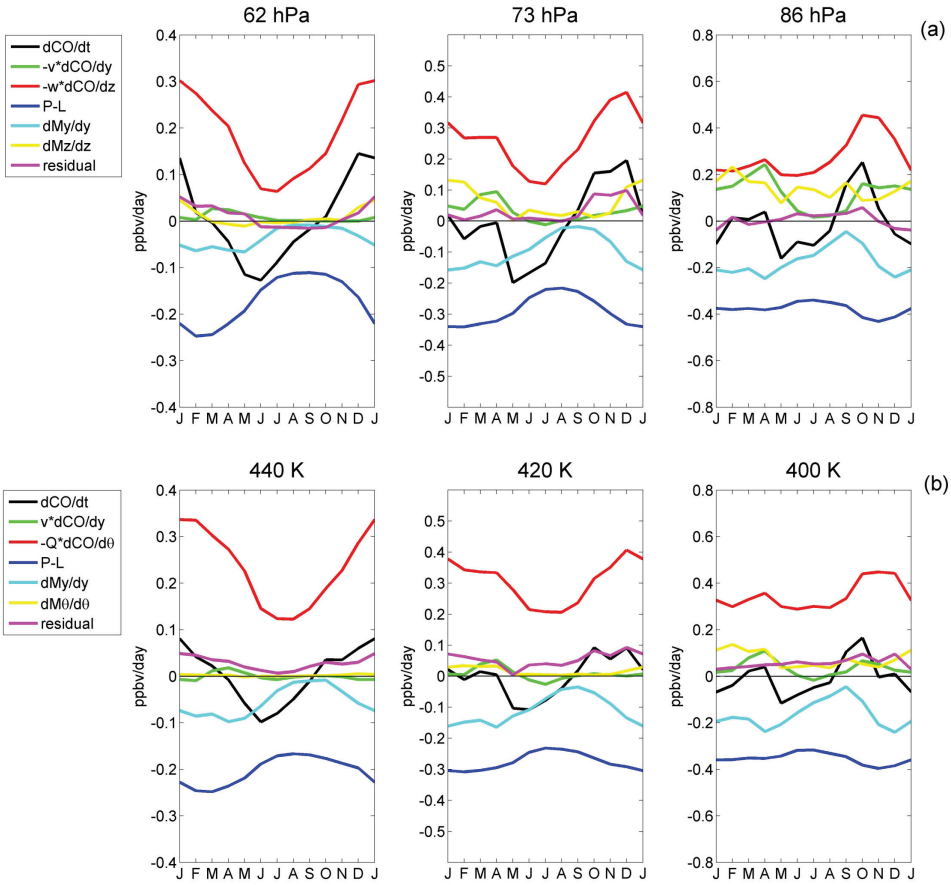


**Fig. A2.** Mean seasonal cycle (monthly means) of the terms in the CO continuity equation averaged over 18° S–18° N on pressure levels (Eq. 2, **a**) and isentropic levels (Eq. 6, **b**).

*Acknowledgements.* We are grateful to R. Garcia and C. Homeyer for constructive comments on the manuscript. We also thank F. Wu and M. Park for providing observational data, and J. A. Añel for facilitating the high-vertical resolution WACCM output. This work was partially supported under the NASA Aura Science Program. The National Center for Atmospheric Research is operated by the University Corporation for Atmospheric Research, under sponsorship of the National Science Foundation. Marta Abalos is funded by the grant BES-2009-013082 and the CGL2012-34997 Project of the Spanish Government. Most of the work has been carried out during visits of M. A. to the Atmospheric Chemistry Division at NCAR.

Edited by: P. Haynes

## References

Abalos, M., Randel, W. J., and Serrano, E.: Variability in upwelling across the tropical tropopause and correlations with tracers in the lower stratosphere, Atmos. Chem. Phys., 12, 11505–11517, doi:10.5194/acp-12-11505-2012, 2012.

Andrews, D. G., Holton, J. R., and Leovy, C. B.: Middle Atmosphere Dynamics, Academic Press, Orlando, Florida, 489 pp., 1987.

Anthes, R. A., Bernhardt, P. A., Chen, Y., Cucurull, L., Dymond, K. F., Ector, D., Healy, S. B., Ho, S.-P., Hunt, D. C., Kuo, Y.-H., Liu, H., Manning, K., McCormik, C., Meehan, T. K., Randel, W. J., Rocken, C., Schreiner, W. S., Sokolovskiy, S. V., Syndergaard, S., Thompson, D. C., Trenberth, K. E., Wee, T.-K., Yen, N. L.,

and Zeng, Z.: The COSMIC/FORMOSAT-3 Mission: Early Results, B. Am. Meteorol. Soc., 89, 313–333, doi:10.1175/BAMS-89-3-313, 2008.

Chen, P., Holton, J. R., O'Neill, A., and Swinbank, R.: Isentropic mass exchange between the Tropics and extra-tropics in the stratosphere, J. Atmos. Sci., 51, 3006–3018, 1994.

Fueglistaler, S., Dessler, A. E., Dunkerton, T. J., Folkins, I., Fu, Q., and Mote, P. W.: Tropical Tropopause Layer, Rev. Geophys., 47, RG1004, doi:10.1029/2008RG000267, 2009.

Garcia, R. R., Marsh, D. R., Kinnison, D. E., Boville, B. A., and Sassi, F.: Simulation of secular trends in the middle atmosphere, J. Geophys. Res., 112, D09301, doi:10.1029/2006JD007485, 2007.

Gettelman, A., Hegglin, M. I., Son, S.-W., Kim, J., Fujiwara, M., Birner, T., Kremser, S., Rex, Añel, J. A., Akiyoshi, H., Austin, J., Bekki, S., Braesike, P., Brül, C., Butchart, N., Chipperfield, M., Dameris, M., Dhomse, S., Garny, H., Hardiman, S. C., Jöckel, P., Kinnison, D. E., Lamarque, J. F., Mancini, E., Marchand, M., Michou, M., Morgenstern, O., Pawson, S., Pitari, G., Plummer, D., Pyle, J. A., Rozanov, E., Scinocca, J., Shepherd, T. G., Shibata, K., Smale, D, Teyssèdre, H., and Tian, W.: Multimodel assessment of the upper troposphere and lower stratosphere: Tropics and global trends, J. Geophys. Res., 115, D00M08, doi:10.1029/2009JD013638, 2010.

Haynes, P. and Shuckburgh, E.: Effective diffusivity as a diagnostic of atmospheric transport: 1. Stratosphere, J. Geophys. Res., 105, 22777–22794, doi:10.1029/2000JD900093, 2000a.

Haynes, P. and Shuckburgh, E.: Effective diffusivity as a diagnostic of atmospheric transport: 2. Troposphere and lower stratosphere, J. Geophys. Res., 105, 22795–22810, doi:10.1029/2000JD900092, 2000b.

Homeyer, C. R. and Bowman, K. P.: Rossby wavebreaking and transport between the tropics and extra-tropics above the subtropical jet, J. Atmos. Sci., 70, 607–626, doi:10.1175/JAS-D-12-0198.1, 2013.

Kinnison, D. E., Brasseur, G. P., Walters, S., Garcia, R. R., Marsh, D. R., Sassi, F., Harvey, V. L., Randall, C. E., Emmons, L., Lamarque, J. F., Hess, P., Orlando, J., Tie, X., Randel, W., Pan, L., Gettelman, A., Granier, C., Diehl, T., Niemeier, U., and Simmons, A. J.: Sensitivity of chemical tracers to meteorological parameters in the MOZART-3 chemical transport model, J. Geophys. Res., 112, D20302, doi:10.1029/2006JD007879, 2007.

Konopka, P., Grooß, J.-U., Ploeger, F., and Müller, R.: Annual cycle of horizontal in-mixing into the lower tropical stratosphere, J. Geophys. Res., 114, D19111, doi:10.1029/2009JD011955, 2009.

Konopka, P., Grooß, J.-U., Günther, G., Ploeger, F., Pommrich, R., Müller, R., and Livesey, N.: Annual cycle of ozone at and above the tropical tropopause: observations versus simulations with the Chemical Lagrangian Model of the Stratosphere (CLaMS), Atmos. Chem. Phys., 10, 121–132, doi:10.5194/acp-10-121-2010, 2010.

Lin, S.-J.: A "vertically lagrangian" finite-volume dynamical core for global models, Mon. Weather Rev., 132, 2293–2307, doi:10.1175/1520-0493(2004)132<2293:AVLFDC>2.0.CO;2, 2004.

Liu, J., Logan, J. A., Murray, L. T., Pumphrey, H. C., Schwartz, M. J., and Megretskaia, I. A.: Transport analysis and source attribution of seasonal and interannual variability of CO in the tropical upper troposphere and lower stratosphere, Atmos. Chem. Phys., 13, 129–146, doi:10.5194/acp-13-129-2013, 2013.

Livesey, N. J., Filipiak, M. J., Froidevaux, L., Read, W. G., Lambert, A., Santee, M. L., Jiang, J. H., Pumphrey, H. C., Waters, J. W., Cofield, R. E., Cuddy, D. T., Daffer, W. H., Drouin, B. J., Fuller, R. A., Jarnot, R. F., Jiang, Y. B., Knosp, B. W., Li, Q. B., Perun, V. S., Schwartz, M. J., Snyder, W. V., Stek, P. C., Thurstans, R. P., Wagner, P. A., Avery, M., Browell, E. V., Cammas, J.-P., E. Christensen, L., Diskin, G. S., Gao, R.-S., Jost, H.-J., Loewenstein, M., Lopez, J. D., Nedelec, P., Osterman, G. B., Sachse, G. W., and Webster, C. R.: Validation of Aura Microwave Limb Sounder $O_3$ and CO observations in the upper troposphere and lower stratosphere, J. Geophys. Res., 113, D15S02, doi:10.1029/2007JD008805, 2008.

Park, M., Randel, W. J., Kinnison, D. E., Emmons, L. K., Bernath, P. F., Walker, K. A., Boone, C. D. D., and Livesey, N. J.: Hydrocarbons in the upper troposphere and lower stratosphere observed from ACE-FTS and comparisons with WACCM, J. Geophys. Res., doi:10.1029/2012JD018327, in press, 2013.

Ploeger, F., Konopka, P., Müller, R., Fueglistaler, S., Schmidt, T., Manners, J. C., Grooß, J.-U., Günther, G., Forster, P. M., and Riese, M.: Horizontal transport affecting trace gas seasonality in the Tropical Tropopause Layer (TTL), J. Geophys. Res., 117, 1–16, doi:10.1029/2011JD017267, 2012.

Plumb, R. A.: A tropical pipe model of stratospheric transport, J. Geophys. Res., 101, 3957–3972, doi:10.1029/95JD03002, 1996.

Plumb, R. A.: Stratospheric transport, J. Meteorol. Soc. Jpn., 80, 793–809, doi:10.2151/jmsj.80.793, 2002.

Randel, W. J. and Held, I. M.: Phase speed spectra of transient eddy fluxes and critical layer absorption, J. Atmos. Sci., 48, 688–697, doi:10.1175/1520-0469(1991)048<0688:PSSOTE>2.0.CO;2, 1991.

Randel, W. J., Park, M., Wu, F., and Livesey, N.: A Large Annual Cycle in Ozone above the Tropical Tropopause Linked to the Brewer-Dobson Circulation, J. Atmos. Sci., 64, 4479–4488, doi:10.1175/2007JAS2409.1, 2007.

Riese, M., Ploeger, F., Rap, A., Vogel, B., Konopka, P., Dameris, M., and Forster, P.: Impact of uncertainties in atmospheric mixing on simulated UTLS composition and related radiative effects, J. Geophys. Res., 117, 1–10, doi:10.1029/2012JD017751, 2012.

Rosenlof, K. H., Tuck, A. F., Kelly, K. K., Russell III, J. M., and McCormick, M. P.: Hemispheric asymmetries in water vapor and inferences about transport in the lower stratosphere, J. Geophys. Res., 102, 13213–13234, doi:10.1029/97JD00873, 1997.

Santee, M. L., Manney, G. L., Livesey, N. J., Froidevaux, L., Schwartz, M. J., and Read, W. G.: Trace gas evolution in the lowermost stratosphere from Aura Microwave Limb Sounder measurements, J. Geophys. Res., 116, D18306, doi:10.1029/2011JD015590, 2011.

Shepherd, T. G.: Transport in the middle atmosphere, J. Meteorol. Soc. Jpn., 85, 165–191, 2007.

SPARC CCMVal Report on the Evaluation of Chemistry-Climate Models, Eyring, V., Shepherd, T. G., and Waugh, D. W. (Eds.), SPARC Report No. 5, WCRP-132, WMO/TD-No. 1526, 2010.

Taguchi, M.: Wave driving in the tropical lower stratosphere as simulated by WACCM. Part I: annual cycle, J. Atmos. Sci., 66, 2029–2043, doi:10.1175/2009JAS2854.1, 2009.

Thompson, A. M., Witte, J. C., Smit, H. G. J., Oltmans, S. J., Johnson, B. J., Kirchhoff, V. W. J. H., and Schmidlin, F. J.: Southern

Hemisphere Additional Ozonesondes (SHADOZ) 1998–2004 tropical ozone climatology: 3. Instrumentation, station-to-station variability, and evaluation with simulated flight profiles, J. Geophys. Res., 112, D03304, doi:10.1029/2005JD007042, 2007.

Thompson, A. M., Miller, S. K., Tilmes, S., Kollonige, D. W., Witte, J. C., Oltmans, S. J., Johnson, B. J., Fujiwara, M., Schmidlin, F. J., Coetzee, G. J. R., Komala, N., Maata, M., Mohamad, M., Nguyo, J., Mutai, C., Ogino, S.-Y., da Silva, F. R., Paes Leme, N. M., Posny, F., Scheele, R., Selkirk, H. B., Shiotani, M., Stübi, R., Levrat, G., Calpini, B., Thouret, V., Tsuruta, H., Valverde Canossa, J., Vömel, H., Yonemura, S., Diaz, J. A., Tan Thanh, N. T., and Thuy Ha, H. T.: Southern Hemisphere Additional Ozonesondes (SHADOZ) ozone climatology (2005–2009): Tropospheric and tropical tropopause layer (TTL) profiles with comparisons to OMI-based ozone products, J. Geophys. Res., 117, D23301, doi:10.1029/2011JD016911, 2012.

Trepte, C. R., Veiga, R. E., and McCormick, M. P.: The poleward dispersal of Mount Pinatubo volcanic aerosol, J. Geophys. Res., 98, 18563–18573, doi:10.1029/93JD01362, 1993.

Volk, C. M., Elkins, J. W., Fahey, D. W., Salawitch, R. J., Dutton, G. S., Gilligan, J. M., Proffitt, M. H., Loewenstein, M., Podolske, J. R., Minschwaner, K., Margitan, J. J., and Chang, K. R.: Quantifying transport between the tropical and mid-latitude lower stratosphere, Science, 272, 1763–1768, doi:10.1126/science.272.5269.1763, 1996.

Waugh, D. W.: Seasonal variation of isentropic transport out of the tropical stratosphere, J. Geophys. Res., 101, 4007–4023, doi:10.1029/95JD03160, 1996.

# 3 Ozone seasonality above the tropical tropopause: reconciling the Eulerian and Lagrangian perspectives of transport processes.

*Abalos, M., Ploeger, F., Konopka, P., Randel, W. J., and Serrano, E., Atmos. Chem. Phys., 13, 10787-10794, doi:10.5194/acp-13-10787-2013, 2013b.*

Atmos. Chem. Phys., 13, 10787–10794, 2013
www.atmos-chem-phys.net/13/10787/2013/
doi:10.5194/acp-13-10787-2013


Atmospheric Chemistry and Physics Open Access

# Ozone seasonality above the tropical tropopause: reconciling the Eulerian and Lagrangian perspectives of transport processes

**M. Abalos[1], F. Ploeger[2], P. Konopka[2], W. J. Randel[3], and E. Serrano[1]**

[1]Universidad Complutense de Madrid, Madrid, Spain
[2]Institute of Energy and Climate Research: Stratosphere (IEK-7), Forschungszentrum Jülich, Jülich, Germany
[3]National Center for Atmospheric Research, Boulder, Colorado, USA

*Correspondence to:* M. Abalos (mabalosa@fis.ucm.es)

Received: 4 June 2013 – Published in Atmos. Chem. Phys. Discuss.: 22 July 2013
Revised: 7 October 2013 – Accepted: 14 October 2013 – Published: 6 November 2013

**Abstract.** We aim to reconcile the recently published, apparently contrasting results regarding the relative importance of tropical upwelling versus horizontal transport for the seasonality of ozone above the tropical tropopause. Different analysis methods in the literature (Lagrangian versus Eulerian, and isentropic versus pressure vertical coordinates) yield different perspectives of ozone transport, and the results must be carefully compared in equivalent terms to avoid misinterpretation. By examining the Lagrangian calculations in the Eulerian formulation, we show here that the results are in fact consistent with each other and with a common understanding of the ozone transport processes near and above the tropical tropopause.

We further emphasize that the complementary approaches are suited for answering two different scientific questions: (1) what drives the observed seasonal cycle in ozone at a particular level above the tropical tropopause? and (2) how important is horizontal transport from mid-latitudes for ozone concentrations in the tropical lower stratosphere? Regarding the first question, the analysis of the transformed Eulerian mean (TEM) ozone budget shows that the annual cycle in tropical upwelling is the main forcing of the ozone seasonality at altitudes with large vertical gradients in the tropical lower stratosphere. To answer the second question a Lagrangian framework must be used, and the results show that a large fraction (∼50 %) of the ozone molecules ascending through the tropical lower stratosphere is of extra-tropical origin and has been in-mixed from mid-latitudes.

## 1 Introduction

Ozone concentrations in the lower tropical stratosphere are determined by photochemical production and by transport processes (e.g., Avallone and Prather, 1996). Photochemical production and horizontal transport of ozone-rich mid-latitude air into the tropics (denoted in-mixing in the following) increase ozone mixing ratios above the tropical tropopause. The vertical upward motion in the tropical lower stratosphere carries air masses from below, with lower ozone concentrations, with seasonally varying strength. Upwelling effectively acts to decrease ozone in the tropical lower stratosphere, where the steepest relative vertical ozone gradients are found, and is balanced in the time mean by photochemical production and in-mixing.

Observations of ozone reveal a large seasonal cycle with a characteristic narrow vertical structure just above the tropical tropopause. Randel et al. (2007) highlighted this behavior and proposed that it was forced by the seasonality in tropical upwelling acting on the strong ozone background vertical gradients. Recently, Abalos et al. (2012) computed the seasonality of the different terms in the transformed Eulerian mean (TEM) transport equation using satellite observations of ozone and reanalysis meteorological fields, and found that the seasonality in ozone mainly followed the seasonality of vertical advection by upwelling at levels with large vertical gradients. Hence, these works concluded that vertical advection within the tropics is the main forcing of the ozone seasonality at a fixed altitude level in the TEM framework.

On the other hand, Konopka et al. (2009) examined the origin of the ozone annual cycle using a conceptual

**Published by Copernicus Publications on behalf of the European Geosciences Union.**

one-dimensional tropical trace gas model, and proposed that quasi-horizontal transport played a primary role in causing the ozone seasonality. Furthermore, Konopka et al. (2010) observed a clear summer maximum in isentropic ozone transport from the northern mid-latitudes into the tropics (in-mixing) associated with the Asian monsoon upper level circulation, in global model simulations with the Chemical Lagrangian Model of the Stratosphere (ClaMS; McKenna et al., 2002). Using three-dimensional back trajectories and a one-dimensional conceptual model, which explicitly included in-mixing from mid-latitudes, Ploeger et al. (2012) further showed that the ozone annual cycle above the tropical tropopause entirely disappeared if in-mixing was inhibited. Consequently, from a Lagrangian perspective following air parcel trajectories, in-mixing of mid-latitude air into the tropics appeared essential for explaining tropical ozone mixing ratios, and particularly the ozone summer maximum.

These results evidence a current lack of understanding regarding the origin of the ozone seasonality in the tropical tropopause layer (TTL) (e.g., Fueglistaler et al., 2009) and tropical lower stratosphere. More specifically, there seems to be a contradiction between the Eulerian results of Randel et al. (2007) and Abalos et al. (2012), who conclude that tropical upwelling is the main driver of the annual cycle in ozone above the tropical tropopause, and the Lagrangian results of Konopka et al. (2009, 2010) and Ploeger et al. (2012), who find that in-mixing is essential for the seasonality. This controversy in the recent literature regarding tropical ozone concentrations is not found for other species (e.g., carbon monoxide, water vapor, nitrous oxide) because the effect of in-mixing is weaker due to the relatively smaller meridional gradients between tropics and extra-tropics in these tracers (Ploeger et al., 2012).

To some extent, the conflict arises from the different vertical coordinates used in the analyses, i.e., pressure versus potential temperature (isentropic) coordinates. As noted by Konopka et al. (2009), the amplitude of the annual cycle in ozone is notably reduced (by ∼60 %) on isentropic levels compared to altitude (or pressure). This is due to the large seasonality in the altitude of the isentropes above the tropical tropopause (linked to temperature changes associated with the seasonality in upwelling). Very recently, Abalos et al. (2013) explicitly compared the differences in the ozone budgets between pressure and isentropic coordinates. Their results show that, on isentropic levels above the tropopause (corresponding to mean log-pressure altitudes with large annual cycles in temperature and ozone) the net tendency is small compared to the other terms in the ozone budget. Thus, despite the overall similarity of the balances in both coordinate systems, on isentropes the reduced ozone seasonality does not follow the larger annual cycle in diabatic advection. However, this fundamental difference only partially explains the apparent contradiction between the above-mentioned works.

In this paper, we demonstrate that the remaining conflict can be reconciled by taking account of the differences between the Eulerian versus Lagrangian perspectives. The Eulerian view separates vertical and horizontal components of transport at each level, such that air parcels are identified as in-mixed only if they are transported horizontally into the tropics at that particular level. The Lagrangian method integrates changes in ozone concentration along each parcel trajectory, so that air parcels are considered in-mixed if they are transported horizontally into the tropics either at that level or at lower levels. Hence, air masses that are in-mixed by the Asian monsoon anticyclone at a given altitude and then vertically advected within the tropics by upwelling will be considered as transported vertically across an upper level in the Eulerian calculations, but represent horizontal transport in the Lagrangian analysis. Abalos et al. (2013) examined the ozone budget using output from a chemistry–climate model, which explicitly resolved all terms in the TEM equation, including eddy transport terms. Their results showed a detailed vertical structure in ozone transport seasonality near the tropical tropopause, with isentropic transport associated with the Asian monsoon dominating around tropopause level and tropical upwelling driving ozone seasonality at higher altitudes (∼2 km above). In the present work we bring together the Eulerian and the Lagrangian analyses to demonstrate that both views are consistent, and provide a complementary understanding of ozone transport near the tropical tropopause.

The used method and models are described in Sect. 2. Section 3 presents the results, concerning the seasonality of ozone in the tropical lower stratosphere from the Eulerian and Lagrangian perspectives. In the following Sect. 4 we discuss these results and implications.

## 2 Model data and method

In order to compare the Lagrangian and Eulerian frameworks, we contrast results from the WACCM (Whole Atmosphere Community Climate Model, Garcia et al., 2007) chemistry climate model, as used by Abalos et al. (2013), with results from the conceptual Lagrangian one-dimensional tropical tracer model (termed "1-D model" in the following), used by Ploeger et al. (2012). The output of the Lagrangian 1-D model will be transformed into Eulerian information, in order to compare equivalent terms.

The conceptual 1-D model for tropical ozone mixing ratio is based on a tropical mean description:

$$\frac{d\chi}{\mathrm{d}t} = P - \alpha_{\mathrm{N}}(\chi - \chi_{\mathrm{N}}) - \alpha_{\mathrm{S}}(\chi - \chi_{\mathrm{S}}). \quad (1)$$

Here, $\chi$ represents a tropical (20° S–20° N) mean, $\frac{d}{\mathrm{d}t}$ is the one-dimensional material derivative following the mean upward motion, $\chi_{\mathrm{N}}$ and $\chi_{\mathrm{S}}$ are the mean Northern Hemisphere (NH) and Southern Hemisphere (SH) mid-latitude annual mean mixing ratios, and $\alpha_{\mathrm{N}}$ and $\alpha_{\mathrm{S}}$ are the inverse

in-mixing damping timescales for the NH and SH, respectively. $P$ is the tropical mean photochemical ozone production rate, taken from the Lagrangian chemistry transport model ClaMS. Horizontal in-mixing (i.e., the sum of advective transport and eddy mixing) is represented as a relaxation against $\chi_N$ and $\chi_S$, which are taken from the 1991–2002 HALOE climatology of Grooß and Russell (2005). The in-mixing inverse damping timescales, $\alpha_N$ and $\alpha_S$, are diagnosed from CLaMS three-dimensional (3-D) back trajectories based on ERA-Interim reanalysis winds, as described in Ploeger et al. (2012). The tropical mean vertical upwelling velocity $\dot{\theta} = Q$ is taken from ERA-Interim, after correcting for the excessively rapid upward transport in the TTL region in this reanalysis by multiplying the heating rate $Q$ by 0.6 (for a more detailed discussion see Ploeger et al., 2012). Note that the in-mixing rates $\alpha_N$ and $\alpha_S$ depend on potential temperature and time and show an annual cycle with maximum during hemispheric summer (as shown in Ploeger et al., 2012, Fig. 5), while the mean extra-tropical mixing ratios used here, $\chi_N$ and $\chi_S$, are annual mean quantities depending only on potential temperature. The results obtained using time-varying (i.e., monthly mean) values for these concentrations are qualitatively similar (not shown).

Equation (1) is formulated in Lagrangian terms, and they state that the rate of change in the concentration of ozone in a given air parcel ascending in the tropics, given by the material derivative ($d\chi/\mathrm{d}t$), is determined exclusively by the sources and sinks ($S$):

$$\frac{d\chi}{\mathrm{d}t} = S, \tag{2}$$

with the source term $S = P - \alpha_N(\chi - \chi_N) - \alpha_S(\chi - \chi_S)$ (see Eq. 1). Ploeger et al. (2012) demonstrated that lateral in-mixing from the extra-tropics must be included in the conceptual 1-D tropical-averaged model in order to obtain a realistic representation of both the mean tropical ozone profile and its seasonality. Consequently, the source term $S$ in this model comprises both photochemical production and lateral in-mixing from the extra-tropics.

From the Lagrangian point of view of Eq. (2) the observer follows the air parcel trajectory, as expressed by the material derivative. From the Eulerian point of view, on the contrary, the observer is fixed at a given location and perceives the flow passing by. In order to transform Eq. (2) into an Eulerian equation, the material derivative is expressed as a function of the local tendency plus the change due to the spatial displacement of the parcel: $\frac{d}{\mathrm{d}t} = \frac{\partial}{\partial t} + \dot{\theta}\frac{\partial}{\partial \theta}$ ($\theta$ is the only spatial coordinate in the tropical 1-D model). The ozone tendency at a fixed level can then be isolated in the Eulerian version of Eq. (2):

$$\frac{\partial \chi}{\partial t} = -\dot{\theta}\frac{\partial \chi}{\partial \theta} + S. \tag{3}$$

While the Lagrangian transport equation (Eq. 2) is integrated along the parcel trajectory to give the ozone concentration of the parcel at a given position, $\chi(\theta(t))$, the Eulerian equation (Eq. 3), is integrated in time at a given position to yield the concentration at this level and time, $\chi(t, \theta)$. This subtle but fundamental difference is key for interpreting the results from different analyses and comparing them unambiguously.

Using $\frac{d}{\mathrm{d}t} = \dot{\theta}\frac{d}{d\theta}$ (which is implied by $\dot{\theta} \equiv \frac{d\theta}{\mathrm{d}t}$), Eq. (1) can be re-written as:

$$\frac{d\chi}{d\theta} = \frac{P}{\dot{\theta}} - \frac{\alpha_N(\chi - \chi_N) - \alpha_S(\chi - \chi_S)}{\dot{\theta}}, \tag{4}$$

which explicitly shows the effect of tropical upwelling in the Lagrangian model. The inverse dependence on $\dot{\theta}$ of the change in ozone along the trajectory implies that slower ascent in summer results in longer transit times for photochemistry and in-mixing to increase ozone concentrations in the air parcel. We calculate the mean tropical ozone mixing ratio from the analytic solution of Eq. (2) (Eq. A1 in Ploeger et al., 2012), using an integration step of 0.5 K potential temperature. The ERA-Interim data used in the 1-D model has been interpolated to isentropic levels with 10 K vertical spacing between 360 K and 500 K.

The 1-D-model results will be compared to results from the WACCM free-running simulation described in Abalos et al. (2013), in terms of the transformed Eulerian mean (TEM) tracer continuity equation for ozone concentration (Eq. 9.4.13 in Andrews et al., 1987), neglecting the small vertical eddy term for simplicity:

$$\frac{\partial \overline{\chi}}{\partial t} = P - \overline{w}^*\frac{\partial \overline{\chi}}{\partial z} + \left[-\overline{v}^*\frac{\partial \overline{\chi}}{\partial y} + \frac{e^{z/H}}{\cos\varphi}\frac{\partial (M_y \cos\varphi)}{\partial y}\right]. \tag{5}$$

Alternatively, the isentropic formulation is (Eq. 9.4.21 in Andrews et al., 1987):

$$\frac{\partial \overline{\chi}}{\partial t} = P - \overline{Q}^*\frac{\partial \overline{\chi}}{\partial \theta} + \left\{-\overline{v}^*\frac{\partial \overline{\chi}}{\partial y} - \overline{\sigma}^{-1}\frac{\partial}{\partial y}\left(\overline{[(\sigma v)'\chi']}\right)\right\} \tag{6}$$

In Eq. (5) overbars indicate zonal mean quantities, $(\overline{v}^*, \overline{w}^*)$ are the meridional and vertical components of the residual circulation, while $\left(\overline{v}^*, \overline{Q}^*\right)$ in Eq. (6) are the isentropic meridional and cross-isentropic velocities weighted by the isentropic mass density $\sigma \equiv -1/g \cdot (\partial p/\partial \theta)$. $\overline{\chi}$ is the zonal mean ozone mixing ratio, $P$ is the net ozone production rate, $\varphi$ is the latitude and $M_y \equiv -e^{-z/H}(\overline{v'\chi'} - \frac{\partial \overline{\chi}}{\partial z}\cdot\overline{v'T'}\Big/S)$ is the horizontal component of eddy transport. The bracketed term on the right-hand side of each equation is the (horizontal or isentropic) in-mixing, which includes both horizontal eddy transport and advection. In particular, the in-mixing term (bracketed term) is equivalent to the term $-\alpha_N(\chi - \chi_N) - \alpha_S(\chi - \chi_S)$ in the 1-D model (Eq. 1). Further details on these equations can be found in Abalos et al. (2013). For our analysis of tropical mean ozone, Eqs. (5) and (6) are averaged over the tropics (20° S–20° N) throughout this paper, and we compute monthly means to examine the seasonality of the different terms. We note here that in the

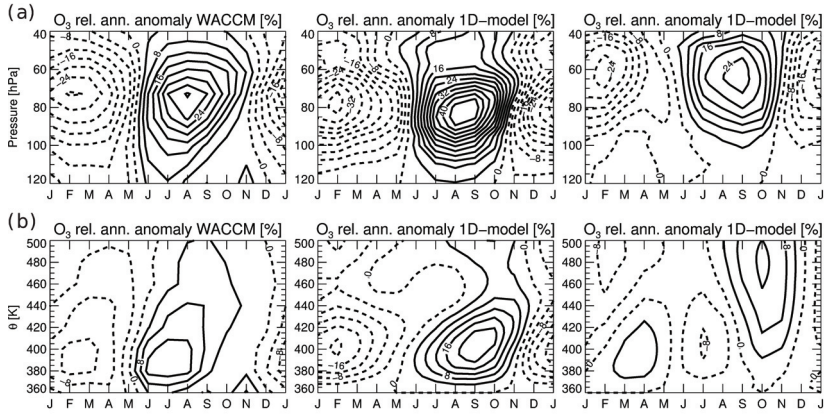


**Fig. 1.** Relative annual anomaly for tropical (20° S–20° N) ozone on pressure levels **(a)** and on isentropes **(b)** [%]. Percentages are relative to the annual mean concentrations. Results are shown from WACCM (left), from the 1-D model (middle) and from the 1-D model without including in-mixing (right). Solid (dashed) contours indicate positive (negative) values. Contour interval: 4 %.

WACCM free-running simulation, the tropical tropopause is approximately 1 km higher than observed. There is a corresponding vertical shift in ozone seasonality so that the maximum amplitude is found approximately 1 km above the level where it is observed by in situ measurements, as discussed in Abalos et al. (2013). The vertical resolution in this WACCM simulation is between 1.1 and 1.4 km in the upper troposphere and lower stratosphere (i.e., pressure levels around the tropical tropopause are ∼118, 101, 86, 73, and 62 hPa).

It is important to bear in mind that our aim is not to compare both models in detail, since they are radically different (a complex global chemistry–climate model versus a conceptual tropical 1-D model), and identical behavior should not be expected in the exact amplitude and timing or the precise levels involved in the ozone seasonality. Instead, our aim is to investigate if there is evidence for a common understanding of the transport processes that cause the ozone seasonality near the tropical tropopause, in spite of the very different nature of the models and the analyses.

## 3 The annual cycle of tropical ozone

Figure 1 shows the tropical mean ozone seasonality obtained with the Lagrangian 1-D model and WACCM. The results are shown on both pressure and isentropic levels, and the decrease in amplitude on isentropic compared to pressure coordinates is evident. Despite the very different nature of the models, the comparison shows similar overall characteristics. In particular, there is a broad maximum in summer centered near ∼80 hPa (∼70 hPa in WACCM), and near the 400–420 K isentropes (380–400 K in WACCM).

Figure 1 also shows the results of the 1-D model if in-mixing is inhibited (right column). On pressure levels, the amplitude of the ozone annual cycle is reduced by ∼50 % and shifted to upper levels. On isentropes, the annual cycle almost completely disappears. This demonstrates that in-mixing is essential for reproducing the observed ozone seasonality in the 1-D model. In particular, on isentropes almost the entire annual cycle of ozone can be attributed to in-mixing (with more ozone in-mixed during boreal summer than winter).

In the next sub-sections we address the question of whether the ozone seasonality in Fig. 1 is driven by the same forcings in both models.

### 3.1 Eulerian view of Lagrangian results

Figure 2 shows the mean seasonal cycle of the terms in the TEM continuity equation for ozone using results from WACCM (Eq. 5) averaged over 20° S–20° N and from the 1-D model after transforming the Lagrangian results to the Eulerian perspective, so that both are directly comparable. This is done by substituting the specific ozone sources in the 1-D model in Eq. (3):

$$\frac{\partial \chi}{\partial t} = -\dot{\theta}\frac{\partial \chi}{\partial \theta} + P - \alpha_{\mathrm{N}}(\chi - \chi_{\mathrm{N}}) - \alpha_{\mathrm{S}}(\chi - \chi_{\mathrm{S}}) \qquad (7)$$

The monthly means are computed over the 2004–2009 period for WACCM and 2005–2006 for the Lagrangian 1-D model. The ozone budget is fairly similar between these two completely different models. The seasonality in the ozone tendency is largest at the upper levels, and it follows the seasonality in upwelling, the dominant term in both models. At lower altitudes (86 hPa in WACCM, 101 hPa in the 1-D model), the seasonality in upwelling and in ozone is smaller,

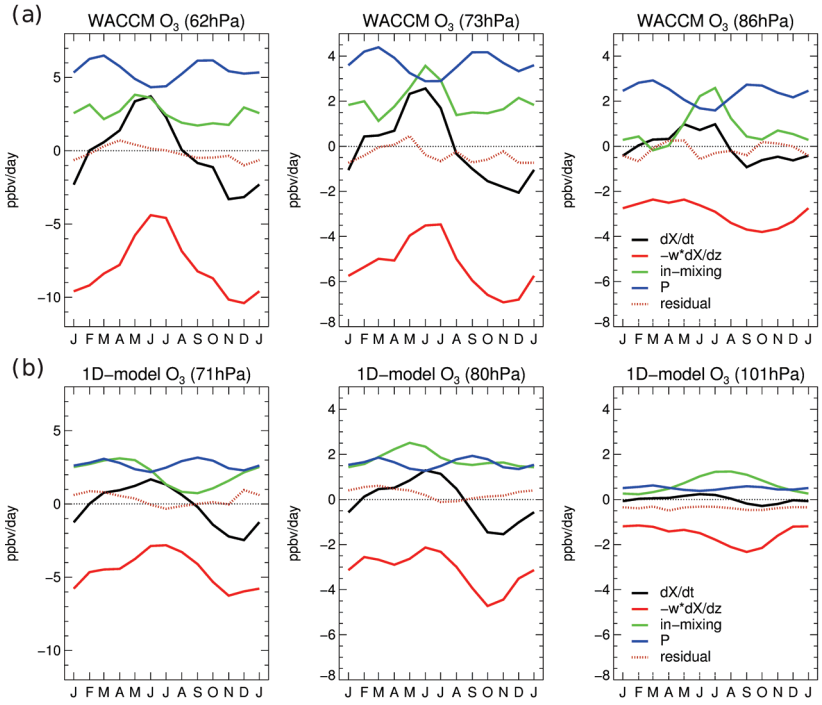


**Fig. 2.** Seasonal cycle of the various tendency terms in the TEM equation for mean tropical ozone concentration (20° S–20° N) computed from WACCM **(a)**, after Abalos et al. (2013), and from the 1-D Lagrangian model results **(b)** at different pressure levels (see text for details). Shown are the net tendency (black), the contributions due to vertical advection (red), horizontal transport (green), photochemical production (blue), and a residual term (red dashed). In order to account for the vertical shift of the tropopause altitude in WACCM, the balances are shown at slightly higher log-pressure altitudes than in the 1-D model (see text for details). Units: [ppbv day$^{-1}$].

and the in-mixing term exhibits a boreal summer maximum in both models, which is smoother and more spread in time in the Lagrangian model than in WACCM. The similarity of the budgets in Fig. 2 demonstrates that the models are consistent, in that similar forcings act to generate the seasonality in ozone at the different levels. Furthermore, in the Lagrangian model the vertical advection term is the leading contribution to the ozone seasonality at levels with strong background gradients, when the results are examined from an Eulerian perspective.

### 3.2 Vertical structure of in-mixing

Figure 3 shows the seasonality of in-mixing, presented as its net effect on tropical ozone tendency (relative to the annual mean ozone mixing ratio), as a function of isentropic levels for both WACCM and the Lagrangian 1-D model. In WACCM, the net effect is computed by averaging the bracketed term in Eq. (6) over the tropical band (20° S–20° N). Again, we note that the magnitude and exact levels are not expected to be comparable, and only broad characteristics should be considered. The seasonality of in-mixing shows a common feature in both models: there is strong in-mixing of ozone during the NH summer limited to isentropic levels below ∼420 K, while at higher levels both models experience slightly more in-mixing in boreal winter–spring compared to summer–autumn.

In both models the strong maximum is clearly identified in the ozone in-mixing during boreal summer at levels around the tropical tropopause, which is associated with the monsoons (as discussed by Konopka et al. (2010) and Ploeger et al. (2012)). The vertical extension of this summer maximum is larger in WACCM, while in the 1-D model the maximum is broader in time. Notwithstanding these differences, both models show this maximum and a consistent transition to a smaller seasonality at higher altitudes, with somewhat larger in-mixing during winter and spring compared to summer and fall.

The overall similarity between the models in the vertical structure of the ozone in-mixing seasonality in Fig. 3 suggests an underlying common understanding of horizontal transport processes, as will be discussed in Sect. 4.

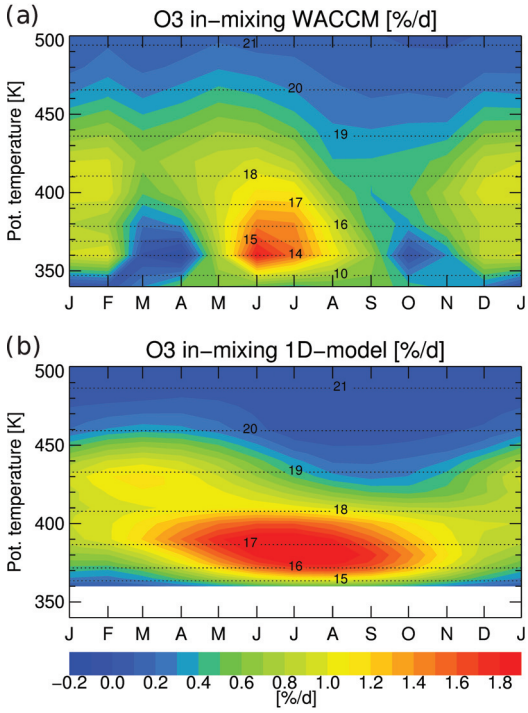


**Fig. 3.** Vertical structure of the seasonal cycle in in-mixing of ozone into the tropics (20° S–20° N). Shown is the in-mixing contribution to the ozone tendency relative to the annual mean ozone concentration in [% day$^{-1}$], from WACCM **(a)** and from the 1-D model **(b)**. See text for details. Log-pressure annual mean altitudes for each model are indicated by the horizontal dotted lines and labeled in km. Color bar range is −0.2 (blue) to 1.8 (red) [% day$^{-1}$].

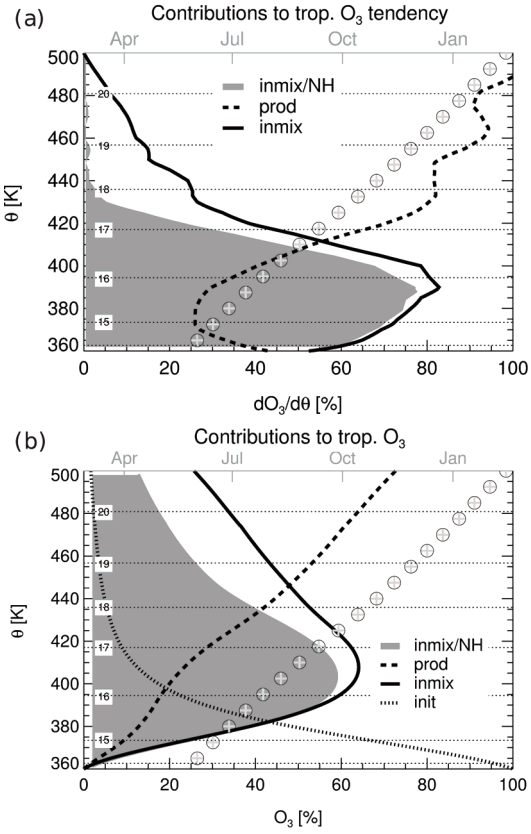


**Fig. 4. (a)** Relative contributions [%] to the change in ozone (i.e., ozone tendency) along an ascending tropical trajectory in the 1-D model. The parcel reaches the level of 500 K on 15 February and hence ascends through the TTL during the previous summer (time along the parcel trajectory is indicated by the gray "+" symbols, with scale shown in the upper x-axis). The different lines show: photochemical production along the ascent (black dashed), total in-mixing (black solid), in-mixing from the NH only (gray shading). The tendency terms are expressed as given on the right-hand side of Eq. (4), and shown relative to the total tendency at each level. **(b)** Same as **(a)**, but for the contributions to mean tropical ozone. The dotted line labeled "init" shows the contribution of the initialization concentration in the 1-D model (i.e., SHADOZ ozone at 360 K). This term is necessary for the lines in **(b)** to sum 100 %. Log-pressure annual mean altitudes are indicated by the horizontal dotted lines and labeled in km.

### 3.3 Contribution of in-mixing to ozone concentrations

From the Lagrangian point of view, air parcels ascending through the tropics during boreal summer may be enriched in ozone either by photochemical production within the tropics or by in-mixing of ozone-rich air from middle latitudes, as expressed by Eq. (4).

Figure 4a shows these contributions (i.e., the two terms on the right-hand side of Eq. 4) to the change in ozone concentration in an ascending tropical air parcel arriving at 500 K on 15 February from the 1-D model. This particular parcel in Fig. 4a ascended through the TTL during the previous summer (time along the trajectory is indicated by the encircled plus symbols), when in-mixing rates in the TTL were largest (see Fig. 3). In Fig. 4, in-mixing of middle latitude ozone (solid line) clearly dominates the increase in ozone along the trajectory at levels below ∼420 K, and this contribution shows a sharp peak just above the tropical tropopause (around 390 K). The rapid decrease in this contribution above ∼420 K is consistent with the vertical structure of in-mixing observed in Fig. 3. Figure 4a further shows that the main contribution to in-mixing originates in the NH (gray shading shows NH contribution to in-mixed ozone) and is related to the Asian monsoon. On the other hand, the increase in ozone due to photochemical production along the trajectory

increases gradually with height (dashed line). Both contributions are comparable around ∼420 K.

Although the relative contribution of in-mixing to the increase in ozone along the trajectory ($d\chi/d\theta$) is largely reduced at higher levels, a significant fraction of the ozone above the TTL is of extra-tropical origin. This is illustrated in Fig. 4b, which shows the contributions to the net ozone mixing ratio of photochemistry and in-mixing integrated (from 360 K to each level above) along the same tropical trajectory discussed above. For instance, as the parcel crosses the 450 K isentrope, in-mixing contributes only about 15 % to the increase in ozone (Fig. 4a). However, a large fraction (about 50 %) of tropical ozone at this level was originally located in mid-latitudes and has been in-mixed at lower levels (the remaining 50 % of ozone molecules have been produced by photochemistry along the trajectory).

The Eulerian calculations do not provide this information on the origin of air parcels (or ozone molecules); it can only be obtained with the Lagrangian analysis, which integrates along the trajectories and hence preserves the memory of air parcels.

## 4 Discussion

There are two main reasons for the apparent discrepancy in the literature regarding the origin of the ozone seasonality in the TTL and lower tropical stratosphere. The first reason is that various analyses use different coordinate systems. On pressure coordinates there is a large seasonal cycle in ozone that peaks near the level of sharpest vertical gradients and follows the seasonality in upwelling. On isentropic coordinates the annual cycle is much reduced and is largest near the tropopause (and not at levels with larger vertical gradients), and completely disappears in the 1-D model if in-mixing is removed (Fig. 1). The effects of using either of these alternative coordinate systems on the ozone budget in the tropical lower stratosphere have been explored by Konopka et al. (2009) and Abalos et al. (2013). They showed that on isentropic coordinates the influence of upwelling on ozone is almost completely removed, and consequently the annual cycle in ozone is reduced due to the large annual cycle of the isentropes relative to pressure levels (induced by upwelling), which is almost in-phase with ozone.

The second reason for the apparent discrepancy regards the difference between the Lagrangian versus the Eulerian transport methodologies. Figure 2 proves that the Lagrangian analysis is consistent with the Eulerian results. On a fixed pressure level above the tropical tropopause (with large background gradients in ozone, e.g., 62 hPa in WACCM and 71 hPa in the 1-D model), the ozone tendency closely follows the vertical advection term in the zonal mean TEM tracer continuity equation and, in this sense, the seasonality of tropical mean ozone is forced by tropical upwelling in both models. However, in the same 1-D model the seasonality in ozone changes substantially if in-mixing is inhibited (50 % reduction on pressure levels, vanishing annual cycle on isentropes), implying that in-mixing makes a significant contribution to high ozone concentrations in boreal summer, and hence to the ozone seasonality. The key information to reconcile this apparent inconsistency is that substantial in-mixing of ozone molecules from the NH mid-latitudes caused by the Asian monsoon anticyclone during summer takes place in the TTL close to the tropopause. Above the TTL, in-mixing rapidly decreases with height, and the ozone seasonality follows the seasonality of vertical advection.

All these features are consistently observed in both models, and consequently there is no actual contradiction between the results of the different analyses. Choosing the Eulerian or the Lagrangian approach depends on the question that one is interested in answering. In particular, two relevant scientific questions are related to this issue: (1) what drives the large annual cycle above the tropical tropopause? and (2) where does the ozone that ascends within the tropical pipe come from? The first question regards the "forcing" of ozone seasonality and the second the "origin" of tropical ozone molecules. Here, the term "forcing" refers to the dominant term in the zonal mean ozone continuity equation at a particular level. In this sense, the TEM framework shows that the seasonality in tropical upwelling constitutes the main "forcing" of the annual cycle in ozone at levels with large vertical gradients. On the other hand, the term "origin" distinguishes between photochemical production within the tropics and in-mixing from mid-latitudes as sources for tropical ozone. In this sense, the Lagrangian approach is suited to understanding the "origin" of ozone molecules entering the tropical stratosphere and shows that, particularly during summer, a substantial amount of tropical ozone originates in middle and high latitudes.

We note that, strictly speaking, neither the Eulerian nor the Lagrangian methodology entirely separates the effects of tropical upwelling and of horizontal in-mixing on tropical ozone. In-mixing at levels of the TTL affects the ozone profile and gradient, and hence may impact the seasonality in the vertical advection term. Near the tropopause (below ∼80 hPa), the vertical gradient in ozone has a seasonal cycle that is almost opposite to the cycle in upwelling, such that the vertical advection term shows relatively little seasonality at this level (Fig. 2). At higher levels, the stronger background gradients are nearly constant and vertical advection follows the seasonality in upwelling. Similarly, the in-mixing term depends on the latitudinal ozone gradient, which seasonality can be affected by upwelling within the tropics. Moreover, as ozone production due to photochemistry and in-mixing along a tropically ascending trajectory both appear weighted with the inverse upwelling velocity (see Eq. 4), a seasonally varying upwelling implies a seasonality in in-mixing of ozone, even if the in-mixing rates were constant throughout the year (result not shown).

Two examples may further illustrate the implications of these results. First, at levels above the TTL (i.e., above about ∼420 K), the seasonality of horizontal in-mixing may be neglected to leading order and the amplitude of the annual cycle in tropical upwelling can be estimated from the amplitude in the ozone tendency (divided by a constant ozone background gradient). Second, for calculating tropical ozone profiles (e.g., in photochemical box models), both photochemical production and in-mixing turn out to be essential in the calculation, and about 50 % of summertime ozone in the TTL and at levels above (up to ∼20 km) is of extra-tropical origin.

## 5 Conclusions

In this paper we reconcile the apparently contrasting views in the literature regarding the seasonality of ozone in the tropical lower stratosphere and its links to tropical upwelling and horizontal in-mixing. By comparing results from a chemistry–climate model and from a one-dimensional Lagrangian transport model, we find that the Eulerian and Lagrangian approaches are consistent and describe different aspects of the ozone transport near the tropical tropopause. Both models show that vertical advection is the main forcing of the tropical mean annual cycle in the lower stratosphere at levels with strong ozone vertical gradients. Additionally, large summertime horizontal in-mixing due to the Asian monsoon circulation is observed in both models near the tropopause. The Lagrangian calculations show that a high fraction of ozone in the TTL and lower stratosphere during summer originates in middle latitudes, and this information cannot be derived from Eulerian budgets. Thus, while the Eulerian and Lagrangian perspectives are consistent, they provide complementary information on transport processes.

*Acknowledgements.* The authors are thankful to Doug Kinnison for providing the WACCM simulation output. The authors also acknowledge stimulating conversations with Stephan Fueglistaler and Markus Rex. This work was partially supported under the NASA Aura Science Program. The National Center for Atmospheric Research is operated by the University Corporation for Atmospheric Research, under sponsorship of the National Science Foundation. M. Abalos acknowledges Grant BES-2009-013082 and Project CGL2012-34997 of the Spanish Government for funding and NCAR for hosting her visits.

Edited by: W. Lahoz

## References

Abalos, M., Randel, W. J., and Serrano, E.: Variability in upwelling across the tropical tropopause and correlations with tracers in the lower stratosphere, Atmos. Chem. Phys., 12, 11505–11517, doi:10.5194/acp-12-11505-2012, 2012.

Abalos, M., Randel, W. J., Kinnison, D. E., and Serrano, E.: Quantifying tracer transport in the tropical lower stratosphere using WACCM, Atmos. Chem. Phys., 13, 10591–10607, doi:10.5194/acp-13-10591-2013, 2013.

Abalos, M., Randel, W. J., Kinnison, D. E., and Serrano, E.: Quantifying tracer transport in the tropical lower stratosphere using WACCM, Atmos. Chem. Phys. Discuss., 13, 13245–13283, doi:10.5194/acpd-13-13245-2013, 2013.

Andrews, D. G., Holton, J. R., and Leovy, C. B.: Middle atmosphere dynamics, Academic Press, Orlando, Florida, 489 pp., 1987.

Avallone, L. M. and Prather, M. J.: Photochemical evolution of ozone in the lower tropical stratosphere, J. Geophys. Res., 101, 1457–1461, 1996.

Fueglistaler, S., Dessler, A. E., Dunkerton, T. J., Folkins, I., Fu, Q. and Mote, P. W.: Tropical tropopause layer, Rev. Geophys., 47, RG1004, doi:10.1029/2008RG000267, 2009.

Garcia R. R., Marsh, D. R., Kinnison, D. E., Boville, B. A., and Sassi, F.: Simulation of secular trends in the middle atmosphere, J. Geophys. Res., 112, 1950–2003, D09301, doi:10.1029/2006JD007485, 2007.

Grooß, J.-U. and Russell III, J. M.: Technical note: A stratospheric climatology for $O_3$, $H_2O$, $CH_4$, $NO_x$, HCl and HF derived from HALOE measurements, Atmos. Chem. Phys., 5, 2797–2807, doi:10.5194/acp-5-2797-2005, 2005.

Konopka, P., Grooß, J.-U., Ploeger, F., and Müller, R.: Annual cycle of horizontal in-mixing into the lower tropical stratosphere, J. Geophys. Res., 114, D19111, doi:10.1029/2009JD011955, 2009.

Konopka, P., Grooß, J.-U., Günther, G., Ploeger, F., Pommrich, R., Müller, R. and Livesey, N.: Annual cycle of ozone at and above the tropical tropopause: observations versus simulations with the Chemical Lagrangian Model of the Stratosphere (CLaMS), Atmos. Chem. Phys., 10, 121–132, doi:10.5194/acp-10-121-2010, 2010.

McKenna, D. S., Konopka, P., Grooß, J.-U., Günther, G., Müller, R., Spang, R., Offermann, D., and Orsolini, Y.: A new Chemical Lagrangian Model of the Stratosphere (CLaMS): 1. Formulation of advection and mixing, J. Geophys. Res., 107, 4309, doi:10.1029/2000JD000114, 2002.

Ploeger, F., Konopka, P., Müller, R., Fueglistaler, S., Schmidt, T., Manners, J. C., Grooß, J.-U., Günther, G., Forster, P. M., and Riese, M.: Horizontal transport affecting trace gas seasonality in the Tropical Tropopause Layer (TTL), J. Geophys. Res., 117, D09303, doi:10.1029/2011JD017267, 2012.

Randel, W. J., Park, M., Wu, F., and Livesey, N.: A Large annual cycle in ozone above the tropical tropopause linked to the Brewer–Dobson circulation, J. Atmos. Sci., 64, 4479–4488, doi:10.1175/2007JAS2409.1, 2007.

# 4 Dynamical forcing of sub-seasonal variability in the tropical Brewer-Dobson circulation.

*Abalos, M., Randel, W. J., and Serrano, E., submitted to J. Atmos. Sci., manuscript number JAS-D-13-0366.*

# Dynamical forcing of sub-seasonal variability in the tropical Brewer-Dobson circulation

Marta Abalos[1]
Universidad Complutense de Madrid, Madrid, Spain

William J. Randel
National Center for Atmospheric Research, Boulder, Colorado

Encarna Serrano
Universidad Complutense de Madrid, Madrid, Spain

Submitted to *Journal of the Atmospheric Sciences*
November 2013

## Abstract

Upwelling across the tropical tropopause exhibits strong sub-seasonal variability superimposed on the well-known annual cycle, and these variations directly affect temperature and tracers in the tropical lower stratosphere. The dynamical forcing of tropical upwelling on sub-seasonal timescales is investigated using the ERA-Interim reanalysis for 1979-2011. Momentum balance diagnostics reveal that transience is linked to the effects of extratropical wave forcing, with centers of action in the extratropical winter stratosphere and in the subtropical upper troposphere of both hemispheres. Zonal mean wind tendencies are important for communicating the high-latitude wave forcing to the tropics, and for extending subtropical forcing to altitudes near and above the tropopause. Dynamical patterns reflect distinctive forcing of the shallow versus deep branches of the Brewer-Dobson circulation; the shallow branch is most strongly correlated with wave forcing in the subtropical upper troposphere and lower stratosphere, while the deep branch is mainly influenced by high-latitude planetary waves.

[1] *Corresponding author address*: Marta Abalos, Depto. Geofísica y Meteorología, Universidad Complutense de Madrid, Facultad de CC. Físicas, Avda. Complutense s/n, 28020, Madrid, Spain.
E-mail: mabalosa@ucm.es.

## 1. Introduction

Tropical upwelling is an important component of the Brewer-Dobson circulation (BDC), strongly influencing temperature and tracer distributions in the tropical lower stratosphere (e.g. Holton et al. 1995, Plumb 2002, Shepherd 2007). The tropical BDC is mainly driven by momentum deposition from large- and small-scale waves, but the relative roles of different forcing regions and their contributions for variability on different time scales are topics of ongoing research (e.g. Randel et al. 2008, Taguchi 2009, Ueyama and Wallace 2010, Zhou et al. 2012, Ueyama et al. 2013). There is empirical evidence that wave activity in the extratropical winter stratosphere influences upwelling and temperatures in the tropical lower stratosphere (e.g. Fritz and Soules 1972, Randel 1993, Randel et al. 2002, Ueyama and Wallace 2010). This influence occurs as the extratropical waves exert a drag on the zonal mean circulation, inducing poleward mass flow, with mass continuity requiring downward flux at high latitudes and upwelling at low latitudes (e.g. Andrews et al. 1987). However, theoretical considerations imply that, in stationary conditions, these induced vertical motions are limited to the latitudinal extension of the forcing (cf. the "downward control principle", Haynes et al. 1991). This suggests that wave forcing needs to occur close to the tropics in order to produce realistic mean tropical upwelling (Plumb and Eluskiewicz 1999, Semeniuk and Shepherd 2001). In contrast, for transient conditions, the influence of extratropical wave forcing can extend into the tropics through nonlocal effects (Garcia 1987, Haynes et al. 1991). The remote connection between high and low latitudes results from the coupled response of the atmospheric zonal wind, temperature and meridional circulation to a transient wave drag (Garcia 1987).

There has been substantial interest in understanding the forcing responsible for the relatively large annual cycle in tropical upwelling, which in turn mainly drives the seasonality in temperature and chemical tracers in the tropical lower stratosphere (e.g. Yulaeva et al. 1994, Randel et al. 2007, Abalos et al. 2012, 2013). However, causality is difficult to untangle for the annual cycle, and the roles of different regions and types of wave forcing have been emphasized in a number of studies (including forcing from high latitudes, subtropics and equatorial waves). Based on the observed coherent temperature annual variations in the tropics and extratropics, some analyses have proposed a primary role of extratropical planetary waves (Yulaeva et al. 1994, Ueyama and Wallace 2010). However, as noted above, strictly high-latitude forcing is difficult to reconcile with theoretical expectations for time mean tropical upwelling. Ueyama et al. (2013) recently suggested that the influence of the extratropical wave drag may involve the latitudinal progression of the forcing towards the tropics on timescales of ~10 days. Wave driving in the subtropics resulting from the dissipation of middle-latitude baroclinic eddies has been emphasized by Taguchi (2009) and Chen and Sun (2011). Furthermore, several studies have highlighted an important role of equatorial planetary waves forced by convection in driving the seasonality in upwelling around the tropical tropopause (Boehm and Lee 2003; Kerr-Munslow and Norton 2006; Ryu

and Lee 2010; Ortland and Alexander 2013). Randel et al. (2008) noted strong seasonal variations for wave forcing in the subtropics, resulting from the combined effects of extratropical and equatorial wave fluxes. The importance of subtropical wave drag has been also noticed in relation to the long-term trends in upwelling predicted by models (Butchart et al. 2006, Garcia and Randel 2008, Calvo and Garcia 2009, Garny et al. 2011, Shepherd and McLandress 2011).

Observations suggest large variability in tropical upwelling on sub-seasonal time scales, although this has received less attention in terms of forcing mechanisms. Zhou et al. (2012) argued that extratropical and subtropical wave drag act cooperatively to drive upwelling on various timescales, and highlighted the importance of including transient variability for determining the specific forcing latitudes. Using high-vertical resolution GPS temperature measurements, Grise and Thompson (2013) analyzed the role of different forcing regions in driving transient variability in upwelling. They found that planetary waves in the extratropical and subtropical stratosphere mainly drive transient upwelling in the lower stratosphere (above ~70 hPa), while equatorial planetary waves and drag in the subtropical troposphere are important for upwelling around the tropopause.

In this work, the dynamical drivers of transient variability in upwelling are investigated from an observational perspective, using daily time series of tropical mean upwelling derived from momentum balance calculations, based on 33 years of ERA-Interim reanalysis. The wave forcing regions relevant for the sub-seasonal fluctuations in upwelling are identified, and the dynamics of the remote connections with the tropical lower stratosphere are explored. The results furthermore evidence the distinct circulations and forcings associated with the shallow versus deep branches of the tropical Brewer-Dobson circulation.

## 2. Data and analyses

Daily mean temperature and three-dimensional wind fields from the ERA-Interim reanalysis are used (Dee et al., 2011), obtained averaging the 6-hourly data, for the period 1979-2011. The data are archived in a 1.5°x1.5° grid, on 37 pressure levels spanning from 1000 hPa to 1 hPa. In order to isolate sub-seasonal variability, a high-pass filter is applied to all the fields, which retains fluctuations on timescales shorter than 90 days. This threshold is chosen to eliminate the influence of the seasonal cycle up to its fourth harmonic.

The analyses are based on the Transformed Eulerian Mean (TEM) framework, where the governing equations can be written as:

$$DF - \frac{\partial \overline{u}}{\partial t} = -\hat{f} \cdot \overline{v}^* \quad (1)$$

$$\frac{\partial \overline{T}}{\partial t} + \overline{v}^* \frac{1}{a}\frac{\partial \overline{T}}{\partial \phi} + \overline{w}^* S = \overline{Q} \quad (2)$$

$$(a\cos\phi)^{-1}\frac{\partial}{\partial \phi}(\overline{v}^*\cos\phi) + e^{z/H}\frac{\partial}{\partial z}(\overline{w}^* e^{-z/H}) = 0 \quad (3)$$

$$f\frac{\partial \overline{u}}{\partial z} + \frac{R}{aH}\frac{\partial \overline{T}}{\partial \phi} = 0 \quad (4)$$

In these equations $DF = \frac{e^{z/H}}{a\cos\phi}\nabla \cdot \mathbf{F}$ is the scaled Eliassen-Palm flux divergence, $(\overline{v}^*, \overline{w}^*)$ is the residual mean meridional circulation, $\hat{f} = f - \frac{1}{a\cos\phi}\frac{\partial}{\partial \phi}(\overline{u}\cos\phi)$ and $S = HN^2/R$, with $N$ the Brunt-Väissälä frequency. These equations

determine the response of the independent variables $\overline{u}$ , $\overline{T}$ , $\overline{v}^*$ and $\overline{w}^*$ to the imposed external forcings, $DF$ and $\overline{Q}$ (in practice, $\overline{Q}$ in the tropical lower stratosphere can be approximated as a linear damping proportional to temperature, so that the primary forcing of the system is by the term $DF$ ). Combining the TEM momentum equation (Eq. (1)) and mass continuity (Eq. (3)), an expression can be derived for tropical upwelling (Randel et al. 2002):

$$\left\langle \overline{w}_m^* \right\rangle (z) = \frac{-e^{z/H}\cos\phi}{\int_{-\phi_0}^{\phi_0} a\cos\phi d\phi} \left\{ \int_z^{\infty} \frac{e^{-z'/H}}{\hat{f}(\phi,z')} \left[ DF(\phi,z') - \overline{u}_t(\phi,z') \right]_{\overline{m}} dz' \right\}_{-\phi_0}^{\phi_0} \quad (5)$$

where $\overline{u}_t$ is the zonal mean wind tendency. This expression gives tropical upwelling at a given level $z$ averaged over a range of latitudes $(-\phi_0, \phi_0)$ as a function of the net forcing integrated over all altitudes above that level and evaluated at the extremes of the latitudinal interval. In this work the focus is on upwelling in the deep tropics, with Eq. (5) evaluated over 18° N-S. Because the zonal mean angular momentum ( $\overline{m}$ ) isolines are almost vertical, the integrand in Eq. (5) can be approximately computed on fixed latitudes. Note that the integrand is a function of the wave forcing ( $DF$ ) minus the tendency in the zonal wind ( $\overline{u}_t$ ). In this sense, $\overline{u}_t$ constitutes an additional forcing of variability in upwelling, and consequently the term $DF - \overline{u}_t$ is denoted *net forcing* of tropical upwelling in this work.

As mentioned in the Introduction, the zonal mean response of the atmosphere to a momentum forcing ( $DF$ ) in the extratropical winter stratosphere, given by Equations (1) to (4), has been extensively studied in theoretical models (Garcia 1987, Haynes et al. 1991, Plumb and Eluskiewicz 1999), and its relation to upwelling in the tropics is fairly well understood for transient wave forcing (e.g. for stratospheric sudden warming events; Dunkerton et al. 1981). Figure 1 illustrates this behavior as derived from one-point correlation cross-sections, calculated from the ERA-Interim reanalysis for sub-seasonal timescales in boreal winter (DJFM). The reference time series for these correlations is $-DF$ (convergence of the EP flux) at one point in the extratropical boreal stratosphere (54°N, 20 hPa), representative of a region with climatological EP flux convergence in DJFM, and Fig. 1 shows the correlations with different fields ( $DF$ , $\overline{u}_t$ , $DF - \overline{u}_t$ and $\overline{T}_t$ ). Wave drag at this particular location is associated with vertical wave propagation from the extratropical troposphere into the stratosphere and a broad region of wave dissipation (EP flux convergence) extending throughout the middle and high latitudes (Fig. 1a). The response in the zonal mean wind (Fig. 1b) shows local deceleration of the zonal mean flow and acceleration on the equatorward side of the forcing (and also negative wind tendencies in the SH subtropics). The net forcing ( $DF - \overline{u}_t$ ) (Fig. 1c) has a broader latitudinal extent than the $DF$ forcing alone, extending into the deep tropics. The residual circulation induced by the

forcing and the associated impact on temperature (Fig. 1d) shows a broad region of upwelling and cooling over the tropical lower stratosphere extending to altitudes near the tropopause, along with downwelling and warming on the poleward side of the forcing. Both the upwelling and the temperature response are found to cross the equator and extend into the SH, a feature clearly seen in satellite observations (Fritz and Soules 1972). The change in temperature gradients in the SH drives a response in the zonal mean wind, which is observed in Fig. 1b as the negative correlations over ~10-40°S. The overall patterns of correlations in Fig. 1 demonstrate the nonlocal response to high-latitude wave forcing, with the residual circulation acting to maintain thermal wind balance between the remote wind and temperature tendencies. A key aspect is that the remote response of the wind tendency ($\overline{u}_t$) extends the net forcing towards low latitudes, so that it reaches the boundaries of the tropics (which are most relevant for tropical upwelling, see Eq. (5)).

## 3. Forcing of sub-seasonal variability in upwelling

The focus of this work is to identify dynamical forcing associated with transient tropical upwelling, and this is done using correlations and regressions applied to the derived upwelling estimate, $\overline{w}^*_m$. Figure 2a shows daily time series of $\overline{w}^*_m$ at 70 hPa averaged over 18°S-18°N for two years (2008-2009), illustrating the annual cycle (maximum during boreal winter-spring) together with substantial sub-seasonal variability. Abalos et al. (2012) showed that these time series of $\overline{w}^*_m$ agree reasonably well (with correlations ~0.7) with two other estimates of upwelling (the residual circulation, $\overline{w}^*$, derived from ERA-Interim, and a thermodynamic estimate, $\overline{w}^*_Q$, based on an accurate radiative transfer code). The thermodynamic estimate is also shown in Fig. 2, highlighting good agreement with $\overline{w}^*_m$. Furthermore, the time series of $\overline{w}^*_m$ are significantly correlated with independent satellite trace gas observations (ozone and carbon monoxide) on sub-seasonal timescales (Abalos et al. 2012). These results suggest the accuracy of the $\overline{w}^*_m$ estimates, and their suitability to investigate the drivers of the variability (i.e. the $DF$ and $\overline{u}_t$ variations that force $\overline{w}^*_m$ via Eq. (5)). The $\overline{w}^*_m$ time series are filtered to isolate sub-seasonal timescales as described above, and the filtered data are shown in Fig. 2b; these form the basis of the correlations and regressions described below (based on the full 33-years record from ERA-Interim); similar results are found for the shorter record 2005-2010 used in Abalos et al. (2012) (not shown).

The time series of tropical upwelling in Fig. 2 are linked to the global zonal mean residual circulation, and Fig. 3 shows the structure of the associated circulations (calculated using the residual circulation $\overline{v}^*$, $\overline{w}^*$ derived from the ERA-Interim reanalysis) together with the patterns of heating and cooling, for DJFM and JJAS. In all the latitude-height cross-sections the regressed zonal mean fields are multiplied by the cosine of latitude to compensate for the increase in variance towards the poles due to spherical geometry (North et al., 1982). In Fig. 3,

both seasons show a broad region of tropical upwelling/cooling and high-latitude downwelling/warming in the winter stratosphere. In addition, shallower cells of circulation close to the tropopause are observed leading to warming in the subtropics in both seasons, although the cell on the summer hemisphere is somewhat stronger in DJFM than in JJAS. Below these warming cells there are cooling regions in the subtropical upper troposphere, associated with ascending motion. Enhanced tropical upwelling is also correlated with warming of the tropical upper troposphere in both seasons. The overall patterns in Fig. 3 are consistent with two branches of the residual circulation, a shallow branch near the tropical tropopause that is symmetric about the equator, and a deeper branch that extends from the tropics into the winter polar stratosphere (e.g. Plumb 2002, Birner and Bönisch 2011). The transition between the two branches is further examined below.

The strong signature of transience in the Brewer-Dobson circulation is also observed in satellite-derived ozone measurements. Figure 4 shows 70 hPa $\overline{w}^*_m$ correlations with zonal mean ozone tendencies ($\partial\overline{O_3}/\partial t$) derived from Aura Microwave Limb Sounder (MLS) satellite observations during DJFM and JJAS of the years 2005-2010 (as described in Abalos et al. 2012). The ozone tendency patterns closely mimic the temperature tendency results (Fig. 3), in particular with patterns in the lower stratosphere that reflect the lower branch of the Brewer-Dobson circulation, and positive correlations in the high latitude winter stratosphere related to the deep branch. This result reflects the strong influence of vertical circulation anomalies on the region of steep ozone gradients in the lower stratosphere. The coupled ozone-temperature signatures are evidence for coherent variability of the BDC on sub-seasonal timescales (for both the deep and the shallow branches).

### *a. Wave drag, wind response and net forcing*

The dynamical driving of transient variability in upwelling is investigated using linear regressions of the different components of the forcing onto the time series of $\overline{w}^*_m$ at 70 hPa (e.g. Fig. 2b). The regressions for boreal winter (DJFM) and summer (JJAS) seasons are shown in Figs. 4 and 5, respectively. Each figure shows the regressions of the (a) EP flux, (b) zonal wind tendency and (c) net forcing ($DF-\overline{u}_t$) onto time series of $\overline{w}^*_m$. The results are qualitatively similar if the residual circulation derived from ERA-Interim at 70 hPa ($\overline{w}^*$) or the thermodynamics estimate ($\overline{w}^*_Q$) is used instead; however, calculations based on $\overline{w}^*_m$ provide a dynamically consistent estimate.

Regressions onto the global EP flux (Figs. 5a and 6a) show that tropical upwelling is highly correlated with vertical wave propagation and convergence in the extratropical winter stratosphere, primarily over latitudes poleward of 30°. Upwelling is also positively correlated with EP flux divergence in the subtropical upper troposphere (in both hemispheres during DJFM in Fig. 5a, only weakly in the summer hemisphere in JJAS, Fig. 6a), with quasi-horizontal EP flux vectors indicating wave propagation away from these regions. The corresponding regressions onto the

zonal mean wind tendencies (Figs. 5b and 6b) show negative correlations (i.e., deceleration of the flow) in the stratosphere centered at the latitude of strongest wave drag in the winter extratropics, and weaker positive correlations (acceleration) on the equatorward side of the forcing, approximately mirroring the patterns in EP flux divergence. The extratropical $\overline{u}_t$ patterns extend over a deep layer with an approximately barotropic vertical structure. There is a global symmetry in the subtropical EP flux and $\overline{u}_t$ patterns in DJFM, which is also evident but less pronounced in JJAS. In addition, there is a relatively small region of wind deceleration centered at the equator near the tropopause during DJFM, coincident with an EP flux convergence in this region seen in Fig. 5a. Regression patterns for the net forcing ($DF-\overline{u}_t$) (Figs. 5c and 6c) in the winter stratosphere extend deeper into the subtropics than those of $DF$ alone, and have a clear maximum near the subtropical edges of the tropopause region. The key point is that, while the wave driving ($DF$) may be remote to the tropical tropopause region, the net forcing ($DF-\overline{u}_t$) extends into the tropical lower stratosphere and is able to drive tropical upwelling (via the balance expressed in Eq. 5).

The temporal evolution of the regressions during DJFM is shown in Fig. 7, which represents lagged regressions onto $\overline{w}^*_m$ of the fields $DF$, $\overline{u}_t$ and $DF-\overline{u}_t$, weighted by density and integrated in log-pressure altitude (as they appear in Eq. 5). The regression of $DF$ (Fig. 7a) shows strongest values in high latitudes and a systematic propagation of the wave forcing towards low latitudes. The largest values of the projections travel from ~65°N to ~40°N in ~5 days. This propagation of the transient wave drag from high to low latitudes was recently highlighted by Ueyama et al. (2013). Variations in the corresponding wind tendency (Fig. 7b) shows patterns of local deceleration and acceleration which also propagate in a coherent manner towards the tropics. The acceleration patterns in the subtropics reach deep into low latitudes, such that the net forcing ($DF-\overline{u}_t$) at low latitudes is substantially stronger than $DF$ alone (Fig. 7c). Figures 5-7 highlight the important role of the zonal wind tendencies for contributing to the net forcing of transient tropical upwelling.

### *b. Composites of extreme events in tropical upwelling*

The regression patterns in Figs. 3-7 show the statistical signatures of circulations linked to transient tropical upwelling, but the patterns of wave and mean flow variability can be better understood by examining composited events of extremes in upwelling (both positive and negative extremes). Extreme events composites are constructed based on the long multi-year record of $\overline{w}^*_m$ (e.g. Fig. 2b), simply choosing the top and bottom 5% $\overline{w}^*_m$ extremes. Figure 8 shows composites of the EP flux averaged over the 5% days of strongest and weakest upwelling in boreal winter (DJFM) for the years 1979-2011, as well as the difference (high minus low). Note that the background climatological EP flux is included in the composited fields in Figs. 8a-b. Figure 8a shows that the strongest

tropical upwelling events are associated with enhanced vertical wave propagation and convergence in the extratropical winter stratosphere, and this behavior is consistent with previous studies (Randel et al. 2002, Ueyama et al. 2013). On the other hand, events of low upwelling (Fig. 8b) are mainly associated with enhanced quasi-horizontal EP flux convergence in the subtropical upper troposphere, with similar patterns observed in both hemispheres, together with weak vertical wave flux in winter high latitudes. The difference in the EP flux between high and low upwelling extremes (Fig. 8c) produces patterns very similar to the correlations in Fig. 5a (and a structure similar to Fig. 6a is observed for composites during JJAS, not shown).

The corresponding composites for the zonal mean wind tendencies are shown in Fig. 9. Since the climatological mean of the wind tendency is near zero, the anomalies coincide with the absolute values. During maximum upwelling events there is deceleration of the stratospheric winds over ~30°-60°N, coincident with the enhanced EP flux convergence in Fig. 8a, and this pattern extends vertically downward across the tropopause. There is also wind acceleration on the equatorward flank of the subtropical jets, extending with a barotropic structure over a deep layer from ~30 hPa to below 400 hPa. Because the EP flux convergence is small at low latitudes, these $\overline{u}_t$ acceleration patterns in the subtropics contribute substantially to $\overline{w}^*_m$ (via Eq. 5), and the net effect is to extend the high-latitude wave forcing to the subtropics (similar to the behavior in Fig. 1). The composited $\overline{u}_t$ for the low $\overline{w}^*_m$ extremes (Fig. 9b) show patterns that are approximately mirror images of Fig. 9a, with coherent wind deceleration on the equatorward flanks of the subtropical jets. These $\overline{u}_t < 0$ coincide with the strong EP flux convergence in Fig. 8b, but the zonal wind tendencies extend to higher altitudes across the tropopause, which results in forced relative downward $\overline{w}^*_m$ across the tropopause level (this behavior is clarified in Section 3c). The zonal wind tendencies in Figs. 9a-b show a symmetric behavior between the two hemispheres, similar to the EP fluxes in Figs. 8a-b), but the overall variations in the two hemispheres are uncorrelated, and this is mainly a statistical result (as discussed further in Section 3d).

### *c. Influence of wave forcing in the subtropical upper troposphere*

Calculations of tropical upwelling using Eq. (5) involve integrating the net forcing above the level where upwelling is computed. Hence, it is not evident how the variability in upwelling at 70 hPa is affected by wave drag below that level (i.e. in the subtropical upper troposphere). To appreciate the mechanism through which this influence occurs, Fig. 10 shows one-point correlations of $-DF$ at one point in the subtropical upper troposphere (24°N, 175 hPa) with different fields (as in Fig. 1). In this case, the wave forcing is localized in a relatively narrow vertical region (Fig. 10a), in contrast to the broader forcing region in Fig. 1a. The EP flux vectors suggest a strong contribution to variability from extratropical waves, and additionally some influence from near-equatorial latitudes (i.e. from equatorial planetary waves, Randel et al. 2008). The zonal wind response

(Fig. 10b) shows deceleration co-located with the wave drag, extending higher in altitude than the forcing (together with accelerations to the north and south). The different vertical extent of the forcing ($DF$) and the local wind response ($\overline{u}_t$) results in a dipolar pattern in the net forcing ($DF - \overline{u}_t$), with opposite signs above and below ~125 hPa (Fig. 10c). Consequently, the remote influence of the upper tropospheric wave forcing on upwelling near and above the tropical tropopause occurs through the deep barotropic response of the zonal wind. In particular, the positive correlations in Fig. 10c imply reduced upwelling near the tropopause associated with enhanced wave drag in the subtropical upper troposphere. To complete the picture, Fig. 10d shows the meridional circulation induced by the forcing and the associated temperature response. Two circulation cells with opposite sense are observed: clockwise circulation below the forcing and anti-clockwise circulation above (resulting in an overall quadrupole temperature structure). The circulation above the forcing shows downwelling and warming near the tropical tropopause (extending across the equator and into the SH subtropics), together with a cooling over the upwelling region over ~25°N-40°N. This is the structure observed in meridional circulation and temperature correlations linked to upwelling near the tropopause (e.g. Fig. 3), and is the statistical signature of the shallow branch of the BDC.

*d. Relations of wave forcing between high and low latitudes and between hemispheres*

The results of $\overline{w}^*_m$ regressions (Figs. 5-6) and extreme upwelling events (Figs. 8-9) demonstrate the combined influence of wave forcing in the high latitude stratosphere and subtropical upper troposphere (regions A and B in Fig. 5a), and also show symmetric patterns between the subtropics in both hemispheres (regions B and C in Fig. 5a; this latter behavior is stronger in DJFM than in JJAS). Whether these patterns represent systematic correlations between these regions or if this is a statistical result from our analyses is verified in the following.

First, the links between high- and low-latitude wave forcing are examined. Figure 11 shows a two-dimensional histogram of wave forcing $DF$ in: a) the extratropical stratosphere (average over 36° N-60°N, 20-10 hPa; region A), and b) the subtropical upper troposphere (21°N-33°N, 300-125 hPa; region B). The black contours in Fig. 11 illustrate the distribution of all daily DJFM samples during 1979/'80-2010/'11 (121 days/year * 32 years = 3872 days), and the overall circular pattern of contours is evidence of weak correlation of wave forcing between these locations. This is consistent with the direct calculation of time series correlation, which is insignificant (~0.03). Figure 11 further includes red and blue dots indicating days with positive and negative extremes in $\overline{w}^*_m$ (the top and bottom 5%, as in the composite events described above). These extreme cases are systematically skewed compared to the background distribution, so that enhanced tropical upwelling corresponds to: a) stronger negative high-latitude $DF$, and b)

weaker negative or positive subtropical $DF$. Weak extremes in tropical upwelling correspond to the opposite behavior: stronger subtropical $DF$ and weaker negative or positive high-latitude $DF$. These are the systematic patterns identified in Fig. 8, and the mean forcing for strong and weak upwelling extremes is significantly different from the mean of the distribution (Student t-test with 99% confidence level). This result suggests that, while the time series of wave forcing in high and low latitudes are generally uncorrelated, random events where the effects reinforce lead to extremes in $\overline{w}^*_m$ (so that compositing extremes leads to patterns that appear linked between high and low latitudes). Similar conclusions are seen when comparing EP fluxes (i.e. high-latitude $\overline{v'T'}$ and subtropical $\overline{u'v'}$) instead of wave forcing $DF$.

Figure 12 shows a similar diagnostic comparing wave forcing in the subtropics of each hemisphere, i.e., $DF$ averaged over 300-125 hPa, for 21°N-33°N (region B) and for 21°S-33°S (region C). Again the overall two-dimensional distribution suggests little correlation between wave forcing in each hemisphere (as also inferred from Fig. 10a). Positive extreme tropical upwelling events (red dots in Fig. 12) occur when $DF$ is less negative or positive in both hemispheres, and the opposite extremes occur when $DF$ is more negative in both hemispheres. While there is no general correlation between hemispheres, events that occur simultaneously lead to tropical upwelling extremes, and appear as symmetric patterns in statistical correlations. Very similar conclusions are found when comparing $\overline{u}_t$ links between hemispheres.

### *e. Shallow and deep branches of the residual circulation*

Analyses of circulation statistics and tracer behavior suggest that the stratospheric Brewer-Dobson circulation can be described by deep and shallow branches, which can evolve in different ways (e.g. Plumb 2002, Birner and Bönisch 2011). This behavior is also found in the analyses of sub-seasonal variability in this work: Fig. 13 illustrates the transition from shallow to deep residual circulation in ERA-Interim data derived by regressing global circulation onto the tropical upwelling at different altitudes. The statistical signature of the lower branch can be identified in correlations with $\overline{w}^*_m$ at 100 hPa (Fig. 13c) as shallow circulation cells centered near the tropical tropopause, with downwelling and warming patterns near ~25°-40°N and ~25°-40°S. In contrast, correlations with $\overline{w}^*_m$ at higher altitudes show less evidence of this behavior, and it is nearly absent from correlations with $\overline{w}^*_m$ at 20 hPa. The 20 hPa correlations reflect mainly the upper branch of the BDC, with tropical upwelling and downwelling in the winter polar stratosphere (Fig. 13a). The change between the low and high branches of the residual circulation appears as a smooth transition between 1) shallow overturning, with downwelling and warming in the subtropics and 2) deep upwelling, broad cooling of the tropical lower and middle stratosphere and warming at high latitudes. Tropical upwelling in the region of ~70 hPa - ~50 hPa is

correlated with both branches. Note that upwelling at 100 hPa still appears connected with the deep branch, as shown by the significant correlations with downwelling and warming at high latitudes. This connection could be linked to the fraction of the mass flux at 100 hPa that is part of the deep branch of the circulation.

The transition of the residual circulation from the lower to the middle stratosphere is also reflected in distinctive patterns of forcing terms influencing upwelling at different levels. Figure 14 shows the regression of the EP flux onto upwelling at the different levels, showing a transition in the dominant forcing associated with upwelling variability at different levels. Near 20 hPa upwelling is most impacted by forcing in the winter stratosphere (Fig. 14a), while the lower branch of the BDC is most influenced by transient wave forcing in the subtropical upper troposphere and lower stratosphere (Fig. 14c). Note that the shallow circulation (Fig. 14c) is negatively correlated with $DF$ in the subtropical lower stratosphere near and above the level of upwelling, while positive correlations are found just below (as discussed in Section 3c). This result is consistent with the calculations of Grise and Thompson (2013) based on high-vertical resolution GPS temperature observations. They show that wave drag in the subtropical lower stratosphere is associated with cooling near the tropical tropopause (~100-70 hPa), while subtropical tropospheric forcing leads to warming. Our analyses demonstrate the dynamical mechanism underlying these relationships. Specifically, subtropical EP flux convergence between 100 hPa and 70 hPa drives stronger upwelling near the tropopause, as follows from Eq. (5), while the wave drag below weakens the upwelling through the remote response in the zonal wind illustrated in Fig. 10. Finally, extratropical wave drag is also correlated with upwelling at 100 hPa, which could be linked to the connection with the deep branch seen in Fig. 13c.

## 4. Summary and discussion

Upwelling across the tropical tropopause is a fundamental part of the global stratospheric circulation. Upwelling cannot be observed directly, but can be inferred from thermodynamic or momentum calculations, or obtained from meteorological reanalyses, and these three estimates agree well for levels in the lower stratosphere (Abalos et al. 2012). Tropical upwelling is fundamentally driven by dynamical forcing (with temperatures and radiative balances responding to this forcing), which is embedded within the $\overline{w}^*_m$ calculations. This work focuses on examining the dynamical forcing of $\overline{w}^*_m$ by quantifying relationships with $DF$ and $\overline{u}_t$, which are the key drivers of $\overline{w}^*_m$ via Eq. (5). Derived estimates of upwelling in the lower stratosphere exhibit a large component of sub-seasonal (week-to-week) variability, in addition to a substantial annual cycle (Fig. 2). Mechanisms contributing to driving the annual cycle include forcing from extratropical waves (Yulaeva et al. 1994, Ueyama and Wallace 2010), baroclinic waves dissipating in the subtropics (Taguchi 2009, Chen and Sun 2011) and equatorial planetary waves (Boehm and Lee 2003, Kerr-Munslow and Norton 2006, Randel et al. 2008, Ortland and Alexander 2013), although causal mechanisms are still a

topic of active research (note that the forcings of the annual cycle are difficult to isolate based simply on correlations). In contrast, the sub-seasonal variations in upwelling (e.g. Fig. 2) have a distinctive temporal signature which can be used to identify transient forcing mechanisms, and this is the goal of this study.

Regression analysis and composites of extreme $\overline{w}^*_m$ events show that key regions of wave forcing ($DF$) for tropical upwelling occur in the extratropical stratosphere and the subtropical upper troposphere (regions A, B and C in Fig. 5a). Enhanced tropical upwelling occurs in conjunction with stronger high-latitude stratospheric wave forcing (enhanced upward EP flux, proportional to $\overline{v'T'}$) and reduced wave forcing in the subtropical upper troposphere (weaker meridional EP flux, proportional to $\overline{u'v'}$). Weaker tropical upwelling occurs with reduced high latitude $\overline{v'T'}$ and enhanced subtropical $\overline{u'v'}$. These represent modulations of the time-mean climatological EP flux and divergence in the extratropics.

A key aspect linking the remote wave forcing ($DF$) to the tropical lower stratosphere involves the associated zonal wind tendencies ($\overline{u}_t$), as the net forcing for upwelling is proportional to $DF - \overline{u}_t$ (Eq. 5). These accelerations $\overline{u}_t$ are part of the overall balanced response to transient localized forcing, wherein the nonlocal residual circulation acts to maintain mass continuity and thermal wind balance. For high-latitude wave forcing, the wind accelerations act to extend the net forcing to tropical latitudes, as illustrated in Fig. 1. For localized forcing in the subtropical upper troposphere, the $\overline{u}_t$ response extends vertically across the tropopause, resulting in an oppositely-signed net forcing in the lower stratosphere (e.g. Fig. 10c). These zonal wind accelerations occur on the equatorward flank of the time-averaged subtropical jets (Fig. 9), and are in thermal wind balance with temperature tendencies in the tropics and middle latitudes, spanning the troposphere to lower stratosphere (e.g. Fig. 3).

The regression and composited $\overline{w}^*_m$ extreme patterns of $DF$ (Figs. 5a and 8c) suggest the combined influence of high- and low-latitude wave forcing on tropical upwelling, and also show highly symmetric patterns of subtropical wave forcing in each hemisphere (at least during DJFM). This begs the question of whether the wave forcings in these regions are intrinsically linked, or if this is a result of the statistical analysis. This question has been addressed by examining cross-correlations and the two-dimensional distribution functions of forcing between the different regions. Results (Figs. 11 and 12) show that there is not a general correlation between wave forcing at high and low latitudes (regions A and B), or between wave forcing in the subtropics between hemispheres (regions B and C). Rather, extreme upwelling events (both positive and negative) occur when the stochastic variations in wave driving in different regions reinforce each other; for example, occasional coincident events of enhanced subtropical wave forcing in both hemispheres leads to extreme minima in tropical upwelling (Fig. 12). Our conclusion is that the coherent global variations suggested in regressions and extreme composites are primarily a statistical result, and do not

signify distant, globally coherent behavior in wave forcing.

The statistical relationships between derived tropical upwelling and temperature/circulation reveal the shallow and deep branches of the Brewer Dobson circulation. The upper branch of the Brewer Dobson circulation is most strongly correlated to tropical upwelling at levels above the lower stratosphere, highlighting a broad-scale deep circulation coupled between the tropics and winter polar stratosphere (Fig. 13a). Variability in the deep branch is primarily linked to wave forcing in the high latitude winter stratosphere (Fig. 14a). In contrast, transient upwelling near the tropopause (~100 or 70 hPa) is strongly correlated with downwelling circulation cells near tropopause level in the subtropics (~25°-40°), and these are reflected in zonal average temperature (Fig. 13c) and ozone tendencies (Fig. 4). This behavior is primarily linked to variability in wave forcing in the subtropical upper troposphere (Fig. 14c), wherein stronger wave forcing drives overturning circulation cells above the forcing, with upwelling in the subtropics and downwelling over the tropical tropopause (Fig. 10d). Likewise, weaker than average wave forcing in the subtropical upper troposphere results in enhanced tropical upwelling and sinking in the subtropics. Note that the shallow branch of the BDC is also intensified by stronger convergence in the tropical lower stratosphere (Fig. 14c). Thus, the exact altitude at which wave dissipation occurs in the subtropics is crucial for the variability of the shallow branch of the BDC, as the drag at slightly different levels can have opposite effects on upwelling near the tropopause.

*Acknowledgements*

We thank Cameron Homeyer for facilitating access to the ECMWF ERA-Interim data used here. This work was partially supported under the NASA Aura Science Program. M.A. thanks the Spanish projects CGL2008-06295 and CGL2012-34997. Most of this work has been carried out at NCAR during visits of M.A. The National Center for Atmospheric Research is operated by the University Corporation for Atmospheric Research, under sponsorship of the National Science Foundation.

## References

Abalos, M., W. J. Randel, and E. Serrano, 2012: Variability in upwelling across the tropical tropopause and correlations with tracers in the lower stratosphere. *Atmos. Chem. Phys.*, **12**, 11505–11517.

Abalos, M., W. J. Randel, D. E. Kinnison, and E. Serrano, 2013: Quantifying tracer transport in the tropical lower stratosphere using WACCM. *Atmos. Chem. Phys.*, **13**, 10591-10607.

Andrews, D. G., J. R. Holton, and C. B. Leovy, 1987: *Middle Atmosphere Dynamics*. Academic Press, 489 pp.

Birner, T. and H. Bönisch, 2011: Residual circulation trajectories and transit times into the extratropical

lowermost stratosphere. *Atmos. Chem. Phys.*, **11**, 817–827.

Boehm, M. T. and S. Lee, 2003: The implications of tropical Rossby waves for tropical tropopause cirrus formation and for the equatorial upwelling of the Brewer–Dobson circulation. *J. Atmos. Sci.*, **60**, 247-261.

Butchart, N., A. A. Scaife, M. Bourqui, J. de Grandpré, S. H. E. Hare, J. Kettleborough, U. Langematz, E. Manzini, F. Sassi, K. Shibata, D. Shindell, and M. Sigmond, 2006: Simulations of anthropogenic change in the strength of the Brewer–Dobson circulation. *Climate Dyn.*, **27**, 727–741.

Calvo, N., and R. R. Garcia, 2009: Wave forcing of the tropical upwelling in the lower stratosphere under increasing concentrations of greenhouse gases. *J. Atmos. Sci*., **66**, 3184-3196.

Chen, P., J. R. Holton, A. O'Neill, and R. Swinbank, 1994: Isentropic mass exchange between the Tropics and extra-tropics in the stratosphere. *J. Atmos. Sci*., **51**, 3006–3018.

Dee, D. P., and 35 coauthors, 2011: The ERA-interim reanalysis: configuration and performance of the data assimilation system. *Q. J. Roy. Meteor. Soc.*, **137**, 553–597.

Dunkerton, T.J., C.-P.F. Hsu, and M. E. McIntyre, 1981: Some Eulerian and Lagrangian diagnostics for a model stratospheric warming. *J. Atmos. Sci*., **38**, 819-843.

Fritz, S., and S. D. Soules, 1972: Planetary variations of stratospheric temperatures. *Mon. Wea. Rev*., **100**, 582–589.

Garcia, R. R., 1987: On the mean meridional circulation of the middle atmosphere. *J. Atmos. Sci*., **44**, 3599-3609.

Garcia, R. R., and W. J. Randel, 2008: Acceleration of the Brewer-Dobson circulation due to increases in greenhouse gases. *J. Atmos. Sci*., **65**, 2731-2739.

Garny, H., Dameris, M., Randel, W. J., Bodeker, G. E., Deckert, R.: Dynamically forced increase of tropical upwelling in the lower stratosphere. *J. Atmos. Sci*., **68**, 1214-1233, 2011.

Haynes, P. H., C. J. Marks, M. E. McIntyre, T. G. Shepherd and K. P. Shine, 1991: On the "downward control" of extratropical diabatic circulations by eddy-induced mean zonal forces. *J. Atmos. Sci*., **48**, 651-678.

Holton, J. R., P. H. Haynes, M. E. McIntyre, A. R. Douglass, R. B. Rood, and L. Pfister, 1995: Stratosphere-troposphere exchange. *Rev. Geophys*., **33**, 403-439.

Kerr-Munslow, A. M., and W. A. Norton, 2006: Tropical wave driving of the annual cycle in tropical tropopause temperatures. Part I: ECMWF analyses. *J. Atmos. Sci*., **63**, 1420-1431.

Ortland, D. A., and M. J. Alexander, 2013: The residual mean circulation in the tropical tropopause layer driven by tropical waves. *J. Atmos. Sci*., in review.

Plumb, R. A., J. Eluszkiewicz, 1999: The Brewer–Dobson Circulation: Dynamics of the Tropical Upwelling. *J. Atmos. Sci*., **56**, 868–890.

Plumb, R. A., 2002: Stratospheric transport. *J. Meteor. Soc. Japan*., **80**, 793–809.

North, G. R., T. L. Bell, R. F. Cahalan, and F. J. Mohen, 1982: Sampling errors in the estimation of Empirical Orthogonal Functions,.*J. Atmos. Sci*., **110**, 699-706.

Randel, W.J., 1993: Global variations of zonal mean ozone during stratospheric warming events. *J. Atmos. Sci.,* **50**, 3308-3321.

Randel, W. J., R. R. Garcia, and F. Wu, 2002: Time-dependent upwelling in the tropical lower stratosphere estimated from the zonal-mean momentum budget. *J. Atmos. Sci*., **59**, 2141–2152.

Randel, W. J., M. Park, F. Wu, and N. Livesey, 2007: A Large Annual Cycle in Ozone above the Tropical Tropopause Linked to the Brewer–Dobson Circulation. *J. Atmos. Sci*., **64**, 4479–4488.

Randel, W. J., R.R. Garcia, and F. Wu, 2008: Dynamical balances and tropical stratospheric upwelling. *J. Atmos. Sci*., 65, 3584-3595.

Ryu, J.-H., and S. Lee, 2010: Effect of tropical waves on the tropical tropopause transition layer upwelling. *J. Atmos. Sci*., **67**, 3130-3148.

Semeniuk, K. and Shepherd, T. G., 2001: Mechanisms for tropical upwelling in the stratosphere, *J. Atmos. Sci.*, **58**, 3097-3115.

Shepherd, T. G., 2007: Transport in the middle atmosphere*., J. Meteor. Soc. Japan*., **85**, 165–191.

Shepherd, T. G. and C. Mc. Landress, 2011: A robust mechanism for strengthening of the Brewer–Dobson circulation in response to climate change: critical-layer control of subtropical wave breaking. *J. Atmos. Sci*., **68**, 784-797.

Taguchi, M., 2009: Wave driving in the tropical lower stratosphere as simulated by WACCM. Part I: annual cycle, *J. Atmos. Sci*., **66**, 2029–2043.

Ueyama, R. and M. J. Wallace, 2010: To what extent does high-latitude wave forcing drive tropical ipwelling in the Brewer–Dobson circulation? *J. Atmos. Sci*., **67**, 1232-3442.

Ueyama, R., E. P. Gerber, J. M. Wallace, and D. M. W. Frierson, 2013: The role of high-latitude waves in the intraseasonal to seasonal variability of tropical upwelling in the Brewer–Dobson circulation. *J. Atmos. Sci*., **70**, 1631–1648.

Yulaeva, E., J. R. Holton, and J. M. Wallace, 1994: On the cause of the annual cycle in tropical lower-stratospheric temperature. *J. Atmos. Sci*., **51**, 169–174.

Zhou, T., M. A. Geller, and W. Lin, 2012: An observational study on the latitudes where wave forcing drives Brewer-Dobson upwelling. *J. Atmos. Sci*., **69**, 1916-1935.

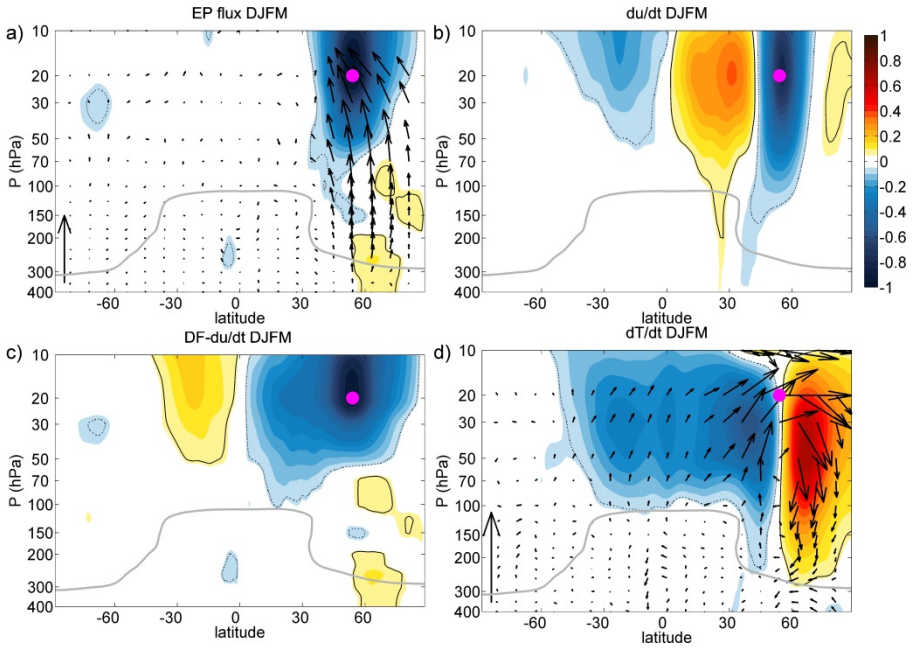


FIG. 1. One-point correlations of EP flux convergence ($-DF$) at 54°N, 20 hPa with (a) EP flux (vectors) and divergence (colors), (b) zonal mean wind tendency, (c) net forcing and (d) temperature tendency (colors) and residual circulation (vectors). The solid and dashed contours show the threshold of 99% significant linear correlations (positive and negative, respectively). The vertical arrows in panels (a) and (d) indicate the length corresponding to a linear correlation of 1. Data: ERA-Interim DJFM 1979-2011.

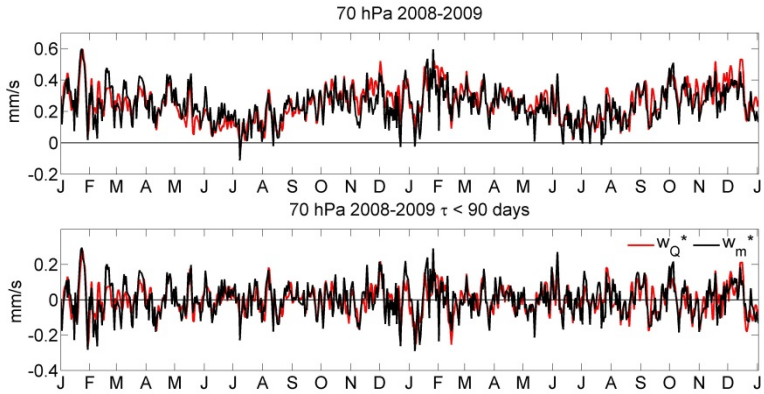


FIG. 2. Time series of upwelling averaged over 18°S-18°N at 70 hPa for the years 2008-2009 estimated indirectly from ERA-Interim data. Black: momentum balance calculation ( $\overline{w}^*_m$ , Eq. 5), red: thermodynamic estimate ( $\overline{w}^*_Q$ , see text for details). Top panel shows the full time series, and the lower panel shows the high-pass filtered series, including only timescales shorter than 90 days. Units: $mm \cdot s^{-1}$.

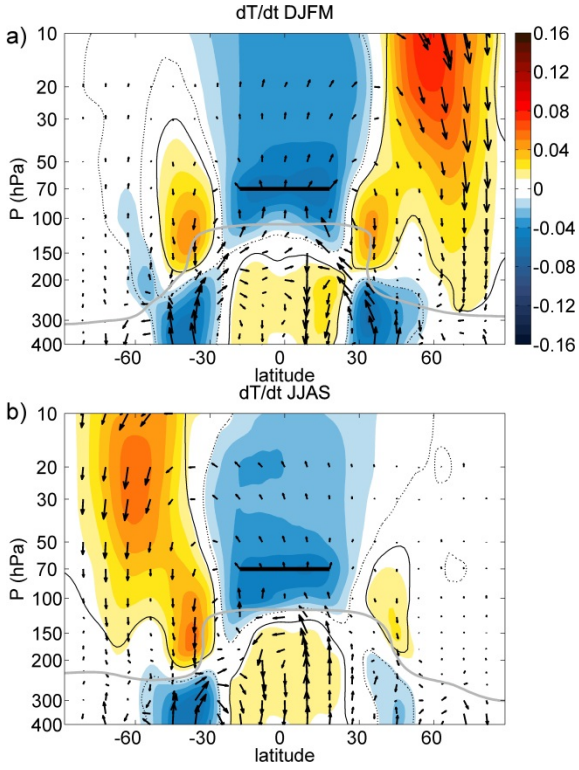


FIG. 3. Regression of the residual circulation (vectors) and temperature tendency (colors) on tropical upwelling ( $\overline{w}_m^*$ ) averaged over 18°S-18°N at 70 hPa for DJFM (upper panel) and JJAS (lower panel). The reference level for upwelling is indicated by the black horizontal bar. The seasonal mean lapse rate tropopause is shown in gray. The solid and dashed contours show the threshold of 99% significant linear correlations (positive and negative, respectively). Data: ERA-Interim 1979-2011. Units: $K \cdot day^{-1}$.

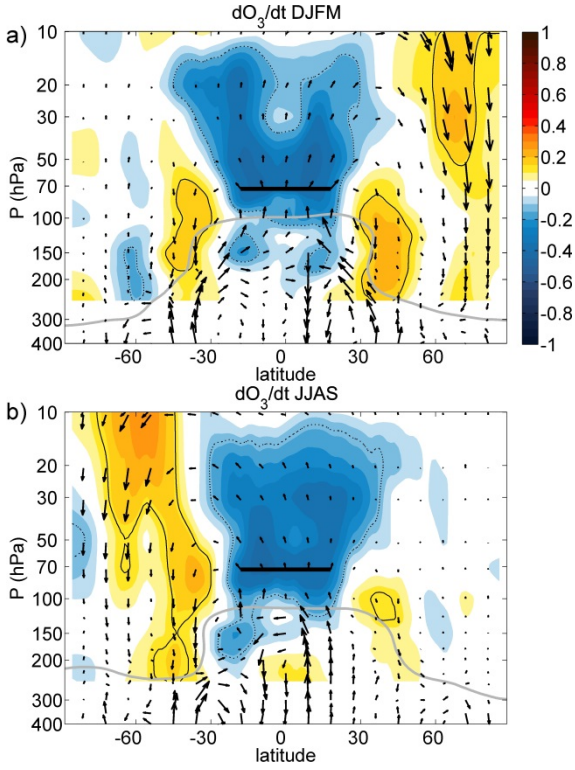


FIG. 4. As Figure 3 but for the regressions of the meridional circulation (vectors) and zonal mean ozone tendency (colors) from the Aura Microwave Limb Sounder (MLS) satellite instrument on upwelling ( $\overline{w}_m^*$ ) averaged over 18°S-18°N at 70 hPa for the period 2005-2010. Units: $ppbv \cdot day^{-1}$ .

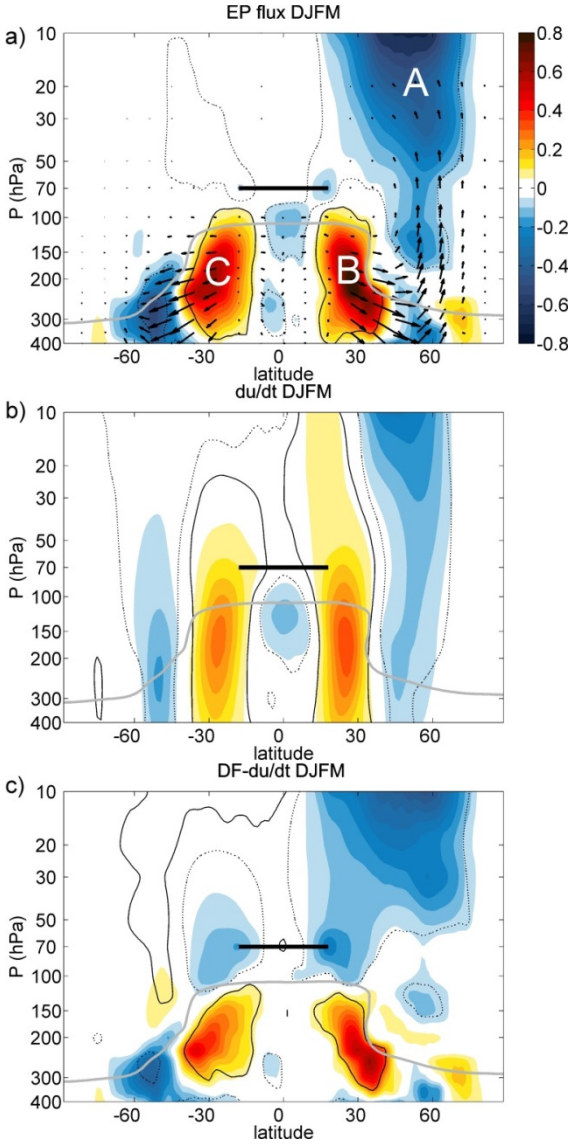


FIG. 5. Regression of (a) EP flux (vectors) and divergence (colors), (b) zonal wind tendency and (c) net forcing onto upwelling ( $\overline{w}_m^*$ ) at 70 hPa averaged over 18°S-18°N in DJFM. The regions A, B and C in (a) denote centers of action for the EP flux divergence, as discussed in text. The time series are filtered to remove timescales longer than 90 days. The reference level for upwelling is indicated by the black horizontal bar. The seasonal mean lapse rate tropopause is shown in gray. The solid and dashed contours show the threshold of 99% significant linear correlations (positive and negative, respectively). Data: ERA-Interim 1979-2011. Units: $m \cdot s^{-1} \cdot day^{-1}$.

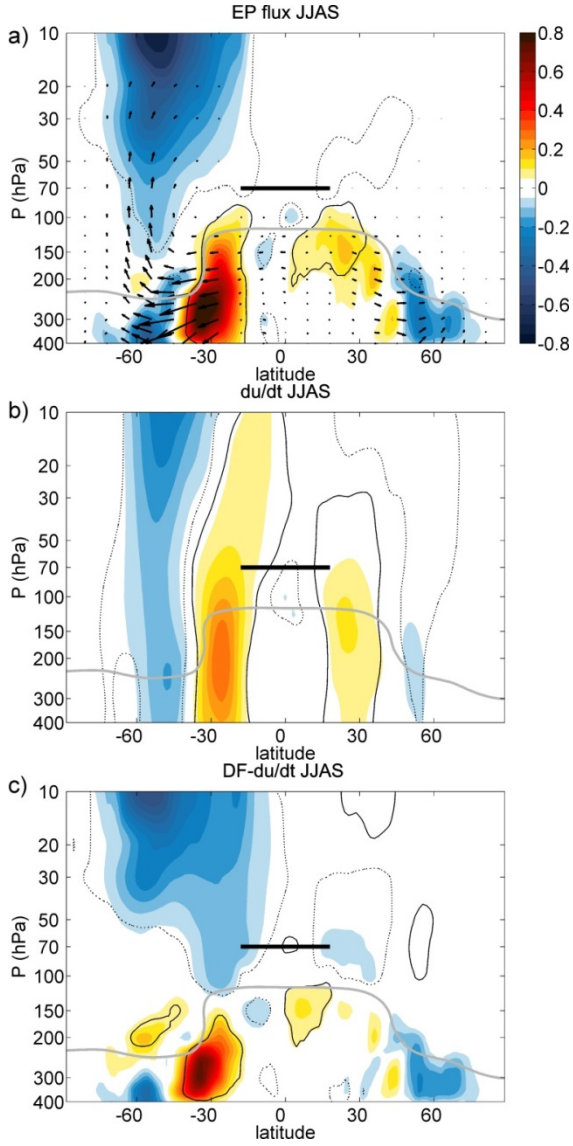


FIG. 6. As Figure 5 but for JJAS.

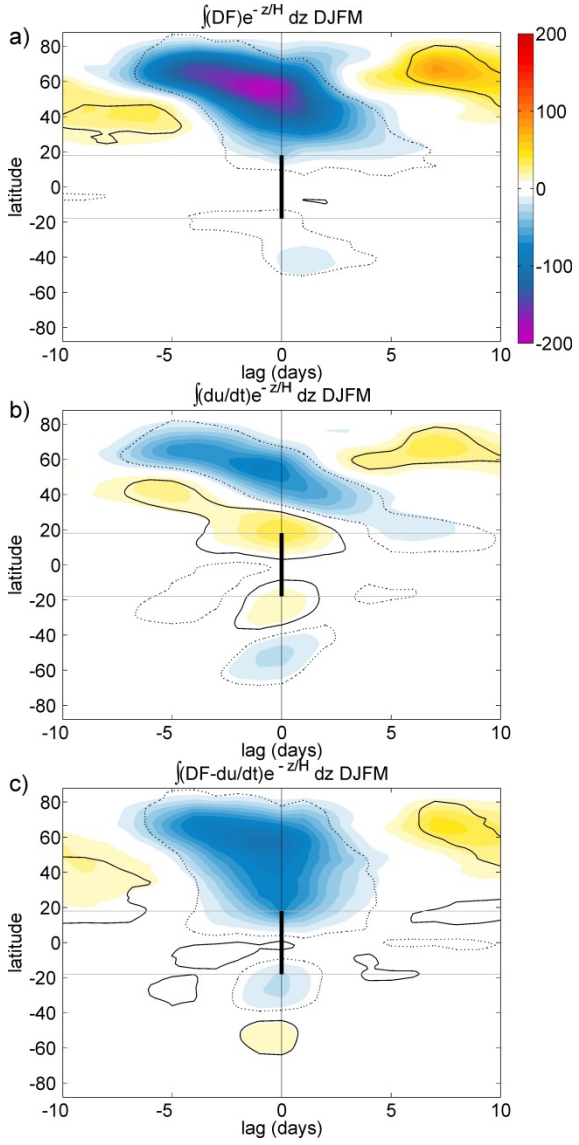


FIG. 7. Lagged regressions as a function of latitude and time (days) of upwelling ( $\overline{w}_m^*$ ) at 70 hPa averaged over 18°S-18°N with the forcing terms integrated in altitude (as in Eq. 5) from 70 hPa to the top. The latitudinal boundaries for upwelling calculations (18°S-18°N) are indicated by gray lines. The solid and dashed contours show the threshold of 99% significant linear correlations (positive and negative, respectively). Units: $m \cdot s^{-1} \cdot day^{-1}$ .

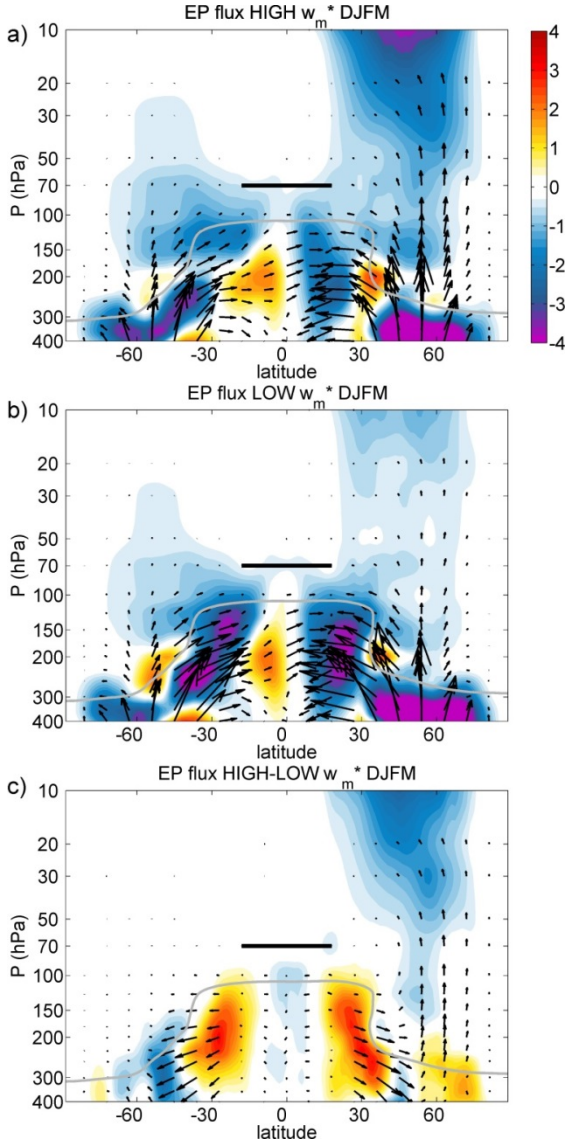


FIG. 8. EP flux and divergence composites for 5% high (a), low (b) and difference high minus low (c) extremes of upwelling at 70 hPa and averaged over 18°S-18°N. The horizontal black bar indicates the location of tropical upwelling used to generate the composites. The seasonal mean lapse rate tropopause is shown in gray. Data: ERA-Interim DJFM 1979-2011. Units: $m \cdot s^{-1} \cdot day^{-1}$.

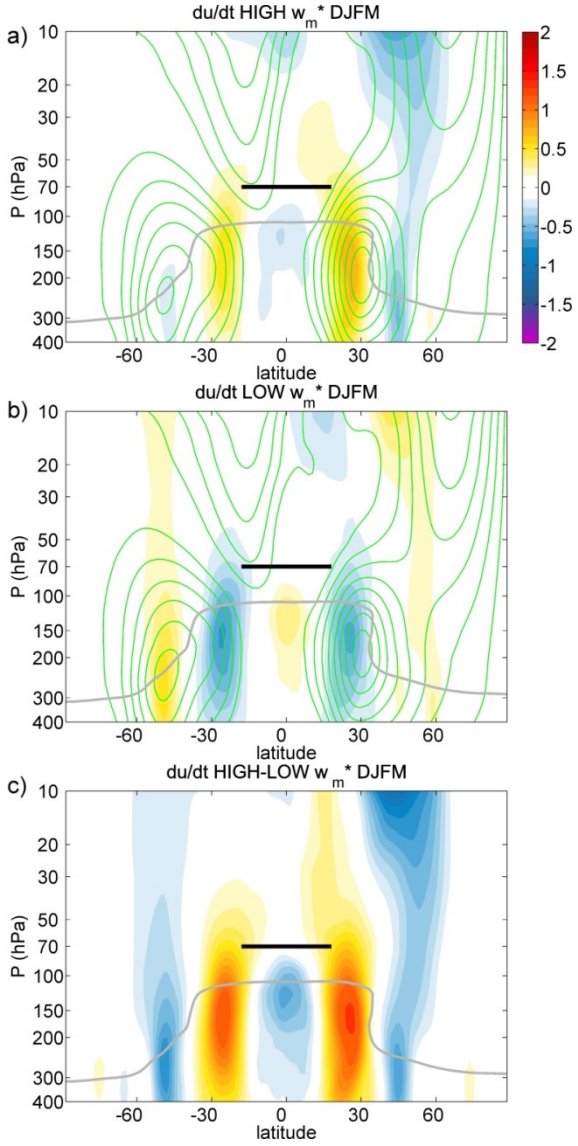


FIG. 9. As Figure 8 but for zonal mean wind tendency. Units: $m\,s^{-1}\,day^{-1}$.

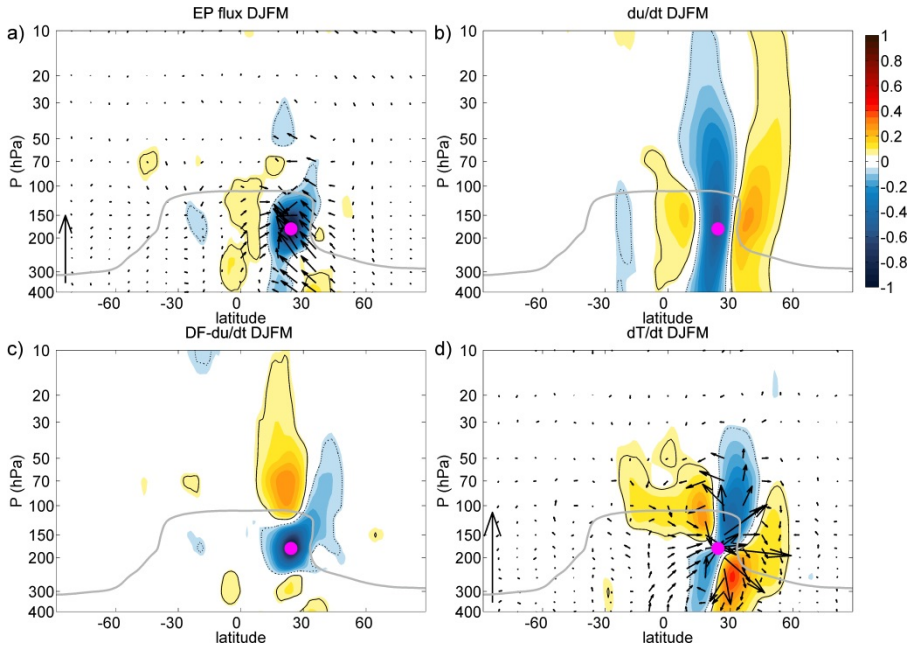


FIG. 10. As Figure 1 but for of EP flux convergence ( $-DF$ ) at 24°N, 175 hPa.

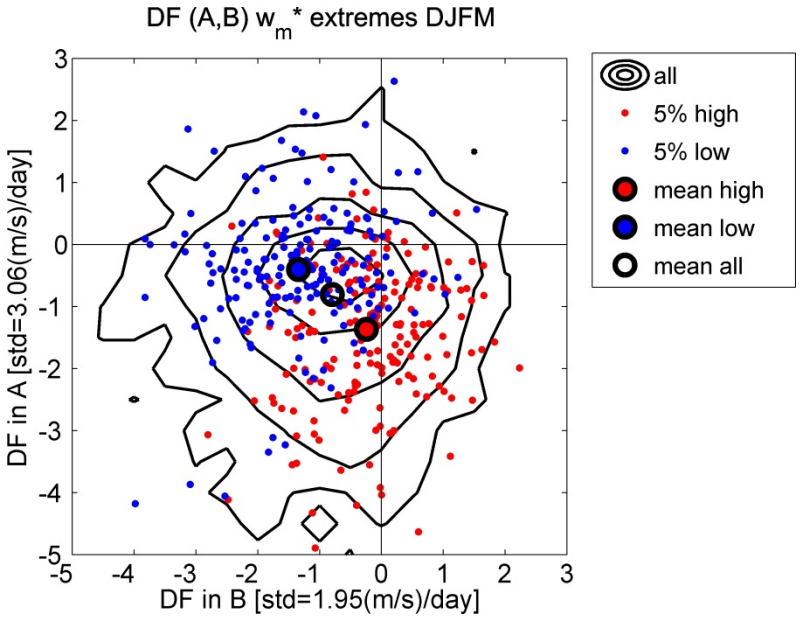


FIG. 11. Two dimensional distribution of wave forcing in the extratropical winter stratosphere (average over 20-10 hPa and 36°N-60°N; region A in Fig. 5a) versus wave forcing in the subtropical upper troposphere (average over 300-125 hPa and 21°N-33°N; region B in Fig. 5a). The axes are normalized to standard deviations in each quantity. Black contours show probability distribution of all DJFM days during 1980-2011 (contours shown are 1, 5, 20, 50 and 80%). Red and blue dots show days with 5% extreme maximum and minimum tropical upwelling. Larger circles indicate the mean of the distribution of all points (no color), high extremes (red) and low extremes (blue).

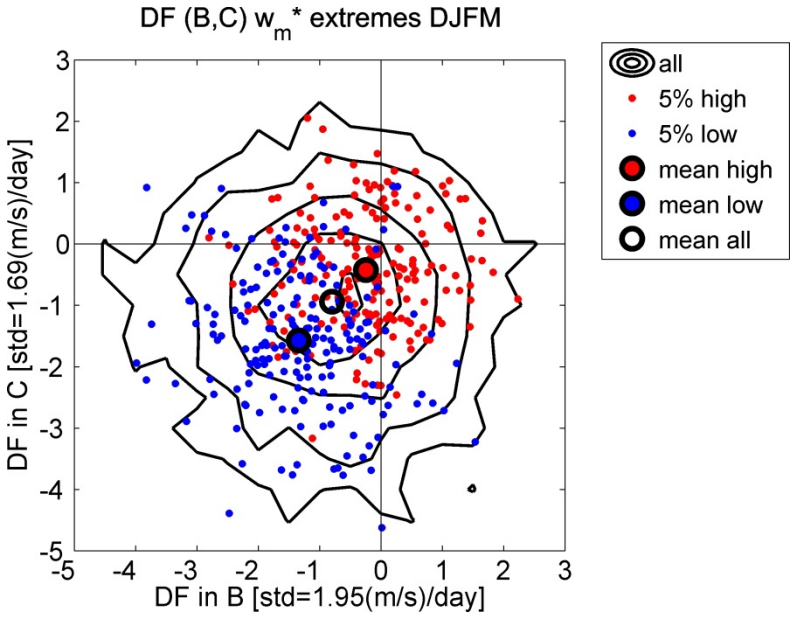


FIG. 12. As figure 11 but for wave forcing in the subtropical upper troposphere in the NH versus the SH (averages over 300-125 hPa and 21°N-33°N and 21°S-33°S respectively; regions B and C in Fig. 5a).

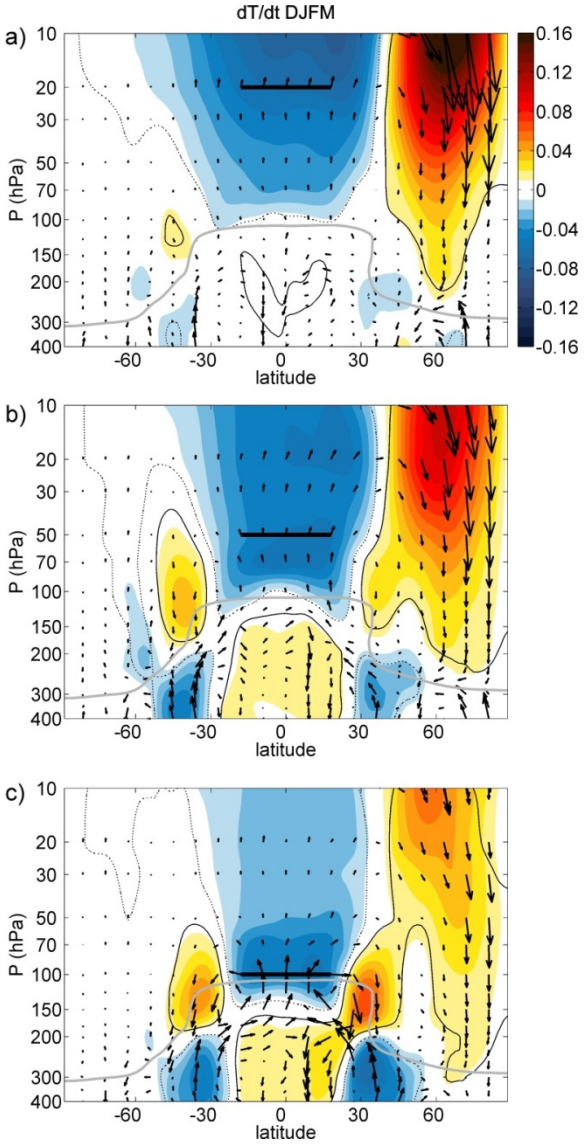


FIG. 13. As Figure 3a but for tropical upwelling ( $\overline{w}^*_m$ ) computed at 20 hPa (a), 50 hPa (b) and 100 hPa (c), as indicated by the black bars.

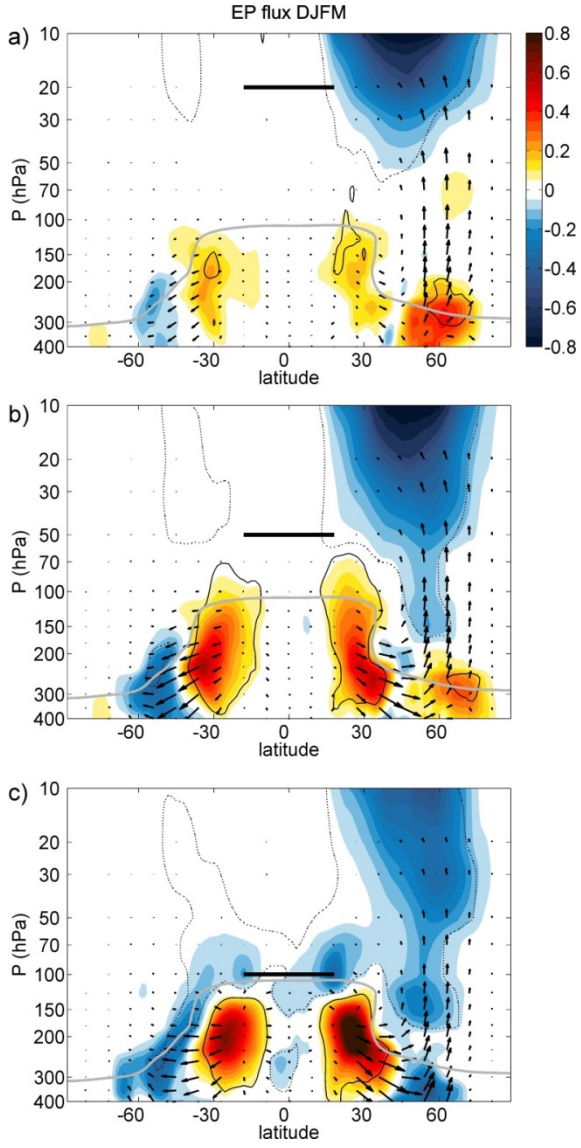


FIG. 14. As Figure 5a but for tropical upwelling ( $\overline{w}_m^*$ ) computed at 20 hPa (a), 50 hPa (b) and 100 hPa (c), as indicated by the black bars.

# 7. Discussion

The primary aim of this Thesis is to investigate the temporal variability in upwelling in the tropical lower stratosphere. For this, tropical mean ascent rates have been inferred in three different ways: directly from ERA-Interim reanalysis, and indirectly from momentum and thermodynamic balance calculations (Abalos et al. 2012). Time series of the three computed estimates of upwelling consistently show large annual cycles, with nearly two times stronger upwelling in boreal winter as compared to summer, consistently with previous works (e.g. Rosenlof 1995, Randel et al. 2002). In addition, substantial variability is observed on sub-seasonal timescales. These independent estimates provide an assessment of the degree of uncertainty in tropical upwelling magnitude and variability. The results show reasonable agreement (linear correlations around ~0.7, statistically significant at 99% confidence level), with best correspondence between the two indirect estimates (Figs. 3 and 4 in Abalos et al. 2012). The fact that the three estimates of upwelling do not exactly coincide highlights their limitations. For instance, it is known that ascent rates in ERA-Interim are around 40% too strong near the tropical tropopause (Simmons et al. 2006, Fueglistaler et al. 2009, Dee et al. 2011, Ploeger et al. 2012). Our calculations are consistent with this result, suggesting that the other two estimates provide more realistic values at 100 hPa. The estimate based on momentum balance calculations does not include a realistic representation of sub-grid scale waves, and their possible contribution to upwelling variability is thus excluded. However, this contribution is estimated to be relatively small for upwelling in the tropical lower stratosphere (Garcia and Randel 2008, Calvo and Garcia 2009). Lastly, the thermodynamic estimate is mainly based on radiative transfer calculations which do not include the clouds effects on radiation. Nevertheless, the net effect of clouds in the tropics has been estimated to be relatively small (Yang et al. 2010). Despite the uncertainties in the

described calculations, the overall agreement among the estimates of upwelling at different levels across the tropical tropopause prompts confidence in the results. Further confirmation of the accuracy of these upwelling calculations comes from the coherent fluctuations that they show with completely independent satellite measurements of ozone and carbon monoxide (CO). All aspects considered, the computed upwelling estimates are suitable for exploring the links with tracer variability in the tropical lower stratosphere.

Time series of temperature and tracer observations above the tropical tropopause show a high degree of common variability on seasonal and sub-seasonal timescales (Fig. 1 in Abalos et al. 2012). Given the strong background vertical gradients in potential temperature and tracers observed in this region, tropical upwelling is a plausible candidate for driving the common fluctuations between temperature and tracers. One feature that stands out in the time series of temperature, ozone and CO just above the tropical tropopause is a large annual cycle. Temperature and ozone cycles are almost in phase, while CO shows approximately opposite phase. The annual cycle in temperature is known to be mainly driven by the large seasonality in upwelling, with stronger ascents in boreal winter carrying more vigorously cold air masses from the tropopause (e.g. Yulaeva et al. 1994, Fueglistaler et al. 2011). Randel et al. (2007) explored the origin of the seasonality in ozone and CO observations, and found evidence that upwelling acting on the strong background vertical gradients is mainly forcing this seasonality. In the present Thesis this relation has been further explored, by computing the monthly mean of the terms in the tracer budgets (for ozone and CO). For this, the upwelling estimates described above have been combined with ERA-Interim meteorological data and tracer satellite observations from MLS (Waters et al. 2006). The results show that the annual cycles in the tracers closely follow the seasonality in vertical advection by upwelling at levels where vertical gradients are strong (Abalos et al. 2012). This analysis is based on the Transformed Eulerian Mean (TEM) equations of transport on log-pressure altitudes. The results are consistent with the work of Randel et al. (2007) and confirm the key

role of upwelling for driving tracer variability in the tropical lower stratosphere.

However, there is one important caveat in the above semi-observational calculations of the tracer budgets. Due to the relatively coarse resolution of the satellite measurements, the eddy transport term in the tracer continuity equation cannot be resolved and thus is included in the residual, computed as the imbalance in the budget considering all the explicitly evaluated terms. The results show a non-negligible residual in the ozone budget. Since it has been argued in previous studies that eddy transport processes can be important for ozone concentrations in the tropical lower stratosphere, it was hypothesized that this relatively large residual might be mainly associated with eddy transport processes, unresolved in the calculations. In order to test this hypothesis, output from the Whole Atmosphere Community Climate Model (WACCM, version 4) has been used to evaluate the TEM tracer budgets (Abalos et al. 2013a). The model analyses support the observational results, highlighting upwelling acting on the strong background vertical gradients as the main cause for tracer seasonality above the tropical tropopause layer. Moreover, eddy transport of ozone explicitly computed from WACCM data shows a very similar structure to the budget residual obtained in the observational calculations (Figure 7.1).

The similarity between these terms is remarkable, especially considering the additional errors that might be included in the observational budget residual and the fact that the model simulation is not nudged in any way to ozone observations. This correspondence supports the validity of the hypothesis proposed above, and thus the residuals in the observational budget can be mostly attributed to the eddy transport. From a complementary perspective, the similarity between the observational and model tracer budgets suggests a realistic representation of transport processes in WACCM, and hence supports its suitability for our purpose.

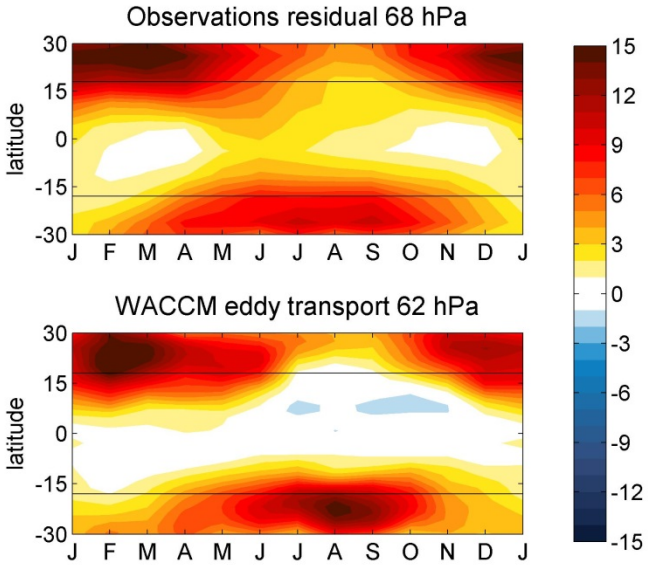


**Figure 7.1**. Monthly evolution as a function of latitude of ozone budget residual in the observations (upper panel) compared to horizontal eddy transport explicitly computed from WACCM output (lower panel) on comparable levels above the tropical tropopause. Units: $ppbv \cdot day^{-1}$.

To this point, the results obtained in this Thesis (both from observations and model data analyses) support the conclusion of Randel et al. (2007) that the annual cycle in ozone above the tropical tropopause is mainly caused by tropical upwelling seasonality acting on the strong vertical gradients. On the other hand, a number of works have recently proposed an alternative explanation for the origin of the ozone seasonality. In particular, results based on simulations with the Chemical Lagrangian transport Model of the Stratosphere (CLaMS) suggest that horizontal transport associated with the Asian monsoon anticyclonic upper-level circulation is mainly responsible for the high tropical ozone concentrations in boreal summer (Konopka et al. 2009, 2010, Ploeger et al. 2012). The anticyclone transports air masses with high ozone concentrations from the extratropical stratosphere into the tropical tropopause layer (TTL), significantly increasing ozone concentrations in this

region. Based on these results from CLaMS, it was proposed that the main driver of ozone seasonality was horizontal transport (or in-mixing) instead of vertical advection by tropical upwelling. In the present Thesis, the details of these contrasting conclusions have been investigated, and it has been found that there is only an apparent discrepancy between the results, which can be reconciled by carefully comparing them in equivalent terms. This reconciliation of the results has been possible thanks to a fruitful collaboration with the *Stratosphere* group of the *Jülich Forschungzentrum* (Germany), in particular with Felix Ploeger and Paul Konopka. Two main reasons have been found for the disagreement regarding the origin of the ozone seasonality above the tropical tropopause.

The first concerns the use of different vertical coordinates. The Lagrangian model is run on isentropic coordinates, which have been proven to provide more accurate and less noisy representation of transport across the TTL (Ploeger et al. 2010). As noted by Konopka et al. (2009), on isentropic coordinates the annual cycle in ozone is much reduced (up to ~60%) as compared to that on log-pressure altitudes. This is because potential temperature undergoes a seasonal cycle as well, which is almost in phase with ozone (as mentioned above). The vertical displacement of the isentropes largely compensates the seasonality in the ozone concentrations. In particular, the fraction of the variability in ozone that is in common with temperature is removed on isentropes. This represents a large fraction of the variability, not only for the annual cycle but also on sub-seasonal timescales. It is important to note that the variability in (potential) temperature is, in turn, mostly driven by upwelling in this region. Thus, in the isentropic frame of reference, the ozone variability associated to upwelling is removed to a large extent. Keeping this difference in mind is essential to interpret the different results. Note that the maximum amplitude of ozone seasonality is found near ~80 hPa in the observations, that is, approximately ~1 km above the cold point tropopause (e.g. Randel et al. 2007). Conversely, on isentropic coordinates the (smaller) maximum amplitude is found near the tropopause, further

highlighting the differences in the ozone seasonality between the two coordinate systems (Abalos et al. 2013a, 2013b).

The second fundamental difference between the analyses from WACCM and CLaMS is that, while the former is based on TEM budgets, the latter consists of Lagrangian calculations. Carefully interpreting the implications of these distinct studies is crucial to understand the origin of the apparent contradiction. In the Lagrangian calculations, ozone concentrations are obtained by integrating material derivatives along parcel trajectories. Consequently, the value of the concentration at a given position and time is determined by the history of the air parcel. If an air parcel has been in-mixed from the extratropics into the TTL near the tropopause and is subsequently transported upwards by the mean tropical upwelling, the two types of analyses lead to apparently contrasting interpretations when evaluated for a given level above the tropopause. On one hand, Lagrangian calculations *remember* that the parcel was originally located outside the TTL, and therefore in this view it is concluded that ozone has been in-mixed from the extratropics. Conversely, in the TEM budgets the air parcel travels across that particular level and is perceived as transported from below by tropical upwelling; hence the change in ozone is due to vertical advection. This example proves the importance of comparing the results from alternative frameworks in equivalent terms (Abalos et al. 2013b).

WACCM results show a transition with height in the seasonality of the explicitly computed ozone horizontal eddy transport (Abalos et al. 2013a). In particular, ~2 km above the tropical tropopause, eddy transport occurs in the winter and spring subtropics of each hemisphere (e.g. Fig. 7.1). On the other hand, at lower levels (near the tropopause), WACCM calculations show a strong effect of eddy transport associated with the summer Asian monsoon on tropical ozone concentrations. Figure 7.2 shows WACCM climatological ozone concentrations and wind vectors for boreal summer (JJA) at one isentropic level close to the tropopause (400 K). A planetary-scale tongue of high-ozone air from the extra-tropics transported towards the tropics by the anticyclonic circulation is clearly

identified to the east of the Asian monsoon (approximately between 120°E-150°W). This horizontal eddy transport significantly increases NH summer tropical mean ozone concentrations near the tropopause, as reflected in the TEM tropical mean budget (Fig. 8 in Abalos et al. 2013). Hence, the TEM budgets based on WACCM data capture the effect of the Asian monsoon near the tropopause first pointed out in the Lagrangian calculations, and this common transport process opens the door for reconciling results.

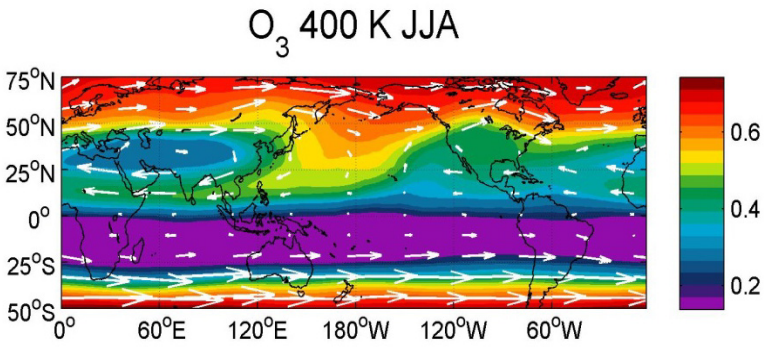


**Figure 7.2**. Seasonal mean boreal summer (JJA) ozone concentration (shading) and horizontal wind (arrows) on the 400 K isentropic surface (near the tropopause) in WACCM4. The tongue of high ozone entering the tropics transported by Asian monsoon makes an important contribution to tropical mean concentrations.

The definitive proof that the results are only apparently contradictory and can be reconciled is obtained when the Lagrangian results are transformed into an Eulerian perspective. The resulting Lagrangian-based budget is similar to that obtained with WACCM, showing a large effect of the Asian monsoon at tropopause levels, but not ~2 km above (Fig. 3 in Abalos et al. 2013b). Moreover, the large annual cycle in upwelling is captured in these calculations as well, and is closely followed by the ozone seasonality at levels with strong vertical gradients (Fig. 2 in Abalos et al. 2013b). These results unequivocally demonstrate the consistency between the Lagrangian model and WACCM TEM calculations. In Abalos et al. (2013b) it is further highlighted that the results from these

different analyses provide complementary information on transport. In particular, while only Lagrangian analyses can offer information on the origin on the air parcels (and tracer molecules in chemistry-including Lagrangian models), TEM budgets are useful for evaluating transport processes affecting tracer concentrations at each level separately.

The analyses in this Thesis highlight the importance of vertical resolution in models for resolving the detailed structure of transport terms near the tropical tropopause and in the lower stratosphere. Current chemistry-climate models usually run with a ~1.1-1.4 km vertical resolution in this region, as used for the WACCM simulation in this Thesis. It was verified before performing the budget analyses that the model accurately reproduces the vertical structure of temperature and tracers in the tropical lower stratosphere, including overall realistic annual cycles peaking just above the tropical tropopause. However, one relevant caveat that was identified is that the cold point tropopause is located at a higher altitude than in the observations. This possibly affects the altitude of the maximum amplitude in temperature and tracer annual cycles, which is also slightly shifted upwards respect to the observations. For the purpose of this Thesis, this issue is accounted for by considering higher levels in WACCM than in the observational analysis.

The vertical shift in the cold point tropopause could be simply due to the limited vertical resolution of the model simulation. This is suggested by the results of a comparison made with a high-vertical resolution version of WACCM (provided by Juan Añel, personal communication). The results show a lower and thus more accurate altitude of the cold point in the high-vertical resolution simulation, as shown in Fig. 7.3. In addition, this simulation provides a more accurate representation of the vertical structure of the ozone annual amplitude (not shown). In view of these results, it might be worthwhile to carry out chemistry-climate model simulations with increased vertical resolution in the upper troposphere and lower stratosphere, in order to improve the current representation of large-scale features such as the location of the cold point, stratospheric water vapor and transport processes affecting other tracers.

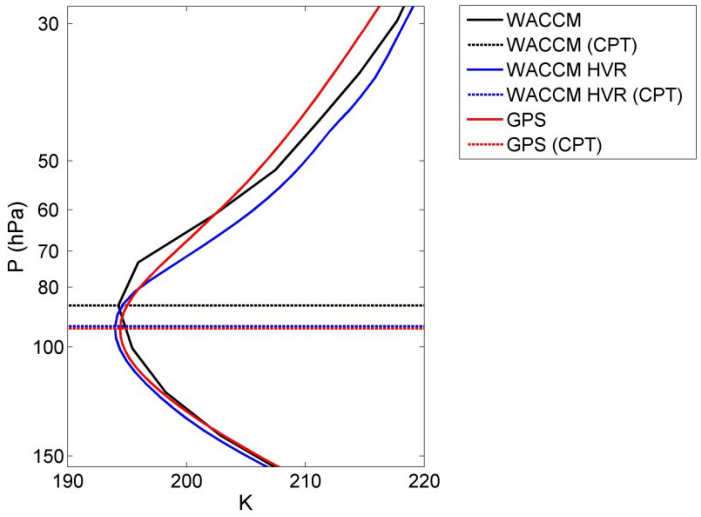


**Figure 7.3.** Vertical structure of tropical annual mean temperature (averaged over 18°S-18°N) from COSMIC GPS observations (red lines) and two versions of WACCM, one with low vertical resolution (labeled WACCM, black lines) and the other one with high vertical resolution (labeled WACCM HVR, blue lines). The height of the cold point tropopause for each dataset is indicated by a horizontal dotted line (labeled CPT). The averaging periods are: 2004-2009 for WACCM data, 1999-2004 for WACCM HVR data and 2007-2010 for GPS data.

Increased vertical resolution in chemistry-climate models could also potentially help improve the characterization of the subtropical transport barriers. The current picture of transport represents the tropical lower stratosphere in partial isolation from the extratropics (e.g. Plumb 2002). The semi-permeable barriers that separate these two regions are known to fluctuate in time and space. In particular, the effective diffusivity calculations of Haynes and Shuckburgh (2000a) highlight a latitudinal swing of the subtropical barriers towards the summer hemisphere, as shown in the panel for 450 K (~20 km) in Fig. 7.4 (from that work). The low values of effective diffusivity in the tropics clearly distinguish this region from the extratropics, where mixing is significantly more frequent. In this Thesis, a seasonal displacement of the mixing barriers is obtained from tracer eddy

transport calculations using the TEM formalism, similar to that obtained by Haynes and Shuckburgh (2000a) (e.g. Fig. 7.1). One key result of this Thesis is that just a few kilometers below, near the cold point tropopause, eddy transport has different seasonal characteristics. In particular, there is more transport within the tropics than at higher levels throughout the year, and the Asian monsoon stands out as a dominant feature producing large-scale mixing in boreal summer (Fig. 9 in Abalos et al. 2013a). An equivalent transition is observed in the results of Haynes and Shuckburgh (2000a, b). The bottom panel of Figure 7.4 shows effective diffusivity at a lower level (370 K, corresponding roughly to ~16 km). In contrast with the higher level, there is high diffusivity across the tropics, with a clear enhancement of mixing in the summer subtropics, likely related to eddy transport from the monsoon circulations. Increasing the vertical resolution in models could help better characterize these characteristics of mixing and the impact on different tracers. Nevertheless, it is important to keep in mind that increasing vertical resolution will not provide any benefit if the underlying processes are not correctly represented in the models.

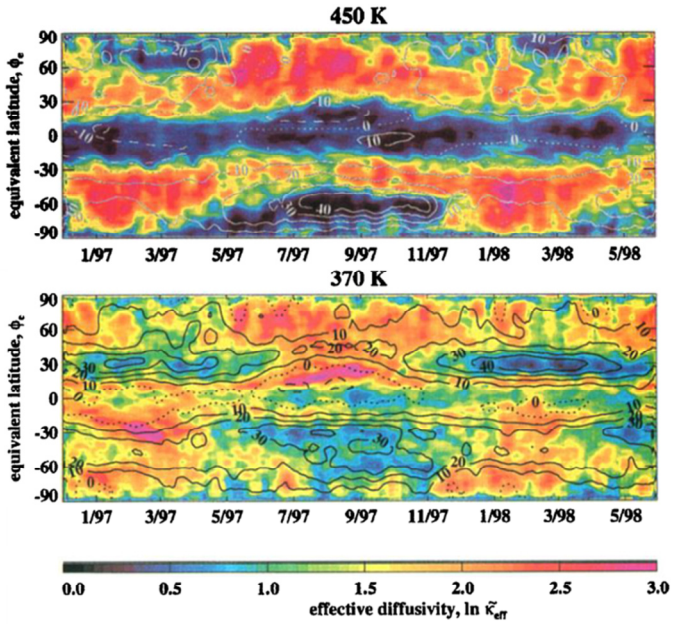


**Figure 7.4**. Effective diffusivity (shading) as a function of latitude and

month computed by Haynes et al. (2000a, upper panel, corresponding to 450 K) and (2000b, lower panel, corresponding to 370 K). The sharp transition in mixing seasonal characteristics across a relatively thin vertical layer is evident, consistently with the results obtained in this Thesis from TEM eddy transport calculations. The contours indicate zonal mean wind in $m \cdot s^{-1}$.

It has been discussed that upwelling estimates provide reasonable approximations to the variability of the real atmosphere, given the good agreement among them and the coherent fluctuations with independent satellite observations (especially for the indirect estimates). From this standpoint, the momentum balance estimate is used in this Thesis to explore the specific dynamical forcing regions driving sub-seasonal fluctuations in upwelling. Theoretical calculations show that transient wave drag drives a global coupled response of the atmosphere, involving remote effects on the zonal mean winds. These dynamical mechanisms have been explored using 33 years of ERA-Interim reanalysis data. The results highlight two main regions of forcing relevant for upwelling transient fluctuations, both associated with wave activity of extratropical origin. Waves propagating deep into the winter extratropical stratosphere and dissipating at high levels (~10 hPa) mainly drive transient upwelling in the so-called deep branch of the Brewer-Dobson circulation. Waves bending towards the equator and dissipating in the subtropical upper troposphere and lower stratosphere are mainly associated with the variability in the shallow branch of the circulation, which is limited to levels below approximately ~70-50 hPa.

The global dynamical patterns obtained in this Thesis demonstrate the important effect of remotely induced transient zonal wind tendencies for communicating the remote wave drag to the low latitudes. From a diagnostic point of view, away from the region of strong wave drag the zonal mean wind response can significantly influence the *net forcing* of upwelling. This result complements the mechanism recently proposed by Ueyama et al. (2013) for the influence of high-latitude wave drag on tropical upwelling. They highlighted a progression of the extratropical

forcing towards low latitudes on timescales of ~10 days. Our analyses show that the nonlocal transient response in the wind travels together with the forcing, on its equatorward flank, directly contributing to upwelling variability. It is important to keep in mind that this remote response in the zonal wind is not a forcing of upwelling itself, but constitutes part of the coupled atmospheric response to the forcing (i.e. the wave drag), in balance with the thermal changes induced by the meridional circulation. However, from the point of view of the upwelling calculations based on momentum balance (Eq. 17), this response has the effect of modifying the effective forcing on upwelling. Also, note that this transient remote connection between extra-tropics and tropics does not hold for the stationary case, since $\overline{u}_t$ is zero in the time mean.

Grise et al. (2013) observed that transient wave drag in the subtropical upper troposphere is related to an increase in temperature in the tropical lower stratosphere just above the tropical tropopause. This second type of remote influence has been confirmed in this Thesis, by direct examination of upwelling (which drives the temperature variations). In addition, the dynamical mechanism for the remote influence of subtropical wave drag on lower stratosphere upwelling has been analyzed, and the results highlight a primary role of the transient zonal wind response, which extends to levels above the forcing. These results contribute to advance in the understanding of dynamical forcing of upwelling variability making use of state-of-the-art reanalysis data (Abalos et al. submitted).

# 8. Conclusions

The main conclusions from this Ph.D. Thesis are:

- **Three different calculations of upwelling show reasonable agreement in the tropical lower stratosphere, validating the suitability of these estimates for investigating 1) the links with tracer variability and 2) the dynamical drivers of upwelling.**

  These quasi-observational estimates of upwelling are computed independently from ERA-Interim reanalysis data, including the reanalysis residual velocity and two indirect estimates based on momentum and thermodynamic balances. The resulting time series show coherent variability on seasonal and sub-seasonal timescales, with linear correlations near ~0.7. Tropical upwelling directly derived from the reanalysis is less correlated with the other two estimates, and its magnitude is overestimated at 100 hPa.

- **Time series of temperature, ozone and carbon monoxide (CO) are highly correlated across the tropical tropopause and in the tropical lower stratosphere, both on seasonal and sub-seasonal timescales.**

  This result, based on tracer satellite measurements from the Microwave Limb Sounder (MLS) instrument onboard the Aura satellite combined with ERA-Interim temperatures, motivates exploring the role of upwelling in driving the common variability.

- **The analysis of the Transformed Eulerian Mean (TEM) budgets demonstrates that tropical upwelling plays a primary role in driving the observed seasonal and sub-seasonal variability in temperature and tracer concentrations (ozone and CO) in the tropical lower**

**stratosphere. This result is obtained for observations and further confirmed using a free-running simulation with the Whole Atmosphere Community Climate Model (WACCM).**

Explicitly computing the terms in the TEM thermodynamic and tracer continuity equations allows evaluating the contribution of upwelling to the observed variability in temperature and tracers. In particular, the model analyses allow closing the balance (i.e. obtaining near zero residuals), and thus comparing the contribution from different terms. WACCM results support the observational results, and provide additional information on other transport terms unresolved in the observations. The ability of the model to accurately represent the main features of the tropical lower stratosphere was evaluated before performing the analyses.

- **Quasi-horizontal eddy transport associated with the Asian monsoon anticyclonic circulation makes an important contribution to ozone summer maximum close to the tropopause. In contrast, tracer eddy transport in the tropical lower stratosphere is linked to transient Rossby wave breaking in the winter and spring subtropics.**

  This sharp change in the seasonality of eddy horizontal (or isentropic) transport with height from near the tropopause (~16.5 km) to a few kilometers above in the lower stratosphere (~18.5 km) has been identified in WACCM data, despite the relatively low vertical resolution of the model (~1.1-1.4 km). The role of horizontal transport is not as large for CO as it is for ozone, because the meridional gradients in CO concentrations between the tropics and the extratropics near the tropopause are smaller (whereas relative vertical gradients are comparable).

- **On isentropic coordinates the effect of upwelling variability on tracers is largely reduced on both seasonal and sub-seasonal**

**timescales as compared to that on log-pressure altitudes, because upwelling drives vertical displacements of the isentropes. On these coordinates horizontal transport mainly drives the remaining sub-seasonal fluctuations in the tracers.**

The relatively large fraction of tracer variability in common with temperature (which is in turn mainly controlled by upwelling) is removed on isentropic coordinates, and the remaining fluctuations are mostly associated with isentropic transport. This is particularly relevant for the annual cycle in ozone, which amplitude is reduced up to ~60% on isentropic coordinates as compared to log-pressure altitudes. The amplitude reduction is larger where the tracer-upwelling correlations are larger, and as a result the vertical structure of the annual cycle is different on isentropes.

- **Lagrangian model results expressed from an Eulerian perspective are consistent with TEM calculations, showing similar transport processes leading to the observed ozone seasonality near and above the tropical tropopause.**

  Apparently contradictory results in the literature are reconciled by comparing the results from a simple one-dimensional Lagrangian model with the TEM results computed from WACCM output. While the TEM analysis considers the budget in each level separately, the Lagrangian perspective provides an integrated view of transport. This fundamental difference must be accounted for in order to accurately compare the results.

- **Sub-seasonal variability in upwelling in lower stratosphere is linked to wave drag in two main centers of action: the extratropical winter stratosphere and the subtropical upper troposphere of both hemispheres.**

These dynamical patterns reflect different forcing regions of the shallow versus deep branches of the Brewer-Dobson circulation. Both centers are mainly associated with waves propagating from the extratropical troposphere. Enhanced planetary wave activity in the extratropical winter stratosphere leads to enhanced upwelling, while wave drag in the subtropics below the tropopause drives transient events of weakened upwelling.

- **The nonlocal transient response of the zonal mean wind to the wave drag is important for remotely communicating the forcing to the tropical lower stratosphere, where it impacts upwelling variability.**

  There is a global coupled response of the mean circulation to an applied wave drag, and this includes remotely induced zonal wind tendencies, which can play an important role by extending the net forcing of upwelling outside the regions of strong wave drag. This effect is observed to communicate the drag in the extratropics with the low latitudes, and also it is found to play a central role in the remote influence that the wave drag at levels below the tropopause exerts on upwelling variability.

# 9. Future work

The results obtained in this Thesis put forward several open questions and call for further research on some issues. Interesting topics to be explored in future works include:

1) **Quantifying inter-annual variability in tropical upwelling by comparing various estimates from different reanalyses.**

The overall good agreement between the time series of the indirect estimates of upwelling found in this Thesis encourages extending the analysis of upwelling variability to timescales longer than the annual cycle. This would allow evaluating how observationally-derived tropical upwelling responds to climate variability and determining the current degree of understanding of the long-term fluctuations by comparing the different estimates.

In addition, the current availability of several state-of-the-art reanalyses (e.g. ERA-Interim, JRA55, MERRA, NCEP-NCAR), providing long-record self-consistent meteorological data, constitutes a unique opportunity for performing an inter-comparison of the upwelling results among different data sets. By quantifying the uncertainties among the different reanalyses, this comparison would provide essential information on the current understanding of upwelling in the scientific community.

Regarding this topic, some of the key questions to address in future works are: Are the effects of ENSO, the QBO and volcanoes observed consistently in all the upwelling estimates? Are the upwelling responses to these long-term fluctuations similar in all reanalyses? Is the background internal climate variability coherent among the estimates and among the reanalyses? Does upwelling reflect long-term changes such as decadal variability? Is there any consistent trend in the estimates?

Furthermore, comparison with independent satellite observations of tracers and temperature could provide an excellent test for the quality of

the upwelling estimates in the reanalyses, allowing the identification of major problems in the representation of the stratospheric circulation in the reanalyses.

2) **Investigating the detailed vertical structure and possible long-term changes of tracer eddy transport.**

In this Thesis, a transition in the characteristics of quasi-horizontal or isentropic transport with height has been observed across the tropical lower stratosphere. In particular, there is a detailed vertical structure in eddy transport processes, with large isentropic mixing associated with the Asian monsoon observed close to the tropopause but absent just a few kilometers above. This transition could be analyzed in model simulations with higher vertical resolution, in order to better constrain the fine vertical structure and advance in understanding the effects of eddy transport on tracer concentrations in the upper troposphere and lower stratosphere.

Higher vertical resolution model simulations could also provide more accurate information on the vertical structure of the other transport terms and their relative influence on tracer seasonality at different levels. Moreover, the spatial structure of tracer eddy transport and mixing could be altered in response to modifications of the background winds such as those associated with climate change. Eddy transport in the tropical lower stratosphere takes place on the upper flank of the subtropical jets, associated with Rossby wave breaking in this region. It has been shown that increased GHG emissions lead to a modification of the subtropical jets, and consequently to an adjustment of the levels of wave breaking.

The question that follows is how do these changes in the critical lines affect tracer eddy transport? In other words, will mixing properties influencing tracer concentrations in the tropical lower stratosphere be modified due to climate change? Could these changes potentially influence the exchange of air between troposphere and stratosphere? Do long-term satellite observations show evidences of any change in lower stratosphere or upper troposphere tracer concentrations?

**3) Exploring the origin of the deep versus shallow wave propagation in relation to upwelling extremes.**

It has been seen in this Thesis that waves propagating from the extratropical troposphere impact the sub-seasonal variability in tropical upwelling, and these waves follow two different paths, either traveling upward into the deeper stratosphere or bending towards the equator. However, it has been shown that, in terms of transient variability, these two regions of wave drag have opposite effects on upwelling in the tropical lower stratosphere. Hence, it is important to understand the specific conditions that determine the direction of propagation of the waves. For this, it is useful to decompose the waves acting in the extratropical stratosphere and in the subtropical upper troposphere as a function of wavenumber, previously separating stationary from transient oscillations. Doing this spectral analysis for high and low upwelling extreme events will allow answering questions such as: Are the waves in the subtropics mostly synoptic-scale eddies? What causes stronger wave drag in the subtropics during low upwelling events? Are synoptic disturbances enhanced during these extremes? Does planetary-scale wave activity in the subtropics increase when deep propagation is reduced? Are upwelling extremes associated with changes in the waves or in the background structure?

On the other hand, it has been shown in this Thesis that wave drag in different regions affects the shallow and deep branches of the Brewer-Dobson circulation differently. Further analyses could be done to understand the gradual transition between these two branches, in relation with the specific wave forcing. Extending these analyses to long-term variability, further questions can be posed: Do the deep and shallow branches of the circulation vary independently? Which waves determine the variability of each branch on long timescales? Are the composites for high and low upwelling cases similar for inter-annual changes?

# 10. Summary

This chapter presents a Summary of the present Ph.D. Thesis, including the state-of-the-art of the subject under study, the motivation for the research carried out, the objectives, the most important results and the main conclusions.

## 1 State-of-the-art and motivation

Tropospheric air masses enter the stratosphere[1] primarily across the tropical tropopause, transported by the upwelling branch of the Brewer-Dobson circulation, which is completed by poleward drift and downwelling over the high latitudes (Brewer 1949, Dobson 1956). Consequently, **tracer concentrations near the tropical tropopause constitute the boundary condition for the chemical composition of the entire stratosphere**, affecting radiative forcing of surface climate (e.g. Fueglistaler et al. 2009a, Riese et al. 2012). Because dynamics, radiation and chemistry are closely coupled in this relatively small region, it is particularly challenging for chemistry-climate models to accurately represent the various processes affecting tracer distribution (e.g. Gettelman et al. 2010, Randel and Jensen 2013). **The structure and variability of constituents in the tropical lower stratosphere are determined mainly by transport processes**, along with chemical sources and sinks. The most important transport mechanisms in this region are large-scale vertical advection by tropical upwelling and quasi-horizontal eddy transport[2]. There are **no direct measurements of vertical velocities in this region, and they need to be inferred indirectly** (e.g. Randel et al. 2008). Estimates in the literature, based either on tracer

[1] Stratosphere: atmospheric layer above the troposphere located approximately between ~10 km and ~50 km and characterized by stable static stratification.
[2] Eddy transport: transport component associated with the zonal anomalies in tracer concentrations. In the Transformed Eulerian Mean formalism this transport is distinguished from mean advection due to the residual circulation.

measurements or dynamical constraints, reveal positive tropical mean vertical velocities throughout the year, featuring a large annual cycle with more intense ascents in boreal winter than summer (e.g. Rosenlof 1995).

Partly as a consequence of the lack of observations, **the specific forcing of variability in tropical upwelling intensity is poorly understood**. The wave-driven nature of the Brewer-Dobson is well-known, and the Transformed Eulerian Mean (TEM) equations provide an advantageous framework for recognizing the dynamical origin of such circulation, denoted *residual* in this formalism (e.g. Andrews et al. 1987). In short, the drag exerted on the background flow by Rossby wave breaking in combination with the Coriolis force produces a poleward mass flow in the extratropical stratosphere, and vertical motion is induced by continuity at the boundaries of the forcing region. However, the current theoretical framework cannot account for tropical annual mean upwelling as inferred from observations (e.g. Plumb and Eluskiewicz 1999). Moreover, significant efforts have been dedicated to disentangle which waves are mainly responsible for the annual cycle in upwelling. Winter planetary wave propagation and breaking is stronger in the NH than in the SH extratropical stratosphere, and this constitutes a first-order explanation for the seasonality in upwelling (e.g. Yulaeva et al. 1994). However, further investigation has highlighted the essential role of other wave forcing in driving the seasonality, including equatorial planetary waves and synoptic baroclinic disturbances in the subtropics (e.g. Bohem and Lee 2003, Norton 2006, Randel et al. 2008, Ueyama and Wallace 2010, Ortland and Alexander 2013). The problem of identifying the specific sources of upwelling variability on sub-seasonal timescales has received attention in recent works (Grise and Thompson 2013, Ueyama et al. 2013). **Understanding the dynamical drivers of upwelling variability on a wide range of timescales is crucial for improving the representation of trace gas transport in Chemistry-Climate models**.

Across the tropical tropopause and in the tropical lower stratosphere, several tracers (such as ozone and carbon monoxide, CO) present sharp vertical gradients. This is also true for potential temperature,

as indicated by the maximum static stability observed just above the tropical tropopause (e.g. Grise et al. 2010). Hence, the effect of upwelling fluctuations on such tracers and temperature is enhanced in this region. Observations reveal a large annual cycle in temperature over a narrow layer just above the tropical tropopause (Reed and Vicek 1969). It has been shown that the cycle in temperature is mainly forced by the upwelling seasonality, with stronger ascents in boreal winter than summer carrying cold air masses from near the cold point tropopause (Yulaeva et al. 1994, Fueglistaler et al. 2011). Using satellite and balloon-borne measurements, Randel et al. (2007) observed large annual cycles in ozone and CO concentrations on a narrow layer above the tropical tropopause, with vertical structures similar to that in the temperature cycle. Randel et al. (2007) further showed that the vertical structure and the phase of the **annual cycles in the tracers can be explained by the seasonality in tropical upwelling acting on the strong background vertical gradients**. In contrast, complementary analyses using a Lagrangian transport model reached a different conclusion. In particular, these works suggested that the large **annual cycle in ozone is mainly caused by horizontal transport** of extratropical ozone into the tropics **by the Asian summer monsoon** upper-level anticyclone (Konopka et al. 2009, 2010, Ploeger et al. 2012). **These contrasting viewpoints call for further research, and this issue has been addressed as part of the analyses carried out in this Thesis**.

**Observations of temperature and tracers near the tropical tropopause show a high degree of common variability**. Figure 1S shows time series of tropical mean temperature from reanalysis (ERA-Interim[3]), together with ozone and CO satellite observations, at three pressure levels across the tropical tropopause for the period 2005-2010. **The co-variability among the series is especially evident for the large annual cycles but is also observed on sub-seasonal timescales**.

[3] Acronym of the ECMWF (European Centre of Medium-Range Weather Forecasts) Interim Re-Analysis.

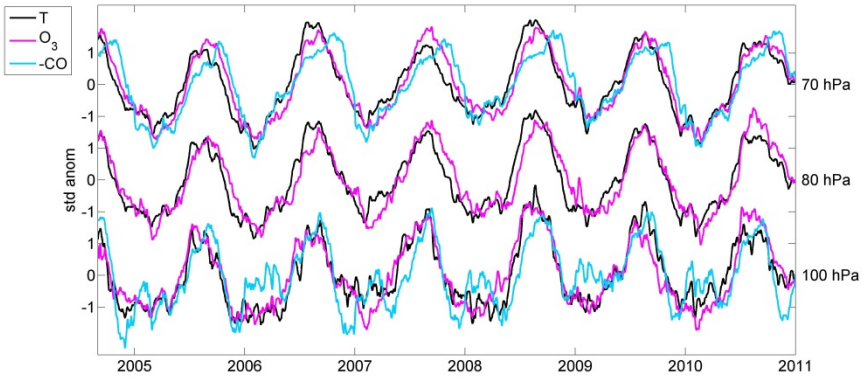


**Figure 1S**. Time series of standardized anomalies of temperature, ozone and CO observations averaged over 20°N-20°S at three pressure levels across the tropical tropopause for 2005-2010. Temperatures are from ERA-Interim, tracer measurements from the Micowave Limb Sounder (MLS) satellite instrument onboard the Aura satellite of NASA (Waters et al. 2006). CO time series are shown on an inverted scale to highlight the common variability.

The observations in Fig. 1 prompt the question of what drives the common fluctuations, and more specifically, **what is the role of tropical upwelling in driving the observed co-variability in temperature and tracers?** These questions constitute the starting point for the present Thesis.

# 2 Objectives

In the context summarized above, the primary objective of this Thesis is **to investigate upwelling in the tropical lower stratosphere, including the variability on different timescales, the impact on temperature and tracer concentrations in this region, and the specific sources of variability**. This general goal has been divided into four specific objectives, which are:

1. **To quantify tropical upwelling and its uncertainty across the tropical tropopause by computing three independent estimates.**

The upwelling estimates include residual velocity from the reanalysis as well as indirect estimates from TEM momentum and thermodynamic balances, and the calculations are based on ERA-Interim reanalysis (Dee et al. 2011).

2. **To investigate the links between upwelling and temperature/tracers variability in the tropical lower stratosphere.**

This objective is carried out first with observational data (tracer satellite measurements plus the upwelling estimates described above) and then with a model simulation of the Whole Atmosphere Community Climate Model, version 4 (WACCM4, Garcia et al. 2007). Both observational and model analyses are based on the TEM formulation of the thermodynamic and the tracer continuity equations, and are focused on seasonal and sub-seasonal timescales.

3. **To evaluate the effects of other transport mechanisms on tracer concentrations in the tropical lower stratosphere.**

The contribution of other processes (besides upwelling) contributing to drive tracer variability is examined by explicitly evaluating all the transport terms in the TEM tracer budgets from WACCM output. These chemistry-climate model results are further compared with those of a conceptual one-dimensional Lagrangian transport model. The comparison between these two very different models provides a comprehensive understanding of tracer transport processes in this region.

4. **To explore the specific dynamical forcing of tropical upwelling variability on sub-seasonal timescales.**

For this, sub-seasonal fluctuations in the upwelling estimate inferred from momentum balance (Objective 1) are projected onto the forcing field. ERA-

Interim daily data for 1979-2011 is used for this Objective, and sub-seasonal variability is isolated by applying spectral filters to the time series.

# 3 Main results and conclusions

The Results Chapter of the Thesis is organized as a collection of four articles written during the Thesis:

1. - *Variability in upwelling across the tropical tropopause and correlations with tracers in the lower stratosphere.* Abalos, M., Randel, W. J. and Serrano, E., Atmos. Chem. Phys., 12, 11505–11517, doi:10.5194/acp-12-11505-2012, 2012.
2. - *Quantifying tracer transport in the tropical lower stratosphere using WACCM*. Abalos, M., Randel, W. J., Kinnison, D. E., and Serrano, E., Atmos. Chem. Phys., 13, 10591-10607, doi:10.5194/acp-13-10591-2013, 2013a.
3. - *Ozone seasonality above the tropical tropopause: reconciling the Eulerian and Lagrangian perspectives of transport processes*. Abalos, M., Ploeger, F., Konopka, P., Randel, W. J. and Serrano, E, Atmos. Chem. Phys. Discuss., 13, 19291–19310, doi:10.5194/acpd-13-19291-2013, 2013b.
4. - *Dynamical forcing of sub-seasonal variability in the tropical Brewer-Dobson circulation*. Abalos, M., Randel, W. J. and Serrano, E., submitted to J. Atmos, Sci.

In this Summary, instead, the most important results are presented following the Objectives listed above. The main conclusions of this Thesis are reported at the end.

## • Objective 1

*To quantify tropical upwelling and its uncertainty across the tropical tropopause by computing three independent estimates.*

Time series of the three semi-observational estimates of tropical upwelling computed for this objective are shown in Figure 2S at the same three pressure levels across the tropical tropopause shown in Fig. 1S. It is important to highlight the uncertainties associated with each of the estimates.

The first estimate is the vertical component of the residual circulation ($\overline{w}^*$), which is mainly a function of the reanalysis zonal mean vertical velocity ($\overline{w}$). Although a number of works have highlighted the improvement in the representation of vertical transport ($\overline{w}$) in ERA-Interim as compared to its predecessor ERA-40, there are still large uncertainties in this magnitude (e.g. Dee et al. 2011 and references therein). The residual velocity is given by:

$$\overline{w}^* \equiv \overline{w} + \frac{1}{a\cos\phi}\left(\cos\phi \frac{\overline{v'T'}}{S}\right)_\phi \qquad (1S)$$

where $\phi$ is the latitude, subscripts indicate partial derivatives, over-bars indicate zonal mean fields and primes are deviations from them (or eddies), $a$ is the Earth radius, $S = HN^2/R$, with $N$ the Brunt-Väissälä frequency, $R$ the gas constant of the dry air and $H$ a constant scale height (Andrews et al. 1987).

A second estimate is obtained combining the TEM momentum balance and mass continuity equations, which gives the following expression for the tropical mean upwelling $\left\langle \overline{w}_m^* \right\rangle$ (Randel et al. 2002):

$$\left\langle \overline{w}_m^* \right\rangle (z) = \frac{-e^{z/H}\cos\phi}{\int_{-\phi_0}^{\phi_0} a\cos\phi d\phi} \left\{ \int_z^\infty \frac{e^{-z'/H}}{\hat{f}(\phi, z')} \left[ DF(\phi, z') - \overline{u}_t(\phi, z') \right]_{\overline{m}} dz' \right\}_{-\phi_0}^{\phi_0} \qquad (2S)$$

where $DF = e^{z/H}\nabla \cdot \mathbf{F} / (a\cos\phi)$ is the Eliassen-Palm flux (EP flux) divergence scaled by density (considering of 1 $kg \cdot m^{-3}$ as the air density value at 1000 hPa), $\overline{u}_t$ is the zonal mean zonal wind tendency and $\hat{f} = f - (\overline{u}\cos\phi)_\phi / (a\cos\phi)$. Equation (2S) gives tropical upwelling at a given level $z$ averaged over a range of latitudes (18°S-18°N in this Thesis) as a function of the dynamical forcing integrated over all altitudes above that level $z$ and evaluated at the boundaries of the latitudinal interval $\pm\phi_0$. The EP flux divergence is a function of heat and momentum eddy fluxes, and these are computed using ERA-Interim data. The main source of uncertainty associated with this estimate $\left\langle \overline{w}^*_m \right\rangle$ is linked to the calculation of the EP flux divergence, because the small-scale waves are not resolved in the ERA-Interim model.

The last upwelling estimate ($\overline{w}^*_Q$) is obtained combining the TEM thermodynamic and mass continuity equations:

$$\overline{T}_t = -\overline{v}^*\overline{T}_y - \overline{w}^* S + \overline{Q} \tag{3S}$$

$$(a\cos\phi)^{-1}(\overline{v}^*\cos\phi)_\phi + e^{z/H}(e^{-z/H}\overline{w}^*)_z = 0 \tag{4S}$$

where $\left(\overline{v}^*, \overline{w}^*\right)$ are the components of the residual circulation and $\overline{Q}$ are the zonal mean radiative heating rates (which in the stratosphere are accurately approximated by the radiative heating rates alone). In this case, the main source of uncertainty is linked to $\overline{Q}$, which is computed using the NCAR-Column Radiation Model, an accurate radiative transfer model with input of ozone satellite observations and ERA-Interim temperatures. One caveat is that this model does not include the radiative effects of clouds, although this effect is likely not large on tropical mean heating rates in the lower stratosphere (Yang et al. 2010). Note that an eddy transport term has been neglected in Eq. (3S), and this is an additional possible source of error in the thermodynamic estimate.

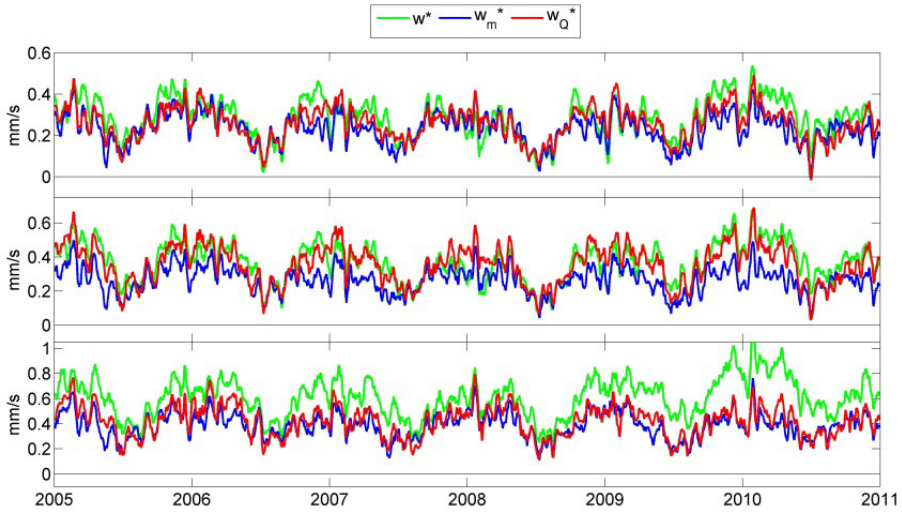


**Figure 2S**. Daily time series of upwelling computed in three different ways (see text for details) for the period 2005-2010 at the pressure levels of 70 hPa (upper panel), 80 hPa (middle panel) and 100 hPa (lower panel). Green: residual circulation. Blue: momentum balance estimate. Red: thermodynamic estimate. 11-points running means are applied to all series. Units: $mm \cdot s^{-1}$.

Despite these uncertainties, **the time series of upwelling** in Fig. 2S **agree reasonably well in the overall magnitude, seasonality and sub-seasonal variability.** The linear correlations among the three estimates at the levels shown in Fig. 2S lay around ~0.7. The strongest correlations in the tropical lower stratosphere are found between the two indirect estimates, computed from momentum and thermodynamic balances. There is less agreement with the residual circulation computed directly from ERA-Interim reanalysis, which is too intense particularly near the tropopause (~100 hPa), in agreement with previous results (e.g. Dee et al. 2011). The results of this objective are published in Abalos et al. (2012).

**The consistency among the independently inferred vertical velocities not only** increases the confidence in these calculations, but also **allows using them to analyze the links between the upwelling fluctuations seen** in Fig. 2S **and the variability in temperature and tracers**

observed in Fig. 1S**,** on both seasonal and sub-seasonal timescales. This analysis is carried out in the second objective.

## • Objective 2

*To investigate the links between upwelling and temperature/tracers variability in the tropical lower stratosphere.*

In order to investigate the influence of upwelling on temperature and tracers in the tropical lower stratosphere, the estimates in Fig. 2S have been combined with ERA-Interim temperatures and satellite measurements of ozone and CO from the MLS instrument. The analyses involve evaluating the terms in the TEM thermodynamic balance (Eq. 3S) and the continuity equation for tracer concentration:

$$\overline{\chi}_t = -\frac{\overline{v}^*}{a}\overline{\chi}_\phi - \overline{w}^*\overline{\chi}_z + e^{z/H}\nabla\cdot\mathbf{M} + P - L \qquad (5S)$$

where $\overline{\chi}$ is the zonal mean tracer concentration, $\overline{w}^*$ represents any of the upwelling estimates, $e^{z/H}\nabla\cdot\boldsymbol{M}$ is the eddy transport term and $P-L$ represents the net tendency due to phochemical reactions (that is, production minus loss rates). Figure 3S shows the resulting observationally-derived monthly evolution of the different terms in thermodynamic balance (Eq. 3S, Fig. 3Sa), together with the ozone (Fig. 3Sb) and CO (Fig. 3Sc) budgets (Eq. 5S), at one level just above the tropical tropopause (i.e. 70 hPa).

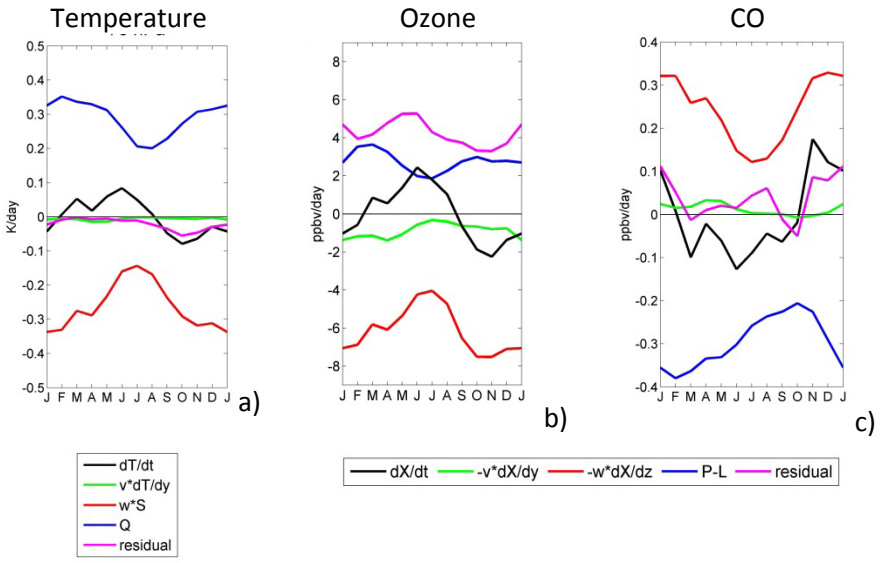


**Figure 3S**. Monthly mean evolution of the terms in the TEM budgets at 70 hPa computed from tracer satellite observations and reanalysis data averaged over (18°S-18°N). The curves represent the different terms in the a) thermodynamic equation (Eq. 3S), b) ozone and c) CO continuity TEM equations (Eq. 5S). Black: tendency of temperature (in a) or tracer (in b and c). Red: Vertical advection by upwelling. Green: meridional advection. Blue: diabatic heating in a), chemical production minus loss in b) and c). Magenta: residuals due to uncertainties in all the terms and also to tracer eddy transport in b) and c). Average over the period 2005-2010.

The thermodynamic balance (Fig. 3Sa) shows that **the annual cycle in adiabatic cooling by tropical upwelling mainly drives the seasonality in temperature** (more intense upwelling of cold air from the tropopause in boreal winter as compared to summer), in agreement with previous works. Radiative heating compensates adiabatic cooling in the annual mean. The ozone and CO budgets (Figs. 3Sb y 3Sc, respectively) share some features. In particular, there is a large annual cycle in the vertical advection by upwelling, which is mirrored by the tracer tendency, indicating that **the seasonality in both tracers is mainly driven by tropical upwelling acting on the strong background vertical gradients**. In the annual mean, CO photochemical destruction balances the increase due to upwelling (Fig. 3Sc). **In the case of ozone**, photochemical production alone is not able to

balance the decrease by upwelling, and **there is a relatively large residual in the balance** (Fig. 3Sb). **This residual** is partly due to uncertainties in all the terms, but it also **includes the eddy transport term** in the TEM continuity equation (Eq. 3S), **which is not explicitly resolved in these observational calculations** (due to the relatively coarse horizontal resolution), and might be important for ozone. The ozone photochemical production shows a weak semi-annual variation, linked to the apparent sun migration over the equator.

**In addition to the large annual cycles, the time series in Fig. 1S show common variability on sub-seasonal timescales**. This is further evidenced in Figure 4S (top series), which shows the time series of temperature, ozone and CO tendencies filtered to remove the annual cycle and longer timescales.

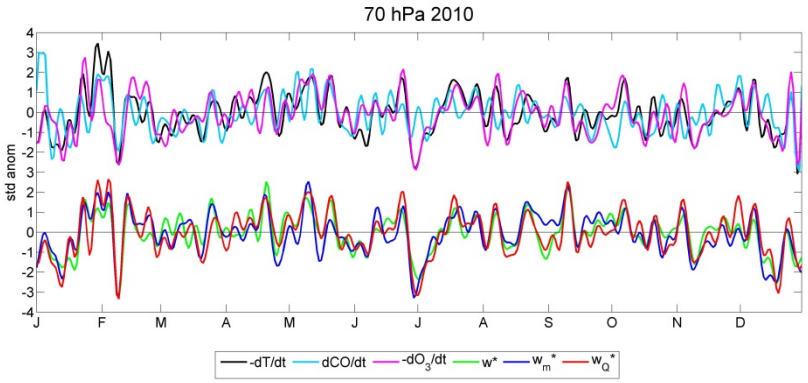


**Figure 4S**. Filtered time series of temperature (black), ozone (magenta) and CO (cyan) tendencies (top) together with upwelling estimates (bottom) for one year (2010) at 70 hPa. The different upwelling estimates are shown in the same colors as in Fig. 2S. The spectral filter is applied to isolate the timescales shorter than the annual cycle (and also timescales longer than 6 days are removed).

The bottom series in Fig. 4S show the estimates of upwelling filtered in the same way. It can be seen that **there are common week-to-week fluctuations between the upwelling estimates and the completely**

**independent tracer satellite observations**. The statistically significant correlations obtained among these series (not shown) demonstrate that **upwelling makes an important contribution in driving the observed variability in temperature and tracers on sub-seasonal timescales above the tropopause**, consistently with the results for the annual cycle. These results are included in Abalos et al. (2012).

To this point, it has been shown that upwelling plays an important role in driving variability in temperature and tracers, both for the seasonal cycle and on sub-seasonal timescales. However, the tracer budgets in Fig. 3S include non-negligible residuals, and in particular there is a relatively large imbalance for ozone (Fig. 3Sb), which could imply that some processes are misrepresented. In order to close the tracer balances (i.e., obtain near-zero residuals), all the terms in the continuity equation (Eq. 5S) must be explicitly evaluated. Because this cannot be accurately done with the observations, output from a model simulation with WACCM4 has been used to complement these results. **WACCM output allows explicitly resolving all the terms in the tracer continuity equation and hence closing the budgets**.

As a previous step to evaluating the balances with WACCM data, the ability of the model to reproduce the main characteristics of the tracer and thermal structure and variability in the region of interest was tested. A slight shift in the height of the tropopause was identified in WACCM output, which is located ~1 km higher than the observations. To illustrate this, Figure 5S shows the vertical structure of tropical mean annual mean temperatures for WACCM data and GPS observations. The cold point tropopause height is identified as the point with the lowest temperature in these profiles (marked by horizontal lines in Fig. 5S). Note that the difference in tropopause location could be due to the limited vertical resolution of the model (1-1.4 km).

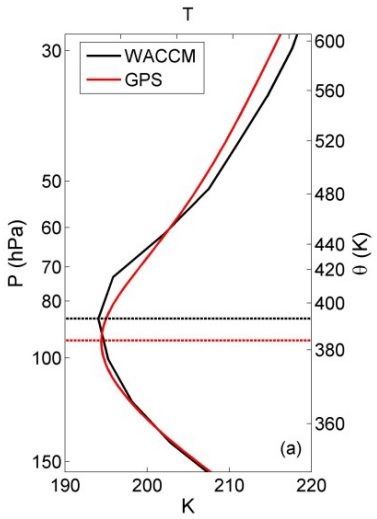


**Figure 5S**. Vertical profile of annual mean temperature in WACCM (black, 2004-2009) and in GPS observations (red, 2006-2011) averaged over 18°S-18°N (WACCM) or over 20°S-20°N (GPS). Horizontal lines indicate the cold point tropopause height. Vertical scale on the right axis shows the height of several potential temperature levels for the annual mean over the same period in WACCM.

In order to account for this difference in tropopause height, the budgets are evaluated on higher log-pressure altitudes in the model than in the observations (for instance the level of 62 hPa WACCM is compared to 70 hPa in the observations). The thermodynamic, ozone and CO balances computed with WACCM at 62 hPa are shown in Fig. 6S.

**Near-zero residuals** are observed in Fig. 6S, implying that the balances are closed in the model. Moreover, **the balances are overall similar to the observational results** (Fig. 3S), confirming the findings based on that data. In particular, **the large annual cycle in ozone tendency closely follows the seasonality in the upwelling term**. The negative tendency due to upwelling is balanced in the annual mean by ozone increase due to net photochemical production plus horizontal transport (which is mainly associated with eddy transport). **This confirms the hypothesis that the large residual in Fig. 3Sb is mainly due to the eddy transport term, unresolved in the observations**. Thus, the analysis with WACCM data supports the results obtained for the observations.

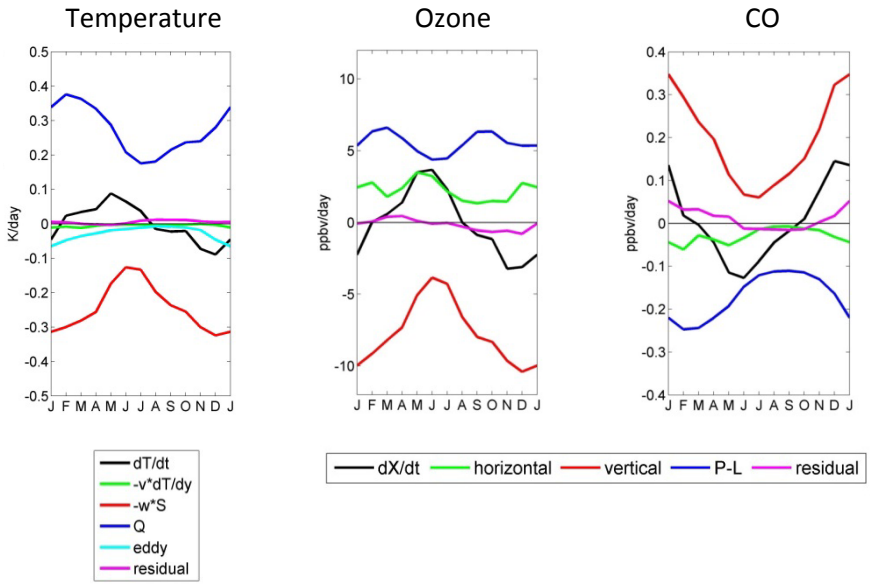


**Figure 6S**. Monthly mean evolution of the terms in the TEM budgets at 62 hPa computed from WACCM data averaged over (18°S-18°N). The curves represent the different terms in the a) thermodynamic equation (Eq. 3S), b) ozone and c) CO continuity TEM equation (Eq. 5S). The transport terms in Eq. (5S) are re-organized for simplicity in horizontal and vertical components of transport. Black: temperature (in a) or tracer (in b and c) tendency. Green: meridional temperature advection in a, meridional transport in b and c (mainly associated with eddy transport). Red: vertical temperature advection in a, vertical transport (mainly associated with upwelling) in b and c. Blue: Radiative heating in a, photochemical production minus loss in b and c. Cyan line in a shows the eddy term in the thermodynamic equation (neglected in Eq. 3S). Magenta: residual due to uncertainties in all the other terms. Average over the period 2004-2009.

## • Objective 3

*To evaluate the effects of other transport mechanisms on tracer concentrations in the tropical lower stratosphere.*

The thermodynamic and tracer budgets in Figures 3S and 6S highlight the annual cycle in tropical upwelling as the main responsible for driving the seasonality in temperature and tracers in the tropical lower

stratosphere. In particular, Fig. 6Sb shows the large annual cycle in ozone tendency closely following upwelling, while horizontal transport shows very little seasonality in the tropical lower stratosphere. Figure 7S shows WACCM results for the ozone balance at 62 hPa (as in Fig. 6Sb) and at two lower pressure levels, including the cold point tropopause (86 hPa in this WACCM simulation).

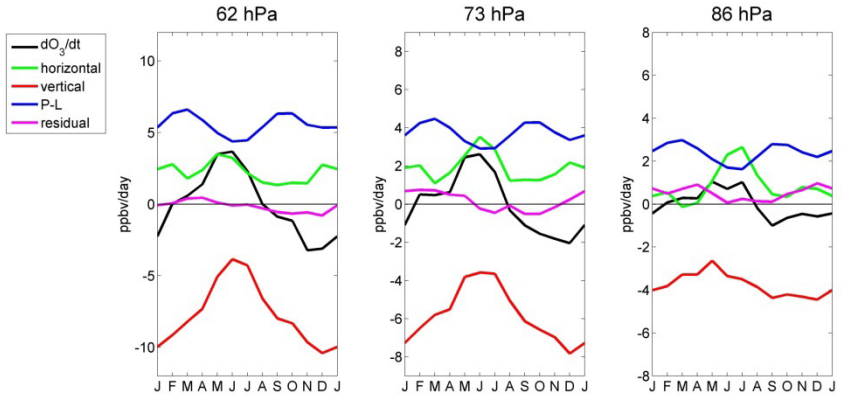


**Figure 7S**. Monthly mean evolution of the terms in the ozone TEM budget at three pressure levels across the tropical tropopause computed from WACCM data averaged over (18°S-18°N). The transport terms in Eq. (5S) are re-organized for simplicity in horizontal and vertical components of transport. Black: ozone tendency. Green: meridional transport (mainly associated with eddy transport). Red: vertical transport (mainly linked to vertical advection by upwelling). Blue: photochemical net tendency (production minus loss). Magenta: residual. Averages are computed over the years 2004-2009. The cold point tropopause is located at 86 hPa in this simulation.

There is a clear transition with height in the balances in Figure 7S, with a largely reduced amplitude of the ozone tendency and the upwelling terms annual cycles at the lowest level (near the tropopause) as compared to the higher levels. In addition, **horizontal transport exhibits a peak in boreal summer near the cold point tropopause**. This transition in the seasonality of quasi-horizontal transport with height is further evidenced in Figure 8S.

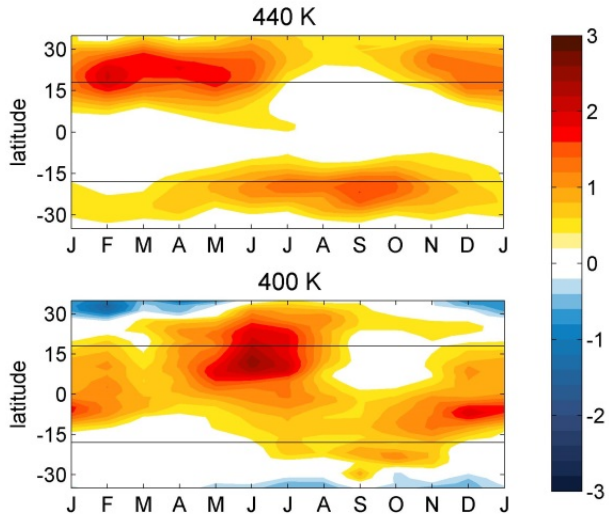


**Figure 8S**. Latitude-versus-month section of ozone tendency due to isentropic transport in WACCM (red values indicate increase in ozone) at two isentropic levels, 440 K (~62 hPa) and 400 K (~86 hPa). The magnitude is represented relative to the annual mean ozone concentration at each location. Averages are computed over the years 2004-2009. In $\% \cdot day^{-1}$.

Figure 8S shows the monthly mean evolution of ozone isentropic transport (mostly eddy transport) as a function of latitude at two isentropic levels which roughly correspond with the highest (62 hPa) and the lowest (86 hPa) levels in Figure 7S. The seasonality of quasi-horizontal ozone eddy transport is notably different between these two levels situated less than 3 km apart. **At the higher level** (440 K, top panel), **ozone eddy transport occurs mainly during winter and spring of each hemisphere**, and is associated with **transient Rossby wave breaking in the subtropics** (not shown). Conversely, **near the tropopause** (~400 K, bottom panel) eddy transport is observed within the tropics throughout the year, and there is a **large increase in tropical ozone in boreal summer,** which is **linked to horizontal transport by the Asian monsoon anticyclone**.

The detailed vertical structure of transport processes driving ozone variability as revealed by WACCM results is summarized in Figure 9S. In particular, this figure shows the vertical structure of the annual cycle

amplitude of all the terms in the ozone budget. In Fig. 9S, **tropical upwelling dominates the ozone seasonality in the lower stratosphere, while the annual cycle in horizontal transport is found** at lower levels, **near the tropopause**.

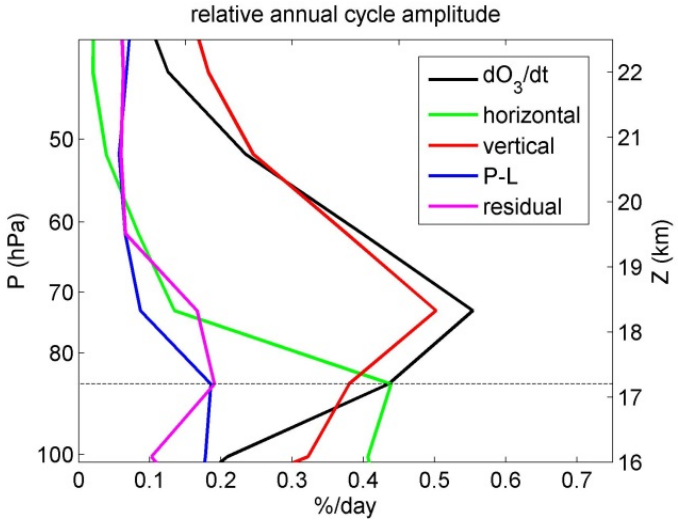


**Figure 9S**. Vertical structure of the annual cycle amplitude of all the terms in the ozone TEM balance computed from WACCM averaged over 18°S-18°N (same terms shown in Fig. 6S). Log-pressure heights are indicated on the right hand-side vertical axis. Terms are expressed relative to the annual mean concentration at each altitude (in $\% \cdot day^{-1}$).

In addition to the annual cycle, the role of different transport processes on ozone and CO variability has been studied on sub-seasonal timescales. **WACCM results highlight upwelling as the main driver of sub-seasonal fluctuations in the tracers**, at levels with strong background vertical gradients in the tropical lower stratosphere. Horizontal eddy transport is also important for week-to-week variability in ozone and CO (although less than upwelling). The results of the budget analyses using WACCM are published in Abalos et al. (2013a).

As briefly mentioned in Section 1 of this Summary, a group of recent works based on Lagrangian model calculations have suggested that the large annual cycle in ozone above the tropical tropopause is mainly caused

by enhanced horizontal transport linked to the Asian monsoon in boreal summer (e.g. Ploeger et al. 2012). This is in contrast with the results shown above, which evidence that the ozone seasonality is mostly driven by upwelling. In order to understand this apparent discrepancy, there are important differences between the analyses that must be taken into account carefully before comparing the results. First, the Lagrangian model calculations are based on isentropic coordinates. Konopka et al. (2009) pointed out that **the tropical ozone seasonality is largely reduced (up to around 60%) on isentropes relative to log-pressure altitudes**. This is because there is a large annual cycle in potential temperature in this region, which is almost in phase with ozone (Fig. 1S). As mentioned earlier, the seasonality in temperature is mainly driven by upwelling (e.g. Fig. 3Sa). Consequently, the effect of upwelling on ozone (and CO) seasonality is mostly removed on isentropes.

In addition to this fundamental difference between the analyses, i**t is crucial to take into account the distinct interpretation of the results obtained using a Lagrangian versus an Eulerian approach.** In order to accurately compare the TEM budgets results, the Lagrangian results have been transformed to an Eulerian representation in this Thesis[4]. Figure 9S shows the Eulerian ozone budget computed from output from a one-dimensional conceptual Lagrangian transport model (1D model in the following, Ploeger et al. 2012). This model computes one-dimensional cross-isentropic back-trajectories from levels in the tropical lower stratosphere. Changes in ozone concentrations along the trajectories are due to photochemical production and in-mixing from the extratropics, both given by the three-dimensional Chemistry Lagrangian Model of the Stratosphere (CLaMS, McKenna et al. 2002, Konopka et al. 2004).

[4] This calculation has been performed by Felix Ploeger from Jülich Forschungzentrum, Germany.

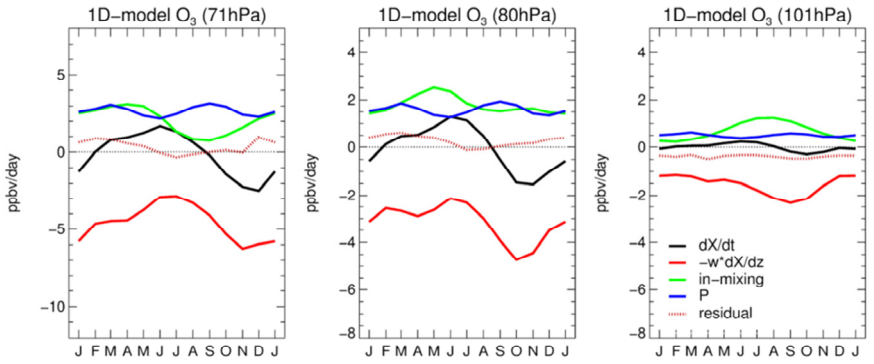


**Figure 10S**. Tropical mean (20°S-20°N) ozone budget derived from output of the one-dimensional Lagrangian model.

Remarkably, despite the profound differences between WACCM and the conceptual 1D-model (a chemistry-climate model versus a simplified one-dimensional model), the ozone balances show common characteristics (compare with Fig. 6S). In particular, in agreement with WACCM, **the Lagrangian results evaluated from an Eulerian perspective exhibit large annual cycles in upwelling, closely followed by the ozone tendency** in the tropical lower stratosphere. Moreover, **there is a change in horizontal transport seasonality with height similar to that observed in WACCM**, with strongest in-mixing in boreal summer observed at the tropopause level (located near 100 hPa in this model), while net horizontal transport is slightly larger in winter and spring at higher levels.

**The similarity between the ozone budgets in both models proves that WACCM and the Lagrangian model are in fact consistent**. The apparent discrepancy originates from the fact that Lagrangian results provide an integrated view of transport, while in the TEM budgets transport terms are evaluated exclusively each fixed level. For instance, air parcel trajectories in-mixed by the Asian monsoon anticyclone that subsequently ascend within the tropics count as horizontally transported in the Lagrangian perspective, but they represent vertical transport in the TEM budgets. Overall, the comparison with Lagrangian results reinforces the picture of transport deduced from WACCM. The results of the

comparison between Eulerian and Lagrangian models are published in Abalos et al. (2013b).

- ## Objective 4.

*To explore the specific dynamical forcing of tropical upwelling variability on sub-seasonal timescales.*

The last part of the Thesis aims to identify the main dynamical forcing mechanisms of sub-seasonal variability in upwelling. Figure 4S (Objective 2) shows common fluctuations on sub-seasonal timescales between the estimates of upwelling and the completely independent satellite tracer measurements. This coherence suggests that a significant fraction of the week-to-week fluctuations reflects variability in the real atmosphere. Hence, these time series can be used to identify the dynamical drivers of sub-seasonal fluctuations in upwelling. In particular, the momentum balance estimate ( $\overline{w}^*_m$ ) will be used, for being dynamically consistent. The analysis is based on projections of the forcing fields onto the time series of upwelling ( $\overline{w}^*_m$ ).

The integrand in Eq. (2S) is a function of $DF - \overline{u}_t$, which is referred to as *net forcing* in this Thesis. Thus, the net forcing of tropical upwelling is given by the combined of effect of the wave drag ( $DF$ , or EP flux divergence) plus the response in the zonal mean wind ( $\overline{u}_t$ ). Figure 11S shows the projection of these two contributions and the net forcing field onto upwelling for the extended winter season (DJFM) of the entire ERA-Interim record (1979-2011). Both the time series and the fields have been previously filtered to isolate sub-seasonal fluctuations (here timescales shorter than 90 days).

This analysis has revealed **two main centers of action of wave drag** $DF$ **relevant for upwelling: the extratropical winter stratosphere and the subtropics of both hemispheres** (Fig. 11Sa). **Corresponding patterns of induced deceleration and acceleration** ( $\overline{u}_t$ ) **are observed in the**

**extratropical stratosphere and the subtropics respectively** (Fig. 11Sb), co-located with the centers of $DF$ . An important result from Fig. 11S is that the effect of the wave drag itself ( $DF$ ) barely reaches the boundaries of the tropics (Fig. 11Sa), which is where it can directly affect upwelling (see Eq. 2S). Given the relatively small values of $DF$ in the (stratospheric) subtropics, **the weak tendency induced remotely in the zonal wind at these low latitudes** ( $\overline{u}_t$ , Fig. 11Sb) **makes a non-negligible contribution to the net forcing** ( $DF - \overline{u}_t$ , Fig. 11Sc), and consequently it **plays an important role in driving upwelling transient fluctuations**.

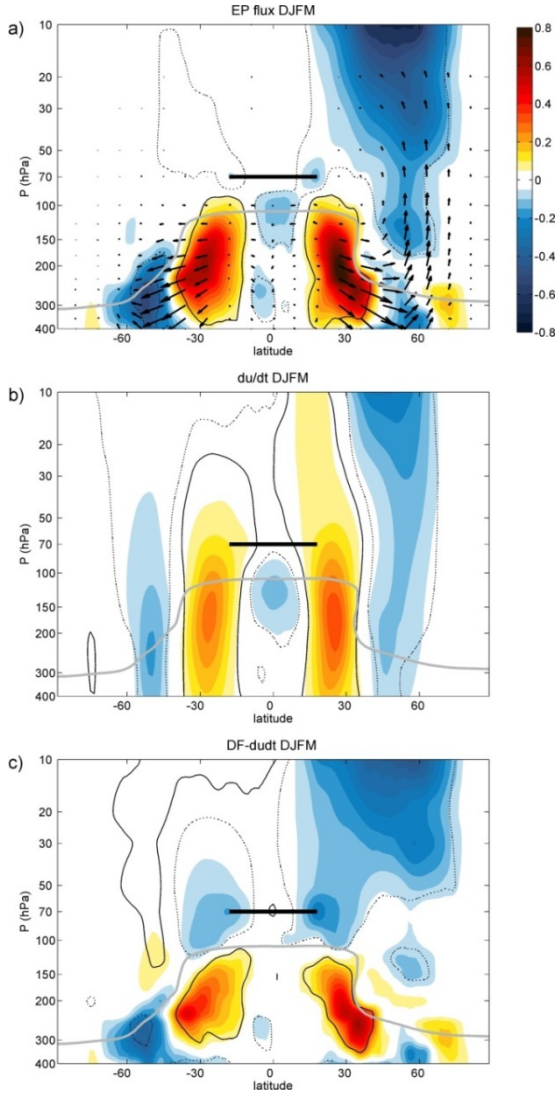


**Figure 11S**. Projections of the forcing fields onto upwelling at 70 hPa averaged over 18°S-18°N for DJFM 1979-2011 (based on daily mean ERA-Interim data). a) EP flux divergence ( $DF$ , shading), EP flux shown by the arrows b) zonal wind tendency ($\overline{u}_t$) and c) $DF - \overline{u}_t$. Contours indicate regions with 99% statistical significance. The gray line depicts the thermal tropopause. The black bar indicates the latitude and altitude of upwelling considered here. The color bar is the same for the three panels. Units: $m \cdot s^{-1} \cdot day^{-1} \cdot std(\overline{w}_m^*)^{-1}$, where $std(\overline{w}_m^*)$ is the unit standard deviation of the upwelling estimate.

In order to interpret correctly the projections in Fig. 11S it is useful to complement this result with the actual values of the EP flux and its divergence $DF$ during particular events of strong and weak upwelling. These extreme cases have been defined as the days with upwelling above the 95$^{th}$ percentile (strong upwelling) and below the 5$^{th}$ percentile (weak upwelling), respectively, of the DJFM time series (for 1979-2011).

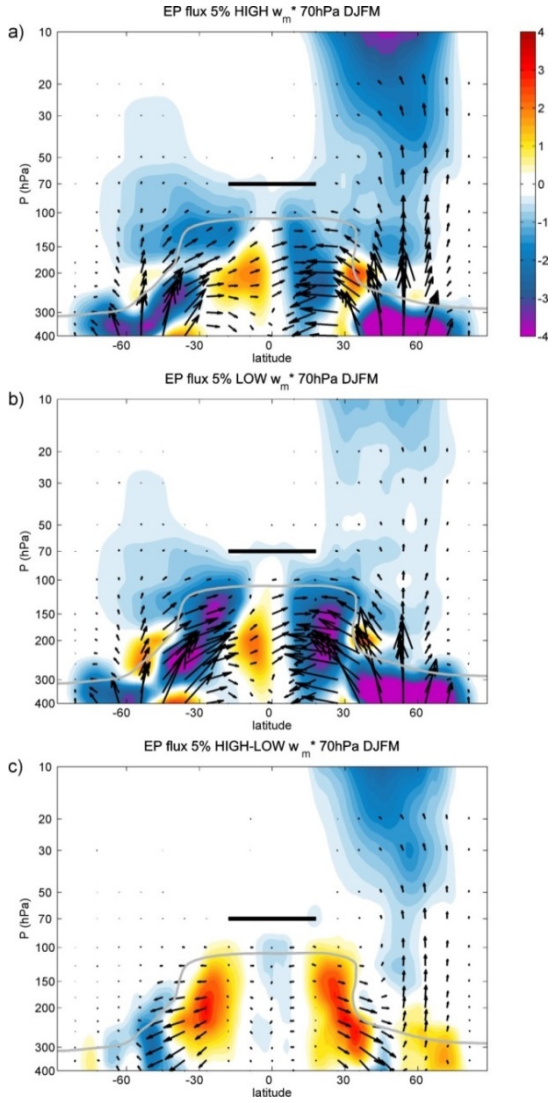


**Figure 12S**. Composite of EP flux (arrows) and divergence ( $DF$ , shading) for the 5% high (a), low (b) and high minus low (c) extremes of tropical upwelling. Same data as in Fig. 11S are used. The gray line depicts the thermal tropopause. The black bar indicates the latitude and altitude of upwelling considered here. Units: $m \cdot s^{-1} \cdot day^{-1}$.

Figure 12S shows that there is EP flux convergence ( $DF < 0$ ) in all centers of action for both high and low extremes. Furthermore, EP flux

convergence is associated with wave activity propagating from the extratropical troposphere, which partly penetrates deep into the stratosphere and partly is refracted towards the equator. **Upwelling is intensified during episodes of deep wave propagation and convergence in the extratropical stratosphere (Fig. 12Sa), and it is weakened when the convergence in the subtropical upper troposphere is enhanced** (Fig. 12Sb). Note that the difference high-minus-low (Fig. 12Sc) resembles the projection patterns shown in Fig. 11Sa. Hence, the composites in Figure 12S allow interpreting the positive and negative signs obtained in the centers of action in Fig. 11Sa as either intensification or weakening of the EP flux convergence in different regions.

The fact that tropical upwelling in the lower stratosphere is linked to EP flux convergence on tropospheric levels apparently contradicts Eq. (2S), which states that upwelling at a given level, $z$, is a function exclusively of the forcing at that level $z$ and above. The analyses carried out evidence the mechanism through which wave drag in the upper troposphere affects levels in the lower stratosphere. In particular, **the barotropic response induced in the zonal wind ($\overline{u}_t$) plays a central role in communicating the signal to higher levels**. Figure 13S illustrates this mechanism. The auto-correlations of the time series of $DF$ at a given location in the subtropical upper troposphere (with $DF$ everywhere else) show that **the extension of the forcing is limited to a relatively reduced region (Fig. 13Sa). In contrast, the response of the zonal wind to the forcing extends vertically across the tropopause (Fig. 13Sb), and as a result the net forcing extends as well into the lower stratosphere (Fig. 13Sc)**. To complete the picture, Fig. 13Sd shows the impact of the drag in the subtropical upper troposphere on the circulation. Two circulation cells with opposite sense are observed, one above and one below the forcing. The upper cell is associated with descent and warming over the tropical tropopause, demonstrating that the forcing in this region leads to a weakening of upwelling (in agreement with Fig. 12Sb).

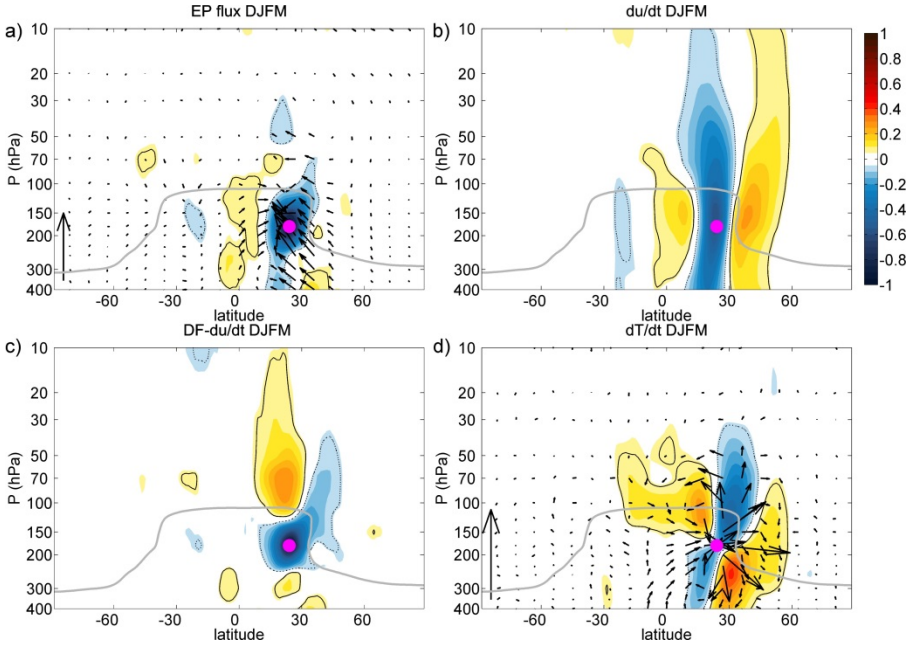


**Figura 13S.** Lineal correlations of the time series of $DF$ at the location indicated by the magenta dot (24°N, 175 hPa) with different fields. a) EP flux divergence (shading) and EP flux (arrows). b) Zonal wind tendency. c) Net forcing. d) Temperature tendency (shading) and residual circulation (arrows). The color bar is the same for all panels. Same data as in Fig. 11S and 12S are used.

In the present analysis, **a partial disconnection between the two branches of the Brewer-Dobson circulation has been identified, in terms of the forcing regions driving transient variability**. In particular, the influence of the wave drag in the subtropical upper troposphere is mainly limited to the lower branch of the circulation (roughly below ~70-50 hPa), while the extratropical stratosphere influences upwelling throughout the depth of the stratosphere. The transition between the two branches in terms of the drivers of the sub-seasonal variability is gradual. These results not only agree with previous studies which have shown that the Brewer-Dobson circulation presents distinct deep and shallow branches which can evolve in different ways (e.g. Bönisch et al. 2011), but it has also provided additional information on the difference between both branches. The

results obtained for this Objective are included in a fourth article that is currently in preparation (Abalos et al. 2013c).

## • Conclusions

The main conclusions of this Ph.D. Thesis can be summarized as follows:

- **Observational and WACCM model analyses based on the TEM budgets show that tropical upwelling drives a large fraction of seasonal and sub-seasonal variability in temperature, ozone and CO in the tropical lower stratosphere, on both seasonal and sub-seasonal timescales.**

- **Eddy quasi-horizontal transport changes seasonality across this region, with the summer Asian monsoon anticyclone strongly affecting ozone concentrations close to the tropopause. In the tropical lower stratosphere eddy transport is mostly linked to Rossby wave breaking in the subtropical winter and spring.**

- **Lagrangian model results on ozone transport near the tropical tropopause are shown to be consistent with the picture derived from TEM analyses, and provide complementary information on the tropical versus extra-tropical origin of the ozone molecules.**

- **Sub-seasonal variability in tropical upwelling is driven by extratropical wave activity, converging in the winter stratosphere and in the upper troposphere subtropics. Induced transient zonal mean wind tendencies are important for remotely communicating the wave drag.**

# 11. Resumen

En este capítulo se resume la Tesis Doctoral, incluyendo una breve descripción del estado del conocimiento en la materia bajo estudio, la motivación de la investigación desarrollada, los objetivos, los resultados más importantes y las conclusiones.

## 1 Estado del conocimiento y motivación

El aire troposférico entra en la estratosfera[1] principalmente en los trópicos, transportado por la rama ascendente de la circulación de Brewer-Dobson (denominada *upwelling* en inglés) que se completa con transporte hacia los polos y descenso sobre latitudes altas (Brewer 1949, Dobson 1956). Por tanto, **la concentración de los gases traza cerca de la tropopausa tropical constituye la condición de frontera para la composición química de toda la estratosfera**, afectando directamente al forzamiento radiativo del clima en superficie (e.g. Fueglistaler et al. 2009a, Riese et al. 2012). Dada la estrecha conexión entre la dinámica, la radiación y la química que tiene lugar en esta región relativamente pequeña caracterizada por temperaturas extremadamente bajas, es particularmente difícil representar todos los procesos que afectan a la distribución de trazadores en los modelos climáticos con química acoplada (e.g. Gettelman et al. 2010, Randel y Jensen 2013).

**La estructura espacial y la variabilidad temporal de los constituyentes atmosféricos en la baja estratosfera tropical están determinadas principalmente por procesos de transporte**, además de por fuentes y sumideros químicos. Los procesos de transporte más importantes en esta región son la advección vertical debida al *upwelling*

[1] Estratosfera: región atmosférica por encima de la troposfera limitada aproximadamente por los niveles de 10 km y 50 km caracterizada por una estratificación estática estable.

tropical y el transporte *eddy*[2] cuasi-horizontal. **No existen actualmente medidas directas de la velocidad vertical en esta región**, y por tanto **debe ser evaluada de forma indirecta** (e.g. Randel et al. 2008). Las estimaciones que se encuentran en la literatura, basadas en observaciones de trazadores o en consideraciones dinámicas, muestran velocidades positivas durante todo el año, y un amplio ciclo anual, con ascensos más intensos durante el invierno boreal que en verano (e.g. Rosenlof 1995).

Debido a la falta de observaciones, **no se conoce con exactitud cuál es el forzamiento de la variabilidad en el *upwelling***. Se ha demostrado que la circulación de Brewer-Dobson está forzada por ondas, y el formalismo denominado *Transformed Eulerian Mean* (TEM) ha demostrado ser particularmente útil para estudiar el origen dinámico de dicha circulación, que se denomina circulación *residual* en este marco teórico (e.g. Andrews et al. 1987). El mecanismo de forzamiento dinámico de la circulación residual se puede resumir brevemente de la siguiente manera. El arrastre ejercido sobre el flujo medio estratosférico por las ondas de Rossby que rompen en la estratosfera extratropical en invierno, en combinación con la fuerza de Coriolis, produce un flujo hacia el polo que a su vez induce ascensos y descensos por continuidad de la masa. Sin embargo, la teoría actual no es capaz de explicar las propiedades del *upwelling* tropical tal como se infieren de las observaciones (e.g. Plumb y Eluskiewicz 1999). Se han realizado importantes esfuerzos para entender qué ondas son principales las responsables del ciclo anual en el *upwelling*. El hecho de que la propagación y ruptura de ondas planetarias sean más intensas en el hemisferio norte que en el sur constituye una explicación de primer orden de la estacionalidad del ascenso (Yulaeva et al. 1994). Sin embargo, se ha observado que otras ondas juegan un papel fundamental en el forzamiento del ciclo estacional, en particular las ondas planetarias ecuatoriales y las ondas baroclínicas de escala sinóptica en los subtrópicos (e.g. Bohem y Lee 2003, Norton 2006, Randel et al. 2008, Ueyama y

[2] Transporte *eddy*: Componente del transporte debida a las anomalías zonales en la concentración de trazadores. En el formalismo *Transformed Eulerian Mean* se distingue entre dicha componente y la advección debida a la circulación residual.

Wallace 2010, Ortland y Alexander 2013). Recientemente, algunos trabajos han centrado la atención en identificar las fuentes de variabilidad del *upwelling* en escalas de tiempo sub-estacionales (Grise et al. 2011, Ueyama et al. 2013). **Comprender el forzamiento dinámico del *upwelling* es crucial para mejorar la representación de los procesos de transporte de trazadores en los modelos climáticos con química acoplada.**

Las concentraciones de muchos gases traza (tales como el ozono o el monóxido de carbono, CO) presentan fuertes gradientes verticales a través de la tropopause tropical y en la baja estratosfera tropical. Esta afirmación es cierta también para la temperatura potencial, como indica el máximo de estabilidad estática observado justo encima de la tropopausa tropical (e.g. Grise et al. 2010). Por tanto, las fluctuaciones en la velocidad vertical tienen un efecto acentuado sobre dichos trazadores y sobre la temperatura en esta región. Las observaciones muestran un importante ciclo anual en la temperatura localizado en una capa relativamente estrecha justo encima de la tropopausa tropical (Reed y Vicek 1969). Se ha demostrado que este ciclo anual es debido a la variación estacional en la intensidad del ascenso (Yulaeva et al. 1994, Fueglistaler et al. 2011). Utilizando tanto observaciones de satélite como de radiosondas, Randel et al. (2008) hallaron ciclos anuales en las concentraciones de ozono y de CO, los cuales presentan una estructura vertical similar a la del ciclo anual de temperatura, es decir, están localizados en una región estrecha y con máxima amplitud sobre la tropopausa tropical. Randel et al. (2007) demostraron que tanto la estructura vertical como la fase de **dichos ciclos en los trazadores pueden explicarse por la estacionalidad del *upwelling* actuando sobre los fuertes gradientes verticales en esta región**. Por otro lado, **análisis complementarios utilizando un modelo lagrangiano de transporte han sugerido que la causa principal del ciclo estacional en el ozono es el transporte horizontal** desde los extra-trópicos originado por el anticiclón en niveles altos **asociado al monzón Asiático**, en vez del *upwelling* (Konopka et al. 2009, 2010, Ploeger et al. 2012). Esta discrepancia de resultados surgida recientemente requiere un análisis al

respecto, el cual ha sido abordado como parte del trabajo desarrollado en esta Tesis Doctoral.

Observaciones recientes de temperatura y trazadores cerca de la tropopausa tropical muestran un alto grado de variabilidad común entre estas magnitudes. La Figura 1S muestra las series temporales de temperatura (datos del reanálisis ERA-Interim[3]), junto con observaciones de satélite de ozono y CO para tres niveles de presión situados en torno a la tropopausa tropical. **La variabilidad en común entre las series es especialmente evidente para los ciclos anuales, pero también se observa en escalas sub-estacionales.**

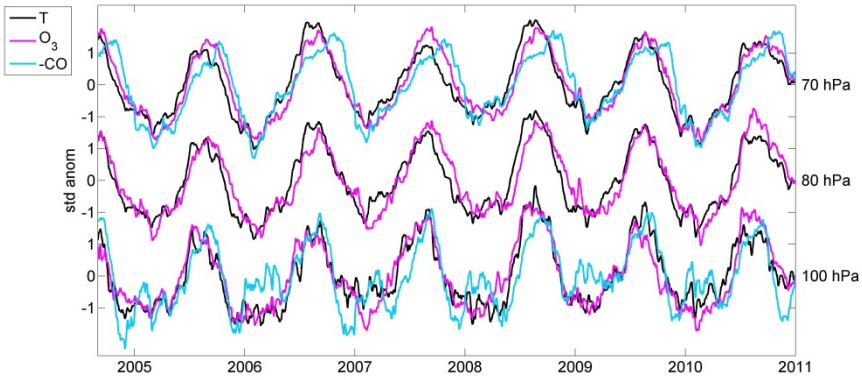


**Figura 1S**. Series temporales de anomalías estandarizadas de temperatura, ozono y CO promediadas entre 20°N-20°S en tres niveles de presión en torno a la tropopausa tropical para el período comprendido entre Septiembre de 2004 y Diciembre de 2010. Los datos de temperatura se han obtenido del reanálisis ERA-Interim, y las observaciones corresponden al instrumento Micowave Limb Sounder (MLS) que viaja a bordo del satélite Aura de la NASA (Waters et al. 2006). La serie de CO se muestra en una escala invertida para ensalzar la variabilidad en común. Figura de Abalos et al. 2012.

Estas observaciones sugieren la pregunta de cuál es el mecanismo que produce estas fluctuaciones comunes, y en particular, **qué papel juega el**

[3] Acrónimo en inglés de Re-Análisis del Centro Europeo de Predicción a Medio Plazo.

***upwelling* tropical en la variabilidad observada en la temperatura y en los trazadores**. Estas preguntas constituyen el punto de partida para esta Tesis Doctoral.

# 2 Objetivos

En el marco del contexto expuesto en la sección anterior, el objetivo general de esta Tesis es **investigar el *upwelling* en la baja estratosfera tropical, incluyendo su variabilidad en distintas escalas temporales, su influencia en la temperatura y en las concentraciones de gases traza en dicha región, y sus fuentes específicas de variabilidad.** Este objetivo general ha sido subdividido en cuatro objetivos específicos, que son los siguientes:

1. **Cuantificar el *upwelling* tropical y su incertidumbre en torno a la tropopausa tropical, calculando tres estimaciones independientes.**

Para ello se utiliza el reanálisis del Centro Europeo de Predicción a Medio Plazo ERA-Interim (Dee et al. 2011). Las tres estimaciones del *upwelling* incluyen la velocidad vertical residual del reanálisis y dos cálculos indirectos basados en los balances de momento y termodinámico.

2. **Investigar la relación entre la variabilidad del *upwelling* y la variabilidad de la temperatura y los trazadores en la baja estratosfera tropical.**

Este objetivo se lleva a cabo con datos observacionales (datos de satélite) y las estimaciones de *upwelling* descritas en el punto anterior, y también con los resultados de una simulación con el modelo WACCM4 (Whole Atmosphere Community Climate Model, version 4, Garcia et al. 2007). El análisis se centra en escalas de tiempo anual e intra-anuales.

3. **Evaluar el efecto de otros mecanismos de transporte sobre la concentración de trazadores en la baja estratosfera tropical.**

La contribución de otros procesos (aparte del *upwelling*) en el forzamiento de la variabilidad de los trazadores se examina en este objetivo a través de la evaluación explícita de todos los términos de transporte en las ecuaciones de balance de los trazadores utilizando datos del modelo climático WACCM4. Estos balances obtenidos con WACCM se comparan además con resultados de un modelo conceptual unidimensional lagrangiano. La comparación con este modelo tan diferente permite obtener una visión más integral de los procesos de transporte en la región bajo estudio.

4. **Explorar el forzamiento dinámico de la variabilidad del *upwelling* en escalas de tiempo sub-estacionales.**

Para ello se proyectan los campos de forzamiento sobre las series temporales de *upwelling* obtenidas a partir de la ecuación de balance de momento para el Objetivo 1. En este último objetivo se utilizan datos diarios de ERA-Interim para el período 1979-2011. Para aislar la variabilidad en escalas de tiempo sub-estacionales en las series temporales, se han aplicado filtros espectrales.

# 3 Resultados principales y conclusiones

El capítulo de Resultados de esta Tesis Doctoral, configurado en formato artículos, se ha subdividido en cuatro secciones, correspondientes a los siguientes artículos que han sido realizados durante el desarrollo de la Tesis:

1. - *Variability in upwelling across the tropical tropopause and correlations with tracers in the lower stratosphere.* Abalos, M., Randel, W. J. y Serrano, E., Atmos. Chem. Phys., 12, 11505–11517, doi:10.5194/acp-12-11505-2012, 2012.

2. - *Quantifying tracer transport in the tropical lower stratosphere using WACCM*. Abalos, M., Randel, W. J., Kinnison, D. E., y Serrano, E., Atmos. Chem. Phys., 13, 10591-10607, doi:10.5194/acp-13-10591-2013, 2013a.

3. - *Ozone seasonality above the tropical tropopause: reconciling the Eulerian and Lagrangian perspectives of transport processes*. Abalos, M., Ploeger, F., Konopka, P., Randel, W. J. y Serrano, E, Atmos. Chem. Phys. Discuss., 13, 19291–19310, doi:10.5194/acpd-13-19291-2013, 2013b.

4. - *Dynamical forcing of sub-seasonal variability in the tropical Brewer-Dobson circulation.* Abalos, M., Randel, W. J. y Serrano, E., enviado a J. Atmos. Sci.

Sin embargo, en este capítulo (Resumen), los principales resultados se presentan agrupados siguiendo el orden de los cuatro objetivos expuestos en la sección anterior. Las conclusiones más importantes se enumeran al final de esta sección.

## • Objetivo 1.

*Cuantificar el upwelling tropical y su incertidumbre en torno a la tropopausa tropical, calculando tres estimaciones independientes.*

La Figura 2S muestra las series temporales de las tres estimaciones semi-observacionales del *upwelling* tropical calculadas como parte de este objetivo, correspondientes a los mismo niveles de presión mostrados en la Fig. 1S, es decir, en torno a la tropopausa tropical. Es importante tener presentes las incertidumbres asociadas a cada una de estas estimaciones.

La primera estimación es la componente vertical de la circulación residual ($\overline{w}^*$), que depende en gran medida del campo de velocidad vertical del reanálisis ($\overline{w}$), producto de los modelos que lleva asociada una gran incertidumbre, a pesar de que algunos trabajos han mostrado una mejora en la representación de la velocidad vertical en el reanálisis ERA-

Interim respecto a su predecesor ERA-40 (e.g. Dee et al. 2011 y referencias). El cálculo de $\overline{w}^*$ a partir de $\overline{w}$ viene dado por:

$$\overline{w}^* \equiv \overline{w} + \frac{1}{a\cos\phi}\left(\cos\phi \frac{\overline{v'T'}}{S}\right)_\phi \tag{1S}$$

donde $\phi$ es la latitud, los subíndices indican derivadas parciales, las barras indican promedio zonal y las primas desviaciones respecto a éstas, $a$ es el radio de la Tierra, $S = H \cdot N^2 / R$, siendo $N$ la frecuencia de Brunt-Väissälä, $R$ la constante del aire seco como gas ideal y $H$ una altura de escala constante (Andrews et al. 1987).

La segunda estimación del *upwelling* ($\overline{w}^*_m$) se obtiene combinando las ecuaciones TEM de conservación del momento y de la masa, de modo que la expresión final tal del valor promedio tropical $\left\langle \overline{w}^*_m \right\rangle$ es la siguiente (Randel et al. 2002):

$$\left\langle \overline{w}^*_m \right\rangle (z) = \frac{-e^{z/H}\cos\phi}{\int_{-\phi_0}^{\phi_0} a\cos\phi d\phi} \left\{ \int_z^\infty \frac{e^{-z'/H}}{\hat{f}(\phi, z')} \left[ DF(\phi, z') - \overline{u}_t(\phi, z') \right]_{\overline{m}} dz' \right\}_{-\phi_0}^{\phi_0} \tag{2S}$$

donde $DF = e^{z/H} \nabla \cdot \mathbf{F} / (a\cos\phi)$ es la divergencia del flujo de Eliassen-Palm (flujo EP) dividida por la densidad (tomando la densidad del aire en el nivel de 1000 hPa como 1 $kg \cdot m^{-3}$), $\overline{u}_t$ es la tendencia de la media zonal del viento zonal y $\hat{f} = f - (\overline{u}\cos\phi)_\phi / (a\cos\phi)$. La Ecuación (2S) proporciona el *upwelling* tropical en un nivel dado $z$ y promediado en un determinado rango de latitudes (18°S-18°N en esta Tesis) en función del forzamiento, integrado para todas las alturas por encima de dicho nivel $z$

y evaluado en las fronteras del intervalo latitudinal $\pm \phi_0$. La divergencia del flujo EP es función a su vez de flujos *eddy* de momento y de calor, los cuales se calculan utilizando datos de ERA-Interim. La mayor fuente de incertidumbre asociada a esta estimación del *upwelling* $\left\langle \overline{w}_m^* \right\rangle$ es el cálculo de la divergencia del flujo de EP, dado que aquellas ondas de escala menor que la resolución horizontal del modelo utilizado en ERA-Interim no están resueltas.

La última estimación ( $\overline{w}_Q^*$ ) se obtiene combinando las ecuaciones TEM de balance termodinámico y de continuidad de la masa:

$$\overline{T}_t = -\overline{v}^* \overline{T}_y - \overline{w}^* S + \overline{Q} \qquad (3S)$$

$$(a\cos\phi)^{-1}(\overline{v}^*\cos\phi)_\phi + e^{z/H}(e^{-z/H}\overline{w}^*)_z = 0 \qquad (4S)$$

siendo $\left(\overline{v}^*, \overline{w}^*\right)$ las componentes de la circulación residual y $\overline{Q}$ la tasa de calentamiento diabático (en la estratosfera se considera buena aproximación utilizar sólo la componente radiativa). En este caso la mayor fuente de incertidumbre está asociada a la tasa de calentamiento radiativo, $\overline{Q}$, que se calcula utilizando un modelo de transferencia radiativa NCAR-CRM, imponiendo como datos de entrada la temperatura de ERA-Interim y observaciones de satélite de ozono. Un inconveniente de este cálculo es que no considera los efectos radiativos de las nubes. Sin embargo, el efecto neto de las nubes sobre el calentamiento radiativo medio en la baja estratosfera tropical es relativamente pequeño (Yang et al. 2010). En la Ecuación (3S) se ha despreciado un término de transporte *eddy* como es común hacer. Sin embargo, esta aproximación puede constituir una fuente de error no del todo despreciable.

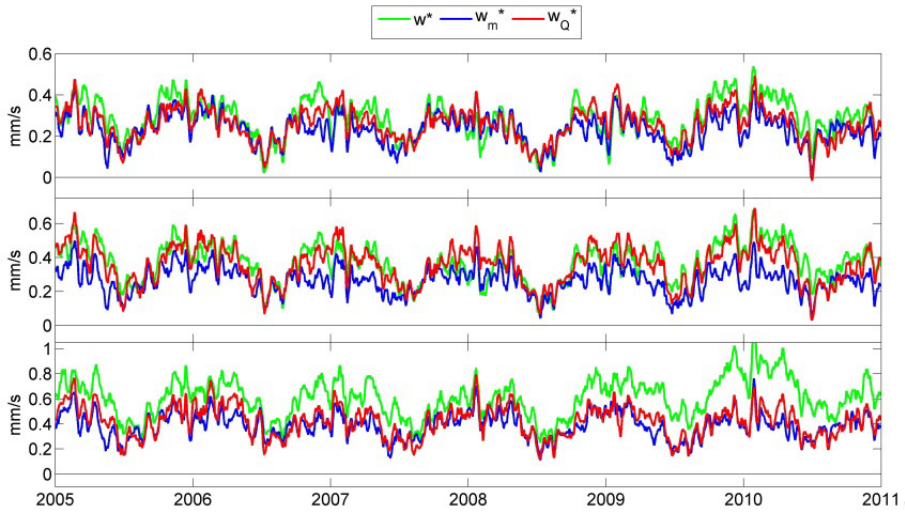


**Figura 2S**. Series temporales diarias de *upwelling* calculado de tres maneras distintas para el período 2005-2010 en los niveles de presión de 70 hPa (panel superior), 80 hPa (panel intermedio) y 100 hPa (panel inferior) (ver texto para más detalles). Verde: circulación residual. Azul: estimación basada en el balance de momento. Rojo: estimación basada en el balance termodinámico. Se han realizado medias móviles de 11-días en todas las series. Unidades: $mm \cdot s^{-1}$.

A pesar de las incertidumbres y fuentes de error descritas, **las series temporales de *upwelling* en la Fig. 2S muestran un acuerdo razonable en general, tanto en la magnitud como en el ciclo estacional y la variabilidad en escalas sub-estacionales**. Las correlaciones lineales entre las tres estimaciones en los niveles mostrados en la Fig. 2S toman valores en torno a ~0.7. Las mayores correlaciones en la baja estratosfera tropical, se obtienen entre las dos estimaciones indirectas, es decir las obtenidas a partir de los balances de momento y termodinámico. La circulación residual calculada directamente con los datos del reanálisis ERA-Interim ( $\overline{w}^*$) presenta un acuerdo menor con las otras dos estimaciones, en particular cerca de la tropopausa (~100 hPa en los trópicos), lo cual es consistente con estudios anteriores (e.g. Dee et al. 2011).

**En resumen, el buen acuerdo entre las velocidades verticales inferidas de manera independiente** induce a confiar en los resultados

obtenidos. En base a ello, **dichas estimaciones pueden ser utilizadas para analizar la relación entre las fluctuaciones en el *upwelling* y aquellas observadas en las series de temperatura y trazadores** (Figura 1S), tanto para el ciclo anual como para escalas de tiempo menores. Los resultados de este objetivo están publicados en Abalos et al. (2012).

- ## Objetivo 2.

*Investigar la relación entre la variabilidad del upwelling y la variabilidad de la temperatura y los trazadores en la baja estratosfera tropical.*

Con el objetivo de investigar la influencia del *upwelling* sobre la temperatura y la concentración de trazadores en la baja estratosfera tropical, se han utilizado las estimaciones mostradas en la Figura 2S en combinación con datos de temperatura de ERA-Interim y observaciones de satélite de ozono y CO (medidas del instrumento MLS). Los análisis realizados consisten en evaluar cada término de las ecuaciones TEM termodinámica (Ec. 3S) y de continuidad para la concentración de trazadores. Esta última se expresa de la siguiente manera:

$$\overline{\chi}_t = -\frac{\overline{v}^*}{a}\overline{\chi}_\phi - \overline{w}^*\overline{\chi}_z + e^{z/H}\nabla\cdot\mathbf{M} + P - L \qquad (5S)$$

siendo $\overline{\chi}$ la concentración zonal media del gas traza, $\overline{w}^*$ representa cualquiera de las tres estimaciones del *upwelling*, $e^{z/H}\nabla\cdot\boldsymbol{M}$ es el término de transporte *eddy*, y $P-L$ cuantifica la tendencia neta de $\overline{\chi}$ debida a las reacciones fotoquímicas (es decir, producción menos pérdida). La Figura 3S muestra los resultados semi-observacionales de la evolución media mensual de los distintos términos de la ecuación termodinámica (Ec. 3S, Fig. 3Sa) y de la ecuación de continuidad (Ec. 5S) para el ozono (Fig. 3Sb) y el monóxido de carbono (Fig. 3Sc), evaluadas en un determinado nivel de presión situado encima de la tropopausa tropical (i.e. 70 hPa).

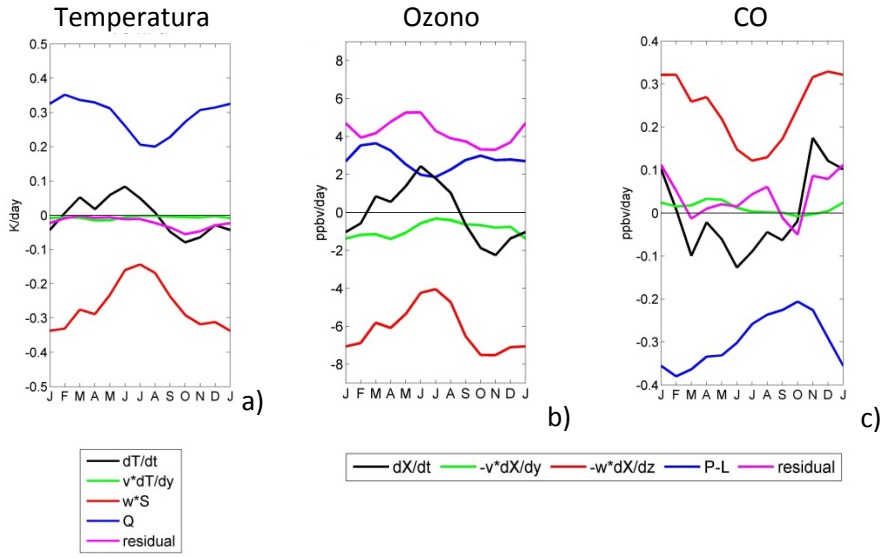


**Figura 3S**. Evolución media mensual de los términos de las ecuaciones TEM (a) termodinámica (Ec. 3S), b) continuidad (Ec. 5S) del ozono y c) continuidad del CO) en 70 hPa calculados con datos observacionales y de reanálisis promediados en el trópico (18°S-18°N). Negro: tendencia de la temperatura (en a) o de los trazadores (en b y en c). Verde: advección meridional. Rojo: Advección vertical debida al *upwelling*. Azul: calentamiento diabático en (a), fuentes y/o sumideros fotoquímicos en b) y en c). Magenta: residuo, debido a incertidumbres en todos los demás términos y también al término *eddy* de transporte de los trazadores en b) and c). Promedio sobre el perído 2005-2010.

El balance termodinámico (Fig. 3Sa) muestra que **el ciclo anual en el enfriamiento adiabático debido al *upwelling*** (es decir, al ascenso más intenso de aire frío proveniente de la tropopausa durante el invierno boreal que durante el verano) **es el principal responsable del ciclo anual en la temperatura**. En promedio anual, el calentamiento radiativo compensa el enfriamiento adiabático producido por el *upwelling*. Los balances de ozono y CO muestran características similares entre sí (Figs. 3Sb y 3Sc, respectivamente). En particular, se observa un amplio ciclo anual en la advección vertical debida al *upwelling*, que se refleja en la tendencia de los gases, indicando que **el ciclo estacional en ambos**

**trazadores se debe principalmente al *upwelling* tropical actuando sobre los fuertes gradientes verticales que existen en esta región**. En promedio anual, la destrucción fotoquímica de CO compensa el aumento debido al *upwelling*. **En el caso del ozono**, la producción fotoquímica por sí misma no es capaz de compensar la disminución debida al *upwelling*, y en consecuencia **hay un residuo relativamente importante en el balance**. **Este residuo** es debido a incertidumbre en todos los términos, pero también **incluye el término de transporte *eddy* en la ecuación de continuidad TEM** (Ec. 5S), el cual **no se puede calcular explícitamente a partir de las observaciones de satélite** (dada la insuficiente resolución horizontal), pero puede jugar un papel importante en el balance de ozono. La producción química de ozono muestra una ligera dependencia semi-anual, debida a la migración aparente del sol sobre el ecuador dos veces al año.

Además de los ciclos anuales, las series temporales en la Figura 1S muestran variabilidad en común en escalas de tiempo intra-anuales. Este hecho se observa claramente en la Figura 4S, que muestra en la parte de arriba las series temporales de la tendencia de la temperatura, el ozono o el CO, filtradas espectralmente para eliminar el ciclo anual y la variabilidad en escalas de tiempo mayores.

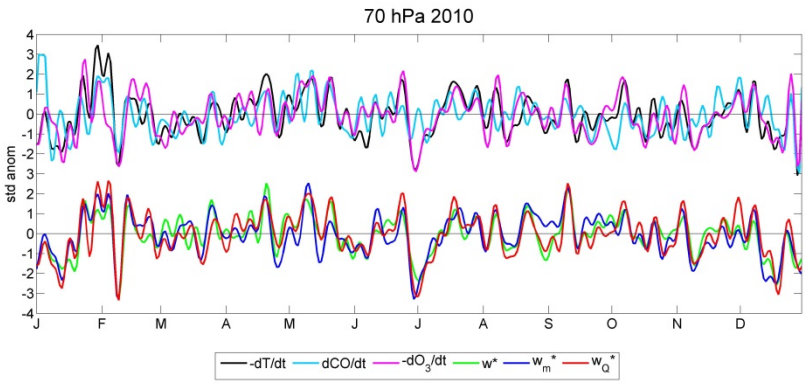


**Figura 4S**. Series temporales filtradas de la tendencia en la temperatura (negro), el ozono (magenta) y el CO (cyan) (arriba), junto a las estimaciones de upwelling tropical (parte inferior) para el año 2010 en el nivel de 70 hPa. Promedio tropical (18°S-18°N). Las estimaciones de upwelling estimates se muestran en los mismos colores que en la Fig. 2S. Para aislar la variabilidad sub-estacional, se ha aplicado un filtro espectral que descarta las escalas de tiempo mayores o iguales que el ciclo anual (también se han eliminado las escalas menores que 6 días).

En la parte inferior de la Fig. 4S se incluyen las series temporales del *upwelling* filtradas de la misma manera que las tendencias. Se observan **fluctuaciones comunes en escalas de tiempo del orden de semanas entre las estimaciones del *upwelling* y las observaciones de satélite de los trazadores, aun siendo series temporales totalmente independientes entre sí**. Las correlaciones lineales entre las series temporales de las tendencias y las estimaciones son estadísticamente significativas (con un nivel de confianza del 99% según el test t-Student), demostrando que **el *upwelling* tropical contribuye notablemente al forzamiento de la variabilidad sub-estacional de la temperatura y de los trazadores**, lo cual es consistente con los resultados obtenidos para el ciclo anual.

Hasta ahora, se ha mostrado que el *upwelling* tropical juega un papel central en el forzamiento de la variabilidad revelada por las observaciones de temperatura, ozono y CO en escalas de tiempo estacional y sub-estaciones. Sin embargo, como se ha mencionado anteriormente, los balances mostrados en la Figura 3S incluyen residuos no despreciables. En

particular, el balance de ozono (Fig. 3Sb) muestra un residuo relativamente grande, pudiendo implicar que ciertos procesos no están correctamente representados en el análisis. Para poder cerrar el balance (es decir, obtener un residuo prácticamente nulo), es preciso evaluar explícitamente todos los términos de la ecuación de continuidad (Eq. 5S). Dado que esto no se puede llevar a cabo con datos observacionales, se ha utilizado una simulación con el modelo WACCM4 para complementar estos resultados. **Los datos de la simulación con el modelo WACCM permiten resolver explícitamente todos los términos en la ecuación de continuidad de los trazadores, y por tanto cerrar los balances**.

Como paso previo al análisis de los balances con datos de WACCM, se ha comprobado la capacidad de este modelo para reproducir las principales características de la estructura térmica y distribución de los trazadores en esta región. Este análisis preliminar ha mostrado que el modelo sobreestima levemente la altura de la tropopausa tropical (en aproximadamente ~1 km). Para ilustrar este punto, la Figura 5S muestra el perfil vertical de la temperatura media anual en el trópico en WACCM y en observaciones de GPS para un período similar (2006-2010). La tropopausa del *punto frío* se identifica como la altura en la que se encuentra el mínimo de temperatura (líneas horizontales en la Fig. 5S). Nótese que esta diferencia puede ser debida a la limitada resolución vertical del modelo (~1-1.4 km).

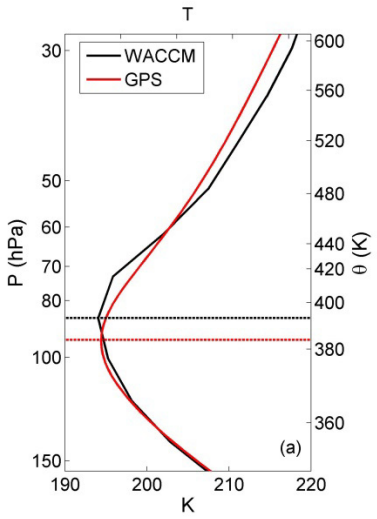


**Figura 5S**. Perfil vertical de la temperatura media anual en el modelo WACCM (negro, período 2004-2009) y en observaciones de GPS (rojo, período 2006-2011) promediada entre 18°S-18°N (WACCM) y entre 20°S-20°N (GPS). Las líneas horizontales muestran la altura de la tropopausa del *punto frío*. La escala vertical de la derecha muestra la localización de los niveles de temperatura potencial media anual para el mismo período en WACCM.

Para tener en cuenta este desplazamiento en la altura de la tropopausa, los balances se evalúan en niveles ligeramente superiores en el modelo respecto a los utilizados para las observaciones (por ejemplo, el nivel de 62 hPa del modelo se compara con el nivel de 70 hPa de las observaciones). Los resultados para el balance termodinámico, del ozono y del CO en el nivel de 62 hPa se muestran en la Fig. 6S.

**Los resultados obtenidos con el modelo** (Fig. 6S) **muestran residuos prácticamente nulos**, lo cual indica que los balances en WACCM están cerrados. **Además, el balance es muy similar al obtenido con las observaciones** (Fig. 3S), confirmando los resultados de las mismas. En particular, **el ciclo anual en la tendencia de ozono sigue de cerca la evolución estacional en el término de *upwelling*** (Fig. 6Sb). En promedio anual, este balance muestra que la tendencia negativa debida al *upwelling* es compensada por la producción fotoquímica de ozono más el transporte horizontal (el cual es principalmente transporte *eddy*). **Esto prueba la**

**hipótesis de que el residuo obtenido en la Figura 3Sb es debido en gran parte al término de transporte *eddy*, que no está explícitamente resuelto en las observaciones**. Por tanto, el análisis con el modelo WACCM apoya los resultados observacionales.

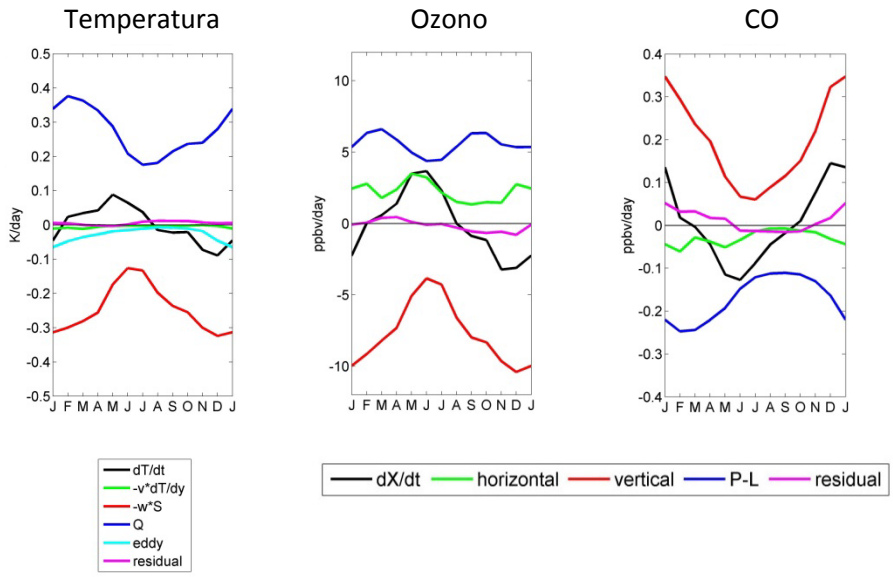


**Figura 6S**. Evolución media mensual de los términos de las ecuaciones TEM (a) termodinámica (Ec. 3S), b) continuidad (Ec. 5S) del ozono y c) continuidad del CO) en 62 hPa calculados con datos del modelo WACCM promediados en el trópico (18°S-18°N). Por simplicidad, los términos de transporte de trazadores de la Ec. 5S se han reagrupado en componentes horizontal y vertical. Línea negra: tendencia de la temperatura (en a) o de los trazadores (en b y en c). Línea verde: Advección meridional de temperatura en a, transporte meridional en b y c (asociado principalmente a transporte *eddy*). Línea roja: Advección vertical de temperatura, transporte vertical en b y c (asociado principalmente al *upwelling*). Línea azul: calentamiento diabático en (a), fuentes y/o sumideros fotoquímicos en b) y en c). Línea cyan (sólo en a)): término *eddy* de transporte de temperatura. Línea magenta: residuo debido a la incertidumbre en todos los demás términos. Promedio sobre el perído 2004-2009.

- ## Objetivo 3.

*Evaluar el efecto de otros mecanismos de transporte sobre la concentración de trazadores en la baja estratosfera tropical.*

Los balances mostrados en las figuras 3S y 6S señalan al *upwelling* como principal responsable del forzamiento del ciclo anual en la temperatura y en los trazadores en la baja estratosfera tropical. En particular, la Figura 6Sb muestra el amplio ciclo anual en el ozono sigue de cerca al término de transporte por parte del *upwelling*, mientras que el término de transporte horizontal muestra muy poca variabilidad estacional en la baja estratosfera tropical. La Figura 7S muestra los resultados de WACCM para el balance de ozono en el nivel de 62 hPa y en otros dos niveles de presión inferiores, incluyendo el nivel en el que se encuentra la tropopausa del punto frío (86 hPa en esta simulación).

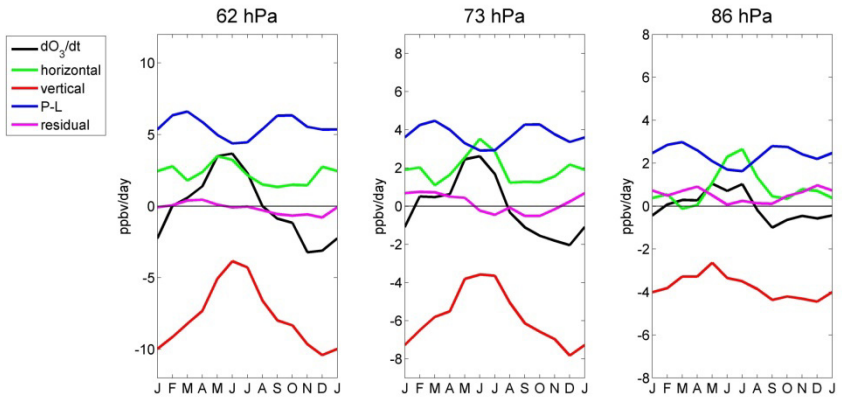


**Figura 7S**. Evolución media mensual del balance TEM de ozono tropical (promediado entre 18°S-18°N) en tres niveles de presión cerca de la tropopausa tropical, calculado con datos del modelo WACCM. La tropopausa (punto frío) se encuentra en el nivel de 86 hPa en esta simulación. Línea negra: tendencia de ozono. Línea roja: transporte vertical (asociado principalmente al *upwelling*). Línea verde: transporte horizontal (asociado principalmente al transporte *eddy* meridional). Línea azul: producción menos pérdida fotoquímica neta. Línea magenta: residuo. Promedio sobre el período 2004-2009.

Se observa claramente una transición con la altura en la estacionalidad de los términos en la Fig. 7S. En particular, la amplitud del ciclo anual del ozono y del *upwelling* es mucho menor en el nivel inferior (junto a la tropopausa tropical) que en los niveles superiores. Además, **el transporte horizontal muestra un máximo en verano del hemisferio norte cerca de la tropopausa tropical**. Esta transición en la evolución estacional del transporte cuasi-horizontal se manifiesta en la Figura 8S.

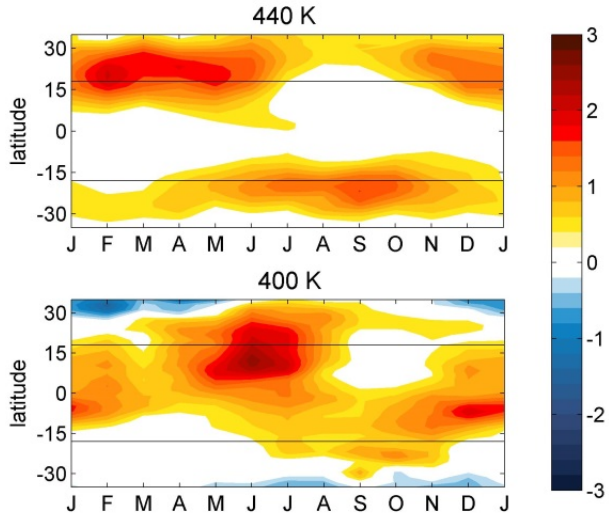


**Figura 8S**. Sección latitudinal de la evolución media mensual del transporte isentrópico de ozono en el modelo WACCM en dos niveles isentrópicos, 440 K (~62 hPa) y 400 K (~86 hPa). La escala de color muestra la tendencia de ozono debida al transporte isentrópico en relación a la concentración media anual en esa posición. Las líneas horizontales muestran los límites del rango de latitudes consideradas en los promedios tropical en la Figura 5S (18°S-18°N). Unidades: $\% \cdot día^{-1}$.

Esta figura muestra la evolución media mensual del transporte isentrópico de ozono (principalmente asociada al transporte *eddy*), en función de la latitud en dos niveles isentrópicos cuya altura corresponde aproximadamente con los niveles más alto (62 hPa) y más bajo (86 hPa) mostrados en la Figura 7S. Las características del transporte *eddy* cuasi-

horizontal son notablemente distintas entre estos dos niveles situados a menos de 3 km de distancia. **En el nivel superior (440 K) el transporte *eddy* de ozono tiene lugar en invierno y primavera en los subtrópicos de cada hemisferio, y está asociado con la ruptura de ondas de Rossby cerca de las líneas críticas** (figura no mostrada en este Resumen). Por otra parte, **cerca de la tropopausa** (~400 K) se observa transporte *eddy* en latitudes tropicales a lo largo de todo el año, siendo destacable un notable incremento en ozono tropical en el verano boreal, asociado con **transporte *eddy* por parte del anticiclón asociado al monzón Asiático**.

La estructura vertical de los procesos de transporte que controlan la variabilidad del ozono en el modelo WACCM se resume en la Figura 9S. En particular, esta figura muestra la amplitud del ciclo anual en cada término del balance TEM de ozono en función de la altura. En la Fig. 9S, el ***upwelling* tropical domina la variabilidad estacional en la baja estratosfera, mientras que el ciclo anual en el transporte horizontal se observa en niveles más bajos, cerca de la tropopausa tropical.**

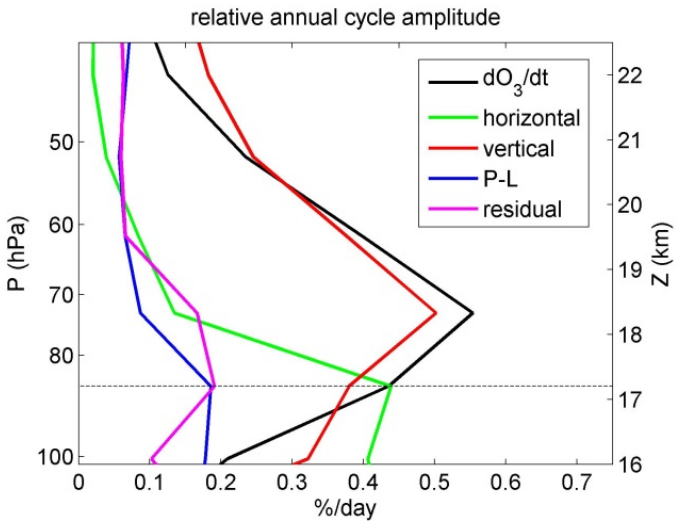


**Figura 9S**. Estructura vertical de la amplitud relativa del ciclo anual de los términos en el balance TEM de ozono calculado para el modelo WACCM (promediado entre 18°S-18°N). La escala en el eje vertical de la derecha muestra la altura obtenida a partir del logaritmo de la presión. La amplitud se expresa en relación a la concentración media anual en cada nivel. Unidades: $\% \cdot día^{-1}$.

Además del ciclo anual, se ha estudiado el papel de los diferentes procesos en la variabilidad del ozono y el CO en escalas de tiempo menores. Los resultados del modelo **WACCM muestran que el upwelling es el principal forzamiento de la variabilidad en estas escalas de tiempo sub-estacionales, en niveles con fuertes gradientes verticales en los trazadores en la baja estratosfera tropical.** El transporte *eddy* horizontal también es importante (aunque en menor medida que el *upwelling*) para la variabilidad sub-estacional en el ozono y el CO. Los resultados sobre el modelo WACCM se recogen en la publicación Abalos et al. (2013a).

Como se ha mencionado brevemente en la Sección 1 de este Resumen, un grupo de trabajos basados en modelos lagrangianos han sugerido recientemente que el ciclo anual en ozono encima de la tropopausa tropical está causado fundamentalmente por transporte horizontal asociado con el monzón Asiático en el verano boreal (e.g.

Ploeger et al. 2012). Esto contradice aparentemente los resultados mostrados más arriba, los cuales evidencian que el ciclo anual en el ozono se produce principalmente en respuesta a la correspondiente evolución en el *upwelling*. La explicación de esta aparente discrepancia radica en que existen diferencias fundamentales entre los análisis que es necesario tener en cuenta a la hora de comparar estos resultados. En primer lugar, los cálculos con el modelo lagrangiano están realizados en coordenadas isentrópicas. Konopka et al. (2009) mostraron que **la amplitud del ciclo estacional del ozono tropical es mucho menor (hasta un 60 %) en coordenadas isentrópicas que en niveles de presión.** Esto es debido a que la temperatura potencial sufre a su vez una gran oscilación anual en esta región, que está prácticamente en fase con el ciclo del ozono (ver Fig. 1S). Como se ha mencionado anteriormente, el ciclo estacional de la temperatura está causado principalmente por el *upwelling* (e.g. Fig. 3Sa). Por tanto, gran parte del efecto del *upwelling* sobre el ozono (y el CO) se elimina cuando se analiza la variabilidad en coordenadas isentrópicas.

Además de esta diferencia clave entre los análisis, es crucial tener en cuenta las distintas interpretaciones de los resultados obtenidos bajo un enfoque lagrangiano o euleriano. Para comparar los resultados adecuadamente, en esta Tesis se han transformado los resultados lagrangianos a una representación euleriana[4]. La Figura 10S muestra el balance de ozono euleriano obtenido a partir de los resultados de un modelo lagrangiano de transporte unidimensional (denominado modelo 1D de ahora en adelante, Ploeger et al. 2012). Este modelo simula retro-trayectorias de parcelas que atraviesan las isentropas partiendo de niveles en la baja estratosfera tropical. Los cambios en la concentración de ozono en cada parcela a lo largo de su trayectoria vienen dados por la producción fotoquímica y el transporte horizontal desde el extra-trópico (*in-mixing* en inglés), valores tomados del modelo lagrangiano tridimensional CLaMS (Chemistry Lagrangian Model of the Stratosphere, McKenna et al. 2002, Konopka et al. 2004).

[4] Este cálculo ha sido realizado por Félix Ploeger del Jülich Forschungzentrum, Alemania.

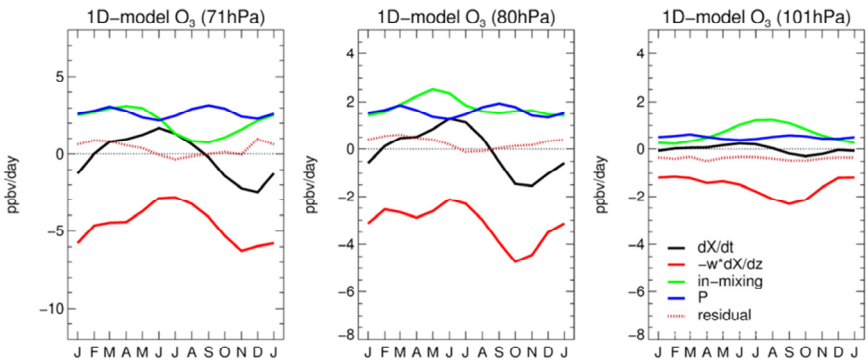


**Figura 10S**. Balance de ozono (promediado entre 20°S-20°N) obtenido a partir de resultados del modelo lagrangiano de transporte unidimensional (modelo 1D) para tres niveles de presión cerca de la tropopausa tropical. Línea negra: tendencia de ozono. Línea roja: advección vertical debida al *upwelling*. Línea verde: transporte horizontal de ozono (*in-mixing*), (incluye advección meridional más transporte *eddy* meridional). Línea azul: producción menos pérdida fotoquímicas. Línea de puntos: residuo.

A pesar de las marcadas diferencias entre el modelo WACCM y el modelo 1D (WACCM es un complejo modelo climático con química acoplada, mientras que el modelo 1D es un modelo simplificado de transporte tropical), el balance de ozono muestra características comunes en los dos modelos (comparar con la Fig. 7S). En particular, **los resultados lagrangianos evaluados desde un punto de vista euleriano confirman que el ciclo anual del *upwelling* causa el ciclo anual de la tendencia de ozono en la baja estratosfera tropical**. Además, **se observa un cambio de la evolución estacional en el transporte horizontal con la altura similar al obtenido en los resultados de WACCM**, con máximo *in-mixing* en el verano boreal cerca de la tropopausa tropical (situada cerca de ~100 hPa en este modelo lagrangiano), mientras que en niveles más altos el transporte horizontal es ligeramente más intenso en invierno y primavera.

**La similitud entre los balances de ozono en los dos modelos demuestra que los resultados de WACCM son consistentes con los del modelo lagrangiano**. La aparente discrepancia tiene origen en el hecho de que los resultados lagrangianos proporcionan una visión integrada del

transporte, mientras que en los balances TEM los términos están evaluados exclusivamente en un determinado nivel de presión. Por ejemplo, las trayectorias de las parcelas de aire transportadas desde el extra-trópico por el anticiclón del monzón Asiático y que seguidamente ascienden en el trópico debido al *upwelling*, serán contabilizadas a su paso por un nivel superior como *in-mixing* desde una perspectiva lagrangiana, mientras que representan transporte vertical en el balance TEM evaluado en ese nivel. En definitiva, la comparación con el modelo lagrangiano refuerza la imagen del transporte de ozono en la baja estratosfera tropical obtenida con el modelo WACCM. Los resultados de la comparación entre las perspectivas euleriana y lagrangiana del transporte de ozono están publicados en Abalos et al. (2013b).

- ## Objetivo 4.

*Explorar el forzamiento dinámico de la variabilidad del upwelling en escalas de tiempo sub-estacionales.*

El siguiente paso en la investigación desarrollada ha sido identificar los principales forzamientos dinámicos de la variabilidad sub-estacional en el *upwelling*. Dada la coherencia observada en las fluctuaciones de escala sub-estacional entre las estimaciones del *upwelling* y las observaciones de trazadores (Figura 4S; Objetivo 2), se ha podido acometer este objetivo empleando una de estas estimaciones; en particular, se utiliza la estimación del *upwelling* basada en el balance del momento ( $\overline{w}^*_m$ ), por su relación directa con el forzamiento dinámico involucrado (Ec. 2S). El análisis se ha llevado a cabo proyectando los campos que constituyen el forzamiento sobre las series temporales de *upwelling*, $\overline{w}^*_m$ (es decir, realizando regresiones lineales entre las respectivas series temporales).

El integrando de la Ec. (2S) es función de $DF - \overline{u}_t$, término que se denomina *forzamiento neto* en esta Tesis Doctoral. Por tanto, el forzamiento neto del *upwelling* viene dado por tanto por el efecto

combinado del arrastre ejercido por las ondas ( $DF$ , divergencia del flujo EP) más la respuesta en el flujo medio zonal ( $\overline{u}_t$ ). La Figura 11S muestra la proyección sobre el *upwelling* de estas dos contribuciones y del forzamiento neto para la estación invernal extendida (DEFM) de todo el período cubierto por ERA-Interim (1979-2011). Tanto las series temporales como los campos han sido previamente filtrados para aislar la variabilidad en escalas temporales sub-estacionales (tomadas aquí como menores de 90 días).

El análisis realizado ha permitido identificar **dos centros de acción de $DF$ principales: en la estratosfera extratropical invernal y en los subtrópicos de ambos hemisferios** (Fig. 11Sa). Asimismo, se han observado **correspondientes patrones de deceleración y aceleración ( $\overline{u}_t$ ) en la estratosfera extratropical y los subtrópicos** respectivamente (Fig. 11Sb), asociados con los centros de acción de $DF$ . Un resultado importante de la Fig. 11S es que el efecto del forzamiento de las ondas en sí, $DF$ , prácticamente no alcanza la frontera de los trópicos (Fig. 11Sa), que es precisamente donde se evalúa el forzamiento en el cálculo del *upwelling* (ver la Ec. 2S). Dado que en latitudes subtropicales el forzamiento ( $DF$ ) toma valores relativamente pequeños, **la débil tendencia del viento zonal inducida de forma remota en dichas latitudes** ( $\overline{u}_t$ , Fig. 11Sb) contribuye de forma no despreciable al forzamiento neto ( $DF - \overline{u}_t$ , Fig. 11Sc), y por consiguiente **tiene un efecto importante en las fluctuaciones sub-estacionales del *upwelling* tropical**.

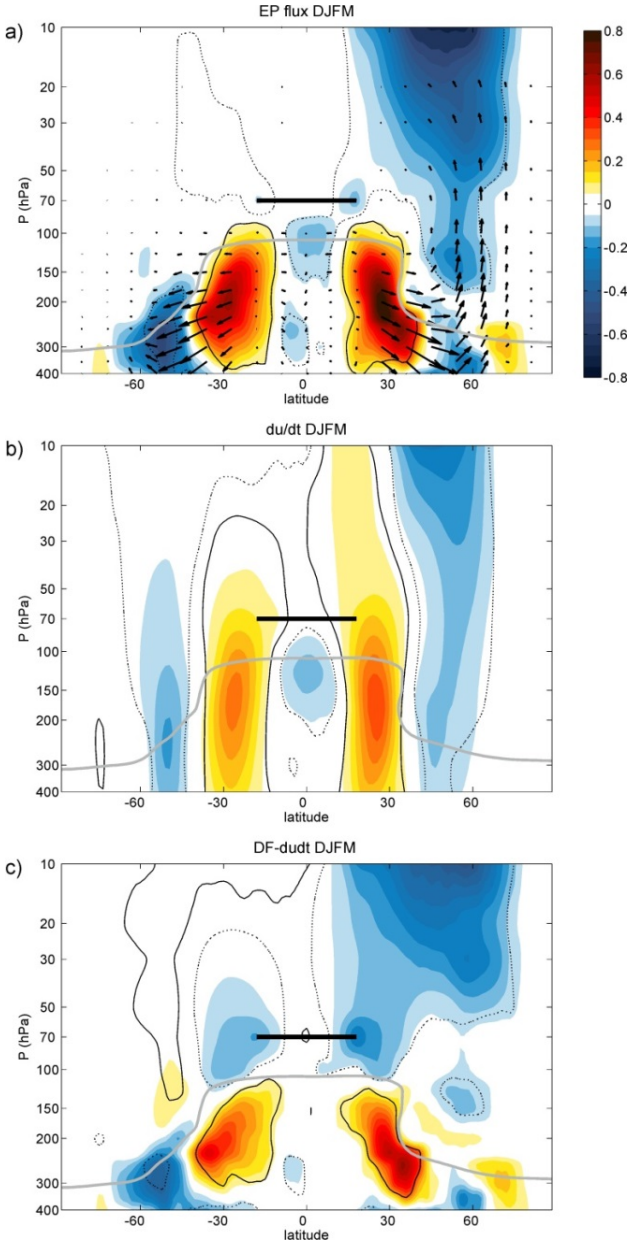


**Figura 11S**. Proyecciones de los campos que definen el forzamiento sobre el *upwelling* tropical en 70 hPa promediado entre 18°S-18°N para los meses DEFM del período 1979-2011 (a partir de datos medios diarios de ERA-Interim). a) Divergencia del flujo EP ( $DF$ , sombreado), el flujo EP se muestra con vectores, b) tendencia del viento medio zonal ( $\overline{u}_t$ ) y c)

$DF - \overline{u}_t$. Los contornos señalan las regiones para las que se tiene un 99% de significación estadística. La línea gris muestra la tropopausa térmica. La barra negra indica el intervalo latitudinal y la altura en los que se ha calculado el *upwelling* para esta figura. La barra de colores es la misma para los tres paneles. Unidades: $m \cdot s^{-1} \cdot day^{-1} \cdot std(\overline{w}_m^*)^{-1}$, donde $std(\overline{w}_m^*)$ representa la unidad de desviación estándar del *upwelling*.

Para interpretar correctamente las proyecciones mostradas en la Fig. 11S, es conveniente complementar este resultado con los valores que toma el flujo EP y su divergencia $DF$ durante eventos de alta y baja intensidad del *upwelling*. Estos casos extremos se han definido como aquellos días con *upwelling* superior al valor percentil P95 (*upwelling* intenso) e inferior al percentil P5 (*upwelling* débil), respectivamente, de la serie temporal correspondiente a la estación DEFM (período 1979-2011).

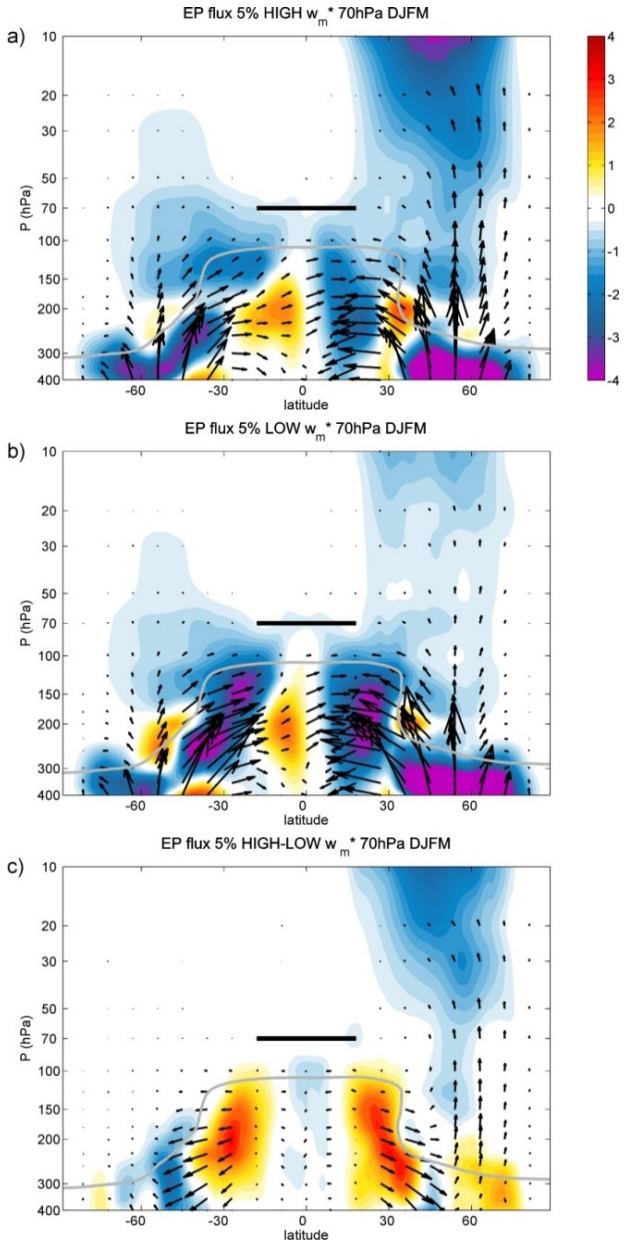


**Figura 12S**. Compuestos del flujo EP (vectores) y su divergencia ( $DF$ , sombreado) para el 5% de casos extremos altos (a), bajos (b) y altos menos bajos (c) del *upwelling*. Los datos utilizados son los mismos que en la Fig. 9S. La línea gris muestra la tropopausa térmica. La barra negra indica el intervalo latitudinal y la altura en los que se ha calculado el *upwelling* para esta figura. Unidades: $m \cdot s^{-1} \cdot day^{-1}$.

La Figura 12S muestra que en todos los centros de acción resaltados en la Fig. 11S la divergencia del flujo EP es negativa ( $DF < 0$ ), es decir el flujo converge, tanto para los extremos altos como para los bajos. Además, esta figura muestra que la convergencia del flujo EP está asociada con actividad de onda que se propaga desde la troposfera extratropical hacia la estratosfera, la cual en parte penetra hacia niveles altos y en parte es refractada hacia el ecuador. **El *upwelling* tropical se intensifica durante episodios de propagación y convergencia en la alta estratosfera extratropical** (Fig. 12Sa)**, y se debilita cuando aumenta la convergencia en la alta troposfera subtropical** (Fig. 12Sb). Nótese que la diferencia entre los extremos de *upwelling* intenso y débil (Fig. 12Sc) presenta una estructura muy parecida a los patrones mostrados en la Fig. 11Sa. Por tanto, los compuestos mostrados en la Fig. 12S permiten interpretar los signos positivo y negativo obtenidos en los centros de acción en la figura 11Sa como intensificación y debilitamiento, respectivamente, de la convergencia del flujo EP en diferentes regiones.

El hecho de que el *upwelling* en la baja estratosfera tropical esté relacionado con la convergencia del flujo de EP en niveles troposféricos aparentemente contradice a la Ec. (2S), que establece que el *upwelling* en un nivel dado, $z$ , es función exclusivamente del forzamiento neto en el mismo nivel $z$ y en niveles superiores. Los análisis realizados muestran el mecanismo por el cual el forzamiento en la alta troposfera afecta a niveles de la baja estratosfera. En particular, **la respuesta barotrópica del viento zonal (es decir, el término $\overline{u}_t$ ) juega un papel fundamental en la comunicación de la señal a los niveles superiores**. La Figura 13S ilustra este mecanismo. Las auto-correlaciones de las series temporales del forzamiento $DF$ en un punto de la alta troposfera subtropical (con $DF$ en todos los demás puntos) muestran que **la extensión del forzamiento está limitada a una región relativamente reducida entorno a dicho punto (Fig. 13Sa). Sin embargo, la respuesta del viento zonal muestra una mayor extensión vertical** (Fig. 13Sb)**, y como resultado el forzamiento neto se extiende por encima de la tropopausa** (Fig. 13Sc). Para completar

el mecanismo, la Figura 13Sd muestra el impacto del mismo forzamiento en la alta troposfera subtropical sobre la circulación. Se observan dos células de circulación con sentido de giro opuesto por encima y por debajo del forzamiento. La célula superior produce descenso y calentamiento por encima de la tropopausa tropical, lo cual demuestra que el forzamiento en esta región produce un debilitamiento del *upwelling* (de acuerdo con las Fig. 12Sb).

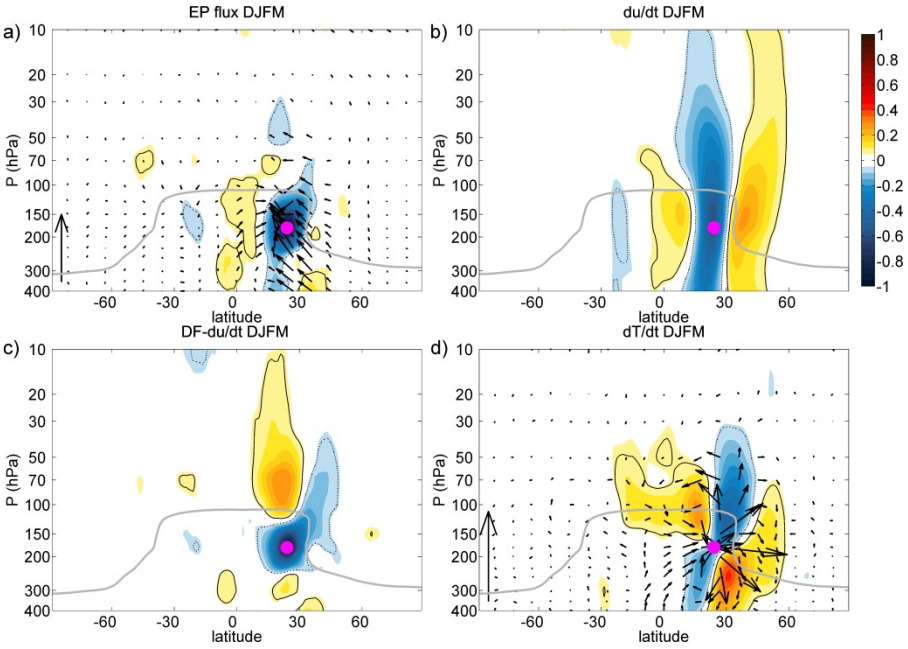


**Figura 13S.** Correlaciones lineales de la serie temporal del forzamiento $DF$ en el punto marcado por el círculo magenta (24°N, 175 hPa) con distintos campos. a) Divergencia del flujo de EP (sombreado) y flujo de EP (vectores). b) Tendencia del viento zonal. c) Forzamiento neto. d) Tendencia de la temperatura (sombreado) y circulación residual (vectores). La barra de colores es la misma para todos los paneles. Los datos utilizados son los mismos que en las Figs. 11S y 12S.

En el presente análisis **se ha identificado una desconexión parcial entre las dos ramas de la circulación de Brewer-Dobson, en relación a las regiones específicas de forzamiento de su variabilidad**. En particular, la influencia del forzamiento localizado en la alta troposfera subtropical está

limitada a la rama superficial de la circulación (situada aproximadamente por debajo de ~70-50 hPa), mientras que $DF$ en la estratosfera extratropical afecta a la variabilidad del *upwelling* a todos los niveles en la estratosfera. La transición entre las dos ramas en términos del forzamiento de la variabilidad sub-estacional es gradual. Estos resultados no sólo están de acuerdo con estudios previos que han mostrado que la circulación de Brewer-Dobson presenta dos ramas bien distinguidas que pueden evolucionar de manera distinta (e.g. Bönish et al. 2011), sino que además aporta aspectos añadidos sobre la diferencia entre ambas ramas. Estos últimos resultados constituyen el material de un cuarto artículo que se encuentra actualmente en preparación (Abalos et al. 2013c).

## • Conclusiones

Las conclusiones más importantes de esta Tesis Doctoral se pueden resumir de la siguiente manera:

- **Análisis basados en tanto en observaciones como en el modelo climático con química acoplada WACCM muestran que el *upwelling* controla una fracción significativa de la variabilidad en la temperatura, el ozono y el monóxido de carbono (CO) en la baja estratosfera tropical, tanto en escalas estacionales como sub-estacionales.**

- **La estacionalidad del transporte *eddy* cuasi-horizontal cambia con la altura, de modo que el monzón Asiático tiene un gran impacto sobre las concentraciones de ozono cerca de la tropopausa. En la baja estratosfera tropical, sin embargo, el transporte *eddy* está asociado a ondas de Rossby que rompen en el subtrópico.**

- **Los resultados de un modelo lagrangiano sobre el transporte de ozono son consistentes con los derivados del análisis de los**

**balances TEM, y proporcionan información complementaria sobre el origen (tropical o extra-tropical) de las moléculas de ozono.**

- **La variabilidad del *upwelling* tropical en escalas de tiempo sub-estacionales está forzada principalmente por la actividad de onda extratropical en invierno, que converge en la estratosfera extratropical y en la alta troposfera subtropical. La respuesta transitoria del viento zonal juega un papel importante en la comunicación remota del forzamiento.**

# References

Abalos, M., Randel, W. J. and Serrano, E.: Variability in upwelling across the tropical tropopause and correlations with tracers in the lower stratosphere, Atmos. Chem. Phys., 12, 11505–11517, doi:10.5194/acp-12-11505-2012, 2012.

Abalos, M., Randel, W. J., Kinnison, D. E., and Serrano, E.: Quantifying tracer transport in the tropical lower stratosphere using WACCM, Atmos. Chem. Phys., 13, 10591-10607, doi:10.5194/acp-13-10591-2013, 2013a.

Abalos, M., Ploeger, F., Konopka, P., Randel, W. J., and Serrano, E.: Ozone seasonality above the tropical tropopause: reconciling the Eulerian and Lagrangian perspectives of transport processes, Atmos. Chem. Phys., 13, 10787-10794, doi:10.5194/acp-13-10787-2013, 2013b.

Abalos, M., Randel, W. J. and Serrano, E.: Dynamical forcing of sub-seasonal variability in tropical upwelling, submitted to J. Atmos. Sci. Manuscript Number: JAS-D-13-0366.

Andrews, D. G. and McIntyre, M. E.: Planetary waves in horizontal and vertical shear: the generalized Eliassen-Palm relation and the zonal mean acceleration, J. Atmos. Sci., 33 (11), 2031-2048, 1976.

Andrews, D. G., and McIntyre, M. E.: Generalised Eliassen-Palm and Charney-Drazin theorems for waves on axisymmetric mean flows in compressible atmospheres, J. Atmos. Sci., 35, 175-185, 1978.

Andrews, D. G., Holton, J. R. and Leovy, C. B.: Middle Atmosphere Dynamics, Academic Press, Orlando, Florida, 489 pp., 1987.

Andrews, A. E., Boering, K. A., Daube, B. C., Wofsy, S. C., Hintsa, E. J., Weinstock, E. M. and Bui T. P.: Empirical age spectra for the lower tropical stratosphere from in situ observations of CO2: Implications for stratospheric transport, J. Geophys. Res., 104, 26,581– 26,595, 1999.

Anthes, R. A., Bernhardt, P. A., Chen, Y., Cucurull, L., Dymond, K. F., Ector, D., Healy, S. B., Ho, S. –P., Hunt, D. C., Kuo, Y.-H., Liu, H., Manning, K.,

McCormik, C., Meehan, T. K., Randel, W. J., Rocken, C., Schreiner, W. S., Sokolovskiy, S. V., Syndergaard, S., Thompson, D. C., Trenberth, K. E., Wee, T.-K., Yen, N. L. and Zeng, Z.: The COSMIC/FORMOSAT-3 Mission: Early Results, B. Am. Meteorol. Soc., 89, 313–333, doi:10.1175/BAMS-89-3-313, 2008.

Bernath, P. F., McElroy, C. T., Abrams, M. C., Boone, C. D., Butler, M., Camy-Peyret, C., Carleer, M., Clerbaux, C., Coheur, P. F., Colin, R., DeCola, P., DeMazière, M., Drummond, J. R., Dufour, D., Evans, W. F. J., Fast, H., Fussen, D., Gilbert, K., Jennings, D. E., Llewellyn, E. J., Lowe, R. P., Mahieu, E., McConnell, J. C., McHugh, M., McLeod, S. D., Michaud, R., Midwinter, C., Nassar, R., Nichitiu, F., Nowlan, C., Rinsland, C. P., Rochon, Y. J., Rowlands, N., Semeniuk, K., Simon, P., Skelton, R., Sloan, J. J., Soucy, M. -A., Strong, K., Tremblay, P., Turnbull, D., Walker, K. A., Walkty, I., Wardle, D. A., Wehrle, V., Zander, R. and Zou, J.: Atmospheric Chemistry Experiment (ACE): Mission overview, Geophys. Res. Lett., 32, L15S01, doi:10.1029/2005GL022386, 2005.

Berrisford P., Dee D. P., Fielding K., Fuentes M., Kallberg P., Kobayashi S., Uppala S. M. The ERA-Interim Archive. ERA Report Series, No. 1. ECMWF: Reading, UK, 2009.

Birner, T. and Bönisch, H.: Residual circulation trajectories and transit times into the extratropical lowermost stratosphere, Atmos. Chem. Phys., 11, 817–827, 2011, doi:10.5194/acp-11-817-2011, 2011.

Bloomfield, P.: Fourier analysis of time series: An introduction, Second Edition, Wiley Series in Probability and Statistics, ISBN: 9780471889489, doi: 10.1002/0471722235, 2000.

Boehm, M. T. and Lee, S.: The implications of tropical Rossby waves for tropical tropopause cirrus formation and for the equatorial upwelling of the Brewer–Dobson circulation, J. Atmos. Sci., 60, 247-261, 2003.

Bönisch, H., Engel, A., Birner, T., Hoor, P. Tarasick, D. W. and Ray, E. A.: On the structural changes in the Brewer-Dobson circulation after 2000, Atmos. Chem. Phys., 11, 3937–3948, doi:10.5194/acp-11-3937-2011, 2011.

Brewer, A. W.: Evidence for a world circulation provided by the measurements of helium and water vapour distribution in the stratosphere, Quart. J. Roy. Meteor. Soc., 75, 351-363, 1949.

Butchart, N., Scaife, A. A., Bourqui, M., de Grandpré, J., Hare, S. H. E., Kettleborough, J., Langematz, U. Manzini, E., Sassi F., Shibata, K., Shindell, D. and Sigmond, M.: Simulations of anthropogenic change in the strength of the Brewer–Dobson circulation, Clim. Dyn., 27, 727–741, doi:10.1007/s00382-006-0162-4, 2006.

Calvo Fernández, N., Garcia, R. R., Garcia-Herrera, R., Gallego Puyol, D., Gimeno Presa, L., Hernández Martín, E. and Ribera Rodríguez, P.: Analysis of ENSO signal in stratospheric and tropospheric temperatures observed by MSU, 1979-2000, J. Climate, 17, 3934-3946, 2004.

Calvo, N. and Garcia, R. R.: Wave forcing of the tropical upwelling in the lower stratosphere under increasing concentrations of greenhouse gases, J. Atmos. Sci., 66, 3184-3196, 2009.

Calvo, N., Giorgetta, M. A., Garcia-Herrera, R. and Manzini, E.: Nonlinearity of the combined warm ENSO and QBO effects on the Northern Hemisphere polar vortex in MAECHAM5 simulations, J. Geophys. Res., 114, D13109, doi:10.1029/2008JD011445, 2009.

Calvo, N., Garcia, R. R., Randel, W. J. and Marsh, D. R.: Dynamical mechanism for the increase in tropical upwelling in the lowermost tropical stratosphere during warm ENSO events, 67, 2331-2340, doi:10.1175/2010JAS3433.1, 2010.

CCMVal SPARC Report No. 5, WCRP-132, WMO/TD-No. 1526, Chemistry-Climate Model Validation by Erying, V., Shepherd, T. and Waugh, D. (Editors), 2010.

Chae, J. H., and Sherwood, S. C.: Annual temperature cycle of the tropical tropopause: A simple model study, J. Geophys. Res., 112, D19111, doi:10.1029/2006JD007956, 2007.

Charney, J. G. and Drazin. P. G.: Propagation of planetary-scale disturbances from the lower into the upper atmosphere, J. Geophys. Res., 66, 83-109, 1961.

Chen, P., Holton, J. R., O'Neill, A. and Swinbank, R.: Isentropic mass exchange between the Tropics and extra-tropics in the stratosphere, J. Atmos. Sci., 51, 3006–3018, 1994.

Chen, G. and Sun, L.: Mechanisms of the tropical upwelling branch of the Brewer–Dobson circulation: The role of extratropical eaves. J. Atmos. Sci., 68, 2878–2892. doi: http://dx.doi.org/10.1175/JAS-D-11-044.1, 2011.

Corti, T., Luo, B. P., de Reus, M., Brunner, D., Cairo, F., Mahoney, M. J., Martucci, G., Matthey, R., Mitev, V., dos Santos,F. H., Schiller, C., Shur, G., Sitnikov, N. M., Spelten, N., Vossing, H. J., Borrmann, S., and Peter, T.: Unprecedented evidence for overshooting convection hydrating the tropical stratosphere, Geophys. Res. Lett., 35, L10810, doi:10.1029/2008GL033641, 2008.

Dee, D. P., Uppala, S. M., Simmons, A. J., Berrisford, P., Poli, P., Kobayashi, S., Andrae, U., Balmaseda, M. A., Balsamo, G., Bauer, P., Bechtold, P., Beljaars, A. C. M., van de Berg, L., Bidlot, J., Bormann, N., Delsol, C., Dragani, R., Fuentes, M., Geer, A. J., Haimberger, L., Healy, S. B., Hersbach, H., Hólm, E. V., Isaksen, L., Kållberg, P., Köhler, M., Matricardi, M., McNally, A. P., Monge-Sanz, B. M., Morcrette, J.-J., Park, B.-K., Peubey, C., de Rosnay, P., Tavolato, C., Thépaut, J.-N., and Vitart, F.: The ERA-interim reanalysis: configuration and performance of the data assimilation system, Q. J. R. Meteorol. Soc., 137, 553–597, doi:10.1002/qj.828, 2011.

Dee, D. P.: ERA-20C production has started, ECMWF Newsletter, 134, 6-9, 2013.

Dickinson, R. E.: Planetary Rossby waves propagating vertically through weak westerly wind waveguides, J. Atmos. Sci., 25, 984-1002, 1968.

Dobson, G. M. B., Harrison, D. N. and Lawrence, J.: Measurements of the amount of ozone in the earth's atmosphere and its relation to other geophysical conditions, Proc. Roy. Soc., Series A, 122, 456-486, 1929.

Dobson, G. M. B.: Origin and distribution of the polyatomic molecules in the atmosphere, Proc. R. Soc. A, 236, 187–193, doi:10.1098/rspa.1956.0127, 1956.

Dunkerton, T.J., Hsu, C.-P.F. and McIntyre, M. E.: Some Eulerian and Lagrangian diagnostics for a model stratospheric warming. J. Atmos. Sci., 38, 819-843, 1981.

Dunkerton, T. J.: Nonlinear Hadley circulation driven by asymmetric differential heating. J. Atmos. Sci., 46, 956–974, 1989.

Edmon, H. J., Jr., B. J. Hoskins, and McIntyre, M. E.: Eliassen-Palm cross sections for the troposphere, J. Atmos. Sci., 37, 2600-2616, 1980.

Eliassen, A.: Slow thermally or frictionally controlled meridional circulation in a frictional vortex, Astrophys. Norv., 5, 19-60, 1951.

Eluszkiewicz, J., Crisp, D., Zurek, R., Elson, L., Fishbein, E., Froidevaux, L. and Waters, J.: Residual circulation in the stratosphere and lower mesosphere as diagnosed from Microwave Limb Sounder data, J. Atmos. Sci., 53, 217–240, 1996.

Engel, A., Möbius, T., Bönisch, H., Schmidt, U., Heinz, R., Levin, I., Atlas, E., Aoki, S., Nakazawa, T., Sugawara, S., Moore, F., Hurst, D., Elkins, J., Schauffler, S., Andrews, A., and Boering, K.: Age of stratospheric air unchanged within uncertainties over the past 30 years, Nat. Geosci., 2, 28–31, doi:10.1038/ngeo388, 2009.

Flury, T., Wu, D. L., and Read, W. G.: Variability in the speed of the Brewer–Dobson circulation as observed by Aura/MLS, Atmos. Chem. Phys., 13, 4563-4575, doi:10.5194/acp-13-4563-2013, 2013.

Folkins, I., Bernath, P., Boone, C., Lesins, G., Livesey, N., Thompson, A. M., Walker, K. and Witte, J. C.: Seasonal cycles of O3, CO, and convective outflow at the tropical tropopause, Geophys. Res. Lett., 33, L16802, doi:10.1029/2006GL026602, 2006.

Fritz, S. and Soules, S. D.: Planetary variations of stratospheric temperatures, Mon. Wea. Rev., 100, 582–589, 1972.

Froidevaux, L., Livesey, N. J., Read, W. G., Jiang, Y. B., Jimenez, C., Filipiak, M. J., Schwartz, M. J., Santee, M. L., Pumphrey, H. C., Jiang, J. H., Wu, D. L., Manney, G. L., Drouin, B. J., Waters, J. W., Fetzer, E. J., Bernath, P. F., Boone, C. D., Walker, K. A., Jucks, K. W., Toon, G. C., Margitan, J.,J., Sen, B., Webster, C. R., Christensen, L. E., Elkins, J. W., Atlas, E., Lueb, R. A., and Hendershot, R.: Early validation analyses of atmospheric

profiles from EOS MLS on the Aura satellite, IEEE Trans. Geosci. Remote Sens., 44, 1106-1121, 2006.

Froidevaux, L., Jiang, Y. B., Lambert, A., Livesey, N. J., Read, W. G., Waters, J. W., Browell, E. V., Hair, J. W., Avery, M. A., McGee, T. J., Twigg, L. W., Sumnicht, G. K., Jucks, K. W., Margitan, J. J., Sen, B., Stachnik, R. A., Toon, G. C., Bernath, P. F., Boone, C. D., Walker, K. A., Filipiak, M. J., Harwood, R. S., Fuller, R. A., Manney, G. L., Schwartz, M. J., Daffer, W. H., Drouin, B. J., Cofield, R. E., Cuddy, D. T., Jarnot, R. F., Knosp, B. W., Perun, V. S., Snyder, W. V., Stek, P. C., Thurstans, R. P. and Wagner P. A.: Validation of Aura Microwave Limb Sounder stratospheric ozone measurements, J. Geophys. Res., 113, D15S20, doi:10.1029/2007JD008771, 2008.

Fueglistaler, S., Dessler, A. E., Dunkerton, T. J., Folkins, I., Fu, Q. and Mote, P. W.: Tropical tropopause layer, Rev. Geophys., 47, RG1004, doi:10.1029/2008RG000267, 2009a.

Fueglistaler, S., Legras, B., Beljaars, A., Morcrette, J. J., Simmons, A., Tompkins, A. M., and Uppala, S.: The diabatic heat budget of the upper troposphere and lower/mid stratosphere in ECMWF reanalysis, Quart. J. Roy. Meteor. Soc., 135, 21– 37, doi:10.1002/qj.361, 2009b.

Fueglistaler, S., Haynes, P. H. and Forster, P. M.: The annual cycle in lower stratospheric temperatures revisited, Atmos. Chem. Phys., 11, 3701–3711, doi:10.5194/acp-11-3701-2011, 2011.

Garcia, R. R.: On the mean meridional circulation of the middle atmosphere, J. Atmos. Sci., 44 (24), 3599-3609, 1987.

Garcia, R. R.: Parameterization of planetary wave breaking in the middle atmosphere, J. Atmos. Sci., 48, 1405-1419, 1991.

Garcia R. R., Marsh, D. R., Kinnison, D. E., Boville, B. A. and Sassi, F.: Simulation of secular trends in the middle atmosphere, J. Geophys. Res., 112, D09301, 1950–2003, doi:10.1029/2006JD007485, 2007.

Garcia, R. R. and Randel, W. J.: Acceleration of the Brewer-Dobson circulation due to increases in greenhouse gases, J. Atmos. Sci., 65, 2731-2739, 2008.

Garcia, R. R., Randel. W. J. and Kinnison, D. E.: On the determination of age of air trends from atmospheric trace species, J. Atm. Sci., 68, 139-154, doi:10.1175/2010JAS3527.1, 2011.

Garcia, R. R., Kinnison, D. E. and Marsh, D. R: "World avoided" simulations with the Whole Atmosphere Community Climate Model, J. Geophys. Res., 117, D23303, doi:10.1029/2012JD018430, 2012.

Garny, H., Dameris, M., Randel, W. J., Bodeker, G. E., Deckert, R.: Dynamically forced increase of tropical upwelling in the lower stratosphere, J. Atmos. Sci., 68, 1214-1233, 2011.

Gerber, E. P.: Stratospheric versus tropospheric control of the strength and structure of the Brewer–Dobson circulation, J. Atmos. Sci., 69, 2857-2877, doi: 10.1175/JAS-D-11-0341.1, 2012.

Gettelman, A., Forster, P., Fujiwara, M., Fu, Q., Vömel, H., Gohar, L., Johason C. and Ammerman, M.: The radiation balance of the tropical tropopause layer, J. Geophys. Res., 109, D07103, doi:10.1029/2003JD004190, 2004.

Gettelman, A., Hegglin, M. I., Son, S.-W., Kim, J., Fujiwara, M., Birner, T., Kremser, S., Rex, Añel, J. A., Akiyoshi, H., Austin, J., Bekki, S., Braesike, P., Brül, C., Butchart, N., Chipperfield, M., Dameris, M., Dhomse, S., Garny, H., Hardiman, S. C., Jöckel, P., Kinnison, D. E., Lamarque, J. F., Mancini, E., Marchand, M., Michou, M., Morgenstern, O., Pawson, S., Pitari, G., Plummer, D., Pyle, J. A., Rozanov, E., Scinocca, J., Shepherd, T. G., Shibata, K., Smale, D, Teyssèdre, H. and Tian, W.: Multimodel assessment of the upper troposphere and lower stratosphere: Tropics and global trends, J. Geophys. Res., 115, D00M08, doi: 10.1029/2009JD013638, 2010.

Gettelman, A., Hamilton, K. P., Morris, G. A., Hasebe, F., Selkirk, H. B.: Report on the U.S. - Japan Bilateral Workshop on the Tropical Tropopause Layer: State of the current science and future observational needs, 15-19 October 2012, Honolulu, HI, USA, SPARC Newsletter, 40, 37-47, 2013.

Gille, J. C., Lyjak, L. V., and Smith, A. K.: The global residual mean circulation in the middle atmosphere for the northern winter period, J. Atmos. Sci., 44, 1437–1452, 1987.

Grise, K. M., Thompson, D. W. J., Birner, T.: A global survey of static stability in the stratosphere and upper troposphere, J. Climate, 23, 2275–2292doi: http://dx.doi.org/10.1175/2009JCLI3369.1, 2010.

Grise, K. M. and Thompson, D. J.: On the signatures of equatorial and extratropical wave forcing in Tropical Tropopause Layer temperatures, J. Atmos. Sci., 70, 1084-1102, doi: 10.1175/JAS-D-12-0163.1, 2013.

Iwasaki, T., Hamada, H. and Miyazaki, K.: Comparisons of Brewer-Dobson circulations diagnosed from reanalyses, J. Meteor. Soc. Japan, 87, 997-1006, 2009.

Hayashi, Y.: Space-time spectral analysis and its applications to atmospheric waves. J. Meteor. Soc. Japan, 60, 156–171, 1982.

Haynes, P. H., Marks, C. J., McIntyre, M. E., Shepherd T. G. and Shine, K. P.: On the "downward control" of extratropical diabatic circulations by eddy-induced mean zonal forces, J. Atmos. Sci., 48, 651-678, 1991.

Haynes, P. and Shuckburgh, E.: Effective diffusivity as a diagnostic of atmospheric transport: 1. Stratosphere, J. Geophys. Res., 105, 22777-22794, doi:10.1029/2000JD900093, 2000a.

Haynes, P. and Shuckburgh, E.: Effective diffusivity as a diagnostic of atmospheric transport: 2. Troposphere and lower stratosphere, J. Geophys. Res., 105, 22795-22810, doi:10.1029/2000JD900092, 2000b.

Haynes, P.: Stratospheric dynamics, Annu. Rev. Fluid Mech. 2005. 37:263–93, doi: 10.1146/annurev.fluid.37.061903.175710, 2005.

Held, I. M. and Hou, A. Y.: Nonlinear axially symmetric circulations in a nearly inviscid atmosphere. J. Atmos. Sci., 37, 515–533,1980.

Held, I. M. and B. J. Hoskins: Large-scale eddies and the general circulation of the troposphere, Advances in Geophysics, 28, 3–31, 1985.

Holton, J. R., Haynes, P. H., Mcintyre, M. E., Douglass, A. R., Rood, R. B. and Pfister, L.: Stratosphere-troposphere exchange, Reviews of Geophysics, 33, 4, 403-439, doi: 10.1029/95RG02097, 1995.

Holton, J. R.: 50 years of the Brewer-Dobson circulation, a personal view, Brewer-Dobson Workshop Report by Norton, W. and Shuckburgh, E. (Editors), SPARC Newsletter 15, 2000.

Holton, J. R.: An introduction to dynamic meteorology, Academic Press, 535 pp., 2004.

Homeyer, C. R. and Bowman, K. P.: Rossby wavebreaking and transport between the tropics and extra-tropics above the subtropical jet, J. Atmos. Sci., 70, 607–626, doi: http://dx.doi.org/10.1175/JAS-D-12-0198.1 2013.

IPCC, Climate Change 2007: The Physical Science Basis, Contribution of Working Group I to the Fourth Assessment Report of the Intergovernmental Panel on Climate Change, S. Solomon et al. (Editors), Cambridge Univ. Press, Cambridge, 2007.

IPCC, Climate Change 2013: The Physical Science Basis, Contribution of Working Group I to the Fifth Assessment Report of the Intergovernmental Panel on Climate Change, Technical Summary, 2013.

Iwasaki, T., Hamada, H. and Miyazaki, K.: Notes and correspondence: Comparison of Brewer-Dobson circulations diagnosed from reanalyses, Journal of the Meteorological Society of Japan, Vol. 87, No. 6, pp. 997--1006, 2009. 997, doi:10.2151/jmsj.87.997, 2009.

Kerr-Munslow, A. M. and Norton, W. A.: Tropical wave driving of the annual cycle in tropical tropopause temperatures. Part I: ECMWF analyses, J. Atmos. Sci., 63, 1420-1431, 2006.

Kinnison, D. E., Brasseur, G. P., Walters, S., Garcia, R. R., Marsh, D. R., Sassi, F., Harvey, V. L., Randall, C. E., Emmons, L., Lamarque, J. F., Hess, P., Orlando, J., Tie, X., Randel, W., Pan, L., Gettelman, A., Granier, C., Diehl, T., Niemeier, U. and Simmons, A. J.: Sensitivity of chemical tracers to meteorological parameters in the MOZART-3 chemical transport model, J. Geophys. Res., 112, D20302, doi:10.1029/2006JD007879, 2007.

Konopka, P., Grooß, J.-U., Ploeger, F. and Müller, R.: Annual cycle of horizontal in-mixing into the lower tropical stratosphere, J. Geophys. Res., 114, D19111, doi:10.1029/2009JD011955, 2009.

Konopka, P., Grooß, J.-U., Günther, G., Ploeger, F., Pommrich, R., Müller, R. and Livesey, N.: Annual cycle of ozone at and above the tropical

tropopause: observations versus simulations with the Chemical Lagrangian Model of the Stratosphere (CLaMS), Atmos. Chem. Phys., 10, 121–132, 2010.

Lin, S. -J.: A "vertically lagrangian" finite-volume dynamical core for global models, Mon. Weather Rev., 132, 2293–2307, doi:10.1175/1520-0493(2004)132<2293:AVLFDC>2.0.CO;2, 2004.

Liu, C., Zipser, E., Garrett, T., Jiang, J. H. and Su, H.: How do the water vapor and carbon monoxide ''tape recorders'' start near the tropical tropopause?, Geophys. Res. Lett., 34, L09804, doi:10.1029/2006GL029234, 2007.

Livesey, N. J., Read, W. G., Lambert, A., Cofield, R. E., Cuddy, D. T., Froidevaux, L., Fuller, R. A., Jarnot, R. F., Jiang, J. H., J. Y. B., Knosp, B. W., Kovalenko, L. J., Pickett, H. M., Pumphrey, H. C., Santee, M. L., Schwartz, M. J., Stek, P. C., Wagner, P. A., Waters, J. W., Wu, D. L.: EOS MLS version 2.2 Level 2 data quality and description document, Tech. Rep. JPL D-33509, Jet Propul. Lab., Pasadena, Calif., 2007.

Livesey, N. J., Filipiak, M. J., Froidevaux, L., Read, W. G., Lambert, A., Santee, M. L., Jiang, J. H., Pumphrey, H. C., Waters, J. W., Cofield, R. E., Cuddy, D. T., Daffer, W. H., Drouin, B. J., Fuller, R. A., Jarnot, R. F., Jiang, Y. B., Knosp, B. W., Li, Q. B., Perun, V. S., Schwartz, M. J., Snyder, W. V., Stek, P. C., Thurstans, R. P., Wagner, P. A., Avery, M., Browell, E. V., Cammas, J. -P., E. Christensen, L., Diskin, G. S., Gao, R. -S., Jost, H. -J., Loewenstein, M., Lopez, J. D., Nedelec, P., Osterman, G. B., Sachse, G. W., and Webster, C. R.: Validation of Aura Microwave Limb Sounder O3 and CO observations in the upper troposphere and lower stratosphere, J. Geophys. Res., 113, D15S02, doi:10.1029/2007JD008805, 2008.

Logan, J. A.: An analysis of ozonesonde data for the lower stratosphere: Recommendations for testing models, J. Geophys. Res., 104, 16151–16170, 1999.

Matsuno, T.: Vertical propagation of stationary planetary waves in the winter Northern Hemisphere, Journal of the Atmospheric Sciences, 27(6), 871-883, 1970.

Matsuno, T.: Lagrangian motion of air parcels in the stratosphere in the presence of planetary waves, 118, 189-216, 1980.

McIntyre, M. E. and Palmer, T. N: Breaking planetary waves in the stratosphere, Nature, 305, 593-600, 1983.

McKenna, D. S., Konopka, P., Grooß, J.-U., Günther, G., Müller, R., Spang, R., Offermann, D. and Orsolini, Y.: A new Chemical Lagrangian Model of the Stratosphere (CLaMS): 1. Formulation of advection and mixing, J. Geophys. Res., 107, D16, 4309, doi: 10.1029/2000JD000114, 2002.

McLandress, C., Plummer, D. A., and Shepherd, T. G.: Technical Note: A simple procedure for removing temporal discontinuities in ERA-Interim upper stratospheric temperatures for use in nudged chemistry-climate model simulations, Atmos. Chem. Phys. Discuss., 13, 25801-25825, doi:10.5194/acpd-13-25801-2013, 2013.

Monge-Sanz B. M., Chipperfield M. P., Simmons A. J., Uppala S. M.: Mean age of air and transport in a CTM: Comparison of different ECMWF analyses, Geophys. Res. Lett., 34, L04801, doi: 10.1029/2006GL028515, 2007.

Montgomery, D. C., Peck, E. A. and Vining, G. G.: Introduction to linear regression analysis, Wiley series in probability and mathematical statistics, Vol. 821, 2012.

Mote, P. W., Rosenlof, K. H., McIntyre, M. E., Carr, E. S., Gille, J. C., Holton, J. R., Kinnersley, J. S., Pumphrey, H. C., Russell III, J. M., and Waters, J. W.: An atmospheric tape recorder: The imprint of tropical tropopause temperatures on stratospheric water vapor, J. Geophys. Res., 101, 3989–4006, 1996.

Newman, P. A., Oman, L. D., Douglass, A. R., Fleming, E. L., Frith, S. M., Hurwitz, M. M., Kawa, S. R., Jackman, C. H., Krotkov, N. A., Nash, E. R., Nielsen, J. E., Pawson, S., Stolarski, R. S. and Velders, G. J. M.: What would have happened to the ozone layer if chlorofluorocarbons (CFCs) had not been regulated?, Atmos. Chem. Phys., 9, 2113–2128, doi:10.5194/acp-9-2113-2009, 2009.

Niwano, M., Yamazaki, K. and Shiotani, M.: Seasonal and QBO variations in ascent rate in the tropical lower stratosphere as inferred from UARS HALOE trace gas data, J. Geophys. Res., 108, 4794, doi:10.1029/2003JD003871, 2003.

North, G. R., Bell, T. L., Cahalan, R. F. and Mohen, F. J.: Sampling errors in the estimation of Empirical Orthogonal Functions, J. Atmos. Sci., 110, 699-706, 1982.

Norton, W. A.: Tropical wave driving of the annual cycle in tropical tropopause temperatures. Part II: Model results, J. Atmos. Sci., 63, 1420-1431, 2006.

Ortland, D. A. and Alexander, M. J.: The residual mean circulation in the tropical tropopause layer driven by tropical waves, J. Atmos. Sci., in review, 2013.

Park, M., W. J. Randel, D. E. Kinnison, L. K. Emmons, P. F. Bernath, K. A. Walker, C. D. D. Boone, and N. J. Livesey: Hydrocarbons in the upper troposphere and lower stratosphere observed from ACE-FTS and comparisons with WACCM, J. Geophys. Res., 118, doi:10.1029/2012JD018327, 2013.

Ploeger, F., Konopka, P., Günther, G., Grooß, J.-U. and Müller, R., Impact of the vertical velocity scheme on modeling transport in the tropical tropopause layer, J. Geophys. Res., 115, D03301, doi:10.1029/2009JD012023, 2010.

Ploeger, F., Konopka, P., Müller, R., Fueglistaler, S., Schmidt, T., Manners, J. C., Grooß, J.-U., Günther, G., Forster, P. M. and Riese, M.: Horizontal transport affecting trace gas seasonality in the Tropical Tropopause Layer (TTL), J. Geophys. Res., 117, 1–16, doi:10.1029/2011JD017267, 2012.

Plumb, R. A.: Zonally-symmetric Hough modes and meridional circulations in the middle atmosphere, J. Atmos. Sci., 39, 983-991, 1982.

Plumb, R. A.: A tropical pipe model of stratospheric transport, J. Geophys. Res., 101, 3957–3972, 10.1029/95JD03002, 1996.

Plumb, R. A., Eluszkiewicz, J.: The Brewer–Dobson Circulation: Dynamics of the Tropical Upwelling. J. Atmos. Sci., 56, 868–890, 1999.

Plumb, R. A.: Stratospheric transport, J. Meteorol. Soc. Jpn., 80, 793–809, doi:10.2151/jmsj.80.793, 2002.

Plumb, R. A.: Tracer interrelationships in the stratosphere, Rev. Geophys., 45, RG4005, doi:10.1029/2005RG000179, 2007.

Pumphrey, H. C., Filipiak, M. J., Livesey, N. J., Schwartz, M. J., Boone, C, Walker, K. A., Bernath, P., Ricaud, P., Barret, B., Clerbaux, C., Jarnot, R. F., Manney, G. L. and Waters J. W.: Validation of middle-atmosphere carbon monoxide retrievals from the Microwave Limb Sounder on Aura, J. Geophys. Res., 112, D24S38, doi:10.1029/2007JD008723, 2007.

Pumphrey, H. C., Boone, C., Walker, K. A., Bernath, P. and Livesey, N. J.: Tropical tape recorded observed in HCN, Geophys. Res. Lett., 35, L05801, doi:10.1029/2007GL032137, 2008.

Randel, W. J. and Held, I. M.: Phase speed spectra of transient eddy fluxes and critical layer absorption, J. Atmos. Sci., 48, 688-697, 1991.

Randel, W. J., Gille, J. C., Roche, A. E., Kumer, J. B., Mergenthaler, J. L., Waters, J. W., Fishbein, E. F. and Lahoz, W. A.: Stratospheric transport from the tropics to middle latitudes by planetary-wave mixing, Nature 365, 533 - 535 (07 October 1993); doi:10.1038/365533a0, 1993.

Randel, W. J., Wu, F., Russell III, J. M., Roche, A. and Waters, J. W.: Seasonal cycles and QBO variations in stratospheric CH4 and H2O observed in UARS HALOE data, 55 (2), 163-185, 1998.

Randel, W. J., Garcia, R. R. and Wu, F.: Time-dependent upwelling in the tropical lower stratosphere estimated from the zonal-mean momentum budget, J. Atmos. Sci., 59, 2141–2152, 2002.

Randel, W. J., Park, M., Wu, F. and Livesey, N.: A Large Annual Cycle in Ozone above the Tropical Tropopause Linked to the Brewer–Dobson Circulation, J. Atmos. Sci., 64 (12), 4479–4488, doi:10.1175/2007JAS2409.1, 2007.

Randel, W. J., Garcia, R.R. and Wu, F.: Dynamical balances and tropical stratospheric upwelling, J. Atmos. Sci., 65, 3584-3595, 2008.

Randel, W. J., Garcia, R. R., Calvo, N. and Marsh, D.: ENSO influence on zonal mean temperature and ozone in the tropical lower stratosphere. J. Geophys. Res., 36, L15822, doi:10.1029/2009GL039343, 2009.

Randel, W. J. and Jensen, E. J.: Physical processes in the tropical tropopause layer and their roles in a changing climate, 6 (3), doi: 10.1038/NGEO1733, 2013.

Ray, E. A., et al., Evidence for changes in stratospheric transport and mixing over the past three decades based on multiple data sets and tropical leaky pipe analysis, J. Geophys. Res., 115, D21304, doi:10.1029/2010JD014206, 2010.

Reed, R. J., and Vicek, C. L.: The annual temperature variation in the lower tropical stratosphere, J. Atmos. Sci., 26, 163–167, 1969.

Riese, M., Ploeger, F., Rap, A., Vogel, B., Konopka, P., Dameris, M. and Forster, P.: Impact of uncertainties in atmospheric mixing on simulated UTLS composition and related radiative effects, J. Geophys. Res., 117(D16), 1–10, doi:10.1029/2012JD017751, 2012.

Rood, R. B.: Reanalysis, in Data assimilation for the Earth system, 26, 361-372, Swinbank et al. (Editors), Kluwer Academic Publishers, The Netherlands, 2003.

Rosenlof, K. H.: Seasonal cycle of the residual mean meridional circulation in the stratosphere, J. Geophys. Res., 100, 5173–5191, 1995.

Rosenlof, K. H., Tuck, A. F., Kelly, K. K., Russell III, J. M. and McCormick, M. P.: Hemispheric asymmetries in water vapor and inferences about transport in the lower stratosphere, J. Geophys. Res., 102(D11), 13213–13234, doi:10.1029/97JD00873, 1997.

Ryu J.-H. and Lee, S.: Effect of tropical waves on the tropical tropopause transition layer upwelling, J. Atmos. Sci., 67, 3130-3148, doi: 10.1175/2010JAS3434.1, 2010.

Santee, M. L., Manney, G. L., Livesey, N. J., Froidevaux, L., Schwartz, M. J. and Read, W. G.: Trace gas evolution in the lowermost stratosphere from Aura Microwave Limb Sounder measurements, J. Geophys. Res., 116, D18306, doi:10.1029/2011JD015590, 2011.

Semeniuk, K. and Shepherd, T. G.: Mechanisms for tropical upwelling in the stratosphere, J. Atmos. Sci., 58, 3097-3115, 2001.

Seviour, W. J. M., Butchart, N. and Hardiman, S. C.: The Brewer–Dobson circulation inferred from ERA-Interim, Quart. J. Roy. Meteor. Soc., 138, 878-888, doi: 10.1002/qj.966, 2011.

Schoeberl, M. R., Duncan, B. N., Douglass, A. R., Waters, J., Livesey, N., Read, W. and Filipiak, M.: The carbon monoxide tape recorder, Geophys. Res. Lett., 33, L12811, doi:10.1029/2006GL026178, 2006.

Schoeberl, M. R., Douglass, A. R., Stolarski, R. S., Pawson, S., Strahan, S. E. and Read, W.: Comparison of lower stratospheric tropical mean vertical velocities, J. Geophys. Res., 113, D24109, doi:10.1029/2008JD010221, 2008a.

Schoeberl, M. R., Douglass, A. R., Newman, P. A., Lait, L. R., Lary, D., Waters, J., Livesey, N., Froidevaux, L., Lambert, A., Read, W., Filipiak, M. J. and Pumphrey, H. C.: QBO and annual cycle variations in tropical lower stratosphere trace gases from HALOE and Aura MLS observations, J. Geophys. Res., 113, D05301, doi:10.1029/2007JD008678, 2008b.

Shepherd, T. G.: Transport in the middle atmosphere, J. Meteorol. Soc. Jpn., 85, 165–191, 2007.

Shepherd, T. G. and Mc. Landress, C.: A robust mechanism for strengthening of the Brewer–Dobson circulation in response to climate change: critical-layer control of subtropical wave breaking, J. Atm. Sci., 68, 784-797, doi:10.1175/2010JAS3608.1, 2011.

Simmons, A., Uppala, S., Dee, D., Kobayashi, S.: ERA-Interim: new ECMWF reanalysis products from 1989 onwards, ECMWF Newsletter, 110, 25-35, 2006.

Solomon, S., Rosenlof, K. H., Portmann, R. W., Daniel, J. S., Davis, S. M., Sanford, T. J., Plattner, G.-K., Contributions of stratospheric water vapor to decadal changes in the rate of global warming, Science 327, 1219, doi:10.1126/science.1182488, 2010.

Stiller, G. P., von Clarmann, T., Haenel, F., Funke, B., Glatthor, N., Grabowski, U., Kellmann, S., Kiefer, M., Linden, A., Lossow, S. and López-Puertas, M.: Observed temporal evolution of global mean age of

stratospheric air for the 2002 to 2010 period, Atmos. Chem. Phys., 12, 3311–3331, doi:10.5194/acp-12-3311-2012, 2012.

Taguchi, M.: Wave driving in the tropical lower stratosphere as simulated by WACCM. Part I: annual cycle, J. Atmos. Sci., 66, 2029–2043, doi:10.1175/2009JAS2854.1, 2009.

Thompson, A. M., Witte, J. C., Smit, H. G. J., Oltmans, S. J., Johnson, B. J., Kirchhoff, V. W. J. H. and Schmidlin, F. J.: Southern Hemisphere Additional Ozonesondes (SHADOZ) 1998–2004 tropical ozone climatology: 3. Instrumentation, station-to-station variability, and evaluation with simulated flight profiles, J. Geophys. Res., 112, D03304, doi:10.1029/2005JD007042, 2007.

Thompson, A. M., Miller, S. K., Tilmes, S., Kollonige, D. W., Witte, J. C., Oltmans, S. J., Johnson, B. J., Fujiwara, M., Schmidlin, F. J., Coetzee, G. J. R., Komala, N., Maata, M., Mohamad, M., Nguyo, J., Mutai, C., Ogino, S. -Y., da Silva, F. R., Paes Leme, N. M., Posny, F.Scheele, R., Selkirk, H. B., Shiotani, M., Stübi, R., Levrat, G., Calpini, B., Thouret, V., Tsuruta, H., Valverde Canossa, J., Vömel, H., Yonemura, S., Diaz, J. A., Tan Thanh, N. T., Thuy Ha, H. T.: Southern Hemisphere Additional Ozonesondes (SHADOZ) ozone climatology (2005–2009): Tropospheric and tropical tropopause layer (TTL) profiles with comparisons to OMI-based ozone products, J. Geophys. Res., 117, D23301, doi:10.1029/2011JD016911, 2012.

Thompson, D. W., Seidel, D. J., Randel, W. J., Zou, C.-Z., Butler, A. H., Mears, C., Osso, A., Long, C., Lin, R.: The mystery of recent stratospheric temperature trends. Nature 491, 692-697, doi: 10.1038/nature11579, 2012.

Thuburn, J. and Craig, G. C.: Stratospheric influence on tropopause height: The radiative constraint, J. Atmos. Sci., 57, 17–28, 2000.

Trepte, C. R., Veiga, R. E. and McCormick, M. P.: The poleward dispersal of Mount Pinatubo volcanic aerosol, J. Geophys. Res., 98, 18563–18573, doi:10.1029/93JD01362, 1993.

Ueyama, R. and Wallace, M. J.: To what extent does high-latitude wave forcing drive tropical ipwelling in the Brewer–Dobson circulation?, J. Atmos. Sci., 67, 1232-3442, doi:10.1175/2009JAS3216.1, 2010.

Ueyama, R., Gerber, E. P., Wallace, J. M., Frierson, D. M. W.: The role of high-latitude waves in the intraseasonal to seasonal variability of tropical upwelling in the Brewer–Dobson circulation, J. Atmos. Sci., 70, 1631–1648, doi: http://dx.doi.org/10.1175/JAS-D-12-0174.1, 2013.

Uppala S. M., Dee D. P., Kobayashi S., Simmons A. J.: 'Evolution of reanalysis at ECMWF'. In Proceedings of Third WCRP International Conference on Reanalysis, 28 January–1 February 2008, Tokyo, Japan, 2008.

Volk, C. M., Elkins, J. W., Fahey, D. W., Salawitch, R. J., Dutton, G. S., Gilligan, J. M., Proffitt, M. H., Loewenstein, M., Podolske, J. R., Minschwaner, K., Margitan, J. J. and Chang, K. R.: Quantifying transport between the tropical and mid-latitude lower stratosphere, Science, 272, 1763–1768, doi:10.1126/science.272.5269.1763, 1996.

von Storch, H., and Zwiers, F. W.: Statistical Analysis in Climate Research, Cambridge University Press, ISBN 0 521 45071 3, 494 pp., ISBN 0-521-01230-9, 1999.

Waters, J. W., Froidevaux, L., Harwood, R. S., Jarnot, R. F., Pickett, H. M., Read, W. G., Siegel, P. H., Cofield, R. E., Filipiak, M. J., Flower, D. A., Holden, J. R., Lau, G. K., Livesey, N. J., Manney, G.L., Pumphrey, H.C., Santee, M. L., Wu, D. L., Cuddy, D. T., Lay, R. R., Loo, M. S., Perun, V. S., Schwartz, M. J., Stek, P. C., Thurstans, R. P., Boyles, M. A., Chandra, K. M., Chavez, M. C., Gun-Shing, C., Chudasama, B. V., Dodge, R., Fuller, R. A., Girard, M. A., Jiang, J. H., Yibo, J., Knosp, B. W., LaBelle, R. C., Lam, J. C., Lee, K. A., Miller, D., Oswald, J. E., Patel, N. C., Pukala, D. M., Quintero, O., Scaff, D. M., Van Snyder, W., Tope, M. C., Wagner, P. A., and Walch, M. J.: The Earth Observing System Microwave Limb Sounder (EOS MLS) on the Aura Satellite, IEEE Trans. Geosci. Remote Sens., 44, 1075-1092, 2006.

Waugh, D. W.: Seasonal variation of isentropic transport out of the tropical stratosphere, J. Geophys. Res., 101, 4007–4023, doi: 10.1029/95JD03160, 1996.

Waugh, D. W. and Hall, T. M.: Age of stratospheric air: theory, observations and models, Reviews of Geophysics, 40 (4), doi:10.1029/2000RG000101, 2002.

Waugh, D.: Age of stratospheric air, Nat. Geosci., 2, 14 – 16, doi:10.1038/ngeo397, 2009.

Wheeler, M. and Kiladis, G. N.: Convectively coupled equatorial waves: Analysis of clouds and temperature in the wavenumber–frequency domain, J. Atmos. Sci., 56, 374-399, 1999.

Yang, Q., Fu, Q., Austin, J., Gettelman, A., Li, F. and Vömel, H.: Observationally derived and general circulation model simulated tropical stratospheric upward mass fluxes, J. Geophys. Res., 113, D00B07, doi:10.1029/2008JD009945, 2008.

Yang, Q., Fu, Q. and Hu, Y.: Radiative impacts of clouds in the tropical tropopause layer, J. Geophys. Res., 115, D00H12, doi:10.1029/2009JD012393, 2010.

Yoshida, K. and Yamazaki, K.: Tropical cooling in the case of stratospheric sudden warming in January 2009: focus on the tropical tropopause layer, Atmos. Chem. Phys., 11, 6325-6336, doi:10.5194/acp-11-6325-2011, 2011.

Yulaeva, E., Holton, J. R. and Wallace, J. M.: On the cause of the annual cycle in tropical lower-stratospheric temperature, J. Atmos. Sci., 51, 169–174, 1994.

Zhou, T., Geller, M. A and Hamilton, K.: The roles of the Hadley circulation and downward control in tropical upwelling, J. Atmos. Sci., 63, 2740-2757, 2006.

Zhou, T., Geller, M. A. and Lin, W.: An observational study on the latitudes where wave forcing drives Brewer-Dobson upwelling, J. Atmos. Sci., 69, 1916-1935, doi: 0.1175/JAS-D-11-0197.1, 2012.

# Acronyms

**ACE**: Advanced Composition Explorer.

**BDC**: Brewer-Dobson circulation.

**CCMVal**: Chemistry-Climate Models Validation Activity.

**CESM:** Community Earth System Model.

**CFCs**: Chloroflourocarbons.

**CLAES**: Cryogenic Limb Array Etalon Sounder.

**CLaMS**: Chemical Lagrangian Model of the Stratosphere.

**CMIP-5**: Coupled Model Intercomparison Project Phase 5.

**COSMIC**: Constellation Observing System for Meteorology Ionosphere and Climate.

**CRM**: Column Radiation Model.

**DJFM**: December, January, February and March.

**ECMWF**: European Centre for Medium-range Weather Forecasts.

**ENSO**: El Niño/Southern Oscillation.

**EOF**: Empirical Orthogonal Function.

**EOS**: Earth Observing System Microwave Limb Sounder.

**ERA-20C**: ECMWF Re-Analysis for the 20th century.

**ERA-Interim**: ECMWF Interim Re-Analysis.

**EP flux**: Eliassen-Palm flux.

**EUMETSAT**: European Organisation for the Exploitation of Meteorological Satellites.

**GEOS**: Goddard Earth Observing System.

**GHG**: Greenhouse gases.

**GPS**: Global Positioning System.

**HALOE**: HAlogen Occultation Experiment.

**HIRDLS**: HIgh Resolution Dynamics Limb Sounder.

**IFS**: Integrated Forecast System.

**IPCC**: Intergovernmental Panel on Climate Change.

**JJAS**: June, July, August and September.

**JRA55**: Japanese 55-year Reanalysis.
**LZRH**: Level of Zero Radiative Heating.
**MERRA**: Modern Era Retrospective-Analysis for Research and Applications.
**MLS**: Microwave Limb Sounder.
**MOZART**: Model of OZone and Related Tracers.
**NASA**: National Aeronautics and Space Administration.
**NCAR**: National Center for Atmospheric Research.
**NOAA**: National Oceanic and Atmospheric Administration.
**NH**: Northern Hemisphere.
**QBO**: Quasi-Biennial Oscillation.
**RO**: Radio Occultation.
**SH**: Southern Hemisphere.
**SHADOZ**: Southern Hemisphere ADditional OZonesondes.
**SMILES**: Superconducting Submillimeter-Wave Limb-Emission Sounder.
**TEM**: Transformed Eulerian Mean.
**TTL**: Tropical Tropopause Layer.
**UARS**: Upper Atmosphere Research Satellite.
**UTLS**: Upper Troposphere/Lower Stratosphere.
**WACCM**: Whole Atmosphere Community-Climate Model.
**WMO**: World Meteorological Organization.